

9374

**TRANSITIONAL ELEMENT AND APPLICATIONS TO FRACTURE MECHANICS**

FORMULATION OF TRANSITIONAL ELEMENTS  
AND  
APPLICATIONS TO LINEAR ELASTIC FRACTURE MECHANICS

By

P. T. PATRICK LEUNG, B.Sc. (CIVIL ENGINEERING)

A Thesis

Submitted to the School of Graduate Studies  
in Partial Fulfilment of the Requirements

for the Degree

Master of Engineering

McMaster University

June, 1982

MASTER OF ENGINEERING (1982)  
(Civil Engineering and Engineering Mechanics)

McMASTER UNIVERSITY  
Hamilton, Ontario

TITLE: Formulation of Transitional Elements and Applications to  
Linear Elastic Fracture Mechanics

AUTHOR: P.T. Patrick Leung, B.Sc. (Civil Engineering), Queen's  
University at Kingston, Ontario

SUPERVISOR: Dr. Farooque A. Mirza

NUMBER OF PAGES: 205

## ABSTRACT

Mixed transitional finite elements, which enable the simultaneous use of the three-node triangular mixed and eight-node isoparametric displacement finite elements, are developed to reduce the amount of computer storage required in the mixed finite element method. Numerical testing of the simultaneous use of the above mixed, mixed transitional and displacement finite elements are also carried out to investigate numerical instability, orientation problems and convergence in the energy sense. The examples of a plane stress cantilever subjected to parabolically varying end shear and a plane strain, square plate with a circular hole in the middle are analyzed and the results obtained are found to be in very good agreement with those reported in the literature.

The three-element scheme above is then applied to problems in linear elastic fracture mechanics. The energy release rate approach using the direct derivative method is incorporated to compute the Mode I stress intensity factor  $K_I$ . Two plane stress isotropic rectangular plates with symmetric edge cracks and a central crack, respectively, and a plane stress orthotropic square plate with a central crack are analyzed. The stress intensity factors obtained are in excellent agreement with the available numerical results, and with significant reduction in computer storage requirements compared to that of the mixed finite element method alone.

Mixed mode linear elastic fracture problems are also considered. In this case, Ishikawa's scheme of decomposing the near crack tip stress and displacement fields is used along with the direct derivative method to compute the mixed mode stress intensity factors  $K_I$  and  $K_{II}$ . The stress intensity factors  $K_I$  and  $K_{II}$  obtained for a deep cantilever with an edge crack subjected to end shear are within 0.62 and 3.74 percent of the numerical results reported in the literature. The prediction of the branching angles for crack extensions are examined and the criterion of maximum energy release rate is used along with Ishikawa's scheme to calculate the angles of crack branching for a plane stress square plate with an oblique crack, subject to uniaxial tension. Good agreement with the results using the maximum stress criterion is observed.

## ACKNOWLEDGEMENTS

In presenting this thesis, the author wishes to express his thanks and gratitude to his supervisor, Dr. F. A. Mirza for his advice and guidance during the research and preparation of this thesis.

The financial support of the Natural Sciences and Engineering Research Council of Canada, Grant A1003 and the McMaster University Sherman Scholarship (1980-1982) are gratefully acknowledged.

Finally, a special thanks to Ms. Marlene Fletcher for her time in typing and making this thesis presentable.

## TABLE OF CONTENTS

	<u>Page</u>
CHAPTER 1 INTRODUCTION	1
CHAPTER 2 FORMULATION OF MIXED FINITE ELEMENT AND MIXED TRANSITIONAL FINITE ELEMENTS	6
2.1 Finite Element Formulation Using Hellinger- Reissner Variational Principle	6
2.2 Formulation of Mixed Finite Element in Plane Elasticity	10
2.3 Mixed Transitional Finite Elements in Plane Elasticity	12
CHAPTER 3 NUMERICAL TESTING OF MIXED TRANSITIONAL WITH MIXED AND ISOPARAMETRIC FINITE ELEMENTS	27
3.1 Solution Technique for the Indefinite System of Matrix Equations	27
3.2 Numerical Instability	31
3.3 Orientation Problem with Four-Node Mixed Transitional Finite Element	35
3.4 Convergence of Mixed Transitional Elements and Combination of Mixed, Mixed Transitional and Isoparametric Finite Elements	44
3.5 Example of Plane Square Plate with a Circular Hole	50

	<u>Page</u>
CHAPTER 4 LINEAR ELASTIC FRACTURE MECHANICS (LEFM) BY FINITE ELEMENT METHOD	72
4.1 Linear Elastic Fracture Mechanics (LEFM)	72
4.2 Application of Finite Element Methods in Lin- ear Elastic Fracture Mechanics	77
4.3 Calculation of Mode I Stress Intensity Factor using Direct Derivative Method in Conjunction with Mixed, Mixed Transitional and Isopara- metric Displacement Elements	81
4.4 Numerical Examples	87
4.4.1 Isotropic Rectangular Plates with Symmetric Edge Cracks and a Central Crack	87
4.4.2 Orthotropic Square Plate with a Central Crack	93
CHAPTER 5 CRACK EXTENSION UNDER COMBINED MODES	108
5.1 Finite Element Analysis for Calculation of Stress Intensity Factors $K_I$ and $K_{II}$ under Combined Modes	108
5.1.1 Calculation of $K_I$ and $K_{II}$ using Energy Approach	109
5.1.2 Numerical Examples	118
5.2 Fracture Criteria for Prediction of Direction of Crack Extension	122

	<u>Page</u>
5.2.1 Maximum Stress Criterion	122
5.2.2 Minimum Strain Energy Density Criterion	123
5.2.3 Maximum Energy Release Rate Criterion	124
5.3 Numerical Examples	129
 CHAPTER 6 CONCLUSIONS	 145
 APPENDIX A Finite Element Matrix for the Three-node Triangular Mixed Element with Linear Displacement and Stress Approximations	 150
APPENDIX B Finite Element Matrix for the Four-node Triangular Mixed Transitional Element (Uncondensed)	156
APPENDIX C Finite Element Equations for Condensed Mixed Transitional Finite Elements	160
APPENDIX D Direct Derivative Method of Calculating Energy Release Rate	166
APPENDIX E Program Listings	173
 BIBLIOGRAPHY	 198

## LIST OF FIGURES

FIGURES	TITLES	<u>Page</u>
2.1	Node numbers and degrees of freedom for a three- node triangular mixed finite element.	22
2.2	Definition of area co-ordinates.	22
2.3	Comparison of three-node triangular mixed and eight-node isoparametric displacement finite ele- ments.	23
2.4	Connection of mixed and isoparametric displacement finite elements by mixed transitional finite ele- ments.	24
2.5	Simultaneous application of mixed variational and minimum potential energy principles to a single domain and stresses on the common boundary.	25
2.6	Four-node triangular mixed transitional finite element and its shape functions.	26
3.1	Premultiplication of the master matrix $\underline{S}$ by its own transpose $\underline{S}^T$ .	53
3.2	Combination of a condensed four-node transitional element, a three-node transitional element and an isoparametric element, used to investigate the effect of the magnitude of the modulus of elastici- ty.	54

3.3	Linear elastic cantilevered beam with fully fixed supports subjected to parabolic end shear.	55
3.4	Node numbers and degrees of freedom for a four-node triangular mixed transitional finite element, uncondensed.	56
3.5	Isoceles four-node triangular mixed transitional finite elements with $m_{12} = -m_{13}$ .	56
3.6	Four-node triangular mixed transitional finite element with a right angle between sides 1-2 and 1-3 and with sides 1-2 and 1-3 parallel to the global coordinate axes.	57
3.7	Plane stress square plate with parabolically varying end loads.	57
3.8	Triangular mixed transitional finite elements used for the finite element analysis of the square plate with parabolically varying end loads - Figure 3.7.	58
3.9	Finite element grids for the square plate with parabolically varying end loads.	59
3.10	Strain energy convergence for the square plate with parabolically varying end loads, using three-node mixed transitional elements, condensed four-node mixed transitional elements and uncondensed four-node mixed transitional elements.	60
3.11	Linear elasticity cantilever with boundary trac-	61

	tions and conditions used.	
3.12	Finite element grids for the mixed, condensed mixed transitional and isoparametric displacement type finite element.	62
3.13	Finite element grids for the mixed, uncondensed mixed transitional and isoparametric displacement type finite elements.	63
3.14	Strain energy convergence for the cantilevered beam in Figure 3.11.	64
3.15	Plots of extreme fibre stress along the axis of the cantilever (Figure 3.11) for various shapes of uncondensed four-node triangular mixed transitional finite elements.	65
3.16	Plane square plate with a circular hole in the middle, isotropic and orthotropic.	66
3.17	Finite element grid for the square plate with a circular hole in the middle, Grid I. Isotropic and orthotropic cases.	67
3.18	Finite element grid for the square plate with a circular hole in the middle, Grid II. Isotropic and orthotropic cases.	68
3.19	Comparison of finite element results for the isotropic square plate with a circular hole in the middle with theoretical results for an infinite plate, uncondensed and condensed mixed transi-	69

	tional finite elements.	
3.20	Comparison of finite element results for the orthotropic square plate with a circular hole in the middle with theoretical results for an infinite plate, uncondensed and condensed mixed transitional finite elements.	70
3.21	Finite element grid for the square plate with a circular hole in the middle, Ref. [8].	71
4.1	Three different modes of fractures.	96
4.2	Stress components near the crack tip in Cartesian rectangular coordinates.	97
4.3	Typical contour for evaluation of J-integral.	97
4.4	Accommodation of crack extension $\Delta a$ by advancing nodes on the path $\Gamma_0$ .	98
4.5(a)	Typical finite element mesh with mixed, mixed transitional and isoparametric displacement type finite elements.	99
4.5(b)	Accommodation of crack extension $\Delta a$ by advancing nodes on path $\Gamma_0$ in Figure 4.5(a).	100
4.6	Rectangular plates with cracks used for determining the crack intensity factors $K_I$ .	101
4.7	Finite element mesh used for determining the crack intensity factor $K_I$ , used for both symmetric edge and central cracks.	102

	<u>Page</u>
4.8	Finite element mesh used for determining the crack intensity factor $K_I$ , used for both symmetric edge and central cracks, Ref. [33]. 103
4.9	Normal stress distribution along the edge OA of the rectangular plate with cracks, Figure 4.6. 104
4.10	Fluctuations of normal stress along the edge OA of the rectangular plate with symmetric edge cracks, Figure 4.6(a). 105
4.11	Orthotropic square plate with a central crack used for determining the crack intensity factor $K_I$ . 106
4.12	Finite element mesh used for determining the crack intensity factor $K_I$ for the square plate with a central crack, Figure 4.11. 107
5.1	Crack tip coordinate system 134
5.2(a)	Finite element grid around the crack tip. 134
5.2(b)	Modelling of crack branching by moving the node at the crack tip only. 135
5.2(c)	Modelling of crack branching by introducing two extra elements. 135
5.3	Deep cantilevered beam subjected to end shear used for determining the crack intensity factor $K_I$ and $K_{II}$ . 136
5.4	Finite element mesh used for determining the crack intensity factors $K_I$ and $K_{II}$ for the deep cantilevered beam subjected to end shear. 137

5.5	Deep cantilevered beam subjected to both tension and end shear used for determining the crack intensity factors $K_I$ and $K_{II}$ .	138
5.6	Plot of energy release rate $G$ against angle of crack extension $\theta$ for the deep cantilevered beam subjected to both tension and end shear, Figure 5.5.	139
5.7	Stress components near the crack tip in polar coordinates.	140
5.8	Problem of a branched crack.	140
5.9	Square plate with an oblique crack subjected to tensile loading used for determining the crack intensity factors $K_I$ and $K_{II}$ and the angle of crack branching $\theta$ .	141
5.10(a)	Finite element mesh used for determining the crack intensity factors $K_I$ and $K_{II}$ and the angle of crack branching $\theta$ for the square plate with an oblique crack subject to uniaxial tension $\tau_0$ .	142
5.10(b)	Details of the finite element mesh around the crack tips for the square plate with an oblique crack subjected to uniaxial tension.	143
5.11	Fracture angle $\theta$ against crack angle $\beta$ for a square plate with an oblique crack subjected to uniaxial tension.	144

## LIST OF TABLES

TABLES	TITLES	<u>Page</u>
3.1	Eigenvalue analysis of a combination of a four-node transitional element, a three-node transitional element and an isoparametric element.	33
3.2	Results for a cantilever analyzed using values of the modulus of elasticity E from 3.0 to $3.0 \times 10^{-6}$ .	35
3.3	Strain energies and percentage errors for the square plate with parabolically varying end loads, Figure 3.7.	45
3.4	Displacements, stresses, and strain energies for the square plate with parabolically varying end loads, Figure 3.7.	47
3.5	Results for the cantilevered beam with three supports, Figure 3.11.	48
3.6	Errors in strain energy and tip displacement for the cantilevered beam with three supports, Figure 3.11.	49
3.7	Comparison of computer storage requirements and stresses at the edge of the hole in a square plate under tension, Figure 3.16. Isotropic and Orthotropic.	52

4.1	Stress intensity factors from the finite element analysis of the rectangular plate with symmetric edge cracks, Figure 4.6(a). (Mixed, Mixed transitional and eight-node isoparametric finite elements.)	90
4.2	Stress intensity factor from the finite element analysis of the rectangular plate with a central crack, Figure 4.6(b). (Mixed, Mixed transitional and eight-node isoparametric finite elements.)	90
4.3	Comparison of stress intensity factors from Reference [33] and the present analysis.	92
4.4	Material properties used for determining the stress intensity factor $K_I$ for a centrally cracked orthotropic square plate.	95
4.5	Comparison of $K_I/K_\infty$ from the present finite element analysis and that from Reference [3].	95
5.1	Results for $K_I$ and $K_{II}$ for a deep cantilevered beam subjected to end shear, Figure 5.3.	119
5.2	Results for $K_I$ and $K_{II}$ for a deep cantilevered beam subjected to both end shear and tension, Figure 5.5.	121
5.3	Energy release rates for different angles of crack extension for the deep cantilevered beam subjected to end shear and tension, Figure 5.5.	121

		<u>Page</u>
5.4	Values of $C_1^*$ and $C_2^*$ (Wang [54]).	127
5.5	Values of $F_{11}(\gamma)$ , $F_{12}(\gamma)$ , $F_{21}(\gamma)$ and $F_{22}(\gamma)$ .	129
5.6	Predicted angles of crack extension for the deep cantilevered beam with end shear and tension, Figure 5.5.	130
5.7	Stress intensity factors for the square plate with an oblique crack subjected to uniaxial tension, Figure 5.9.	131
5.8	Predicted angles of crack extension for the square plate with an oblique crack subjected to uniaxial tension, Figure 5.9.	133

## CHAPTER 1

### INTRODUCTION, PURPOSE AND SCOPE

#### 1.1 Introduction

The finite element method is currently the most widely used numerical method for analyzing boundary value problems for which no closed form solutions exist or are extremely difficult to obtain.

For decades the use of either displacement or equilibrium finite element method based on the principles of minimum potential energy and minimum complimentary energy, respectively, have dominated analyses of problems in continuum mechanics. The mixed finite element method in plane elasticity, based on the Hellinger-Reissner variational principle has been investigated by Oden [4], Oden and Reddy [5], Oden and Lee [6], Mirza and Olson [7] and Mirza [8]. Mirza [8] established the energy convergence in plane elasticity problems. A three-node triangular mixed finite element with linear stress and displacement approximations was applied to plane elasticity with improvements in accuracy and the energy convergence rate over the constant stress triangular displacement finite element which uses the same linear displacement approximations. The computer storage required in the mixed finite element method is, however, much larger than the corresponding displacement finite element method, in spite of the aforementioned improvements.

The mixed finite element method in conjunction with the energy release rate concepts has also been applied to stress singular problems with cracks by Mirza and Olson [33]. It was shown to possess an excellent potential for analysis of stress singular problems in terms of improved convergence in energy and accuracy in stresses. However, again, very large computer storage is required in such analyses.

## 1.2 Purpose and Scope

In order to reduce the amount of computer storage inherent in the mixed finite element method, transitional mixed finite elements are developed in this thesis to enable the simultaneous use of the three-node triangular mixed finite elements [7] and the eight-node isoparametric displacement finite elements in a single finite element domain. Such simultaneous use of the mixed and displacement finite elements is then applied to the analyses of mixed mode stress singular crack problems in linear elastic fracture mechanics with the mixed finite elements used in the region immediately surrounding the crack tip with a stress singularity and the isoparametric displacement finite element in the region where stresses are more regular. Stress intensity factors  $K_I$  and  $K_{II}$  are calculated and the angles of crack branching in mixed mode fracture problems are predicted using the energy approach.

The Hellinger-Reissner variational principle in plane elasticity is introduced in Chapter 2 where the formulations of mixed finite elements are discussed. Four-node triangular mixed transitional finite elements (uncondensed and condensed versions) are formulated in detail.

The condensed version also necessitates the use of a three-node triangular transitional mixed element with only stress degrees of freedom at two of its nodes to connect the three-node triangular mixed and the eight-node isoparametric finite elements.

Numerical testings of the simultaneous use of the three-node triangular mixed and eight-node isoparametric displacement finite elements, connected by the mixed transitional elements are given in Chapter 3. A solution technique for matrix equations, involving transformation of indefinite matrices to positive definite matrices, is also presented in Chapter 3. Numerical instability of the mixed finite element method and orientation problems of the four-node mixed transitional finite elements are investigated. The rates of energy convergence of the mixed transitional elements are studied through analysis of a plane stress, square plate with parabolically varying end loads. When the mixed, mixed transitional and the isoparametric displacement finite elements are used simultaneously, the energy convergence rate is investigated by analyzing a plane stress cantilever subjected to a parabolically varying end shear. The plane strain problem of a square plate with a circular hole in the middle is also analyzed for stress concentrations.

Chapters 4 and 5 are devoted to applications of the simultaneous use of the three types of elements mentioned above to problems in linear elastic fracture mechanics. A brief account of linear elastic fracture mechanics is presented in Chapter 4. Applications of the finite element method to fracture problems are also given and, in particular, the direct derivative energy approach [7, 38] is described in detail and

applied to calculate the stress intensity factor  $K_I$  for mode I (opening mode) cracking. Three problems are analyzed and the finite element solutions are compared with the results available in the literature. The problems include an isotropic plane stress rectangular plate, first with symmetric edge cracks, then a central crack and an orthotropic plane stress square plate with a central crack.

Mixed mode fracture problems are considered in Chapter 5. The energy approach of analyzing such problems is discussed and the use of Ishikawa's scheme [39, 40] to determine the stress intensity factors  $K_I$  (mode I) and  $K_{II}$  (mode II, in plane sliding) using only a single virtual crack extension is presented. This is then used to analyze deep cantilevered beams with an edge crack subject to loads which caused mixed mode fracture. Crack branching theory due to Hellen et al., [41] is also presented and compared with the energy approach utilizing Ishikawa's scheme. The calculation and prediction of the angle of crack branching is also attempted. Various mixed mode fracture criteria are examined and, in particular, the criterion of maximum energy release rate is adopted. Finally the criterion of maximum energy release rate, using results by Wang [54] together with the stress intensity factors calculated using Ishikawa's scheme, is used to calculate the angles of crack branching for a plane stress, square plate under tension with an oblique crack in the middle. The results are compared with those obtained by using the maximum stress criterion by Erdogan and Sih [48] and the criterion of maximum energy release rate via the approach due to Hellen et al., [41].

Lastly, some general conclusions, limitations and suggestions are presented in Chapter 6.

## CHAPTER 2

### FORMULATION OF MIXED FINITE ELEMENT AND MIXED TRANSITIONAL FINITE ELEMENTS

In linear elasticity, finite elements can be formulated using the variational principles [1]. A finite element formulated using the Hellinger-Reissner variational principle [2] based on assumed displacement and stress fields is called the mixed finite element. A detailed derivation of the mixed transitional finite element using the Hellinger-Reissner variational principle is presented in this chapter. The mixed triangular, transitional elements enable the use of the three-node mixed triangular elements in conjunction with the eight-node isoparametric displacement finite elements [9]. A brief account of triangular mixed and eight-node isoparametric elements is also included.

#### 2.1 Finite Element Formulation Using Hellinger-Reissner Variational Principle

The differential equations to be satisfied in linear elasticity include the equilibrium equations, the constitutive relationships and the compatibility equations which are also subjected to some boundary conditions [3]. Reissner [2] developed a functional which, for plane elasticity, takes the following form:

$$I_R = \iiint_V [\tau_{11}\epsilon_{11} + \tau_{22}\epsilon_{22} + \tau_{12}\gamma_{12} - W]dV - \iiint_V [\bar{F}_1 u_1 + \bar{F}_2 u_2]dV - \iint_{S_1} [\bar{P}_1 u_1 + \bar{P}_2 u_2]dS. \quad (2.1.1)$$

Where  $\tau_{11}, \tau_{22}, \tau_{12}$  are the stress components;  
 $\epsilon_{11}, \epsilon_{22}, \gamma_{12}$  are the strain components;  
 $W$  is the complimentary energy density;  
 $\bar{F}_1, \bar{F}_2$  are the prescribed body forces in the  $x_1$  and  $x_2$  directions;  
 $\bar{P}_1, \bar{P}_2$  are the prescribed surface tractions in the  $x_1$  and  $x_2$  directions;  
 $u_1, u_2$  are the displacements in the  $x_1$  and  $x_2$  directions;  
 $S_1$  is that part of the surface where surface tractions are prescribed; and  
 $V$  is the volume.

The variational theorem can be stated in the following manner

[2]:

"Among all states of stress and displacement which satisfy the boundary conditions of prescribed surface displacement, the actually occurring state of stress and displacement is determined by the variational equation  $\delta I = 0$ ."

$$\delta \left\{ \iiint_V [\tau_{11}\epsilon_{11} + \tau_{22}\epsilon_{22} + \tau_{12}\gamma_{12} - W]dV - \iiint_V [\bar{F}_1 u_1 + \bar{F}_2 u_2]dV \right.$$

$$\left( -\iint_{S_1} [\bar{P}_1 u_1 + \bar{P}_2 u_2] dS \right) = 0 \quad (2.1.2)$$

Furthermore, if the kinematic strain-displacement equations of elasticity

$$\epsilon_{11} = \frac{\partial u_1}{\partial x_1}, \quad \epsilon_{22} = \frac{\partial u_2}{\partial x_2}, \quad \gamma_{12} = \frac{\partial u_1}{\partial x_2} + \frac{\partial u_2}{\partial x_1} \quad (2.1.3)$$

are employed, thus assuring kinematic compatibility, the Euler equations at stationarity of the variational principle are the equilibrium equations, the constitutive relations and the boundary conditions. In fact,

$$\begin{aligned} \delta I_R = & \iiint_V \left[ \left( \frac{\partial u_1}{\partial x_1} - \frac{\partial W}{\partial \tau_{11}} \right) \delta \tau_{11} + \left( \frac{\partial u_2}{\partial x_2} - \frac{\partial W}{\partial \tau_{22}} \right) \delta \tau_{22} + \dots \right. \\ & \left. - \left( \frac{\partial \tau_{11}}{\partial x_1} + \frac{\partial \tau_{12}}{\partial x_2} + \bar{F}_1 \right) \delta u_1 + \dots \right] dV \\ & + \iint_{S_1} [(P_1 - \bar{P}_1) \delta u_1 + (P_2 - \bar{P}_2) \delta u_2] dS = 0. \end{aligned} \quad (2.1.4)$$

Since  $\delta \tau_{11}$ ,  $\delta \tau_{22}$ ,  $\delta \tau_{12}$ ,  $\delta u_1$  and  $\delta u_2$  are arbitrary variations, the aforementioned system of equations is obtained in the following manner:

$$\tau_{ij,j} + \bar{F}_i = 0 \quad i,j = 1, 2 \quad (2.1.5)$$

$$\tau_{ij} = E_{ijkl} \epsilon_{kl} \quad i,j = 1, 2 \quad (2.1.6)$$

$$P_i = \bar{P}_i \quad \text{on } S_1 \quad i = 1, 2 \quad (2.1.7)$$

Oden [4], Oden and Reddy [5], Oden and Lee [6] and Mirza and Olson [7] studied the convergence and performance of the mixed finite element method in plane elasticity. It was reported in reference [7] that when the approximations for stresses and displacements are chosen independently, the following completeness criterion has to be satisfied:

"The strains from the stress approximations should possess at least all the strain modes that are present in the strains derived from the displacement approximations, with rigid body modes precluded."

Violation of this criterion will lead to "mechanisms", i.e. non-stressing strain modes. This means that the strain energy of the system will not be definite and the matrix equations for an application will be singular. Such "mechanisms" cannot be removed by simply removing the rigid body modes.

The convergence studies carried out in reference [7] also indicated that, provided both the stresses and displacements are made continuous across interelement boundaries, the error in strain energy is governed by the mean square error in the stress approximations. This means that if the error in stresses is  $O(\ell_e^2)$ , where  $\ell_e$  is the largest

diameter within an element, the error in strain energy is expected to be  $O(\ell_e^4)$  which is  $O(N^{-4})$  for a uniform grid, where  $N$  is the number of elements along a typical length of a finite element grid.

## 2.2 Formulation of Mixed Finite Element in Plane Elasticity

In the formulation of the element matrices, it is convenient to write the functional in Equation (2.1.1) using matrix notations. Thus

$$I_R(\underline{\Lambda}) = \int_V [\underline{\tau}^T \underline{T} \underline{u} - \frac{1}{2} \underline{\tau}^T \underline{C} \underline{\tau}] dV - \int_V \underline{\bar{F}}^T \underline{u} dV - \int_{S_1} \underline{\bar{P}}^T \underline{u} dS \quad (2.2.1)$$

where, for plane elasticity,

$$\underline{\tau} = \langle \tau_{11} \ \tau_{22} \ \tau_{12} \rangle^T \quad (2.2.2)$$

$$\underline{u} = \langle u_1 \ u_2 \rangle^T \quad (2.2.3)$$

$$\underline{\Lambda} = \langle \underline{\tau}^T \ \underline{u}^T \rangle^T \quad (2.2.4)$$

$$\underline{\bar{F}} = \langle \bar{F}_1 \ \bar{F}_2 \rangle^T \quad (2.2.5)$$

$$\underline{\bar{P}} = \langle \bar{P}_1 \ \bar{P}_2 \rangle^T \quad (2.2.6)$$

$$\underline{T} = \begin{bmatrix} \frac{\partial}{\partial x_1} & 0 \\ 0 & \frac{\partial}{\partial x_2} \\ \frac{\partial}{\partial x_2} & \frac{\partial}{\partial x_1} \end{bmatrix} \quad \underline{C} = \begin{bmatrix} \alpha & -\beta & 0 \\ -\beta & \gamma & 0 \\ 0 & 0 & \delta \end{bmatrix} \quad (2.2.7)$$

The matrix C above is the compliance matrix. It is shown here in a symbolic form. For the isotropic plane stress case,  $\alpha = \gamma = 1/E$ ,  $\beta = \nu/E$  and  $\delta = E/2(1 + \nu)$ , where  $E$  is the modulus of elasticity and  $\nu$  is Poisson's ratio.

The element matrix for plane stress linear elasticity for linear displacements and linear stresses is given in reference [7]. As shown in Figure (2.1), it is a three node triangular element with  $u_1, u_2, \tau_{11}, \tau_{22}$  and  $\tau_{12}$  as nodal degrees of freedom. Using area coordinates, the linear approximations for displacements and stresses can be written as

$$u_i = \langle L_1 \ L_2 \ L_3 \rangle \begin{Bmatrix} 1 \\ u_i \\ 2 \\ u_i \\ 3 \\ u_i \end{Bmatrix} \quad ; \ i = 1, 2 \quad (2.2.8)$$

$$\tau_{ij} = \langle L_1 \ L_2 \ L_3 \rangle \begin{Bmatrix} 1 \\ \tau_{ij} \\ 2 \\ \tau_{ij} \\ 3 \\ \tau_{ij} \end{Bmatrix} \quad ; \ i = j = 1, 2 \quad (2.2.9)$$

where  $L_1$ ,  $L_2$ , and  $L_3$  are the area coordinates as defined in Figure (2.2).

Derivation of the element matrix for this element is similar to the derivation of the element matrix for the mixed transitional element to be presented in the next section. All relevant matrices for this element are given in Appendix A.

Applications of the mixed element above have been demonstrated by Mirza and Olson [7]. Improved accuracy of the three-node triangular mixed element over the constant stress triangular displacement element (C.S.T.), which uses the same linear displacement approximations, was observed. Also, the predicted strain energy convergence rate of the mixed element has been confirmed through applications on various examples in reference [8].

### 2.3 Mixed Transitional Finite Elements in Plane Elasticity

The mixed finite element method has been applied to stress singular problems in plane elasticity by Mirza and Olson [33]. It was concluded that the strain energy convergence rate is at least  $O(N^{-1})$  and the numerical results from the mixed finite element analysis of a plane stress square plate with symmetric edge cracks, using the three-node triangular mixed elements, yielded a strain energy convergence rate of nearly  $O(N^{-2})$ . Moreover, it was observed that in order to achieve the same accuracy as obtained with displacement elements, much fewer total degrees of freedom were needed in spite of more degrees of freedom per

node needed for the mixed finite elements. Therefore, the mixed finite element method seems to have an excellent potential for numerical analysis of stress singular problems.

In spite of the improved accuracy and convergence, the use of mixed elements alone, when applied to stress singular problems, requires a much larger amount of computer storage because of the larger half-band widths due to increased number of degrees of freedom per node. It is therefore proposed to use the three-node triangular mixed elements in conjunction with the conventional displacement elements, with the mixed elements used exclusively over part of the region where the stress gradients are expected to be very large. Since the energy convergence rate of the three-node triangular mixed elements is  $O(N^{-4})$ , it is desirable to use a displacement type element which exhibits the same energy convergence rate. The eight-node isoparametric element is considered here. Formulation of the eight-node isoparametric element can be found in most text books on finite element method, e.g. Zienkiewicz [9].

The displacement variation along the sides of the eight-node isoparametric element is quadratic whereas that along the sides of the mixed element is linear. Moreover, the mixed element has nodal degrees of freedom in both displacements and stresses whereas the eight-node isoparametric element has only displacements as nodal degrees of freedom, Figure (2.3). Therefore, one or more types of transitional elements have to be developed to connect the above-mentioned two types of elements.

There are two possible ways of connecting the three-node triangular mixed and eight-node isoparametric elements. These are illustrated in Figure (2.4). Since the displacement variation is quadratic along the sides of the eight-node isoparametric element, a triangular transitional element with three corner nodes and one mid side node along one of its sides is used. Hence displacement compatibility along the interelement boundary would be guaranteed through a proper choice of displacement polynomials. As shown in Figure (2.4a), one option is to use both stress and displacement degrees of freedom at all nodes of the transitional element. Since the isoparametric element has only displacement degrees of freedom, double nodes (which have the same coordinates) would have to be used along the interelement boundary between the transitional and the isoparametric elements. Thus, equating only the displacements at the double nodes would ensure displacement continuity provided that the variation is quadratic.

The second option (Figure (2.4b)) is to condense out the stress degrees of freedom at the three nodes of the transitional element which connect it to the isoparametric element. In this case, however, another type of transitional element, which is formed by condensing out the stress degrees of freedom at only one node of the three-node triangular mixed element, also has to be used. Assemblage of the various elements follows the usual routines of finite element analysis. Both types of transitional elements will be used in investigating the energy convergence rate in the next chapter. It should be pointed out here that both the uncondensed and condensed, transitional elements are also mixed formulations.

The use of the mixed finite elements in conjunction with the isoparametric displacement finite elements involves the use of Hellinger-Reissner mixed variational principle over the region where mixed elements are used and the principle of minimum potential energy in the region where the isoparametric displacement elements are employed, Figure (2.5). In the region where the mixed finite elements via Hellinger-Reissner principle are used, both stresses and displacements are required to be continuous across the interelement boundaries for faster convergence [8]. Whereas in the region where the displacement finite elements via the principle of minimum potential energy are employed, only the displacements are required to be continuous across the interelement boundaries. These continuity requirements are satisfied within the two regions, respectively. The question remains as to what continuity requirements are needed along the common boundary of the two regions where the mixed variational principle is used on one side and the principle of minimum potential energy on the other side. For quadratic variation along the common boundary, displacement continuity is ensured by equating the displacement degrees of freedom at the common nodes. However, the stress continuity along the common boundary is not maintained. Stresses calculated on one side of the common boundary can be considered as the stress boundary conditions for the region on the other side. Stress continuity can then be attempted by introducing the following boundary integrals in the formulation of the finite elements adjacent to the common boundary:

$$\int_{S_c} (\tau_{nn}^{MT} - \tau_{nn}^I) \tilde{u}_n dS \quad (2.3.1)$$

$$\int_{S_c} (\tau_{ns}^{MT} - \tau_{ns}^I) \tilde{u}_s dS \quad (2.3.2)$$

Where  $n, s$  are the outward normal and tangential directions at the common boundary

$\tau_{nn}^{MT}, \tau_{ns}^{MT}$  are the normal and tangential stresses calculated for the mixed element edge;

$\tau_{nn}^I, \tau_{ns}^I$  are the normal and tangential stresses calculated for the isoparametric element edge;

$\tilde{u}_n, \tilde{u}_s$  are the normal and tangential displacements;

$S_c$  is the element edge length along the common boundary.

These integrals imply continuity only in a weighted integral sense and not pointwise. It is hoped that at extremum the error, due to lack of stress continuity required by the mixed and mixed transitional elements and not required by the displacement isoparametric finite elements, will be minimum.

The incorporation of boundary integrals in expressions (2.3.1) and (2.3.2) will, however, lead to very complicated element formulations and perhaps to no avail. Numerical results of the finite element analyses, using both triangular mixed and isoparametric displacement

elements, reveal that reasonably accurate results can be obtained without incorporating such integrals. It is thus expected that the boundary integrals for the mixed transitional and isoparametric elements lying alongside the common boundary must have a cancelling effect and the stress values along this common boundary adjust themselves even if no such boundary integrals are employed. Therefore, in subsequent element formulations, the boundary integrals in expressions (2.3.1) and (2.3.2) will be deleted.

The four-node triangular, transitional element and its shape functions are shown in Figure (2.6). The following approximations are used for both stresses and displacements.

$$u_i = \langle N_1 \ N_2 \ N_3 \ N_4 \rangle \begin{Bmatrix} 1 \\ u_i \\ 2 \\ u_i \\ 3 \\ u_i \\ 4 \\ u_i \end{Bmatrix} ; i = 1, 2 \quad (2.3.3)$$

$$\tau_{ij} = \langle N_1 \ N_2 \ N_3 \ N_4 \rangle \begin{Bmatrix} 1 \\ \tau_{ij} \\ 2 \\ \tau_{ij} \\ 3 \\ \tau_{ij} \\ 4 \\ \tau_{ij} \end{Bmatrix} ; i = j = 1, 2 \quad (2.3.4)$$

Where



Substitution of (2.3.9) and (2.3.10) into (2.2.1) yields

$$I_R(\tilde{\Lambda}) = \int_V [\tilde{\tau}^T \bar{N}^T \underline{T} \bar{N} \tilde{u} - \frac{1}{2} \tilde{\tau}^T \bar{N} \underline{C} \bar{N} \tilde{\tau}] dV - \int_V \bar{F}^T \bar{N} \tilde{u} dV - \int_{S_1} \bar{P}^T \bar{N} \tilde{u} dS \quad (2.3.15)$$

where  $\tilde{\Lambda} = \langle \tilde{u} \quad \tilde{\tau} \rangle^T$ .

Now for stationarity of the mixed variational principle

$$\frac{\partial I_R(\tilde{\Lambda})}{\partial \tilde{u}} = 0 \quad \text{and} \quad \frac{\partial I_R(\tilde{\Lambda})}{\partial \tilde{\tau}} = 0. \quad (2.3.17)$$

These then lead to the following element matrix equation,

$$\begin{bmatrix} \underline{0} & \left\{ \int_V \bar{N}^T \underline{T} \bar{N} dV \right\}^T \\ \int_V \bar{N}^T \underline{T} \bar{N} dV & - \int_V \bar{N}^T \underline{C} \bar{N} dV \end{bmatrix} \begin{Bmatrix} \tilde{u} \\ \tilde{\tau} \end{Bmatrix} = \begin{Bmatrix} \left\{ \int_V \bar{F}^T \bar{N} dV \right\}^T \\ \underline{0} \end{Bmatrix} + \begin{Bmatrix} \left\{ \int_{S_1} \bar{P}^T \bar{N} dS \right\}^T \\ \underline{0} \end{Bmatrix} \quad (2.3.18)$$

which can be rewritten as

$$\begin{bmatrix} \underline{0} & \underline{0} & \underline{a}^T & \underline{0} & \underline{b}^T \\ \underline{0} & \underline{0} & 0 & \underline{b}^T & \underline{a}^T \\ \underline{a} & 0 & \underline{\alpha c} & -\underline{\beta c} & \underline{0} \\ 0 & \underline{b} & -\underline{\beta c} & \underline{\gamma c} & \underline{0} \\ \underline{b} & \underline{a} & \underline{0} & \underline{0} & \underline{\delta c} \end{bmatrix} \begin{Bmatrix} \underline{u} \\ \underline{v} \end{Bmatrix} = \begin{Bmatrix} \underline{d} \\ \underline{e} \\ \underline{0} \end{Bmatrix} + \text{Consistent Load Vector} \quad (2.3.19)$$

$$\text{Where } a_{ij} = \int_V N_i N_{j,x_1} dV \quad i, j = 1, 2, 3, 4 \quad (2.3.20)$$

$$b_{ij} = \int_V N_i N_{j,x_2} dV \quad i, j = 1, 2, 3, 4 \quad (2.3.21)$$

$$c_{ij} = - \int_V N_i N_j dV \quad i, j = 1, 2, 3, 4 \quad (2.3.22)$$

$$d_i = \int_V \bar{F}_1 N_i dV \quad i = 1, 2, 3, 4 \quad (2.3.23)$$

$$e_i = \int_V \bar{F}_2 N_i dV \quad i = 1, 2, 3, 4 \quad (2.3.24)$$

and  $\alpha$ ,  $\beta$ ,  $\gamma$  and  $\delta$  are elements of the compliance matrix as defined previously. The element matrix is symmetric but in general indefinite. The submatrices and the element matrix are listed in Appendix B.

The element matrix for the four-node transitional element with stress degrees of freedom at only one of its nodes is derived by condensing out  $\tau_{11}^2, \tau_{11}^3, \tau_{11}^4, \tau_{22}^2, \tau_{22}^3, \tau_{22}^4, \tau_{12}^2, \tau_{12}^3$  and  $\tau_{12}^4$ . The resulting element matrix is given in Appendix C along with the element matrix for the transitional element obtained by condensing out

the stress degrees of freedom at one node only (node 3) of the three-node triangular mixed element.

The linear variation in displacements and stresses along two edges and quadratic variation along the third edge of the four-node mixed transitional element suggest that the chosen polynomial may lack spatial isotropy. As such, some orientation problems with the transitional element are anticipated. It should also be pointed out that because of the mixed variational formulation of the element, there are doubts about the proper representation of strain modes derived from the assumed displacement fields and the dependence of the stress modes possessed by the independently assumed stress fields on the strain modes through the constitutive equations. A numerical investigation into this problem is presented in the next chapter.

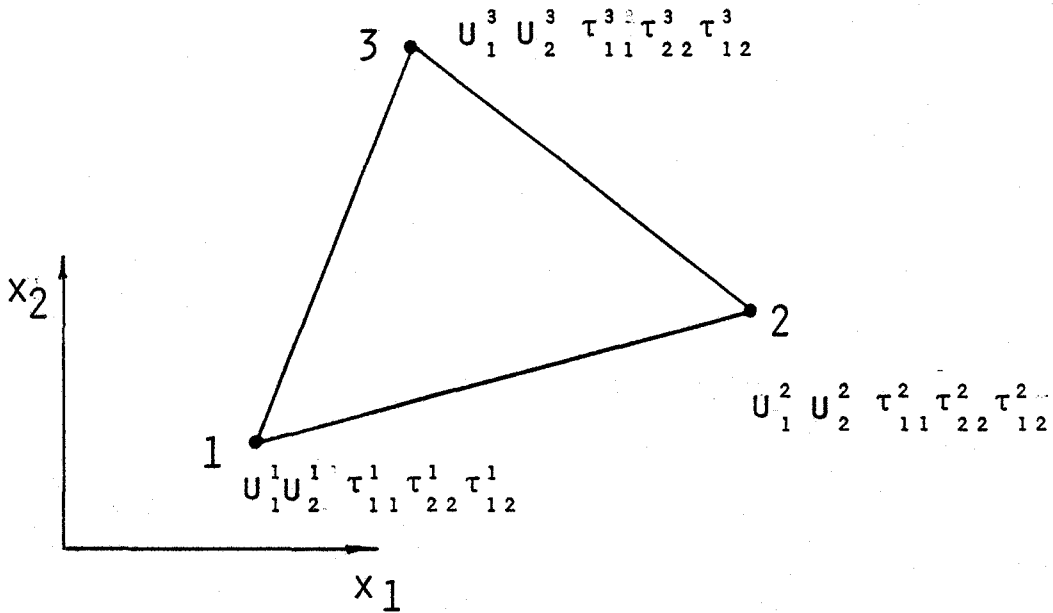


FIG. 2.1: NODE NUMBERS AND DEGREES OF FREEDOM FOR A THREE-NODE TRIANGULAR MIXED FINITE ELEMENT.

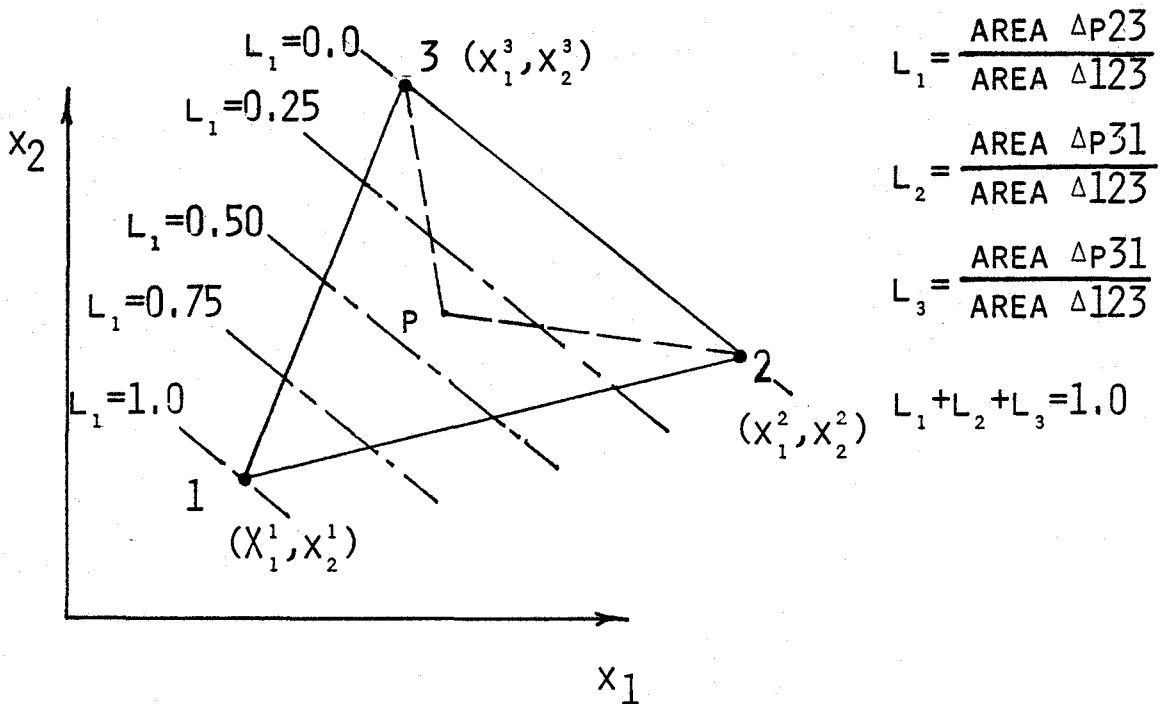
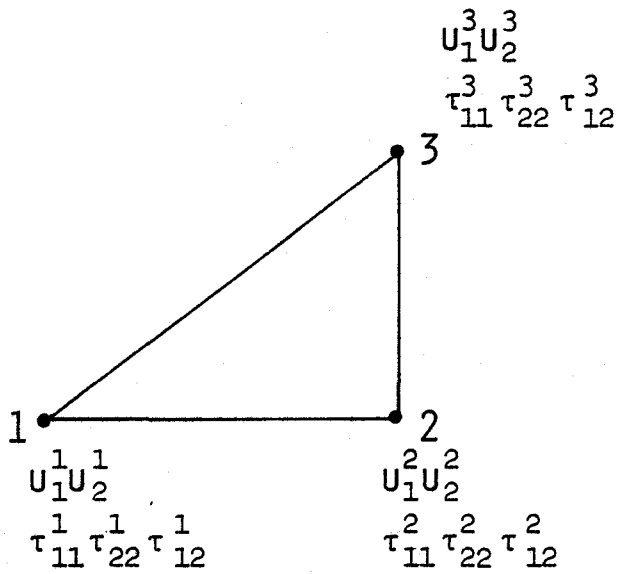
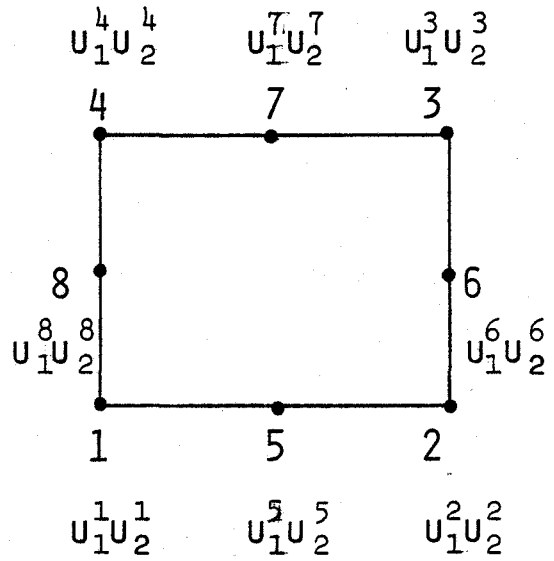


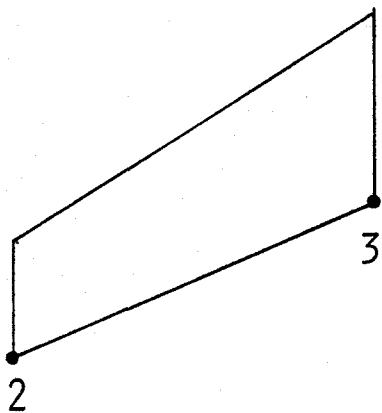
FIG. 2.2: DEFINITION OF AREA COORDINATES.



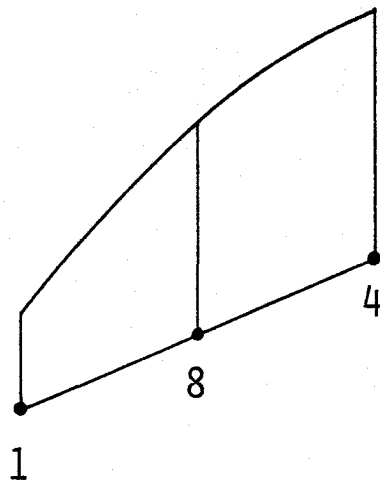
a) THREE-NODE TRIANGULAR MIXED FINITE ELEMENT.



b) EIGHT-NODE ISOPARAMETRIC DISPLACEMENT FINITE ELEMENT.

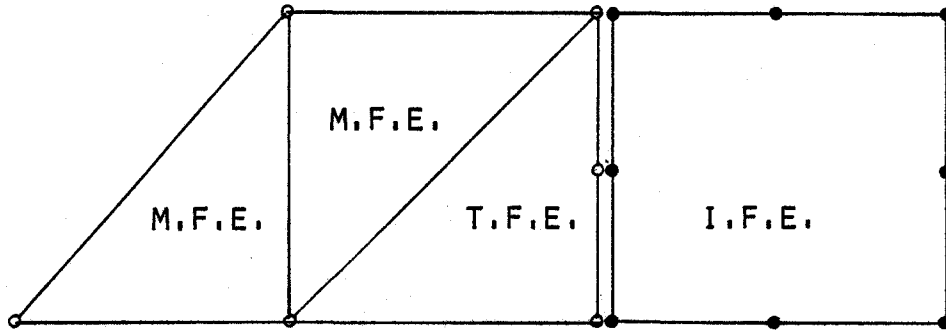


c) LINEAR VARIATION OF DISPLACEMENT ALONG EDGE 2-3 OF THE MIXED FINITE ELEMENT.

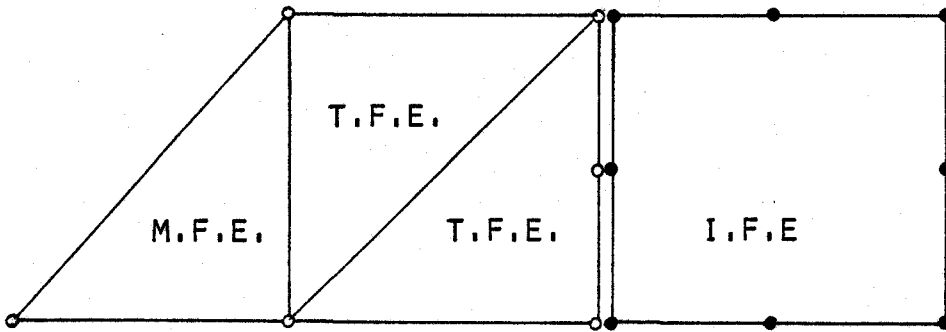


d) QUADRATIC VARIATION OF DISPLACEMENT ALONG EDGE 1-8-4 OF THE ISOPARAMETRIC DISPLACEMENT FINITE ELEMENT.

FIG. 2.3: COMPARISON OF THREE-NODE TRIANGULAR MIXED AND EIGHT-NODE ISOPARAMETRIC DISPLACEMENT FINITE ELEMENTS.



a) SCHEME FOR UNCONDENSED TRANSITIONAL FINITE ELEMENTS.



b) SCHEME FOR CONDENSED TRANSITIONAL FINITE ELEMENTS.

- NODES WITH STRESS AND DISPLACEMENT DEGREES OF FREEDOM.
- NODES WITH DISPLACEMENT DEGREES OF FREEDOM.

M.F.E. MIXED FINITE ELEMENT.  
T.F.E. TRANSITIONAL FINITE ELEMENT.  
I.F.E. ISOPARAMETRIC FINITE ELEMENT.

FIG. 2.4: CONNECTION OF MIXED AND ISOPARAMETRIC DISPLACEMENT FINITE ELEMENTS BY MIXED TRANSITIONAL FINITE ELEMENTS.

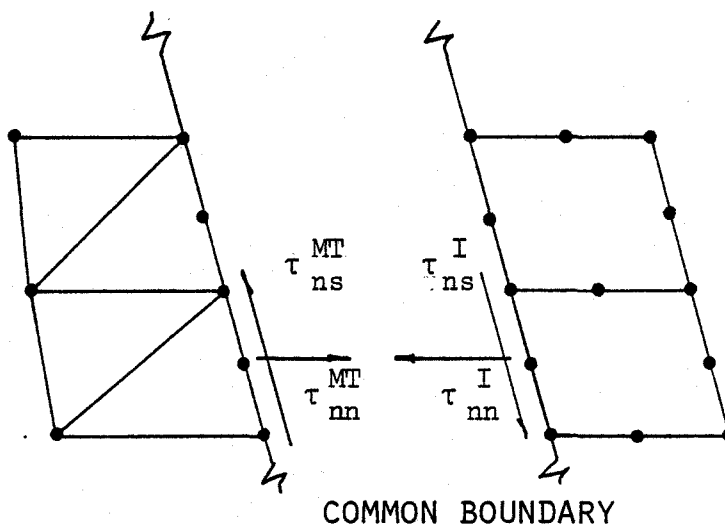
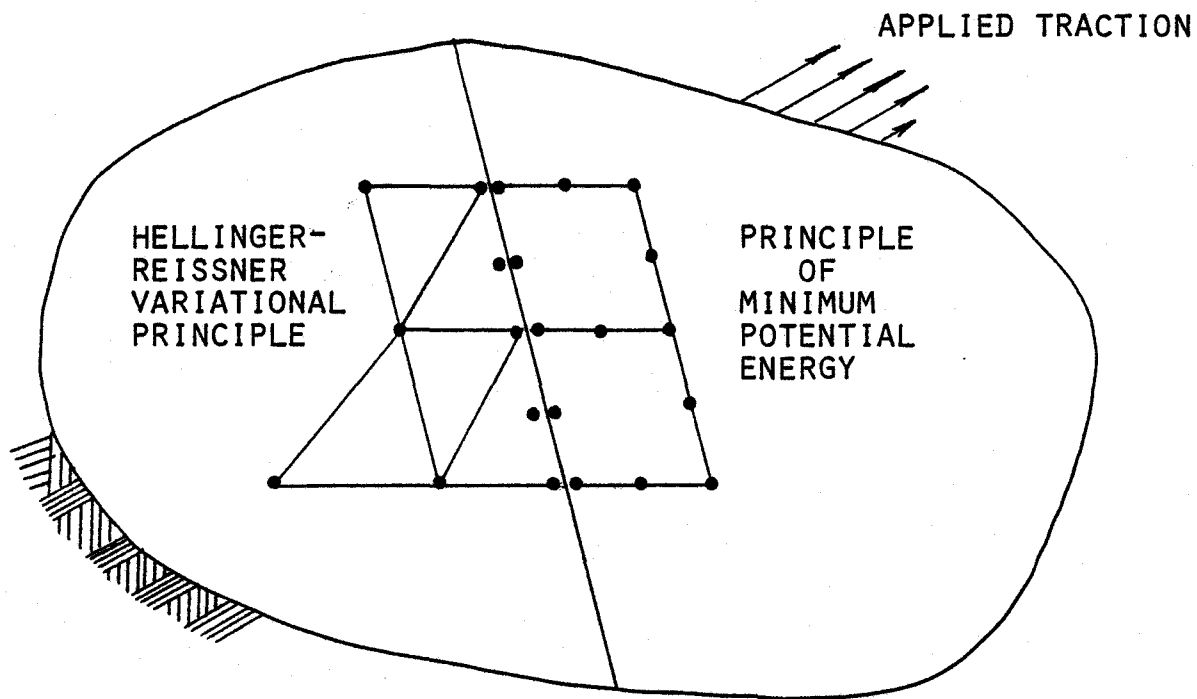


FIG. 2,5: SIMULTANEOUS APPLICATION OF MIXED VARIATIONAL AND MINIMUM POTENTIAL ENERGY PRINCIPLES TO A SINGLE DOMAIN AND STRESSES ON THE COMMON BOUNDARY.

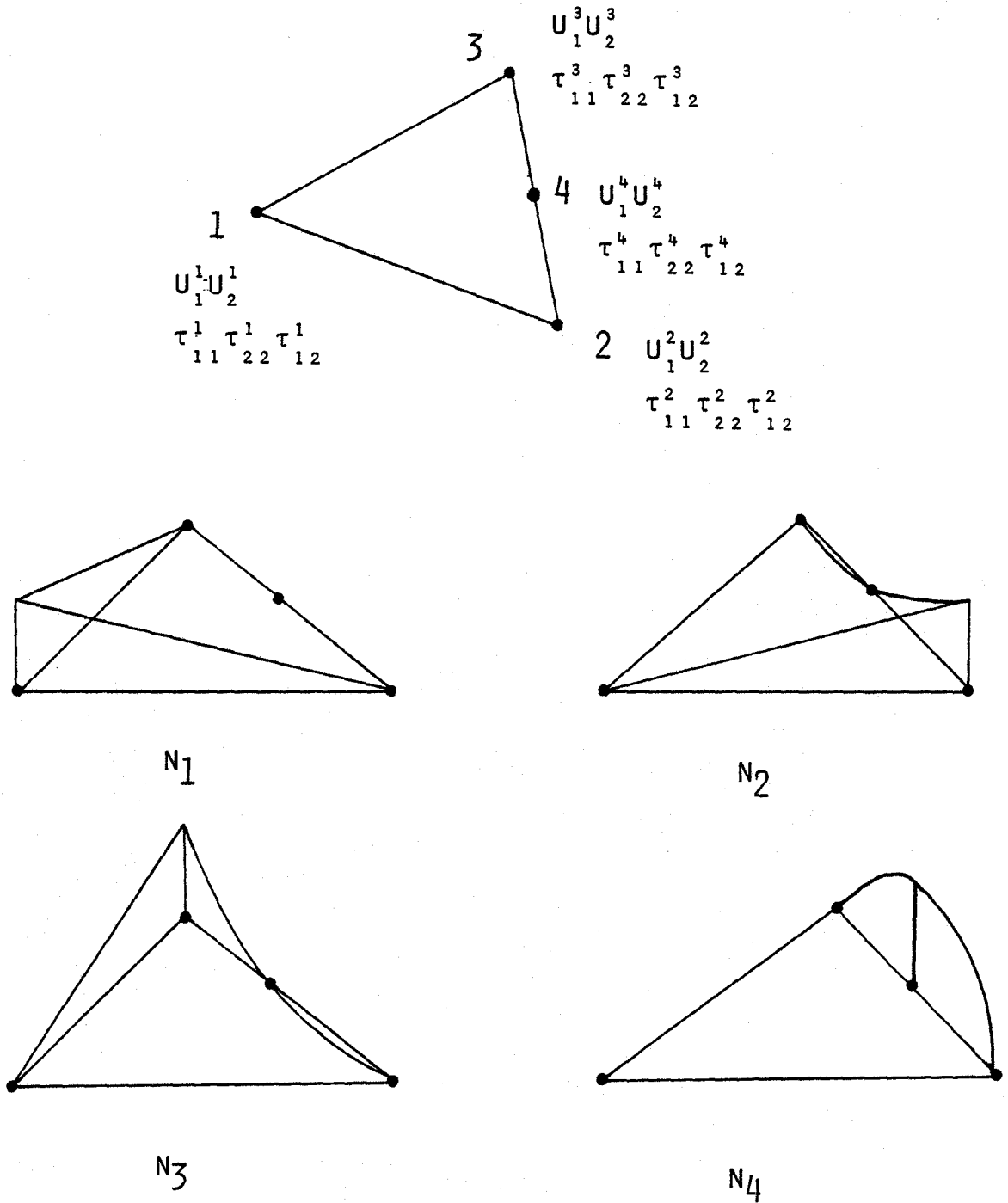


FIG. 2.6: FOUR-NODE TRIANGULAR MIXED TRANSITIONAL FINITE ELEMENT AND ITS SHAPE FUNCTIONS.

CHAPTER 3

NUMERICAL TESTING OF MIXED TRANSITIONAL WITH MIXED AND  
ISOPARAMETRIC FINITE ELEMENTS

The use of triangular mixed finite elements in conjunction with eight-node isoparametric displacement finite elements has been proposed in the previous chapter. The mixed transitional finite elements, which connect the two types of elements above, have been formulated. Results of numerical tests carried out for investigating performance of the proposed three or four element combination schemes are presented in this chapter. After presenting the solution technique adopted, numerical instability and orientation problems of the transitional elements are studied through eigenvalue analyses and applications of the proposed procedure to some boundary value problems for which the exact or nearly exact solutions are available in the literature. The convergence of the mixed transitional finite elements in the energy sense, and that of the combined elements, is also studied and presented. Finally, the use of mixed transitional finite elements with mixed and isoparametric elements is illustrated through more elaborate examples.

3.1 Solution Technique for the Indefinite System of Matrix Equations

The element matrix for the mixed finite elements (Appendix A) is of the form,

$$\begin{matrix} \underline{S}^e \\ (m+n) \times (m+n) \end{matrix} = \begin{bmatrix} \frac{0}{m \times m} & \frac{A^e}{m \times n} \\ \frac{A^e T}{n \times m} & \frac{-B^e}{n \times n} \end{bmatrix} \quad (3.1.1)$$

where  $m$  and  $n$  are the numbers of degrees of freedom in displacements and stresses, respectively. The matrix  $\underline{S}^e$  is real, symmetric and would have real eigenvalues. The submatrix  $\underline{B}^e$  is positive definite. It is shown in Appendix B of reference [8] that if  $r$  is rank of the matrix  $\underline{S}^e$ , then the eigenvalue distribution is of the following type:

- (i)  $m$  positive and  $n$  negative eigenvalues if  $r = m + n$ ;
- (ii)  $(r - n)$  positive,  $(m + n - r)$  zero and  $n$  negative eigenvalues if  $r < m + n$ .

If the completeness criterion stated in Section 2.1 is satisfied by the assumed displacement and stress approximations for the plane elasticity mixed finite elements, rank  $r$  of the element matrix in Equation (3.1.1) is equal to  $m + n - 3$ . The element matrix will then have  $(m - 3)$  positive, 3 zero and  $n$  negative eigenvalues where the zero eigenvalues correspond to the rigid body modes. Upon elimination of the rigid body modes, the element matrix will have both positive and negative eigenvalues and is therefore indefinite. The global matrix equations for mixed elements used in conjunction with the isoparametric elements will also be indefinite in general, with both positive and negative eigenvalues after rigid body modes have been removed.

Although the method of Gaussian elimination with partial pivoting can be employed to solve such indefinite equations, the central memory storage required for the global matrix would be very large. An alternative scheme is proposed to help reduce the storage requirements and presented here.

The global matrix equation can be written as

$$\underline{S} \underline{\Lambda} = \underline{F} \quad (3.1.2)$$

where  $\underline{S}$  is the global matrix which is real but indefinite,  $\underline{\Lambda}$  is the vector of unknowns which consists of both stresses and displacements, and  $\underline{F}$  is the consistent load vector. If the total displacement and stress degrees of freedom are  $M$  and  $N$ , respectively, then for a properly constrained body there will be  $M$  positive and  $N$  negative eigenvalues  $(+\lambda_1, +\lambda_2, \dots, +\lambda_M, -\lambda_{M+1}, -\lambda_{M+2}, \dots, \lambda_{M+N})$ . It can be shown [10] that if  $\lambda_1$  is an eigenvalue of  $\underline{S}$  associated with the eigenvector  $\underline{\Lambda}_1$ , i.e.

$$\underline{S} \underline{\Lambda}_1 = \lambda_1 \underline{\Lambda}_1 \quad (3.1.3)$$

then for any positive integer  $K$ , the following is true.

$$\underline{S}^K \underline{\Lambda}_1 = \lambda_1^K \underline{\Lambda}_1 \quad (3.1.4)$$

In particular, if  $K = 2$ ,  $\underline{S}^2 \underline{\Lambda}_1 = [\underline{S} \underline{S}] \underline{\Lambda}_1 = [\underline{S}^T \underline{S}] \underline{\Lambda}_1 = \lambda_1^2 \underline{\Lambda}_1$  for symmetric  $\underline{S}$ . Therefore, if we premultiply the global matrix  $\underline{S}$  by its transpose, a matrix with eigenvalues equal to the squares of the corresponding eigenvalues of  $\underline{S}$  is obtained and the resulting matrix  $\underline{S}^T \underline{S}$  will be positive definite, i.e. all eigenvalues are positive. From the above consideration, it is obvious that the indefinite global matrix equation can be transformed into a positive definite matrix equation by premultiplying both sides of Equation (3.1.2) by the transpose of  $\underline{S}$ .

$$[\underline{S}^T \underline{S}] \underline{\Lambda} = [\underline{S}^T \underline{F}] \tag{3.1.5}$$

The solution to Equation (3.1.5) is the same as that of Equation (3.1.2) provided the rank of  $\underline{S}^T \underline{S}$  is the same as that of  $\underline{S}$ . The solution scheme indicated by Equation (3.1.5) is also referred to as the discretized least square method [11]. To minimize the amount of computer storage required, the global matrix equations are stored using the skyline technique [12] in which variable half bandwidths are used. Premultiplying a matrix stored using this technique by its transpose requires special attention to storage addressing. A computer subroutine MULTIP has been written to perform such manipulations and is given in the program listing in Appendix E. Figure (3.1) shows a premultiplication of  $\underline{S}$  with  $\underline{S}^T$  and indicates doubling of variable half bandwidths excluding the diagonal. It should be noted that the storage required to carry out the Gaussian elimination process for the  $12 \times 12$  matrix of Figure (3.1) would require matrix size of 156, i.e.

$$N(3LB + 1) = 12(3 \times 4 + 1) = 156$$

where  $N$  = total degrees of freedom and  $LB$  = half bandwidth excluding the diagonal. On the other hand, the matrix size required for the positive definite  $\underline{S}^T \underline{S}$  matrix using the skyline technique is 51, a substantially smaller storage requirement.

### 3.2 Numerical Instability

The uncondensed element matrix equation (2.3.19) for isotropic elastic properties can be written as

$$\begin{bmatrix}
 \underline{0} & \underline{0} & \underline{a}^T & \underline{0} & \underline{b}^T \\
 \underline{0} & \underline{0} & \underline{0} & \underline{b}^T & \underline{a}^T \\
 \underline{a} & \underline{0} & + \frac{1}{E} \underline{C} & - \frac{\nu}{E} \underline{C} & \underline{0} \\
 \underline{0} & \underline{b} & - \frac{\nu}{E} \underline{C} & + \frac{1}{E} \underline{C} & \underline{0} \\
 \underline{b} & \underline{a} & \underline{0} & \underline{0} & \frac{2(1+\nu)}{E} \underline{C}
 \end{bmatrix}
 \begin{Bmatrix}
 \underline{u} \\
 \underline{v} \\
 \underline{\tau}
 \end{Bmatrix}
 =
 \begin{Bmatrix}
 \underline{d} \\
 \underline{e} \\
 \underline{0}
 \end{Bmatrix}
 \quad (3.2.1)$$

It should be noted that the submatrix  $\underline{C}$  is divided by the modulus of elasticity  $E$ . Usually a large value of  $E$  leads to a very large ratio between the largest and the smallest matrix elements, which can lead to ill-conditioning of the system matrix. The condensed element matrix equations given in Appendix C also show that, after condensation, in addition to having some elements of the condensed matrix divided by

E, there are also some elements which are multiplied by E. Ratio between the largest and the smallest elements of the condensed matrix will then be much larger than that for the uncondensed matrix. Therefore, perhaps, a more severe ill-conditioning may result for large E values.

Eigenvalue analyses are performed on the triangular mixed element, the mixed transitional elements and a combination of mixed, mixed transitional and eight-node isoparametric element matrices. The modulus of elasticity has been varied from 1.0 to 100,000,000.0.

It is observed that for all eigenvalue analyses performed, the order of magnitude of the negative eigenvalues decreases as the value of E increases, with the first few significant figures varying slightly at the same time. Except for the uncondensed elements, the order of magnitude of the positive eigenvalues increases as the value of E increases. The first few significant figures of the positive eigenvalues remain essentially constant. Results of the eigenvalue analysis for a combination of a condensed four-node mixed transitional element, a three-node mixed transitional element and an isoparametric element, as shown in Figure (3.2), are given in Table (3.1).

For E increasing from 1.0 to 100,000,000.0, the order of magnitude of the negative eigenvalues decreases from about  $10^{-1}$  to  $10^{-8}$  while that of the positive eigenvalues increases from about  $10^1$  to  $10^{+9}$ . Thus for large values of E, the ratio of the largest positive and negative eigenvalues is of the order  $10^{17}$ . Moreover, for small values of E,

	1	100	1,000	10,000	100,000	1,000,000	10,000,000	100,000,000
1	-0.3516	-0.3874E-01	-0.3876E-03	-0.3880E-04	-0.3408E-05	-0.1853E-05	-0.6483E-07	-0.5891E-06
2	-0.1844	-0.1995E-02	-0.1992E-03	-0.1995E-04	-0.1919E-05	-0.1372E-06	-0.3260E-07	-0.4191E-06
3	-0.1444	-0.1454E-02	-0.1454E-03	-0.1445E-04	-0.1402E-05	-0.6493E-06	-0.1344E-07	-0.3260E-08
4	-0.1153	-0.1192E-02	-0.1192E-03	-0.1197E-04	-0.1350E-05	0.7436E-08	-0.1262E-07	-0.1624E-08
5	-0.7479E-01	-0.7565E-03	-0.7565E-04	-0.6025E-05	-0.8180E-06	0.5098E-06	-0.7228E-08	-0.1334E-08
6	-0.4401E-01	-0.4411E-03	-0.4411E-04	-0.5979E-05	-0.8172E-06	0.2736E-05	0.4704E-06	-0.1259E-08
7	-0.2956E-14	-0.1789E-12	-0.7592E-11	-0.3128E-10	0.2846E-09	0.4331E-05	0.6808E-05	-0.7228E-09
8	-0.1738E-14	-0.1029E-12	-0.1040E-12	0.6096E-08	0.1967E-08	0.2890E-02	0.1162E-02	-0.6999E-09
9	0.6272E-14	0.9486E-08	0.1625E-12	0.2234E-04	0.1237E-05	0.4295E-02	0.1409E-02	0.4618E-02
10	0.1167	0.1144E+02	0.1143E+03	0.1143E+04	0.1143E+05	0.1428E+06	0.1428E+07	0.1428E+06
11	0.2128	0.2115E+02	0.2115E+03	0.2115E+04	0.2115E+05	0.2115E+06	0.2115E+07	0.2114E+08
12	0.3810	0.3646E+02	0.3646E+03	0.3646E+04	0.3646E+05	0.3646E+06	0.3646E+07	0.3646E+08
13	0.4032	0.3994E+02	0.3997E+03	0.3997E+04	0.3997E+05	0.3997E+06	0.3997E+07	0.3997E+08
14	0.5944	0.5565E+02	0.5565E+03	0.5565E+04	0.5565E+05	0.5565E+06	0.5565E+07	0.5565E+08
15	0.6717	0.6438E+02	0.6438E+03	0.6438E+04	0.6438E+05	0.6438E+06	0.6438E+07	0.6438E+08
16	0.7050	0.6917E+02	0.6917E+03	0.6917E+04	0.6917E+05	0.6917E+06	0.6917E+07	0.6917E+08
17	0.1055E+01	0.1043E+03	0.1043E+04	0.1043E+05	0.1043E+06	0.1043E+07	0.1043E+08	0.1043E+09
18	0.1103E+01	0.1095E+03	0.1095E+04	0.1095E+05	0.1095E+06	0.1095E+07	0.1095E+08	0.1095E+09
19	0.1402E+01	0.1399E+03	0.1399E+04	0.1399E+05	0.1399E+06	0.1399E+07	0.1399E+08	0.1399E+09
20	0.1440E+01	0.1437E+03	0.1437E+04	0.1437E+05	0.1437E+06	0.1437E+07	0.1437E+08	0.1437E+09
21	0.1704E+01	0.1702E+03	0.1702E+04	0.1702E+05	0.1702E+06	0.1702E+07	0.1702E+08	0.1702E+09
22	0.1931E+01	0.1929E+03	0.1929E+04	0.1929E+05	0.1929E+06	0.1929E+07	0.1929E+08	0.1929E+09
23	0.2752E+01	0.2752E+03	0.2752E+04	0.2752E+05	0.2752E+06	0.2752E+07	0.2752E+08	0.2752E+09
24	0.3577E+01	0.3576E+03	0.3576E+04	0.3576E+05	0.3576E+06	0.3576E+07	0.3576E+08	0.3576E+09
25	0.5113E+01	0.5113E+03	0.5113E+04	0.5113E+05	0.5113E+06	0.5113E+07	0.5113E+08	0.5113E+09
26	0.6801E+01	0.6801E+03	0.6801E+04	0.6801E+05	0.6801E+06	0.6801E+07	0.6801E+08	0.6801E+09

TABLE 3.1 Eigenvalue Analysis of a Combination of a Four-node Transitional Element, a Three-node Transitional Element and an Isoparametric Element.

computer results give zero eigenvalues as of the order  $10^{-14}$  which depends upon the machine accuracy, and is much smaller than the orders of magnitude of the positive and negative eigenvalues. As the value of  $E$  becomes very large, the 'zero eigenvalues' given by the computer are of the order  $10^{-5}$  to  $10^{-9}$ , while the orders of magnitude of the negative eigenvalues are of the order  $10^{-6}$  to  $10^{-8}$ . The 'zero' and negative eigenvalues become much closer and numerical instability is expected as the 'zero' eigenvalues given by computer results are not small enough to be regarded as zero eigenvalues. It is to be noted that after premultiplication of the matrix by its own transpose as indicated in the previous section, the ratio of the largest positive and negative eigenvalues of the resulting matrix will be  $10^{34}$  instead of  $10^{17}$ . Thus the solution technique adopted in the previous section will suffer from a further magnified numerical instability.

One can overcome the problem of numerical instability by employing double precision arithmetic on the computer or through some improved iterative techniques. Since only linear elasticity problems are considered in this work, it is sufficient to perform all computer calculations with a small value for the modulus of elasticity  $E$ , say 1.0, and the resulting solutions can be scaled accordingly for appropriate large  $E$  values. Moreover, the stress results should theoretically be independent of the  $E$  value and need not be scaled.

In order to demonstrate the effects of numerical instability, consider the cantilevered beam shown in Figure (3.3). (The same cantilever, with slightly different support conditions, will be analyzed in

subsequent convergence studies.) The Poisson's ratio is 0.25 and the modulus of elasticity  $E$  is varied from 3.0 to  $3.0 \times 10^6$ . Results are given in Table (3.2). It is observed that as  $E$  value increases, value of  $\tau_{11}$  at node 10 loses accuracy and eventually an ill-conditioned matrix results for very large  $E$  values using the solution technique described in the previous section.

Modulus of Elasticity (E)	Strain Energy (U)	Tip Displacement ( $\delta_T$ )	$\tau_{11}$ at Node 10
3.0	$.6992217735744 \times 10^5$	$.34959359 \times 10^4$	24.194055
30.0	$.6992217529958 \times 10^4$	$.34959358 \times 10^3$	24.194054
300.0	$.6992217599054 \times 10^3$	$.34959358 \times 10^2$	24.194054
3,000.0	$.6992218558375 \times 10^2$	$.34959363 \times 10^1$	24.194033
30,000.0	$.6992217225374 \times 10^1$	.34959349	24.191548
300,000.0	.6991962855168	$.34957418 \times 10^{-2}$	23.862192
3,000,000.0	$.6961538016872 \times 10^{-1}$	$.3476489 \times 10^{-2}$	- 15.291709
10,000,000.0	$.1917723486110 \times 10^{-1}$	$.92138441 \times 10^{-3}$	191.13958
25,000,000.0	ill conditioned		
30,000,000.0	ill conditioned		

TABLE 3.2: Results for a cantilever analyzed using values of the modulus of elasticity from 3.0 to  $3.0 \times 10^{-6}$ .

### 3.3 Orientation Problem with Four-Node Mixed Transitional Finite Element

The approximations for both displacements and stresses for the four-node mixed transitional element are given by Equations (2.3.3) and (2.3.4) in terms of area coordinates. However, the same approximations can be derived by starting with a complete quadratic polynomial with six arbitrary constants, i.e.

$$u_i = a_1^i + a_2^i x_1 + a_3^i x_2 + a_4^i x_1^2 + a_5^i x_1 x_2 + a_6^i x_2^2; \quad i = 1, 2 \quad (3.3.1)$$

$$\tau_{ij} = b_1^{ij} + b_2^{ij} x_1 + b_3^{ij} x_2 + b_4^{ij} x_1^2 + b_5^{ij} x_1 x_2 + b_6^{ij} x_2^2; \\ i, j = 1, 2, 3 \quad (3.3.2)$$

Variations of  $u_i$  and  $\tau_{ij}$  along edge 1-2 of the four-node mixed triangular element, Figure (3.4), can be obtained by substituting  $x_2 = m_{12}x_1$  in equations (3.3.1) and (3.3.2):

$$u_i = a_1^i + a_2^i x_1 + a_3^i (m_{12}x_1) + a_4^i x_1^2 + a_5^i (m_{12}x_1)^2 + a_6^i (m_{12}x_1)^2; \\ i = 1, 2 \quad (3.3.3)$$

$$\tau_{ij} = b_1^{ij} + b_2^{ij} x_1 + b_3^{ij} (m_{12}x_1) + b_4^{ij} x_1^2 + b_5^{ij} (m_{12}x_1)^2 + b_6^{ij} (m_{12}^2 x_1^2); \\ i = j = 1, 2 \quad (3.3.4)$$

where  $m_{12}$  is the slope of edge 1-2.

In order to force linear variations of displacements and stresses along edge 1-2, the coefficient of  $x_1^2$  term in Equations (3.3.3) and (3.3.4) must vanish, i.e.,

$$a_4^i + m_{12} a_5^i + m_{12}^2 a_6^i = 0 \quad i = 1, 2 \quad (3.3.5)$$

$$b_4^{ij} + m_{12} b_5^{ij} + m_{12}^2 b_6^{ij} = 0 \quad i = j = 1, 2 \quad (3.3.6)$$

Similarly, for linear variations of displacements and stresses along edge 1-3, the following constraints result,

$$a_4^i + m_{13} a_5^i + m_{13}^2 a_6^i = 0 \quad i = 1, 2 \quad (3.3.7)$$

$$b_4^{ij} + m_{13} b_5^{ij} + m_{13}^2 b_6^{ij} = 0 \quad i, j = 1, 2 \quad (3.3.8)$$

where  $m_{13}$  is the slope of edge 1-3. Equations (3.3.5) to (3.3.8) can be used to solve for  $a_5^i$  and  $a_6^i$  in terms of  $a_4^i$  and for  $b_5^{ij}$  and  $b_6^{ij}$  in terms of  $b_4^{ij}$ , respectively. The displacement and stress variations are then given by

$$u_i = a_1^i + a_2^i x_1 + a_3^i x_2 + a_4^i (x_1^2 + \alpha x_1 x_2 + \beta x_2^2) \quad (3.3.9)$$

$$\tau_{ij} = b_1^{ij} + b_2^{ij} x_1 + b_3^{ij} x_2 + b_4^{ij} (x_1^2 + \alpha x_1 x_2 + \beta x_2^2) \quad (3.3.10)$$

where

$$\alpha = \frac{(m_{12} + m_{13})}{m_{12}m_{13}} \quad (3.3.11)$$

$$\beta = \frac{1}{m_{12}m_{13}} \quad (3.3.12)$$

Equation (3.3.9) is differentiated to obtain strains as follows:

$$\epsilon_{11} = \frac{\partial u_1}{\partial x_1} = a_2^{11} + a_4^{11} (2x_1 + \alpha x_2) \quad (3.3.13)$$

$$\epsilon_{22} = \frac{\partial u_2}{\partial x_2} = a_3^{22} + a_4^{22} (\alpha x_1 + 2\beta x_2) \quad (3.3.14)$$

$$\gamma_{12} = \frac{\partial u_2}{\partial x_1} + \frac{\partial u_1}{\partial x_2} = a_3^{12} + a_2^{12} + a_4^{12} (\alpha x_1 + 2\beta x_2) + a_4^{12} (2x_1 + \alpha x_2) \quad (3.3.15)$$

Inspection of Equations (3.3.13) to (3.3.15) and Equation (3.3.10) shows that the strains from the stress approximations possess all of the strain modes that are present in the strains derived from the displacement approximations. The completeness criterion stated in Section (2.1) is therefore satisfied by the displacement and stress approximations given by Equations (3.3.9) and (3.3.10) and mechanisms, non stressing strain modes, will not be present. However, examination of Equation (3.3.10) indicates that for a general state of stress, the stress approximations will have difficulties in satisfying the equilibrium equations  $\tau_{ij,j} = 0$ ,  $i, j = 1, 2$ . This is explained next.

Substitution of the stress approximations given by Equation (3.3.10) gives the relationships that have to be satisfied by the arbitrary constants for exact satisfaction of the equilibrium equations. For example, if the approximations for  $\tau_{11}$  and  $\tau_{12}$  are substituted into the equilibrium equation  $\tau_{11,1} + \tau_{12,2} = 0$ , we obtain

$$\begin{aligned} \frac{\partial \tau_{11}}{\partial x_1} + \frac{\partial \tau_{12}}{\partial x_2} &= b_2^{11} + b_4^{11}(2x_1 + \alpha x_2) + b_3^{12} + b_4^{12}(\alpha x_1 + 2\beta x_2) = \\ &= (b_2^{11} + b_3^{12}) + (2b_4^{11} + \alpha b_4^{12})x_1 + (\alpha b_4^{11} + 2\beta b_4^{12})x_2 = 0. \end{aligned} \quad (3.3.16)$$

Similarly, if the approximations for  $\tau_{22}$  and  $\tau_{12}$  are substituted into the equation  $\tau_{12,1} + \tau_{22,2} = 0$ , the following is obtained.

$$\begin{aligned} \frac{\partial \tau_{12}}{\partial x_1} + \frac{\partial \tau_{22}}{\partial x_2} &= b_2^{12} + b_4^{12}(2x_1 + \alpha x_2) + b_3^{22} + b_4^{22}(\alpha x_1 + 2\beta x_2) = \\ &= (b_2^{12} + b_3^{22}) + (2b_4^{12} + \alpha b_4^{22})x_1 + (\alpha b_4^{12} + 2\beta b_4^{22})x_2 = 0. \end{aligned} \quad (3.3.17)$$

Thus for the equilibrium equations to be satisfied at every point within the element, the following two sets of relationships have to be satisfied by the arbitrary constants in the approximations for stresses, Equation (3.3.10).

$$b_2^{11} + b_3^{12} = 0 \quad (3.3.18)$$

$$2b_4^{11} + \alpha b_4^{12} = 0 \quad (3.3.19)$$

$$\alpha b_4^{11} + 2\beta b_4^{12} = 0 \quad (3.3.20)$$

$$\text{and } b_2^{12} + b_3^{22} = 0 \quad (3.3.21)$$

$$2b_4^{12} + \alpha b_4^{22} = 0 \quad (3.3.22)$$

$$\alpha b_4^{12} + 2\beta b_4^{22} = 0 \quad (3.3.23)$$

It is observed that for non-trivial values of  $b_4^{11}$ ,  $b_4^{12}$  and  $b_4^{22}$ ,  $\alpha$  and  $\beta$  as defined in Equations (3.3.11) and (3.3.12) have to satisfy the following equality.

$$4\beta - \alpha^2 = 0 \quad (3.3.24)$$

$$\text{or } \beta = \alpha^2/4 \quad (3.3.25)$$

Equation (3.3.25) is satisfied only when  $m_{12} = m_{13}$ , i.e., the triangular transitional element degenerates into a straight line. Therefore, for exact satisfaction of the equilibrium equations at every point within the element,  $b_4^{11}$ ,  $b_4^{12}$  and  $b_4^{22}$  should vanish. With  $b_4^{11}$ ,  $b_4^{12}$  and  $b_4^{22}$  equal to zero, the stress approximations given by Equation (3.3.10) will reduce to linear variations of  $\tau_{11}$ ,  $\tau_{12}$  and  $\tau_{22}$  over an element. However, in finite element analyses, equilibrium equations are satisfied only approximately in a weighted integral sense and not pointwise. Therefore, for a general state of stress,  $b_4^{11}$ ,  $b_4^{12}$  and  $b_4^{22}$  given by a finite element analysis will not be expected to vanish and the stress approximations will be better than just linear. Results from examples to be presented subsequently do show non-linear stress variations along side 2-4-3 of the transitional elements, thus indicating non zero values

of  $b_4^{11}$ ,  $b_4^{12}$  and  $b_4^{22}$ .

Equilibrium Equations (3.3.16) and (3.3.17) also reveal that for lines  $2x_1 + \alpha x_2 = 0$  and  $\alpha x_1 + 2\beta x_2 = 0$ , the equilibrium equations can be satisfied for arbitrary values of  $b_4^{11}$ ,  $b_4^{12}$  and  $b_4^{22}$ . This means that along these two lines,  $b_4^{11}$ ,  $b_4^{12}$  and  $b_4^{22}$ , can attain non unique values. Again, as the equilibrium equations are satisfied only in a weighted integral sense and not pointwise in a finite element analysis, this is expected to give rise to some oscillations in stress values.

The aforementioned oscillations of stresses are expected to vanish if lines, for which equilibrium equations can be satisfied with non unique values of  $b_4^{11}$ ,  $b_4^{12}$  and  $b_4^{22}$ , do not exist. This condition is met when  $\alpha$  in Equations (3.3.16) and (3.3.17) vanishes. In this case Equations (3.3.16) and (3.3.17) reduce to

$$b_2^{11} + b_3^{12} + 2b_4^{11} x_1 + 2\beta b_4^{12} x_2 = 0 \quad (3.3.26)$$

$$\text{and } b_2^{12} + b_3^{22} + 2b_4^{12} x_1 + 2\beta b_4^{22} x_2 = 0. \quad (3.3.27)$$

Thus for equilibrium to be satisfied anywhere within the element  $b_4^{11}$ ,  $b_4^{12}$  and  $b_4^{22}$  should vanish provided there are no body forces.

From Equation (3.3.11),  $\alpha$  vanishes if

$$m_{13} = -m_{12} \quad (3.3.28)$$

for non-zero  $m_{12}$  and  $m_{13}$ . This corresponds to configurations of isocetes triangles shown in Figure (3.5). Apparently, there is no need for restrictions on the orientation of side 2-4-3.

One special case for which the lines with non unique  $b_{ij}^4$ 's do not exist is when  $m_{12} = 0$  and  $m_{13}$  is infinity, Figure (3.6). For side 1-2,  $x_2 = 0$  and Equation (3.3.2) gives

$$\tau_{ij} = b_1^{ij} + b_2^{ij} x_1 + b_4^{ij} x_1^2, \quad i, j = 1, 2 \quad (3.3.29)$$

Similarly, for side 1-3,  $x_1 = 0$  and

$$\tau_{ij} = b_1^{ij} + b_3^{ij} x_2 + b_6^{ij} x_2^2, \quad i, j = 1, 2 \quad (3.3.30)$$

For linear variations of stresses along edges 1-2 and 1-3,  $b_4^{ij}$  and  $b_6^{ij}$  vanish and stress approximations reduce to

$$\tau_{ij} = b_1^{ij} + b_2^{ij} x_1 + b_3^{ij} x_2 + b_5^{ij} x_1 x_2, \quad i, j = 1, 2 \quad (3.3.31)$$

and for the equilibrium equations to be satisfied, we have

$$(b_2^{11} + b_3^{12}) + b_5^{11} x_2 + b_5^{12} x_1 = 0 \quad (3.3.32)$$

$$(b_2^{12} + b_3^{22}) + b_5^{12} x_2 + b_5^{22} x_1 = 0. \quad (3.3.33)$$

Thus there exist no lines along which  $b_5^{11}$ ,  $b_5^{12}$  and  $b_5^{22}$  are undetermined when equilibrium is satisfied and stress oscillations are not expected.

It is then postulated that oscillations of stresses will not be expected for four-node transitional mixed elements which satisfy either of the following conditions:

- 1) the element sides form a triangle with  $m_{12} = -m_{13}$ , Figure (3.5);
- 2) the element sides form a right angle triangle with the right angle between sides 1-2 and 1-3 and with sides 1-2 and 1-3 parallel to the global coordinate axes, Figure (3.6).

A rigorous mathematical justification will not be attempted. However, through various numerical applications of the transitional elements, together with the mixed and isoparametric displacement elements (to be presented in subsequent sections), it is found that good accuracy is obtained by using the orientations and shapes indicated in Figures (3.5) and (3.6), i.e.,  $m_{12} = -m_{13}$  and  $m_{12} = 0$ ,  $m_{13} = \infty$ . For other orientations and shapes of the transitional elements, oscillations of stresses over the full domain have indeed been observed. Thus numerical results do confirm that if no lines with non unique arbitrary constants  $b_4^{ij}$  exist, the four-node mixed transitional element does seem to perform reasonably well.

It is to be noted that by performing a patch test with the mixed transitional elements, constant stress state is reproduced with any arbitrary orientation and shape of the element. This is because only the constants  $b_1^{ij}$  in the stress approximation will attain constant stress values. Consequently the problem of non unique values of  $b_4^{ij}$  does not arise. This suggests that if, within a finite element grid, the mixed transitional elements are located where the stress state is approximately constant, the mixed transitional element should work reasonably well even if the orientations and shapes are not in accordance with those indicated in Figure (3.5) and (3.6) and stipulated in configurations (1) and (2) earlier.

### 3.4 Convergence of Mixed Transitional Elements and Combinations of Mixed, Mixed Transitional and Isoparametric Finite Elements

The three-node triangular mixed and the eight-node isoparametric displacement finite elements both have predicted energy convergence rates of  $O(N^{-4})$ . The use of the three-node triangular mixed finite elements and the eight-node isoparametric displacement elements connected by the mixed transitional elements involves using both the Hellinger-Reissner principle and the principle of minimum potential energy in a finite element application. In order to predict the strain energy convergence rate in such an application, the strain energy convergence rates of the mixed transitional elements are investigated first.

A square plate (plane stress) with parabolically varying end loads, Figure (3.7), is analysed using only the mixed transitional finite elements. The analytical solution [13] is known and hence it has been used to study convergence in strain energy. Due to symmetry, only one quarter of the plate ABCD needs to be analyzed with forced boundary conditions  $u_1 = 0$  on AD and  $u_2 = 0$  on AB. The mixed transitional elements are shown in Figure (3.8). The finite element grids used for studying the energy convergence rate for each type of mixed transitional finite elements are shown in Figure (3.9). Table (3.3) gives the calculated strain energies in the square plate and percentage errors. Plots of the errors in strain energy versus grid size are shown in Figures (3.10a) to (3.10c).

Finite Element Grid	$10Et^2U/(1-\nu^2)L^2N_0$	Error (%)
N = 2	2.652491	5.050
N = 4	2.738196	1.982
N = 8	2.779601	0.500
Exact Solution	2.79357	

(a) Condensed mixed element (3-node transitional element)

Finite Element Grid	$10Et^2U/(1-\nu^2)L^2N_0$	Error (%)
N = 2	2.676449	4.192
N = 4	2.747999	1.631
N = 8	2.782233	0.406
Exact Solution	2.79357	

(b) 4-node transitional element, condensed

Finite Element Grid	$10Et^2U/(1-\nu^2)L^2N_0$	Error (%)
N = 2	2.709306	3.016
N = 4	2.775975	0.629
N = 8	2.791582	0.071
Exact Solution	2.79357	

(c) 4-node transitional element, uncondensed

TABLE 3.3: Strain energies and percentage errors for the square plate with parabolically varying end loads, Figure (3.7).

The calculated values of strain energy seem to be in good agreement with the exact value. The strain energy convergence rate for the three-node transitional and the condensed four-node transitional elements is  $O(N^{-2})$ , Figure (3.9a and b). The numerical results for the uncondensed four-node transitional elements indicate the strain energy convergence rate of  $O(N^{-4})$ , Figure (3.10c), which is the same as the strain energy convergence rate of the three-node triangular mixed and the eight-node isoparametric elements. The displacements and stresses given in Table (3.4) are also in good agreement with the analytical values.

The strain energy convergence rate when the three-node triangular, the mixed transitional and the eight-node isoparametric displacement elements are used together is studied next. For this purpose, the cantilevered beam shown in Figure (3.11) is analyzed. The analyses are carried out with condensed transitional elements first and repeated using the uncondensed transitional elements. The finite element grids are given in Figures (3.12) and (3.13). Comparisons of the finite element solutions with the exact solution [8] are presented in Table (3.5). The computed results appear to be in good agreement with the analytical solution. It is observed, however, that the stresses calculated using the uncondensed transitional finite elements have an error of about 11% whereas the stresses calculated using the condensed transitional finite elements resulted in an error of about 2% in the vicinity of the transitional elements.

Grid Size	$u_{2D}$			$u_{1D}$			$T_{22A}$			U Strain Energy		
	MFE	T.F.E.		MFE	T.F.E.		MFE	T.F.E.		MFE	T.F.E.	
	Condensed	Condensed	Uncondensed	Condensed	Condensed	Uncondensed	Condensed	Condensed	Uncondensed	Condensed	Condensed	Uncondensed
N = 2	0.448260	0.4613412	0.4792811	-0.149604	-0.1578762	-0.1734217	0.823924	0.936512 <sup>*</sup>	0.970385	0.2413767	0.2435569	0.2465469
N = 4	0.461474	0.4654755	0.4727769	-0.141383	-0.1466588	-0.1406876	0.837352	0.912827 <sup>*</sup>	0.952797	0.2491758	0.2500697	0.2526137
N = 8	0.461414	0.4627559	0.4644919	-0.139133	-0.1404195	-0.1390017	0.853500	0.904356 <sup>*</sup>	0.881212	0.2529436	0.2531832	0.2540340
Exact		0.4616885			-0.1383109			0.85909			0.2542149	

\* Calculated from displacement field.

TABLE 3.4: Displacements, stresses and strain energies for the square plate with parabolically varying end loads, Figure 3.7

Elements	Mesh	Strain Energy (U)	Tip Displacement ( $\delta_T$ )	$\tau_{11}$ at $x_1 = 18''$ at $x_2 = 6''$
Condensed	N = 2	0.6869276367E5	3.440875E4	30.856607
	N = 4	0.7112716533E5	3.537654E4	29.361476
Uncondensed	N = 2	0.697070443E5	3.491264E4	37.323863
	N = 4	0.713329153E5	3.548020E4	26.742277
Exact		0.714666666E5	3.553333E4	30.000000

TABLE 3.5 Results for the cantilevered beam with three supports, Figure 3.11.

Errors in the calculated strain energy are presented in Table (3.6) and plotted against grid size "N" in Figure (3.14). The strain energy convergence rate when using the uncondensed transitional elements to connect the mixed and the isoparametric finite elements, is found to be  $O(N^{-4})$ , hence maintaining the strain energy convergence rates of all three types of finite elements used in the analyses. When condensed transitional elements, with energy convergence rate of  $O(N^{-2})$ , are used, the strain energy convergence rate is close to  $O(N^{-3})$ . Thus, with the condensed transitional elements, energy convergence rate is lower.

Elements	Mesh	Error in		Convergence Rate
		U(%)	$\delta_T$ (%)	
Uncondensed	N = 2	2.462	1.747	$N^{-4}$
	N = 4	0.187	0.149	
Condensed	N = 2	3.880	3.165	$\approx N^{-3}$
	N = 4	0.475	0.441	

TABLE 3.6: Errors in strain energy and tip displacement for the cantilevered beam with three supports, Figure 3.11.

To illustrate the shape restrictions on the uncondensed four-node transitional element, the cantilever of Figure (3.13) is reanalyzed by distorting shapes of the transitional elements. Figure (3.15) shows plots of the extreme fibre stress along the beam axis for the different transitional element shapes as indicated. It is observed that when edge 2-4-3 of the transitional elements, Figure (3.4), is parallel to one of the global axes and the other two sides being equal in length, thus forming an isocoles triangle ( $m_{12} = -m_{13}$ ), reasonably accurate results for the extreme fibre stresses are obtained. However, when the shapes of the transitional elements deviate from the condition  $m_{12} = -m_{13}$ , large fluctuations of stresses result, especially in the vicinity of the transitional elements. This confirms the earlier findings that the non unique problem with the quadratic stress modes for non zero  $\alpha$  condition does lead to oscillations of the calculated stresses.

### 3.5 Example of Plane Square Plate with a Circular Hole

The three-node triangular mixed, mixed transitional and the isoparametric displacement finite elements are used to analyze the problem of a plane square plate with a circular hole in the middle, under uniform tension  $\tau_0$ , Figure (3.16). The diameter of the hole is taken as one-eighth of the plate width and the plate is of unit thickness. The plane strain state is analyzed for both isotropic and orthotropic cases. Because of symmetry, only one quarter of the plate is analyzed and the two finite element grids used are shown in Figures (3.17) and (3.18). All four-node mixed transitional elements in both grids are isosceles triangles with right angles between sides 1-2 and 1-3. However in the first grid, side 2-4-3 of each transitional element is not parallel to any of the global axes whereas in the second grid, side 2-4-3 of each transitional element is kept parallel to one of the global axes.

The calculated stresses are plotted in Figures (3.19) and (3.20) along with the analytical solution for an infinite plate [13, 14]. Results obtained with the two different grids are almost the same. In both cases, the finite element solutions over predict the stress concentration at the circular hole. This is expected for a finite plate.

The same problem has been analyzed by Mirza [8] using a more refined grid shown in Figure (3.21). In one case, only the mixed finite elements are used and in the other the constant stress triangular element (CST's). A comparison of the results obtained with the present analyses with that obtained using mixed elements and CST's, respect-

ively, is given in Table (3.7). The amount of computer storage required in each case, except that for the CST elements, is also indicated. In the present analyses the skyline storage technique has been used, while for the other cases the uniform half bandwidth storage scheme was used.

It is observed that the present analyses give less accurate results than that obtained using mixed elements alone. This can be explained by the relatively coarse grids used. However, reasonably accurate results are obtained and the number of degrees of freedom and computer storage required are very much reduced. The number of degrees of freedom is almost halved and the storage requirement for the global matrix reduced from about 45000 to about 10000. Therefore, the present scheme of mixed and the isoparametric elements does indicate the advantage in both lesser storage requirements and relative accuracy.

Finally, it should be pointed out that the four-node mixed transitional element performs well when  $m_{12}$  is not equal to minus  $m_{13}$  ( $m_{12} \neq -m_{13}$ ). This is because the transitional elements are located in a region of approximately constant stresses where the severity of the orientation problem is very much reduced. Thus no oscillations of stresses have been observed.

(a) ISOTROPIC

	$\tau_{11}(C)/\tau_0$	$\tau_{22}(B)/\tau_0$	Storage $\underline{S} \rightarrow \underline{S}^T \underline{S}$	DOF	NB*
Uncondensed					
Grid #1	3.4972671	-0.9982387	5615 + 10508	188	100
Grid #2	3.5115569	-0.9537004	5904 + 11157	193	102
Condensed					
Grid #1	3.4917262	-0.9937126	3857 + 7187	161	73
Grid #2	3.5109618	-0.9620834	4131 + 7905	166	75
Ref. [8] (All MIXEL)	3.2630492	-1.0931845	43434	342	42
CST (extrapolated)	2.910	-0.878			
Infinite Plate	3.00	-1.00			

(b) ORTHOTROPIC

	$\tau_{11}(C)/\tau_0$	$\tau_{22}(B)/\tau_0$	Storage $\underline{S} \rightarrow \underline{S}^T \underline{S}$	DOF	NB*
Uncondensed					
Grid #1	3.2743412	-1.2010702	5615 + 10508	188	100
Grid #2	3.3049690	-1.1193274	5904 + 11157	193	102
Condensed					
Grid #1	3.2684212	-1.1925217	3857 + 7187	161	73
Grid #2	3.3038854	-1.1291649	4131 + 7905	166	75
Ref. [8] (All MIXEL)	3.0852018	-1.6463486	43434	342	42
CST (extrapolated)	2.920	-0.888			
Infinite Plate	2.83	-1.75			

\* Half bandwidth excluding the diagonal.

TABLE 3.7: Comparison of computer storage requirements and stresses at the edge of the hole in a square plate under tension, Figure 3.16. Isotropic and Orthotropic.

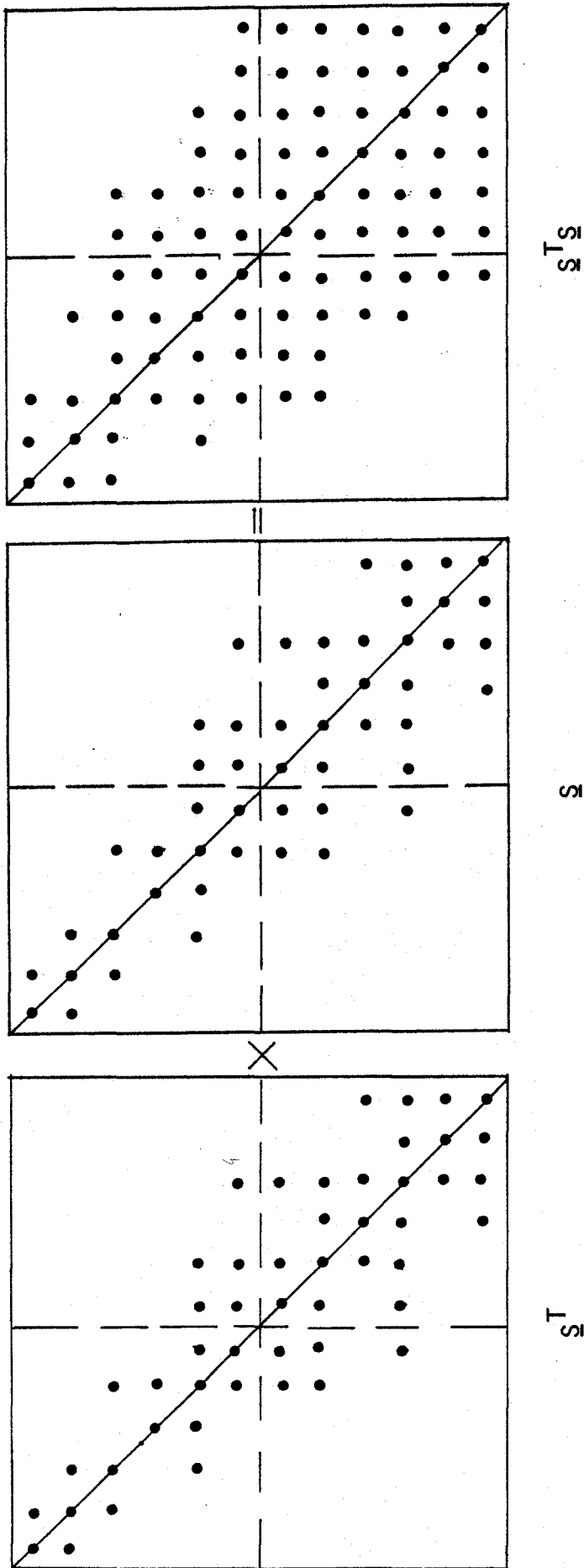
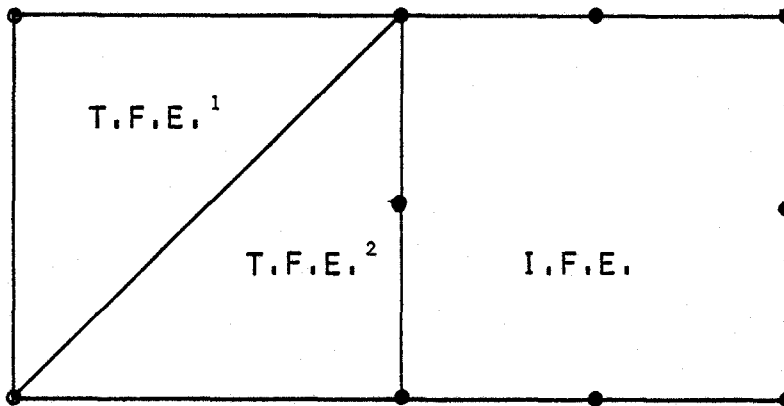


FIG. 3.1: PREMULIPLICATION OF THE MASTER MATRIX  $S$  BY ITS OWN TRANSPOSE  $S^T$ .



○ NODES WITH STRESS AND DISPLACEMENT D.O.F.

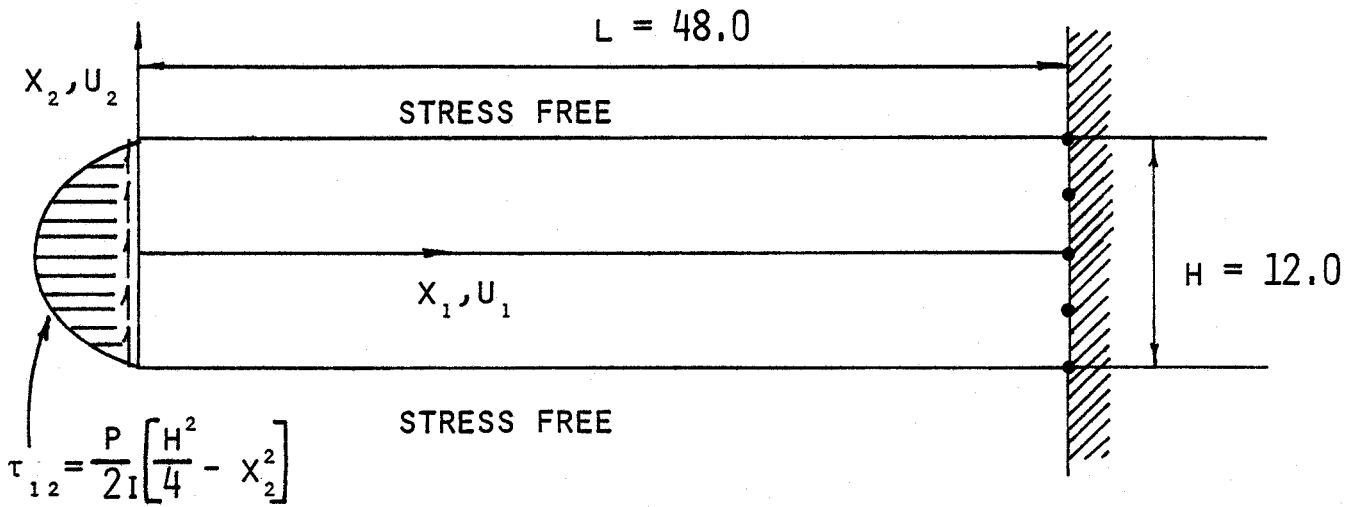
● NODES WITH DISPLACEMENT D.O.F.

T.F.E.<sup>1</sup> - THREE-NODE TRANSITIONAL FINITE ELEMENT, CONDENSED.

T.F.E.<sup>2</sup> - FOUR-NODE TRANSITIONAL FINITE ELEMENT, CONDENSED.

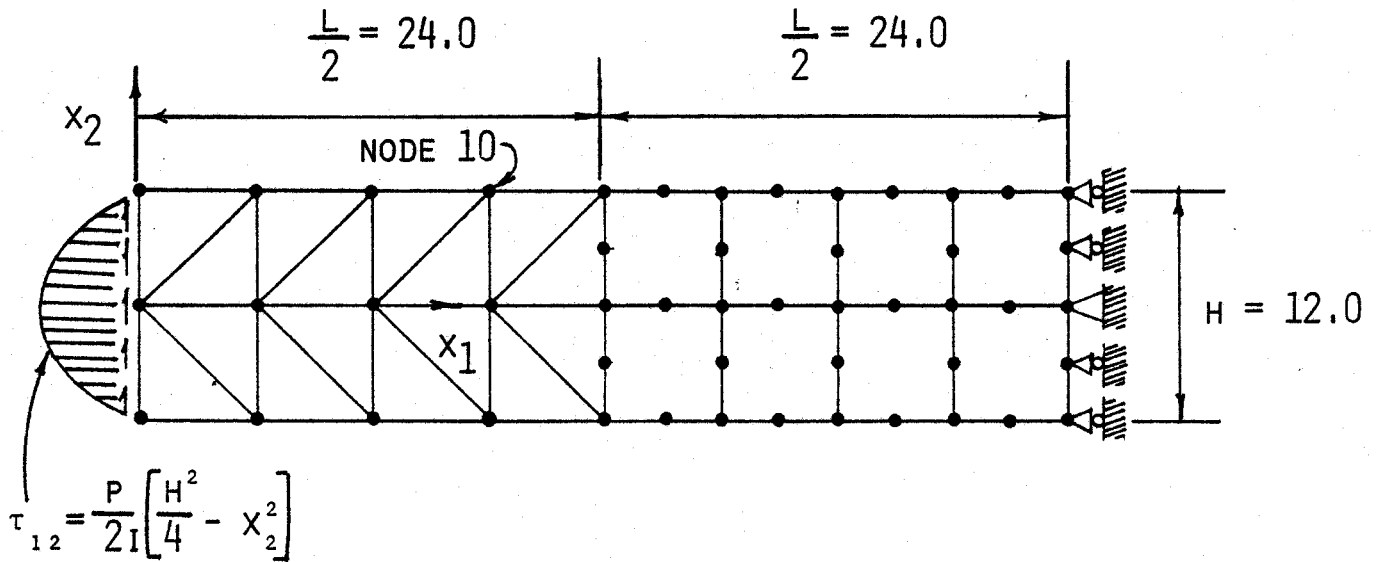
I.F.E. - ISOPARAMETRIC DISPLACEMENT FINITE ELEMENT.

FIG. 3.2: COMBINATION OF A CONDENSED FOUR-NODE TRANSITIONAL ELEMENT, A THREE-NODE TRANSITIONAL ELEMENT AND AN ISOPARAMETRIC ELEMENT, USED TO INVESTIGATE THE EFFECT OF THE MAGNITUDE OF THE MODULUS OF ELASTICITY.



PARABOLICALLY VARYING END SHEAR,  $P = 40^k$

a) CANTILEVER WITH LOAD SYSTEM AND SUPPORT CONDITIONS.



b) FINITE ELEMENT IDEALIZATION ALONG WITH BOUNDARY CONDITIONS.

FIG. 3.3: LINEAR ELASTICITY CANTILEVER BEAM WITH FULLY FIXED SUPPORTS SUBJECTED TO PARABOLIC END SHEAR.

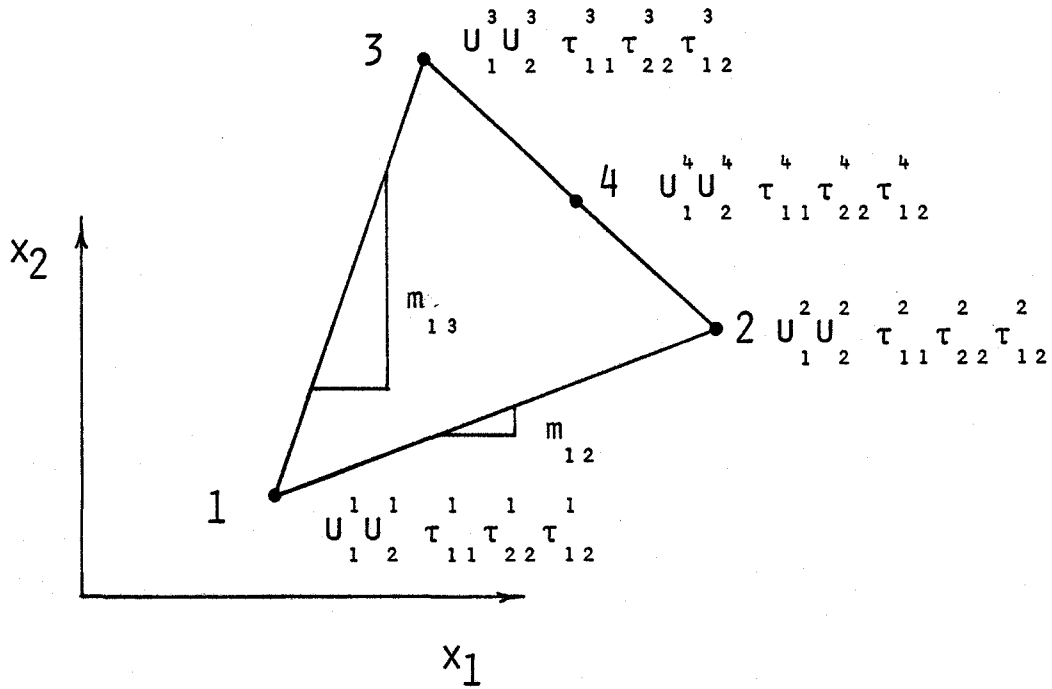


FIG. 3.4 NODE NUMBERS AND DEGREES OF FREEDOM FOR A FOUR-NODE TRIANGULAR MIXED TRANSITIONAL FINITE ELEMENT, UNCONDENSED

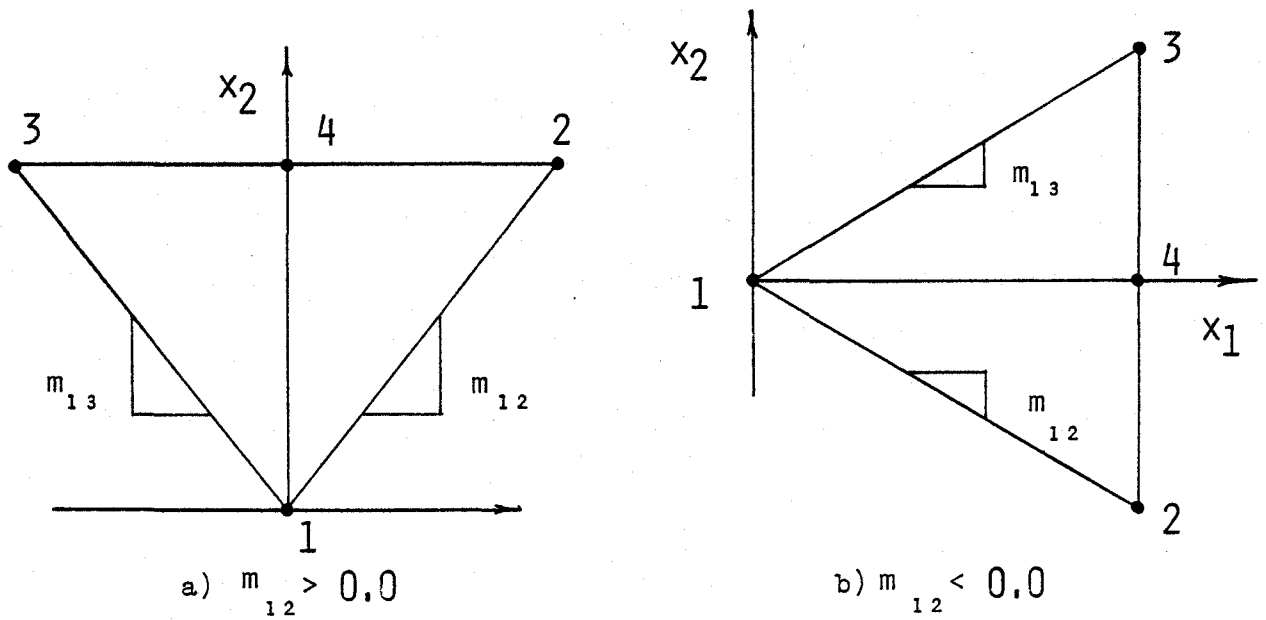


FIG. 3.5: ISOCELES FOUR-NODE TRIANGULAR MIXED TRANSITIONAL FINITE ELEMENTS WITH  $m_{12} = -m_{13}$ .

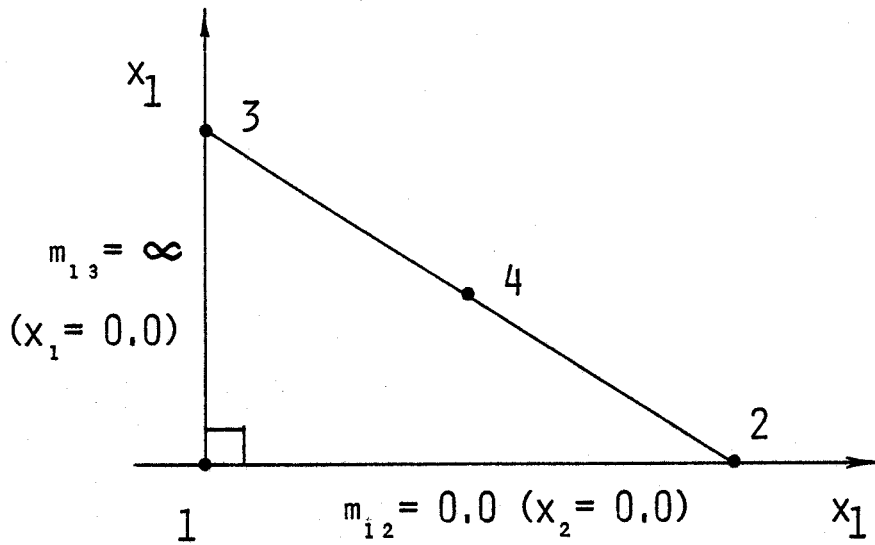


FIG. 3.6: FOUR-NODE TRIANGULAR MIXED TRANSITIONAL FINITE ELEMENT WITH A RIGHT ANGLE BETWEEN SIDES 1-2 AND 1-3 AND WITH SIDES 1-2 AND 1-3 PARALLEL TO THE GLOBAL COORDINATE AXES.

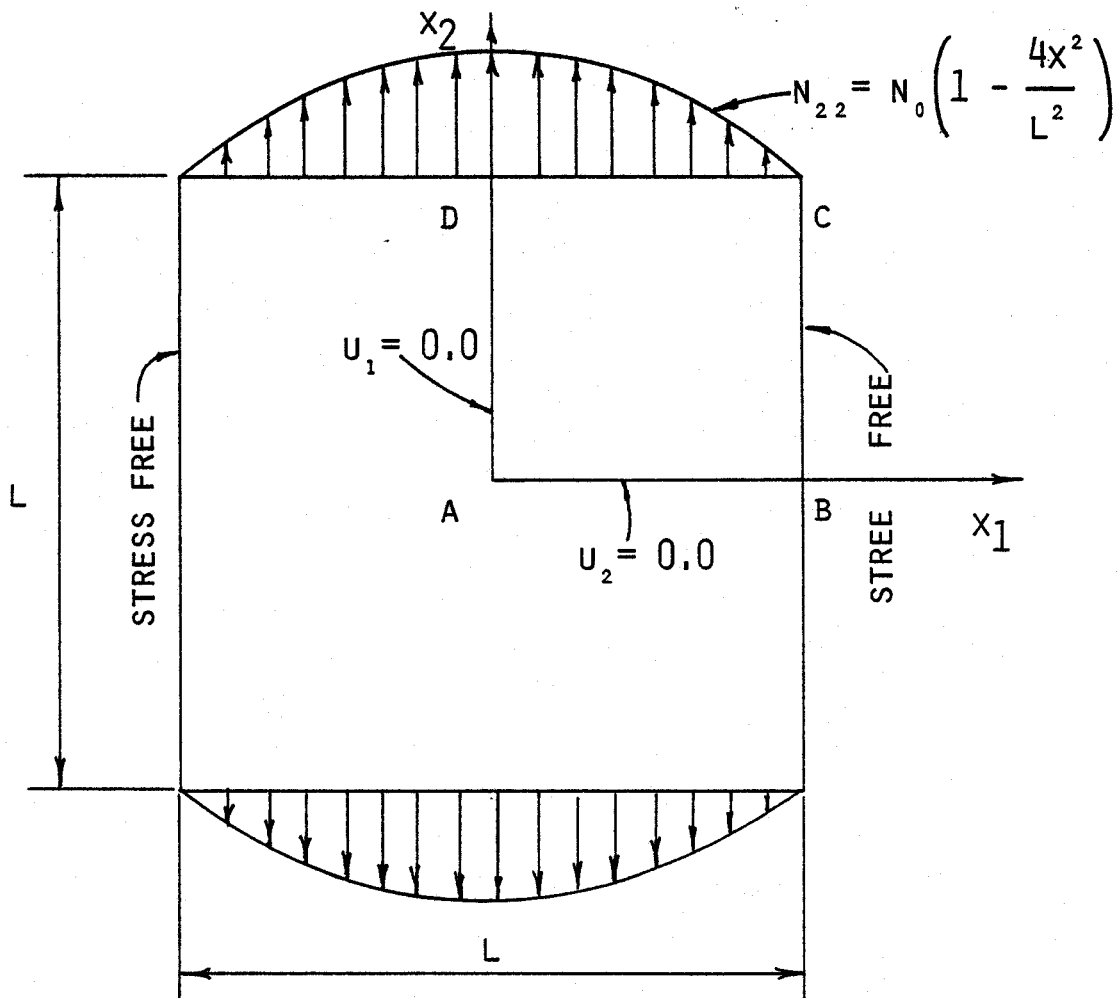


FIG. 3.7: PLANE STRESS SQUARE PLATE WITH PARABOLICALLY VARYING END LOADS.

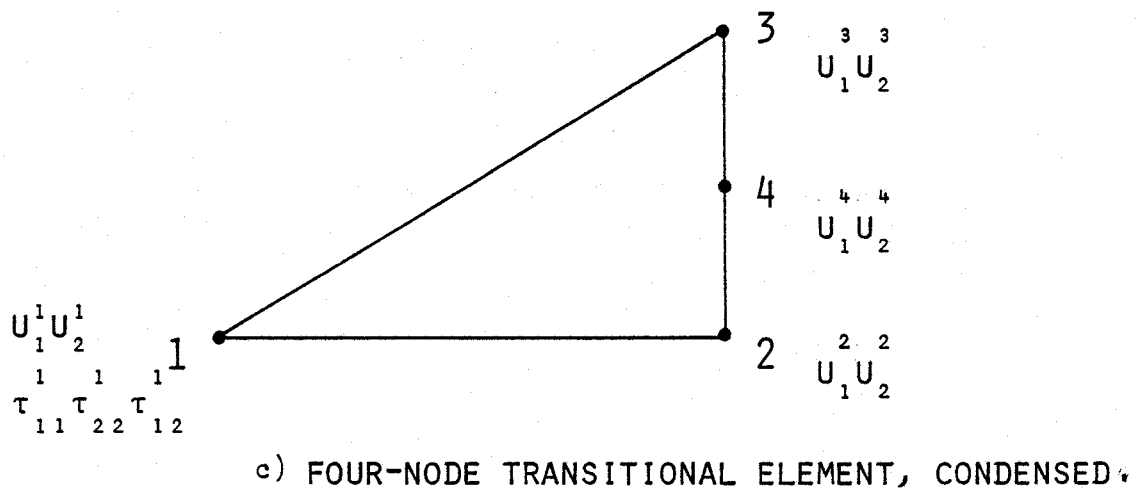
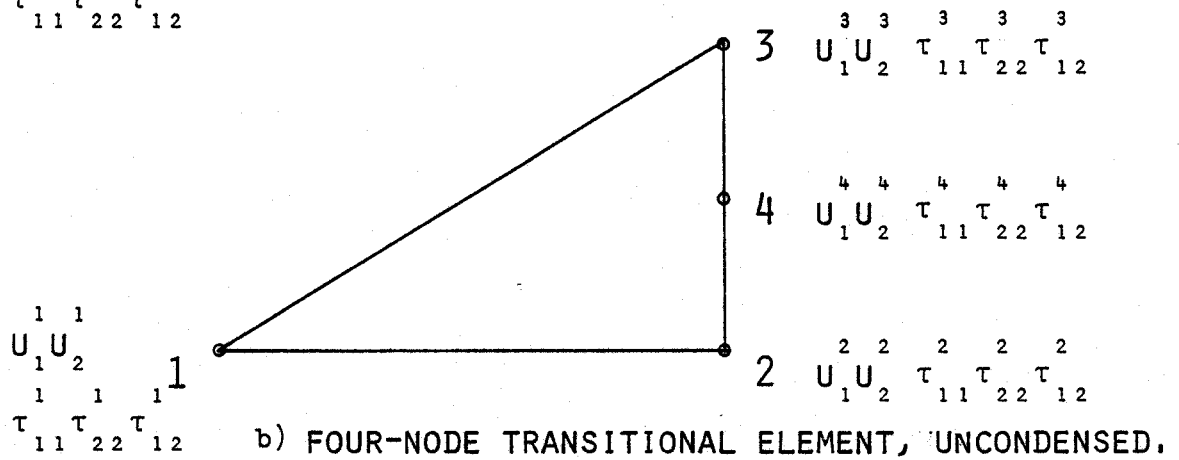
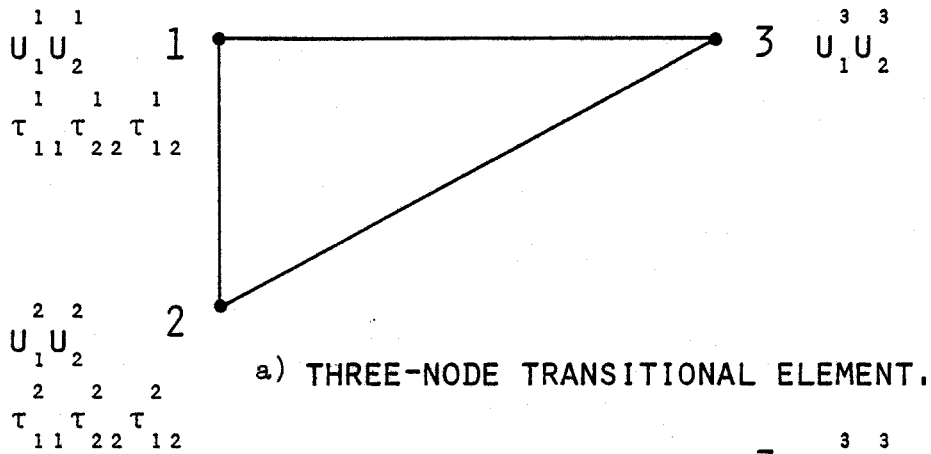
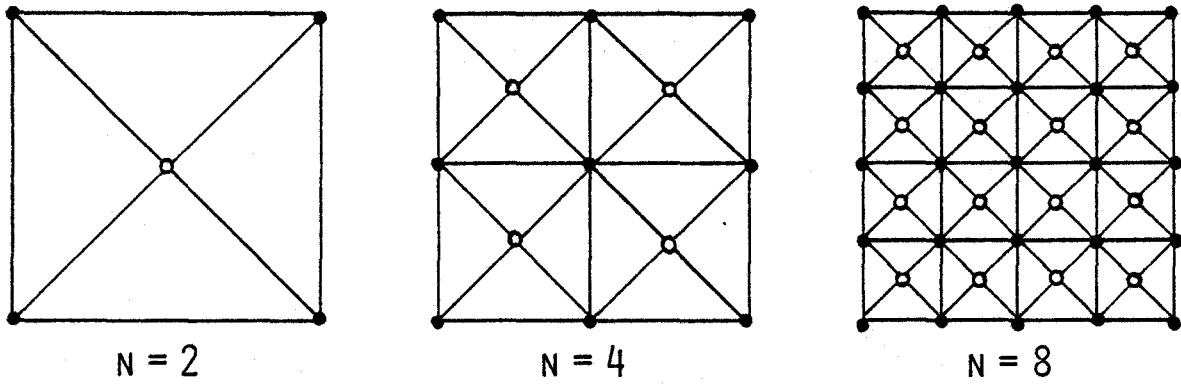
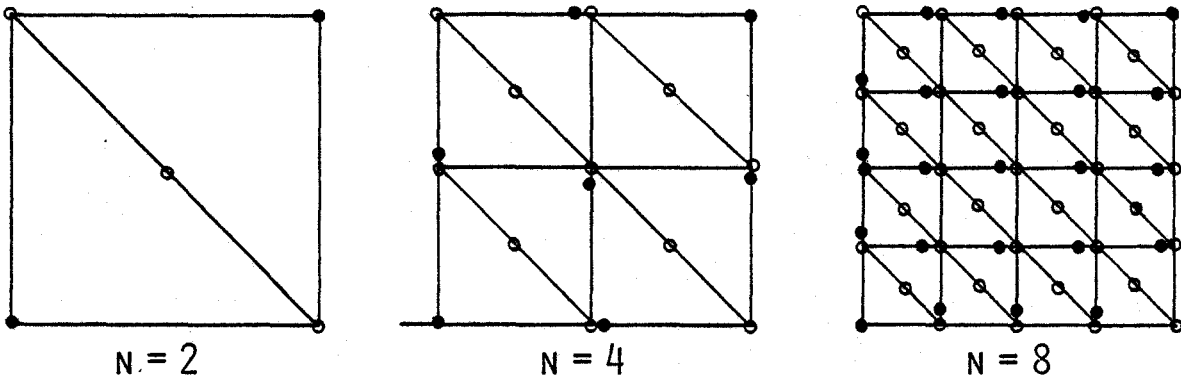


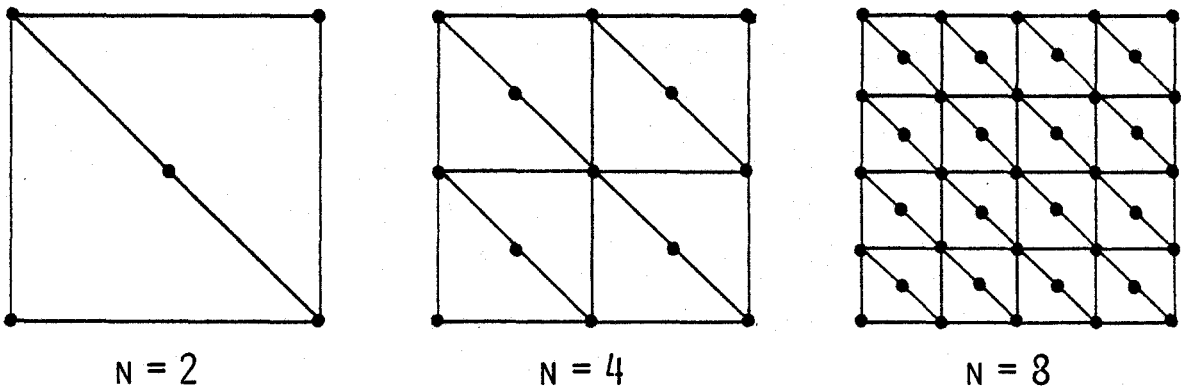
FIG. 3.8: TRIANGULAR MIXED TRANSITIONAL FINITE ELEMENTS USED FOR THE FINITE ELEMENT ANALYSIS OF THE SQUARE PLATE WITH PARABOLICALLY VARYING END LOADS-FIGURE. 3.7.



a) THREE-NODE TRANSITIONAL ELEMENTS.



b) FOUR-NODE TRANSITIONAL ELEMENTS, CONDENSED.



c) FOUR-NODE TRANSITIONAL ELEMENTS, UNCONDENSED.

- NODES WITH STRESS AND DISPLACEMENT DEGREES OF FREEDOM.
- NODES WITH DISPLACEMENT DEGREES OF FREEDOM.

FIG. 3.9: FINITE ELEMENT GRIDS FOR THE SQUARE PLATE WITH PARABOLICALLY VARYING END LOADS.

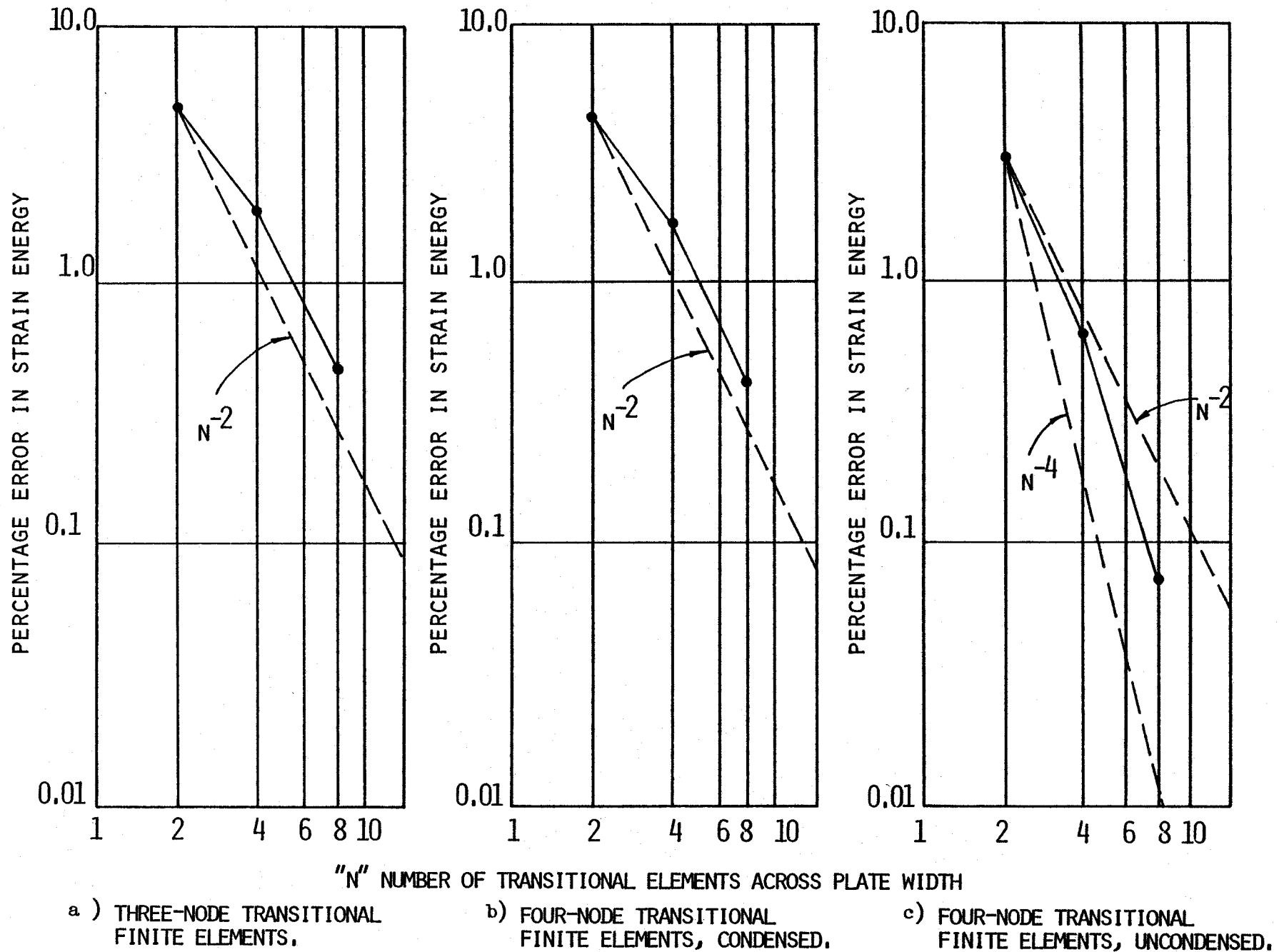
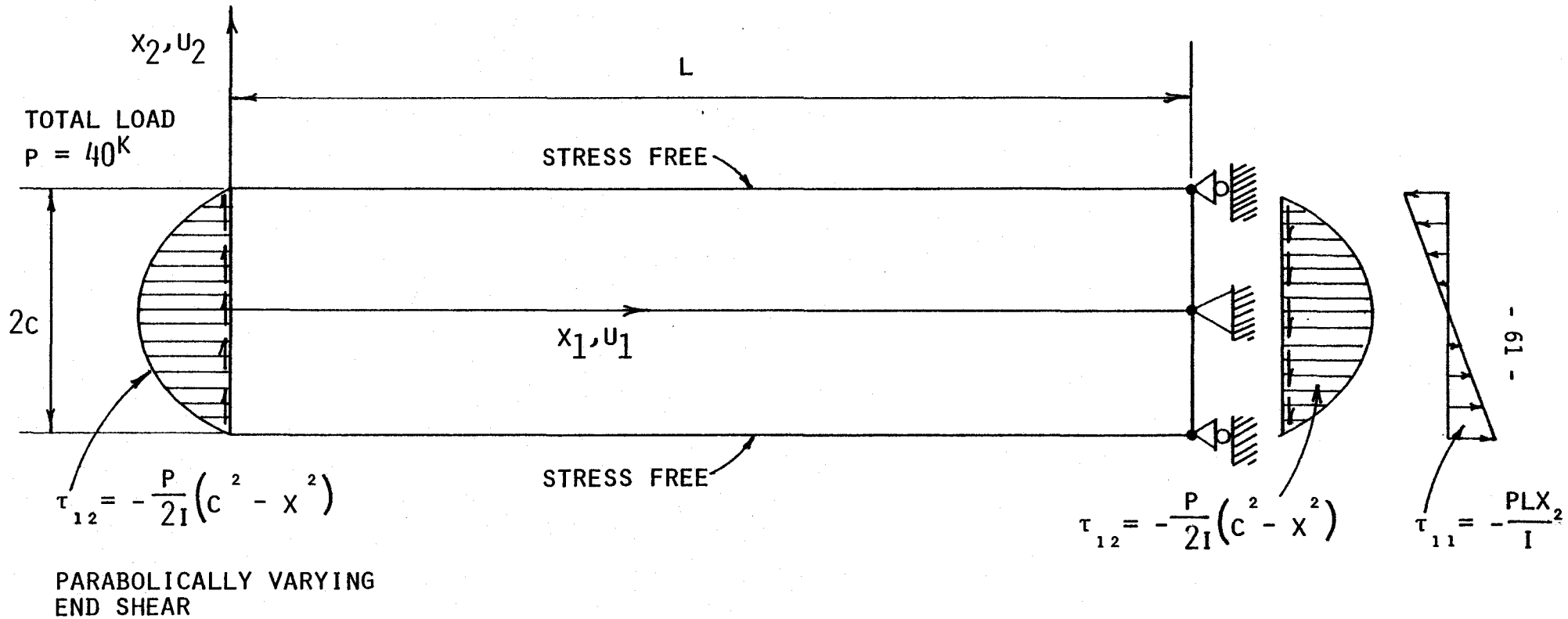
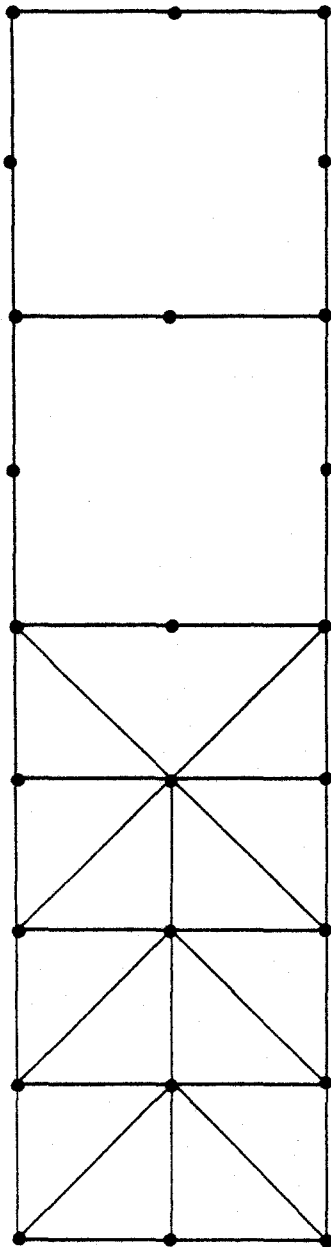


FIG. 3.10: STRAIN ENERGY CONVERGENCE FOR THE SQUARE PLATE WITH PARABOLICALLY VARYING END LOADS.

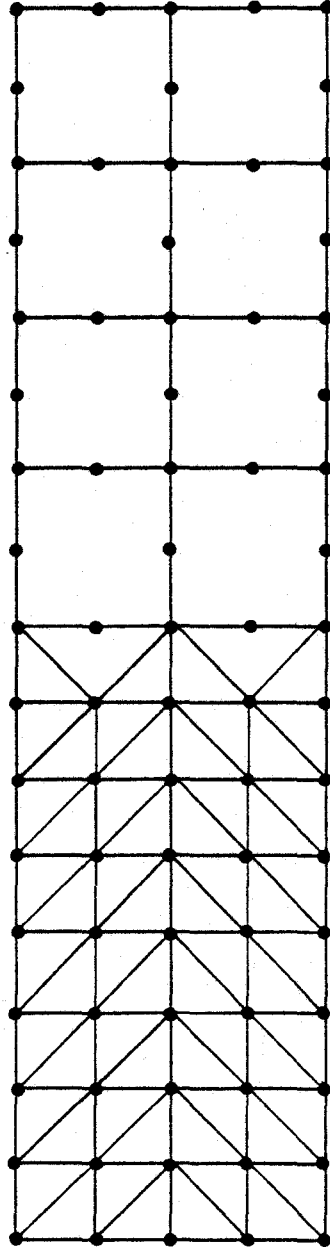


BOUNDARY CONDITIONS:  $u_1(L,0) = u_2(L,0) = u_1(L,-c) = u_1(L,c) = 0$

FIG. 3.11: LINEAR ELASTIC CANTILEVER WITH BOUNDARY TRACTION AND CONDITIONS USED.

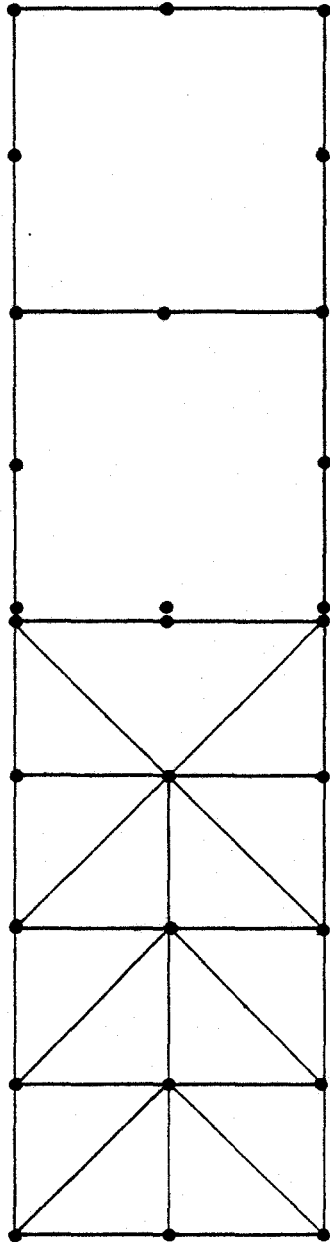


$N = 2$

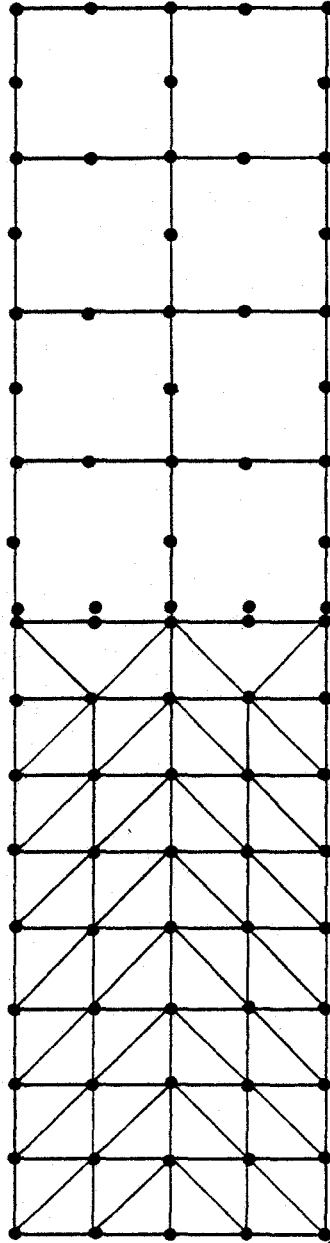


$N = 4$

FIG. 3.12: FINITE ELEMENT GRIDS FOR THE MIXED, CONDENSED MIXED TRANSITIONAL AND ISOPARAMETRIC DISPLACEMENT TYPE FINITE ELEMENTS.



$N = 2$



$N = 4$

FIG. 3.13: FINITE ELEMENT GRIDS FOR THE MIXED, UNCONDENSED MIXED TRANSITIONAL AND ISOPARAMETRIC DISPLACEMENT TYPE FINITE ELEMENTS.

- WITH CONDENSED MIXED TRANSITIONAL ELEMENTS.
- ▲ WITH UNCONDENSED MIXED TRANSITIONAL ELEMENTS.

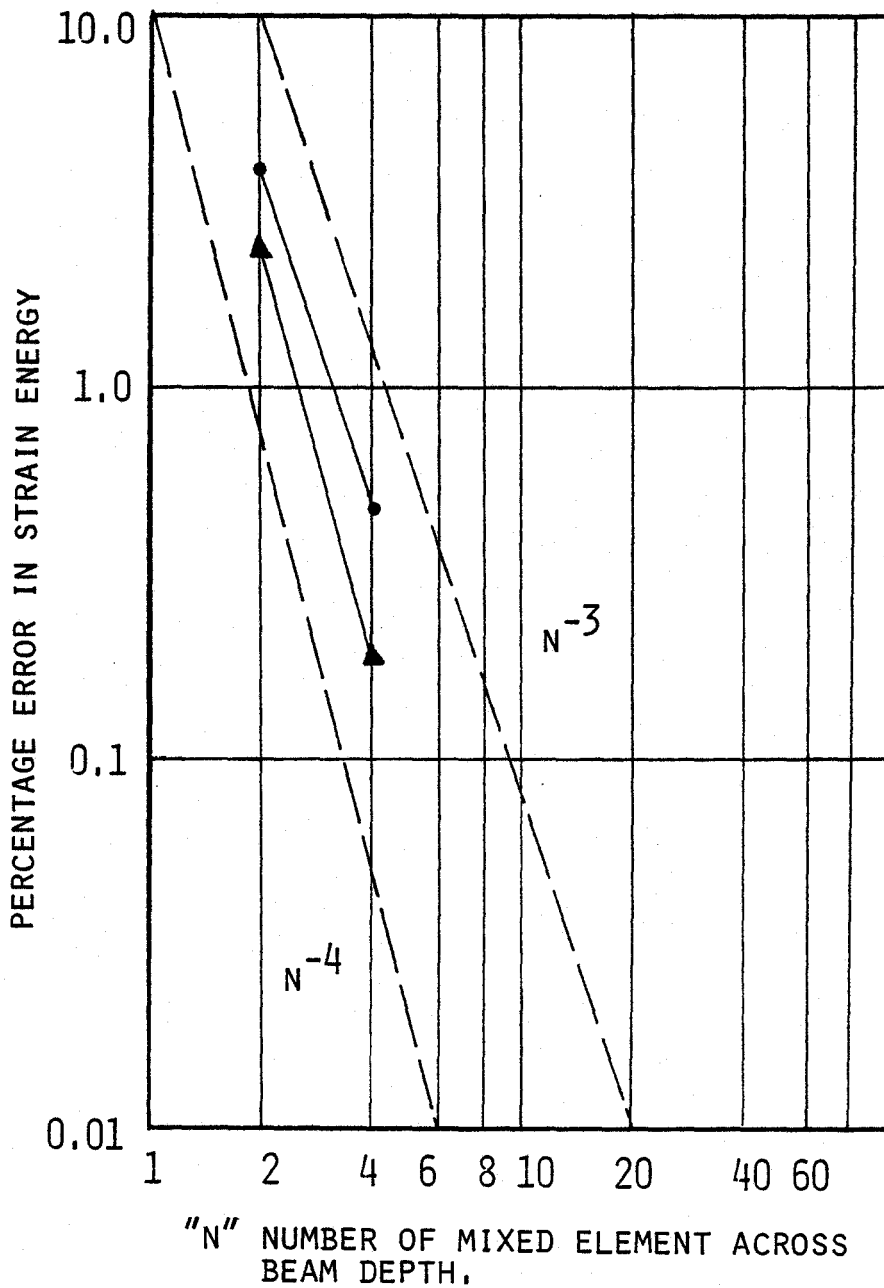


FIG.3.14: STRAIN ENERGY CONVERGENCE FOR THE CANTILEVERED BEAM IN FIGURE 3.11.

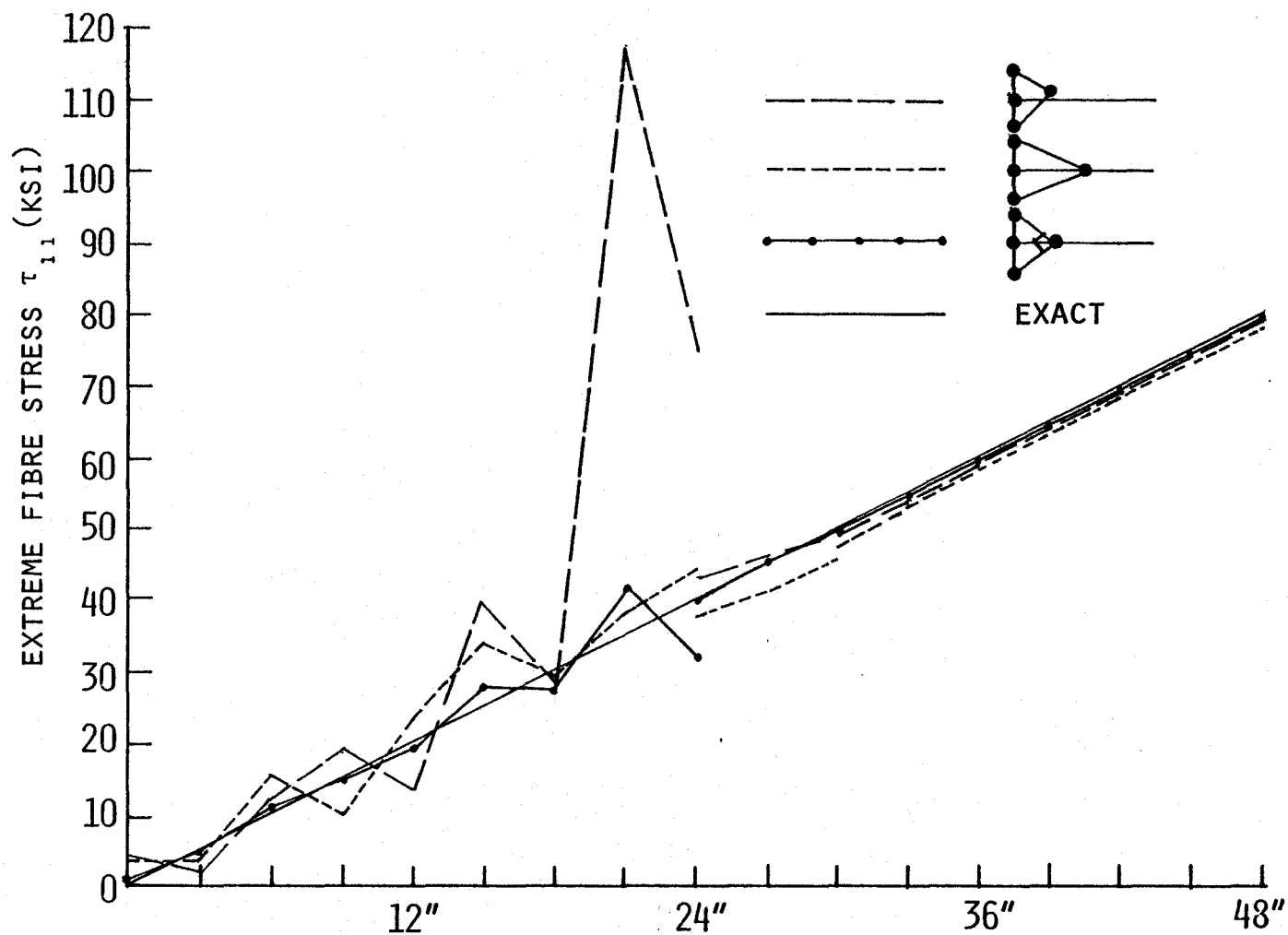
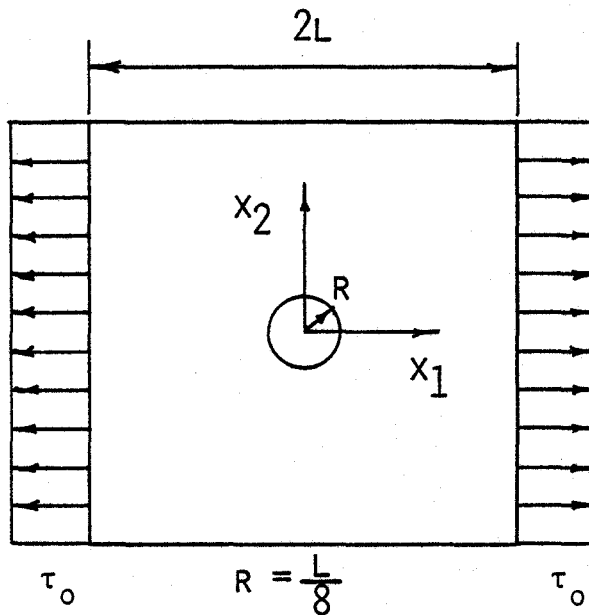


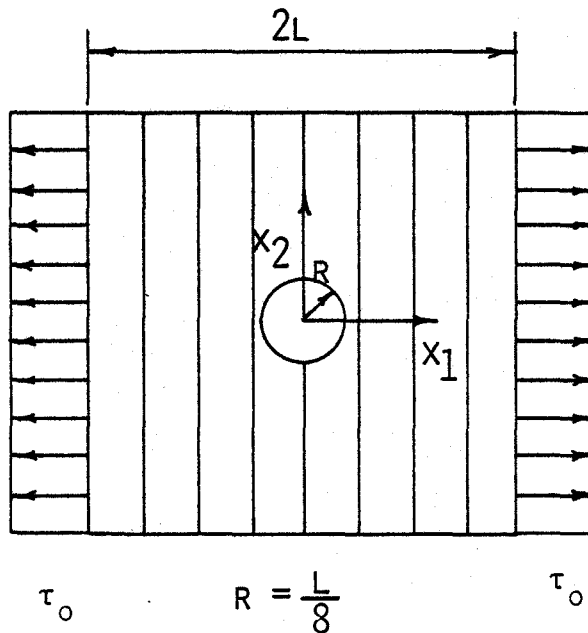
FIG. 3.15: PLOTS OF EXTREME FIBRE STRESS ALONG THE AXIS OF THE CANTILEVER (FIGURE 3.11) FOR VARIOUS SHAPES OF UNCONDENSED FOUR-NODE TRIANGULAR MIXED TRANSITIONAL FINITE ELEMENT.



UNIT THICKNESS

$E = 1.0, \nu = 0.1, \mu = E/2(1+\nu)$

a) ISOTROPIC CASE.



UNIT THICKNESS

$E_1 = 1.0, E_2 = 3.0, \nu_{21} = 0.1, \nu_{12} = 0.3, \mu_{12} = 0.42$

b) ORTHOTROPIC CASE.

FIG. 3.16: PLANE SQUARE PLATE WITH A CIRCULAR HOLE IN THE MIDDLE, ISOTROPIC AND ORTHOTROPIC.

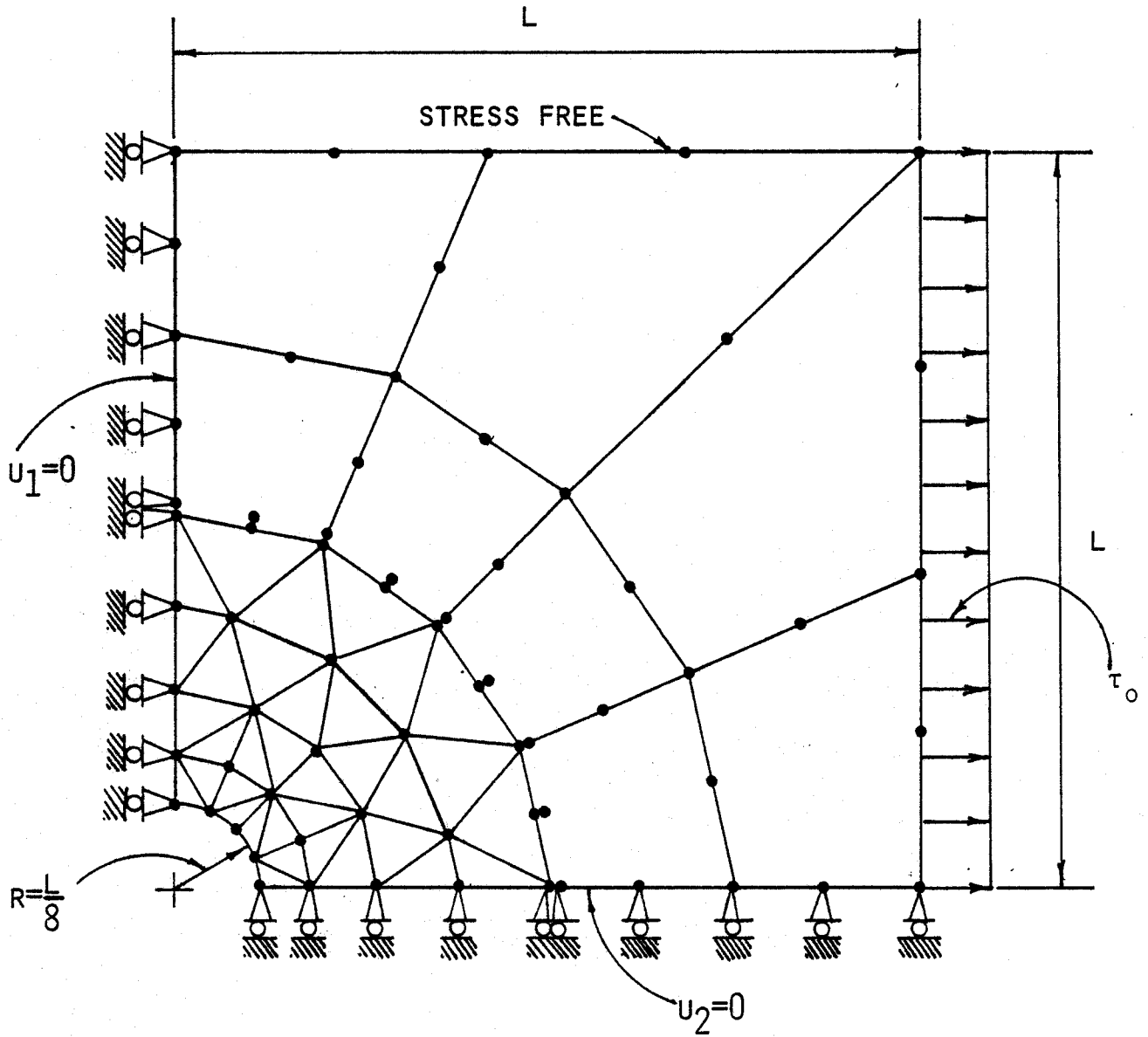


FIG. 3.17: FINITE ELEMENT GRID FOR THE SQUARE PLATE WITH A CIRCULAR HOLE IN THE MIDDLE, GRID I, ISOTROPIC AND ORTHOTROPIC CASES.

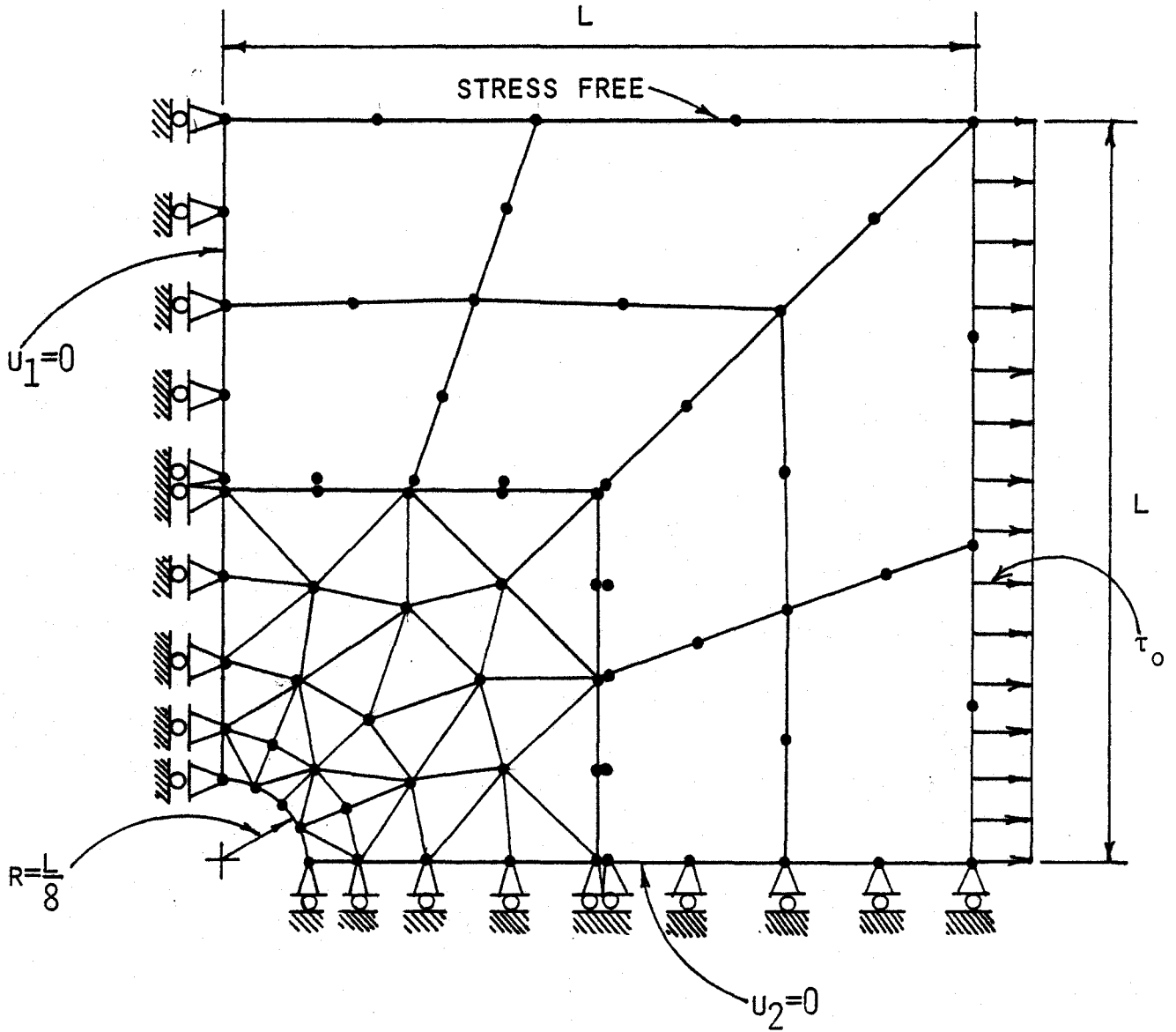
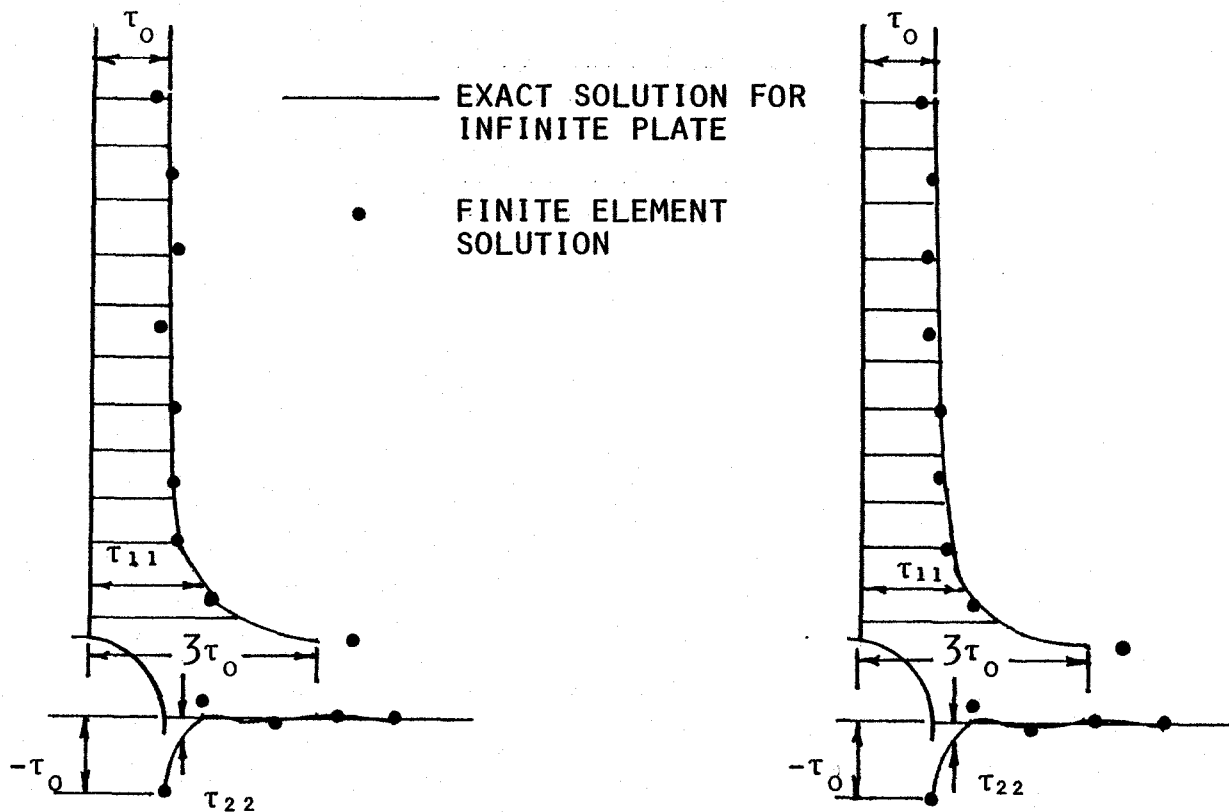


FIG. 3.18: FINITE ELEMENT GRID FOR THE SQUARE PLATE WITH A CIRCULAR HOLE IN THE MIDDLE, GRID II, ISOTROPIC AND ORTHOTROPIC CASES.



a) UNCONDENSED MIXED TRANSITIONAL FINITE ELEMENTS.

b) CONDENSED MIXED TRANSITIONAL FINITE ELEMENTS.

FIG. 3.19: COMPARISON OF FINITE ELEMENT RESULTS FOR THE ISOTROPIC SQUARE PLATE WITH A CIRCULAR HOLE IN THE MIDDLE WITH THEORETICAL RESULTS FOR AN INFINITE PLATE, UNCONDENSED AND CONDENSED MIXED TRANSITIONAL FINITE ELEMENTS.

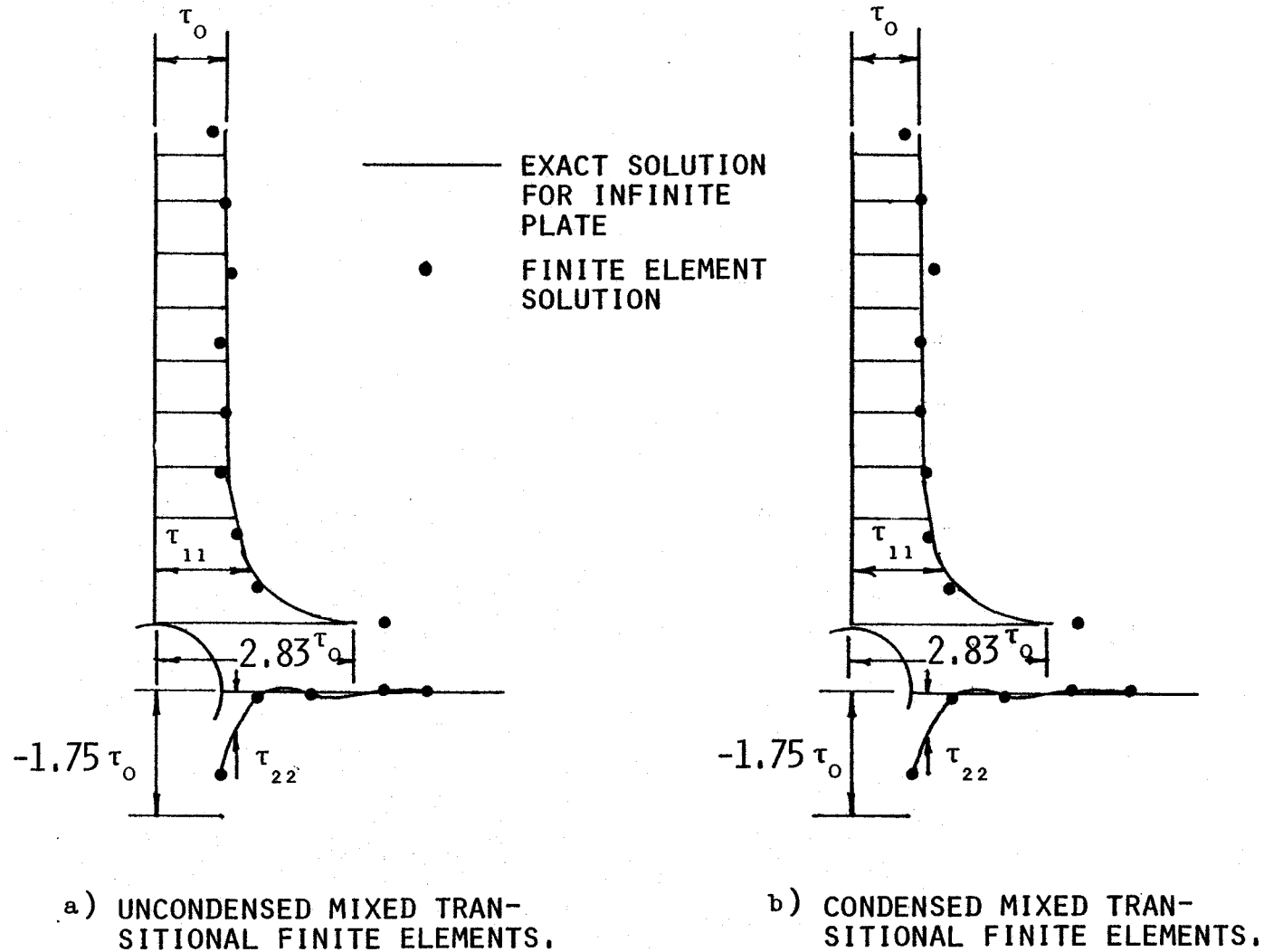


FIG. 3.20: COMPARISON OF FINITE ELEMENT RESULTS FOR THE ORTHOTROPIC SQUARE PLATE WITH A CIRCULAR HOLE IN THE MIDDLE WITH THEORETICAL RESULTS FOR AN INFINITE PLATE, UNCONDENSED AND CONDENSED MIXED TRANSITIONAL FINITE ELEMENTS.

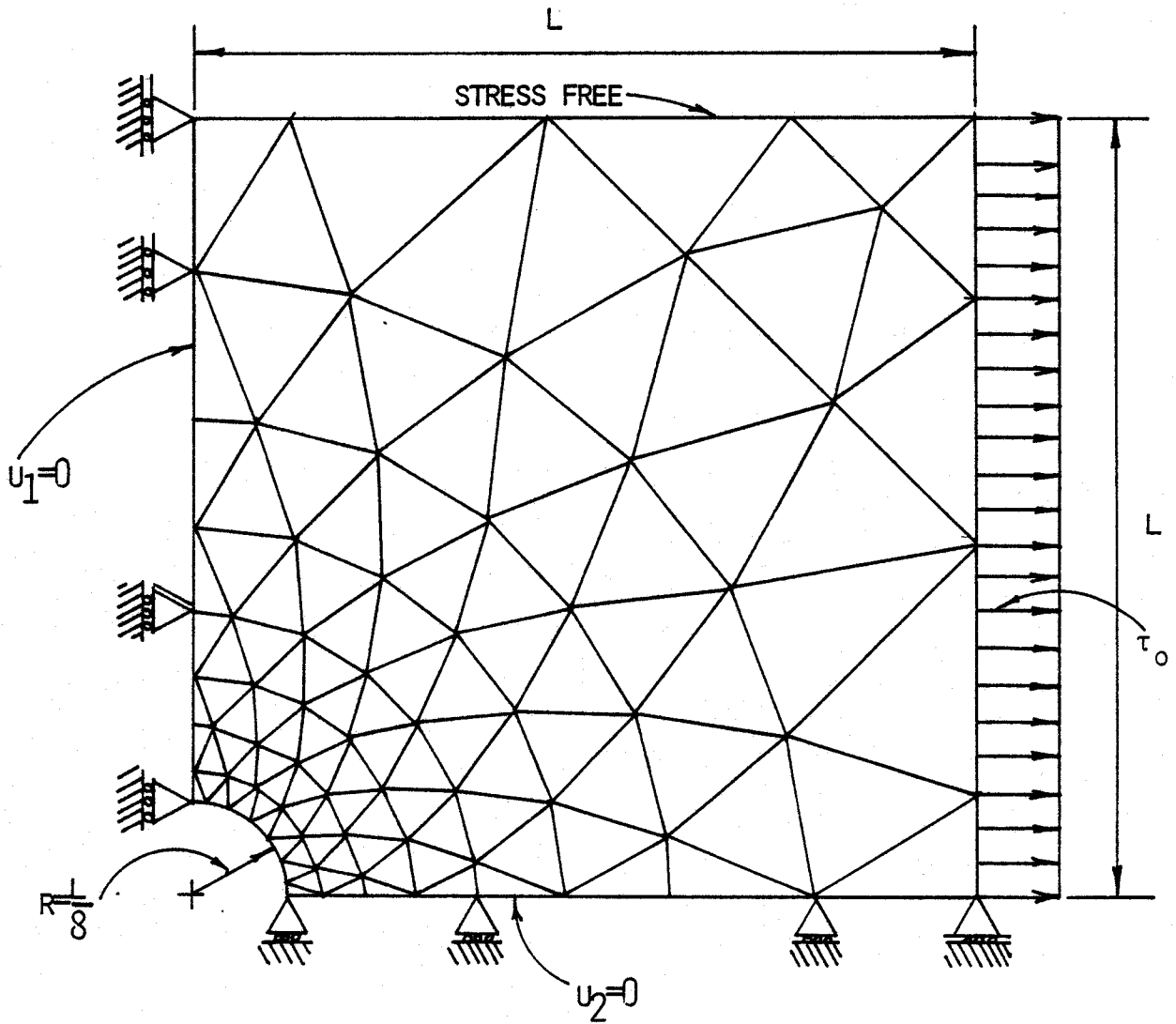


FIG. 3.21: FINITE ELEMENT GRID FOR THE SQUARE PLATE WITH A CIRCULAR HOLE IN THE MIDDLE, REFERENCE [8].

## CHAPTER 4

### LINEAR ELASTIC FRACTURE MECHANICS (LEFM) BY FINITE ELEMENT METHOD

The formulations and numerical tests of the triangular mixed and mixed transitional finite elements have been carried out in the previous chapters. Application of the finite element method to linear elastic fracture mechanics (LEFM) will be presented in this chapter and, in particular, the use of finite element scheme for using the mixed, mixed transitional and isoparametric displacement finite elements in a single finite element mesh. Following a brief account of linear elastic fracture mechanics, various finite element approaches in determining the stress intensity factors are discussed. Details of the direct derivative approach are then given and the classical problems of plates with symmetric edge cracks and a central crack under in-plane loads are analyzed.

#### 4.1 Linear Elastic Fracture Mechanics (LEFM)

Fracture or cracking of a material is the physical separation under severe stress conditions in the presence of a notch or crack in a structure. The concepts and results of LEFM have been used successfully to predict the strength and life of cracked structures, particularly when yielding of the material is confined to a very small region around the crack tip. A brief account of LEFM is presented here.

Generally speaking, there are two approaches for studying fracture, the energy approach and the stress parameter approach. Griffith in 1920 [15, 16] proposed an energy balance argument for coplanar crack growth of a sharp crack. The idea behind Griffith's concept is that a crack will begin to propagate if the energy released during a crack front growth is equal to the energy required to form the new crack surface. This theory, which is valid for brittle materials where the deformations are essentially elastic prior to onset of fracture and where the plastic yielding is confined to a very small region around the crack tip, has been the basis of determining the fracture of cracked bodies. Alternatively Irwin [17], in applying Griffith's concept to solve fracture problems, emphasized the stress conditions in the vicinity of the crack tip. In various papers [17, 18, 19], Irwin pointed out, mostly from a mathematical viewpoint, that in fracture mechanics three basic modes of crack extension can be distinguished. These are:

- a) Mode I - the opening mode where the displacement discontinuity is perpendicular to the plane of the crack;
- b) Mode II - the sliding mode where the displacement discontinuity is in the plane and parallel to the direction of the crack;
- c) Mode III - the tearing mode where the displacement discontinuity is in the plane of the crack but perpendicular to it.

The three different modes of crack extension are illustrated in Figure (4.1). In all these cases, it is assumed that the crack is a straight through cut perpendicular to the plane of the material.

In the case of plane strain or plane stress, where the material contains a straight crack subject to in-plane loadings, only the first two modes of crack extension, Modes I and II, are relevant. For these cases, nonzero stress components are mathematically infinite at the crack tip and the stress state in the neighborhood of the crack can be expressed as follows [17, 20, 21], Figure (4.2):

$$\begin{aligned} \tau_{11} = & \frac{K_I}{(2r)^{1/2}} \cos(\theta/2)[1 - \sin(\theta/2) \sin(3\theta/2)] \\ & - \frac{K_{II}}{(2r)^{1/2}} \sin(\theta/2)[2 + \cos(\theta/2) \cos(3\theta/2)] + \dots \end{aligned} \quad (4.1.1.a)$$

$$\begin{aligned} \tau_{22} = & \frac{K_I}{(2r)^{1/2}} \cos(\theta/2)[1 + \sin(\theta/2) \cos(3\theta/2)] \\ & + \frac{K_{II}}{(2r)^{1/2}} \sin(\theta/2) \cos(\theta/2) \cos(3\theta/2) + \dots \end{aligned} \quad (4.1.1.b)$$

$$\begin{aligned} \tau_{12} = & \frac{K_I}{(2r)^{1/2}} \cos(\theta/2) \sin(\theta/2) \cos(3\theta/2) \\ & + \frac{K_{II}}{(2r)^{1/2}} \cos(\theta/2)[1 - \sin(\theta/2) \sin(3\theta/2)] + \dots \end{aligned} \quad (4.1.1.c)$$

where the non-singular stress terms have been dropped and  $r$  and  $\theta$  are the polar coordinates in the  $x_1$ - $x_2$  plane.  $K_I$  and  $K_{II}$  in Equations (4.1.1a, b and c) are called the stress intensity factors and are

measures of the intensity of the stress singularities at the crack tip.  $K_I$  and  $K_{II}$  are the symmetric and skew-symmetric components of the stress intensity factors and they are associated with the opening (Mode I) and sliding (Mode II) modes of crack extension, respectively. In general, the stress intensity factors are functions of the crack length, the geometry and the external loadings.

The generalized Griffith-Irwin fracture theory states that under external loading, slow crack extension will start when the corresponding stress intensity factors reach their critical values. The critical values of  $K_I$  and  $K_{II}$  for which a crack becomes unstable and propagates are designated as  $K_{IC}$  and  $K_{IIC}$  respectively.  $K_{IC}$  is also sometimes referred to as the fracture toughness. For design purposes, the critical value of a stress intensity factor is assumed to be a material property. For a given crack configuration and principal mode of fracture, a theoretical stress intensity factor is computed and compared with the critical value of stress intensity factor for the same material. The critical value of stress intensity factor is determined experimentally for the same principal mode of fracture and the same environmental conditions as in the actual application. If the computed theoretical stress intensity factor is less than the critical value, then the crack will not propagate. Otherwise, crack propagation will result. Thus, estimation of the critical state of stress at the crack tip reduces to determination of the elastic stress intensity factors.

Irwin [19] also showed that the stress intensity factors are related to the decrease in potential energy of the cracked system per

unit area of crack advance, i.e., the potential energy release rate  $G$ .

For plane problems, the following equations hold:

$$G_I = \frac{-\partial \Pi}{\partial a} \text{ mode I} = \frac{(\kappa + 1) K_I^2}{8\mu} \quad (4.1.2)$$

$$G_{II} = \frac{-\partial \Pi}{\partial a} \text{ mode 2} = \frac{(\kappa + 1)}{8\mu} K_{II}^2 \quad (4.1.3)$$

where  $G_I$  and  $G_{II}$  are the potential energy release rates for Mode I and Mode II, respectively;  $\Pi$  is the potential energy;  $\mu$  is the shear modulus; and the elastic constant  $\kappa$  takes the value  $(3 - 4\nu)$  for plane strain and  $(3 - \nu)/(1 + \nu)$  for plane stress where  $\nu$  is the Poisson's ratio. It should be noted that  $G_I$  and  $G_{II}$  are formally computed by assuming that the crack extends in a plane collinear with the original crack as in Mode I (which is not necessarily the actual direction of crack propagation under a general state of stress, with both  $K_I$  and  $K_{II}$  having nonzero values) and  $G_I$  is in fact the energy release rate in Griffith's theory.

From Equations (4.1.2) and (4.1.3) it is seen that the stress intensity factors and the energy release rates are related and the problem of crack instability can be addressed either in terms of stress intensity factors or energy release rates. Under a general state of loading, both  $K_I$  and  $K_{II}$  corresponding to the opening and sliding modes will attain nonzero values. In this chapter, discussion will be

restricted to those cases where the loadings are symmetric about the crack plane (Mode I type). Consequently, the stress state in the vicinity of the crack tip is symmetric about the crack plane and can be adequately described by the first term in Equation (4.1.1), i.e. only  $K_I$  will attain a nonzero value. Therefore, the crack will extend in an opening mode and only  $K_I$  and  $G_I$  have to be calculated.

#### 4.2 Application of Finite Element Method in Linear Elastic Fracture Mechanics

In any application of LEFM principles, the crack tip stress intensity factors have to be determined. A rigorous determination of the stress intensity factors requires an exact solution of the elasticity problem formulated for the cracked body. In most cases, highly sophisticated mathematical analysis is required and exact solutions are either very difficult or impossible to obtain. The stress intensity factors have been calculated for varying crack size and relatively simple-shaped plates by Paris and Sih [22]. For the more realistic complex shapes encountered in practice, however, numerical techniques are generally required and the finite element method has been successfully used to evaluate the stress intensity factors.

When conventional finite elements with polynomial interpolation functions are used in the crack tip region, the characteristic elastic stress singularity can not be represented and as such indirect procedures have been used. Basically there are two different approaches: the extrapolation of a field parameter near the crack tip using the

calculated displacement or stress fields, or an energy method whereby the potential energy release rate is calculated which is then used to determine the stress intensity factors using Equations (4.1.2) and (4.1.3).

The extrapolation approach has been used by Chan et al. [23] in conjunction with constant stress triangular elements. The product of  $r^{1/2}$  with a stress component as a function of distance  $r$  along a ray emanating from the crack tip is plotted and a tangential extrapolation of this quantity to the crack tip at  $r = 0$  is performed from which the stress intensity factors can be determined using the singular stress solution in Equation (4.1.1). Alternatively, the extrapolation can be based on the product of  $r^{1/2}$  with a displacement. Stress intensity factors within five percent of the accepted values of  $K_I$  are reported. However, such procedures require extremely fine grid refinements near the crack tip and could easily exhaust the storage capacity of most computers. Approximately 2000 degrees of freedom were used to obtain the five percent accuracy reported.

The energy method of calculating the stress intensity factor  $K_I$  has been used by Mowbray [24] and Hayes [25]. The energy method used in reference [24] is very similar to experimental compliance method. The same specimen was analyzed for several cracks of slightly varying length and the compliance was obtained as a function of crack length  $a$ . Numerical differentiation of this relationship with respect to the crack length enables determination of  $G_I$ , and  $K_I$  can be calculated from

Equation (4.1.2). Using this method, again about five percent accuracy was obtained for 1000 degrees of freedom with the constant stress elements. The procedure above, however, requires a separate analysis to be performed for each crack configuration with slightly different crack length and therefore can be very costly.

A path independent integral in plane elasticity, called the J-integral, has been introduced by Rice [26, 27] and is defined as:

$$J = \int_{\Gamma} W dy - \bar{T} \cdot \frac{\partial \bar{u}}{\partial x} ds \quad (4.2.1)$$

where  $W = \int_0^{\epsilon_{ij}} \sigma_{ij} d\epsilon_{ij}$  is the strain energy density,  $\bar{T}$  is the traction vector on curve  $\Gamma$  around the crack tip in relation to a unit outward normal vector  $\bar{n}$ ,  $\bar{u}$  is the displacement vector and  $ds$  is an element of arc-length along the curve  $\Gamma$ , Figure (4.3). It can be shown that the J-integral is equal to the potential energy release rate for a crack assumed to propagate in its own plane. For mode I loading,

$$J = G_I = - \frac{\partial \Pi}{\partial a} = \frac{(\kappa + 1)}{8\mu} K_I^2 \quad (4.2.2)$$

Hence the potential energy release rate for a particular crack configuration can be obtained by evaluating the J-integral and the stress intensity factor  $K_I$  can be determined using Equation (4.2.2) without performing a second analysis for a configuration with a slightly different crack length. The path independence of the J-integral allows its evalu-

ation along a contour far enough away from the crack tip where the finite element solution would be more representative, thus resulting in a better accuracy.

A direct derivative finite element technique, based on the energy release rate, similar to the J-integral, was introduced by Park [28]. Again, a solution for only the original crack length is required and for constant stress triangular elements, it was shown that the direct derivative technique is in fact a numerical analog of the J-integral. Details of the direct derivative method are given in the next section where the method is applied to determine  $K_I$  for linear elasticity problems using the mixed, mixed transitional and isoparametric displacement finite elements. This procedure is adopted because the extreme grid refinement in the crack tip region needed for the extrapolation method is not required and there is no need for a second analysis to determine the potential energy release rate.

Instead of using the aforementioned indirect methods to determine the stress intensity factors, special crack tip elements with direct incorporation of the stress singularity in the interpolation functions can be employed [29 to 32]. Improved accuracy is generally obtained by using such special elements and the stress intensity factors can be obtained directly from the finite element solutions. For example, Tracey [29], using a mesh of isocelus trapezoidal special elements surrounding the crack tip was able to obtain five percent accuracy for  $K_I$  with only 248 degrees of freedom. Although the special singularity elements can be readily incorporated into an existing finite element

program, their versatility in terms of energy convergence rate, changing crack direction and propagation for mixed mode cracking is not clear and are not discussed here.

#### 4.3 Calculation of Mode I Stress Intensity Factor using Direct Derivative Method in Conjunction with Mixed, Mixed Transitional and Isoparametric Displacement Elements

The stress intensity factor  $K_I$  is related to the potential energy release rate  $G_I$  and for plane strain and plane stress problems with unit thickness, this relationship is given by

$$G_I = - \frac{\partial \Pi}{\partial a} = \frac{(\kappa + 1)}{8\mu} K_I^2 \quad (4.3.1)$$

where  $a$  is the crack length and  $\Pi$ ,  $\mu$  and  $\kappa$  have been defined previously (Equation (4.1.2)). The direct derivative approach has been used by Park [28] and Mirza [8, 33] using constant strain triangular finite elements and triangular mixed finite elements, respectively. It has been shown by Tong and Pian [34] that in stress singular problems, the use of high order displacement finite elements will not be able to improve the energy convergence rate and the convergence in strain energy is only linear in plane elasticity, i.e.,  $O(N^{-1})$ . However, it was shown in reference [33] that with mixed finite elements, the strain energy convergence rate is at least  $O(N^{-1})$  and using triangular mixed finite element with linear stress and displacement approximations, a strain energy convergence rate of  $O(N^{-2})$  has been obtained. Also, improved accuracies were demonstrated for the energy release rate and  $K_I$  values

with mixed finite elements. It has been pointed out in Chapter 2, however, that the use of mixed finite elements alone requires a much larger computer storage. Therefore it is proposed to use the mixed finite elements near the crack tip where there is a stress singularity and large stress gradients, and to use the eight-node isoparametric displacement finite elements in the region away from the crack tip where stress distribution is more regular. The isoparametric finite elements are connected to the mixed finite elements via the mixed transitional elements developed in Chapter 2. It is expected that the proposed scheme will reduce the computer storage required while maintaining the advantage of improved convergence rate over that when only the displacement type finite elements are used.

In the mixed finite element analysis, the element matrix equations (Equations (2.3.19) and (3.1.1)) are assembled using the usual routines of finite element analysis. The global matrix equation is given by:

$$\begin{bmatrix} \underline{0} & \underline{A}^T \\ \underline{A} & \underline{-B} \end{bmatrix} \begin{Bmatrix} \underline{u} \\ \underline{\tau} \end{Bmatrix} = \begin{Bmatrix} \underline{f} \\ \underline{0} \end{Bmatrix} \quad (4.3.2)$$

and the potential energy can be expressed as [33]:

$$\Pi_M = \frac{1}{2} \langle \underline{u}^T \quad \underline{\tau}^T \rangle \begin{bmatrix} \underline{0} & \underline{A}^T \\ \underline{A} & \underline{-B} \end{bmatrix} \begin{Bmatrix} \underline{u} \\ \underline{\tau} \end{Bmatrix} - \underline{u}^T \underline{f} \quad (4.3.3)$$

where matrices  $\underline{A}$  and  $\underline{B}$  are global matrices obtained by assembling the

element matrices  $\underline{A}^e$ 's and  $\underline{B}^e$ 's (see Equation (3.1.1)),  $\underline{f}$  is the generalized load vector and  $\underline{u}$  and  $\underline{\tau}$  are the unknown nodal displacements and stresses. The potential energy release rate is obtained by differentiating  $\Pi_M$  with respect to the crack length  $a$  in the following manner:

$$\frac{\partial \Pi_M}{\partial a} = \left\langle \frac{\partial \underline{u}^T}{\partial a} \quad \frac{\partial \underline{\tau}^T}{\partial a} \right\rangle \begin{bmatrix} \underline{0} & \underline{A}^T \\ \underline{A} & -\underline{B} \end{bmatrix} \begin{Bmatrix} \underline{u} \\ \underline{\tau} \end{Bmatrix} - \begin{Bmatrix} \underline{f} \\ \underline{0} \end{Bmatrix} + \frac{1}{2} \langle \underline{u}^T \quad \underline{\tau}^T \rangle \frac{\partial}{\partial a} \begin{bmatrix} \underline{0} & \underline{A}^T \\ \underline{A} & -\underline{B} \end{bmatrix} \begin{Bmatrix} \underline{u} \\ \underline{\tau} \end{Bmatrix} - \underline{u}^T \frac{\partial \underline{f}}{\partial a} \quad (4.3.4)$$

However, the first term in Equation (4.3.4) is zero because Equation (4.3.2) has been satisfied exactly in the finite element analysis. Therefore the potential energy release rate becomes:

$$\frac{\partial \Pi_M}{\partial a} = \frac{1}{2} \langle \underline{u}^T \quad \underline{\tau}^T \rangle \frac{\partial}{\partial a} \begin{bmatrix} \underline{0} & \underline{A}^T \\ \underline{A} & -\underline{B} \end{bmatrix} \begin{Bmatrix} \underline{u} \\ \underline{\tau} \end{Bmatrix} - \underline{u}^T \frac{\partial \underline{f}}{\partial a} \quad (4.3.5)$$

Furthermore, if the body is loaded by surface tractions applied on the boundary other than the crack surface, then the load vector  $\underline{f}$  is independent of the infinitesimal change in the crack length, i.e.,  $\partial \underline{f} / \partial a = 0$ . Thus from Equations (4.3.1) and (4.3.5):

$$\frac{-\partial \Pi_M}{\partial a} = \frac{(\kappa + 1)}{8\mu} K_I^2 = -\frac{1}{2} \langle \underline{u}^T \quad \underline{\tau}^T \rangle \frac{\partial \underline{S}}{\partial a} \begin{Bmatrix} \underline{u} \\ \underline{\tau} \end{Bmatrix} \quad (4.3.6)$$

where  $\underline{S}$  is the master finite element matrix in Equation (4.3.2) and  $\partial \underline{S} / \partial a$  represents the change in the master finite element matrix per unit crack extension.

A crack extension can be accommodated using the mesh shown in Figure (4.4) by rigidly translating all nodes on and within the contour  $\Gamma_0$  about the crack tip by a very small amount  $\Delta a$  in the  $x_1$ -direction. All other nodes remain fixed. Thus the master finite element matrix, which depends on individual element geometries and elastic properties, remain unchanged in the region interior to  $\Gamma_0$  and exterior to  $\Gamma_1$ . Therefore the contributions to  $\partial S / \partial a$  come from only the band of elements between the contours  $\Gamma_0$  and  $\Gamma_1$ , Figure (4.4) and:

$$\frac{\partial \Pi_M}{\partial a} = \frac{1}{2} \langle \underline{u}^T \quad \underline{\tau}^T \rangle \frac{\partial S}{\partial a} \begin{Bmatrix} \underline{u} \\ \underline{\tau} \end{Bmatrix} = \frac{1}{2} \langle \underline{u}^T \quad \underline{\tau}^T \rangle \sum_{i=1}^{E^0} \frac{\partial S_i^0}{\partial a} \begin{Bmatrix} \underline{u} \\ \underline{\tau} \end{Bmatrix} \quad (4.3.7)$$

where  $\underline{u}$  and  $\underline{\tau}$  are the nodal variables for the nodes on  $\Gamma_0$  and  $\Gamma_1$ ;  $E^0$  is the number of elements between the contours  $\Gamma_0$  and  $\Gamma_1$ ; and  $S_i^0$  are the element matrices. The change in the element matrix can be calculated directly as:

$$\frac{\partial S_i}{\partial a} = \frac{\partial S_i}{\partial x_{1j}} \frac{\partial x_{1j}}{\partial a} \quad (4.3.8)$$

where the nodal coordinates are thought of as functions of the crack length  $a$ . The derivatives  $\partial x_{1j} / \partial a$  are then either unity or zero, depending on whether  $x_{1j}$  is the  $x_1$ -coordinate of a node located on  $\Gamma_0$  or not. Alternatively,  $\partial S_i / \partial a$  can be approximated by a forward finite difference scheme as:

$$\frac{\partial S_i^0}{\partial a} = \frac{\Delta S_i^0}{\Delta a} = \frac{1}{\Delta a} [S_i^0_{a + \Delta a} - S_i^0_a] \quad (4.3.9)$$

where  $S_i^0$  is calculated for the initial crack length  $a$ ; and  $S_i^0_{a + \Delta a}$  the same matrices when the  $x_1$  coordinates of all of the nodes lying on  $\Gamma_0$  have been incremented by an amount  $\Delta a$ . Thus from Equation (4.3.7), the potential energy release rate can be calculated as follows.

The master finite element matrix equations need only be solved once, i.e., for the initial crack length  $a$ . After obtaining this solution, the potential energy release rate can be calculated in a discrete manner by pre- and post-multiplying the differentiated matrices of Equation (4.3.9) with the solution vectors for the corresponding nodal variables and then summing these over all the elements between  $\Gamma_0$  and  $\Gamma_1$ , i.e.,

$$\frac{\Delta \Pi_M}{\Delta a} = \frac{1}{2} \sum_{i=1}^{E^0} \frac{\langle \underline{u}_i^e \quad \underline{\tau}_i^e \rangle^T [S_i^0_{a + \Delta a} - S_i^0_a]}{\Delta a} \begin{Bmatrix} \underline{u}_i^e \\ \underline{\tau}_i^e \end{Bmatrix} \quad (4.3.10)$$

where  $\underline{u}_i^e$  and  $\underline{\tau}_i^e$  are the nodal displacement and stress degrees of freedom for the nodes corresponding to the  $i^{\text{th}}$  element within the contour  $\Gamma_0$  and  $\Gamma_1$ . After computing  $\Delta \Pi_M / \Delta a$  using Equation (4.3.10), the stress intensity factor  $K_I$  can be calculated as:

$$K_I = \sqrt{\frac{8\mu}{(\kappa + 1)} \left[ \frac{-\Delta\Pi_M}{\Delta a} \right]} \quad (4.3.11)$$

It should be pointed out that the contour  $\Gamma_0$  to be translated has to lie inside the body and enclose the crack tip. However, it can be shrunk to a single node at the crack tip so that the summation in Equation (4.3.10) extends over the elements adjacent to the crack tip only.

A typical finite element mesh, when the direct derivative method is used in conjunction with the mixed, mixed transitional and isoparametric displacement finite elements, is shown in Figure (4.5a). The change in the finite element mesh is illustrated in Figure (4.5b). The crack extension is accommodated by rigidly translating all nodes on and within a contour  $\Gamma_0$  about the crack tip by a small amount  $\Delta a$  as explained previously. However, it should be noted that the contours  $\Gamma_0$  and  $\Gamma_1$  are kept within the region where only mixed finite elements are used. The change in potential energy is again given by Equation (4.3.7) and can be calculated as described earlier in this section. A subroutine (DENERG) has been written to perform the calculations described above for the direct derivative method of evaluating the potential energy release rate. For the purpose of computer programming, it is convenient to classify the mixed finite elements within the contours  $\Gamma_0$  and  $\Gamma_1$  into two categories; mixed elements with two nodes on contour  $\Gamma_0$  are classified as element type I and elements with only one node on contour  $\Gamma_0$  are classified as element type II. Derivations of the changes in element matrices in Equation (4.3.9), i.e.  $S_{-1}^0 + \Delta a$  -  $S_{-1}^0$ ,

are presented in Appendix D for both types of mixed elements. The subroutine DENERG is included in the program listing in Appendix E.

#### 4.4 Numerical Examples

Applications of the energy approach described in the previous section are presented in this section. The stress intensity factor  $K_I$  for plates with symmetric edge cracks and a central crack under inplane loads are computed and compared with results available in the literature. Three different problems are analyzed and presented below.

##### 4.4.1 Isotropic Rectangular Plates with Symmetric Edge Cracks and a Central Crack

Two plane strain problems, isotropic rectangular plates one with symmetric edge cracks and the other with a central crack are analyzed. The details of the two plates are shown in Figure (4.6). Because of symmetry about the  $x_1$  and  $x_2$  axes, only a quarter of the plate is analyzed in each case and this is shown in Figure (4.6) as shaded areas along with the respective boundary conditions. The finite element mesh used in both problems is shown in Figure (4.7). Mixed finite elements are used in the near crack tip region and only four eight-node isoparametric displacement finite elements are used in the region away from the crack tip as indicated. Two four-node and four three-node mixed transitional (only for condensed version) elements are used to connect the mixed and isoparametric finite elements. It should be noted that the configuration of the four-node mixed transitional finite

elements (uncondensed) conforms with the requirements discussed in Section 3.3. Also indicated in Figure (4.7) are the ratios of the radii  $r_{\Gamma_0}$  to the crack length  $a$  (0.0, 0.1, 0.2). These are used to calculate the potential energy release rates for a crack extension of  $\Delta a$  in the finite element analyses as described in the previous section. Although it is sufficient to solve each problem once for the initial crack length  $a$ , the finite element analysis is performed every time here when the contour  $\Gamma_0$  (with  $\frac{r_{\Gamma_0}}{a} = 0.0, 0.1, 0.2$ ) is translated by the amount  $\Delta a = 5 \times 10^{-6} a$  in the direction of the crack. The analyses are carried out first with uncondensed transitional finite elements (which require no three-node transitional elements) and then repeated with condensed transitional finite elements.

The potential energy release rate, in the discretized form, can be expressed as

$$G_I = \frac{-\Delta\Pi}{\Delta a} \quad (4.4.1.1)$$

$$\text{and } \Delta\Pi = \Pi_{r_{\Gamma_0}} - \Pi_0$$

where  $\Pi_0$  is the potential energy associated with the initial crack and  $\Pi_{r_{\Gamma_0}}$  when the crack tip has been moved by an amount  $\Delta a$ . The crack intensity factor is then calculated by using Equation (4.3.11) which for plane strain problems reduces to the following:

$$K_I = \sqrt{\frac{E}{(1 - \nu^2)} \left( \frac{-\Delta\Pi}{\Delta a} \right)}. \quad (4.4.1.2)$$

The results obtained with the uncondensed transitional elements are very nearly the same as those obtained with the condensed transitional elements. Only the uncondensed elements results will be presented here. The numerical results for the plate with symmetric edge cracks are given in Table (4.1) and those for the plate with a central crack in Table (4.2). The crack stress intensity factor for the former is compared with nearly exact  $K_I$  obtained by Bowie [35] and that for the plate with a central crack with  $K_I$  by Bowie and Neal [36]. In both cases, very satisfactory results are obtained (using a reasonably crude grid), with the smallest percentage errors obtained for the contour  $\Gamma_0$  with radius  $r_{\Gamma_0} = 0.1 a$ . The errors in  $K_I$  for the plate with symmetric edge cracks and that with a central edge crack are 3.71% and 5.74%, respectively. In general, the accuracy of the value of  $K_I$  calculated will depend on the contour  $\Gamma_0$  used to calculate the potential energy release rate and personal judgement and experience have to be relied upon to determine the best values.

$\frac{r_{\Gamma_0}}{a}$	$-\frac{E\Pi}{\tau_0^2 hbt}$	$-\frac{10^6 E\Delta\Pi}{\tau_0^2 hbt}$	$-\frac{aE \Delta\Pi}{\tau_0^2 hbt \Delta a}$	$\frac{K_I}{\tau_0 \sqrt{a}}$	Error %
0.0	1.05748361	1.281555	0.256311	1.83845	14.04
0.1	1.05748394	1.609364	0.321873	2.05939	3.71
0.2	1.05748389	1.557822	0.311564	2.02614	5.27
Initial Crack	1.05748233	EXACT $K_I$ ; ref, [35]		2.13884	

TABLE 4.1: Stress intensity factors from the finite element analysis of the rectangular plate with symmetric edge cracks, Figure 4.6(a). (Mixed, Mixed Transitional and 8-node isoparametric finite elements.)

$\frac{r_{\Gamma_0}}{a}$	$-\frac{E\Pi}{\tau_0^2 hbt}$	$-\frac{10^6 E\Delta\Pi}{\tau_0^2 hbt}$	$-\frac{aE \Delta\Pi}{\tau_0^2 hbt \Delta a}$	$\frac{K_I}{\tau_0 \sqrt{a}}$	Error %
0.0	1.0456331	1.302753	0.260551	1.85286	16.20
0.1	1.0456335	1.548342	0.329668	2.08418	5.74
0.2	1.0456334	1.614274	0.322855	2.06253	6.72
Initial Crack	1.0456318	EXACT $K_I$ ; ref, [36]		2.10922	

TABLE 4.2: Stress intensity factors from the finite element analysis of the rectangular plate with a central crack, Figure 4.6(b). (Mixed, Mixed Transitional and 8-node isoparametric finite elements.)

The sensitivity of the calculated values of the energy release rate  $G_I$  to the magnitude of  $\Delta a$  used is also studied. It is found that the calculated  $G_I$  values are relatively insensitive to the magnitude of

$\Delta a$  used for these problems. In general, of course, the size of  $\Delta a$  will affect accuracy of  $G_I$ . Thus the values of  $\Delta a = 5 \times 10^{-6} \times a$  used in the present analyses is very reasonable.

The same problems have been analyzed by Mirza and Olson [33] using the mixed finite elements alone and the finite element grid used is shown in Figure (4.8). It was found that the results with the least percentage error were also obtained for the contour  $\Gamma_0$  with radius  $r_{\Gamma_0} = 0.1 a$ . Errors in the stress intensity factors  $K_I$  obtained for the plate with symmetric edge cracks and that with a central crack were 1.97% and 0.89%, respectively. A comparison of the results in reference [33] with that from the present analysis is given in Table (4.3). It is observed that the stress intensity factors  $K_I$  from the present analysis are not as accurate because of the cruder finite element grids used. However, these are still very reasonably accurate. The computer storage requirement for the global matrix in the present analyses is reduced by more than 10 times which is a very significant improvement. Also, the number of elements and degrees of freedom required are reduced. The calculated values of  $K_I$  from the present analysis can be improved by refining the finite element grid in the crack tip region. The storage requirement is still expected to be much less than that reported in reference [33]. Plots of normal stresses on the crack face OA (Figure (4.6)) are shown in Figure (4.9). The values of the peak stress obtained at the crack tip are about 5.2 times  $\tau_0$ .

Author(s)	Number of Elements	Degrees of Freedom	Storage Req'd for Global Matrix	Accuracy of $K_I$ Error %	Type of Element
Mirza [8]	174	505	111,100	1.97	Mixed triangles*, (Symmetric edge cracks).
Mirza [8]	174	505	111,100	0.89	Mixed triangles*, (Central crack).
Present	52	190	10,807	3.71	Mixed triangles*, transitional elements, 8-node isoparametric finite elements, (Symmetric edge cracks).
Present	52	190	10,807	5.74	Mixed triangles*, transitional elements, 8-node isoparametric finite elements, (Central crack).

TABLE 4.3: Comparison of stress intensity factors from the present analyses and reference [33].

\* Plane strain mixed finite elements; displacement and stress linear.

Finally, it should be emphasized that the four-node mixed transitional finite element configuration (shape and orientation) used satisfies the requirement in Section (3.3) regarding the orientation problems. In fact, in this work, the stress fluctuations due to orientation problems of the four-node mixed transitional element were first observed when the problem of a rectangular plate with symmetric edge cracks was analysed, Figure (4.10). When uncondensed transitional elements, which

fail to comply with the requirements in Section (3.3) were used, the calculated stress intensity factor  $K_I$  indicated an error of more than 50%. Thus the present analysis also serves to confirm the orientation problems discussed previously.

#### 4.4.2 Orthotropic Square Plate with a Central Crack

A square orthotropic plate ( $2b \times 2c$ ) with a central crack of length  $2a$  as shown in Figure (4.11) is analysed for the plane stress state. The lines of material symmetry coincide with the  $x$  and  $y$  axes. Again, due to symmetry, only one quarter of the plate is analysed and the finite element grid used is shown in Figure (4.12). Note that due to the geometry of the problem, it is found convenient to use only the mixed finite elements. Values of  $K_I$  are calculated for different ratios of the principal moduli of elasticity,  $E_x/E_y$ . The results are then compared with the numerical results obtained by Bowie and Freese [37] through an extension of the modified mapping-collocation technique. The analytical solution given in [37] is characterized by two parameters,  $\eta_1$  and  $\eta_2$ , which are related to the material properties by the following:

$$\eta_1 \eta_2 = (E_x/E_y)^{1/2} \tag{4.4.2.1}$$

$$\eta_1 + \eta_2 = \sqrt{2} \left\{ (E_x/E_y)^{1/2} + E_x/2\mu_{xy} - \nu_{yx} \right\}^{1/2}. \tag{4.4.2.2}$$

In determining the stress intensity factor  $K_I$ , the parameter  $\eta_1$  is kept

as unity and  $\eta_2^2 (= E_x/E_y)$  is left as the parameter to be varied. For the present finite element analysis, however, all values of the material properties are needed. The value of the shear modulus of elasticity is taken to be unity in all of the analyses and for different values of  $\eta_2^2$ , i.e.  $E_x/E_y$ , the principal Moduli ( $E_x$  and  $E_y$ ) and the Poisson's ratios are chosen so that Equation (4.4.2.2) is satisfied. Table (4.4) summarizes the material properties used. The potential energy release rate  $G_I$  is calculated using the contour  $\Gamma_0$  as indicated in Figure (4.12). To compare with the results in [37],  $G_I$  is converted to the stress intensity factor  $K_I$ . In the case of a crack propagating in its own plane in an orthotropic body,  $G_I$  and  $K_I$  are related by [38]:

$$G_I = \pi K_I^2 \left( \frac{1}{2E_x E_y} \right)^{1/2} \left\{ \left( \frac{E_x}{E_y} \right)^{1/2} + \frac{2 \left( \frac{\nu_{yx}}{E_x} \right) + \frac{1}{\mu_{xy}}}{\frac{2}{E_x}} \right\}^{1/2} . \quad (4.4.2.3)$$

A comparison of the results from the present analysis and those of Bowie and Freese is given in Table (4.5). It is observed that an excellent agreement is obtained and differences in  $K_I/K_\infty$  are less than 1% except or  $E_x/E_y = 4.5$  where the difference is 1.16%. In order to test the sensitivity of the finite element solutions to different values of material properties while keeping  $\eta_1$  and  $\eta_2$  constant, a different set of elastic properties were used for the case  $\eta_2^2 = 0.7$ . It was found that the values of  $K_I$  calculated are almost the same as that given in Table (4.5). This agrees with Bowie's results that  $K_I$  depends only on the two parameter  $\eta_1$  and  $\eta_2$  given by Equations (4.4.2.1) and (4.4.2.2).

$\eta_2^2 = E_x/E_y$	$E_x$	$E_y = E_x/\eta_2^2$	$\mu_{xy}$	$\nu_{yx}$	$\nu_{xy} = \frac{\nu_{yx}}{E_x/E_y}$
0.3	1.50	5.00	1.0	0.1	0.33333
0.7	2.16667	3.09523	1.0	0.23333	0.33333
1.0	2.16667	2.66667	1.0	0.33333	0.33333
1.5	3.16667	2.11111	1.0	0.33333	0.22222
4.5	6.16667	1.37037	1.0	0.33333	0.074074

TABLE 4.4: Material Properties used for determining the stress intensity factor  $K_I$  for a centrally cracked orthotropic square plate.

$\eta_2^2 = \frac{E_x}{E_y}$	$K_I/K_\infty$ Bowie & Freese	$K_I/K_\infty$ Present Analysis	Accuracy (% Error)
0.3	1.37	1.363	0.51
0.7	1.26	1.250	0.79
1.0	1.22	1.213	0.57
1.5	1.18	1.181	0.08
4.5	1.12	1.133	1.16

$K_\infty = \sqrt{a} = \sqrt{2.4}$

TABLE 4.5: Comparison of  $K_I/K_\infty$  from the present finite element analysis and results by Bowie and Freese [37].

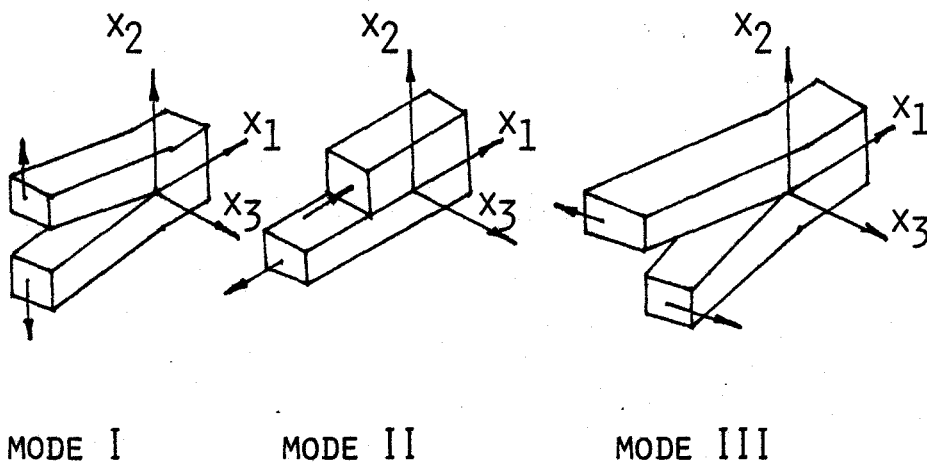


FIG. 4.1: THREE DIFFERENT MODES OF FRACTURE.

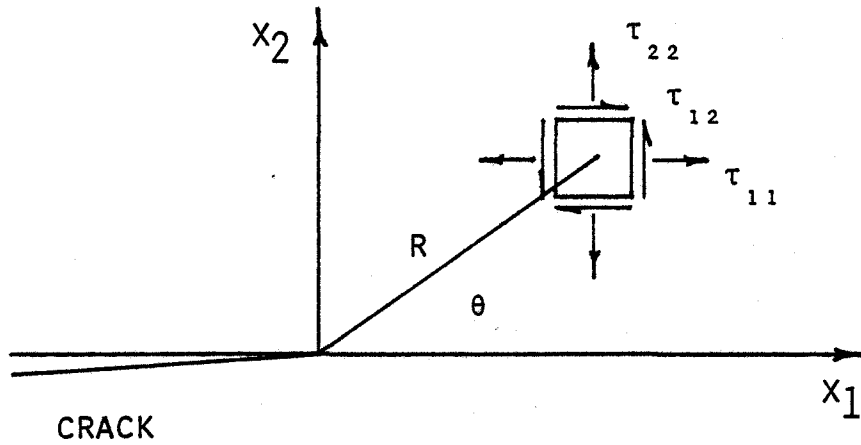


FIG. 4.2: STRESS COMPONENTS NEAR THE CRACK TIP IN CARTESIAN RECTANGULAR COORDINATES.

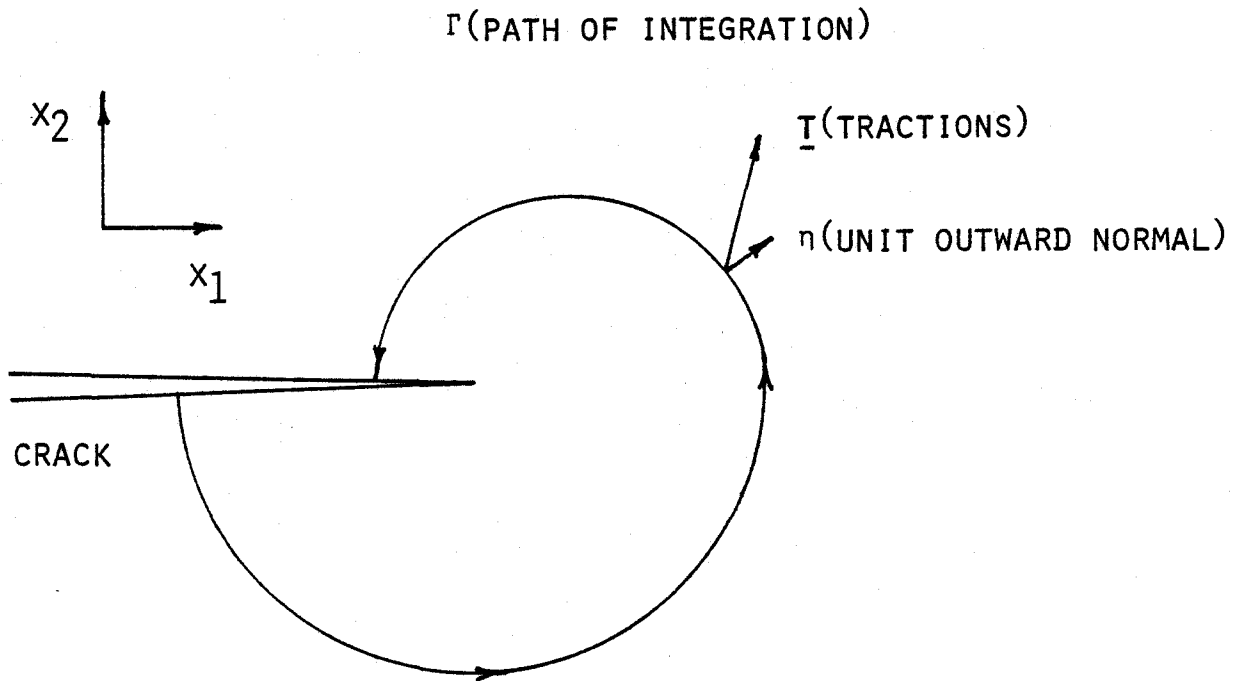


FIG. 4.3: TYPICAL CONTOUR FOR EVALUATION OF J-INTEGRAL.

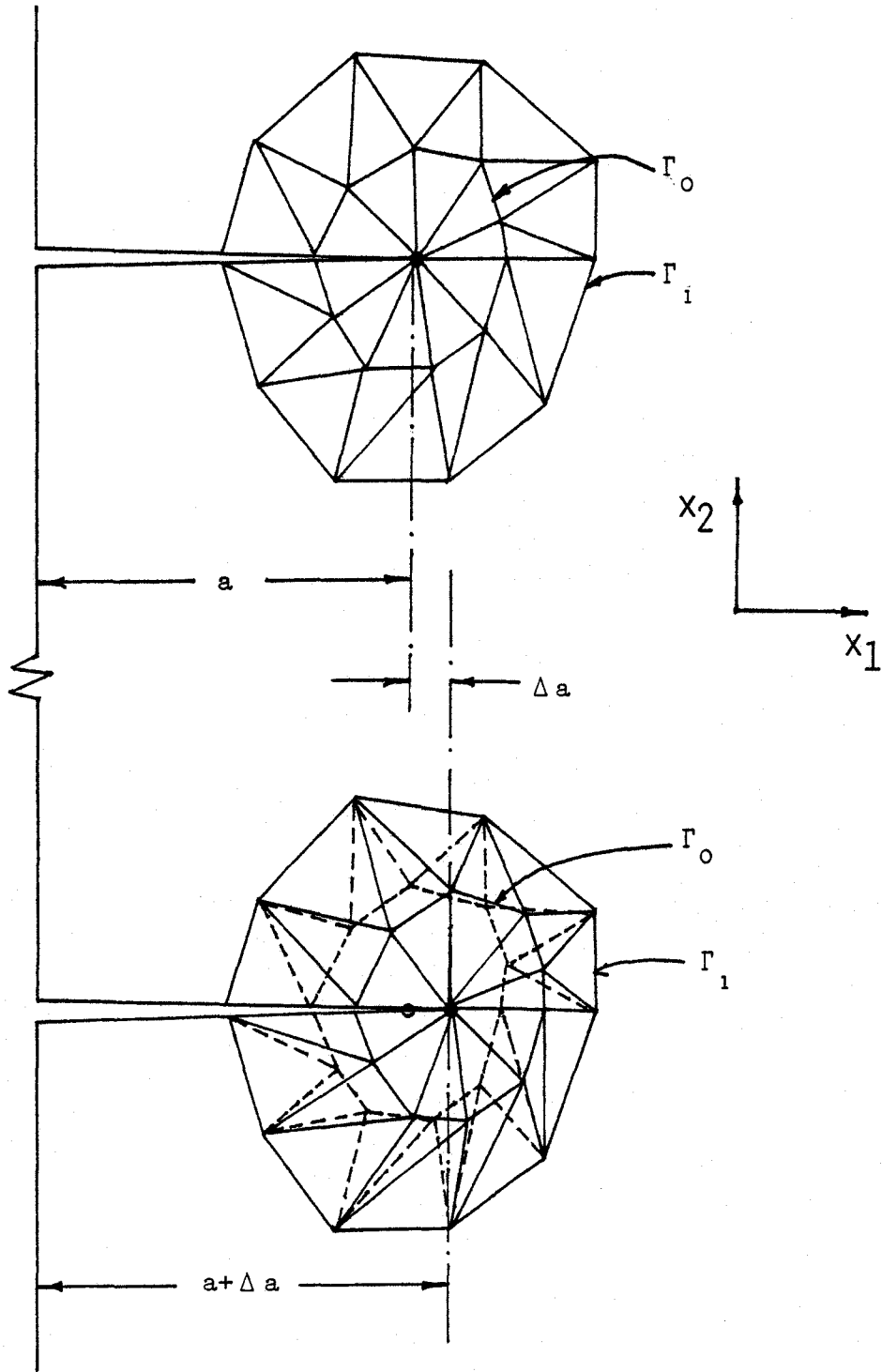


FIG. 4.4: ACCOMODATION OF CRACK EXTENSION  $\Delta a$  BY ADVANCING NODES ON THE PATH  $\Gamma_0$ .

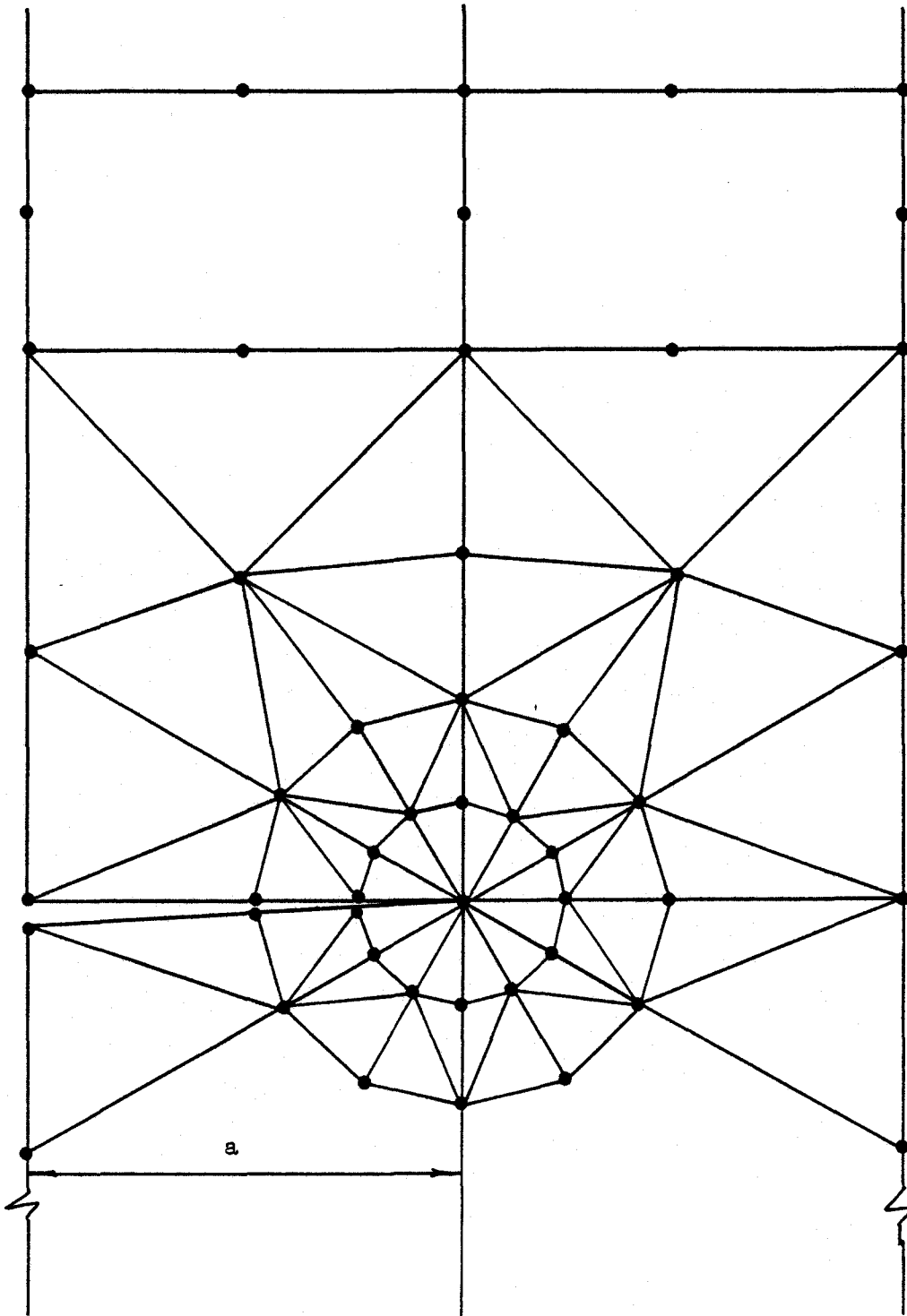


FIG. 4.5<sup>a</sup> : TYPICAL FINITE ELEMENT MESH WITH MIXED, MIXED TRANSITIONAL AND ISOPARAMETRIC DISPLACEMENT TYPE FINITE ELEMENTS.

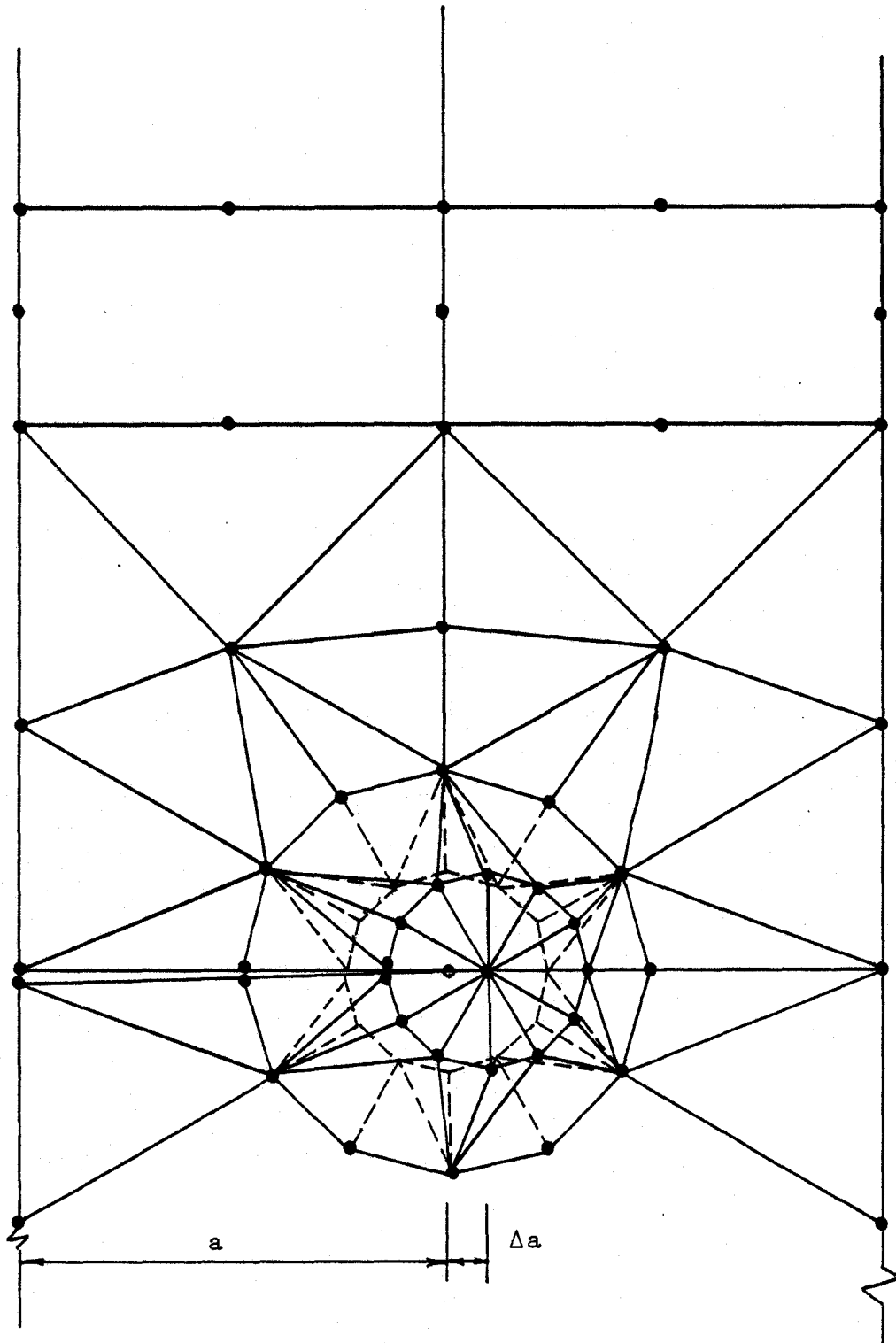
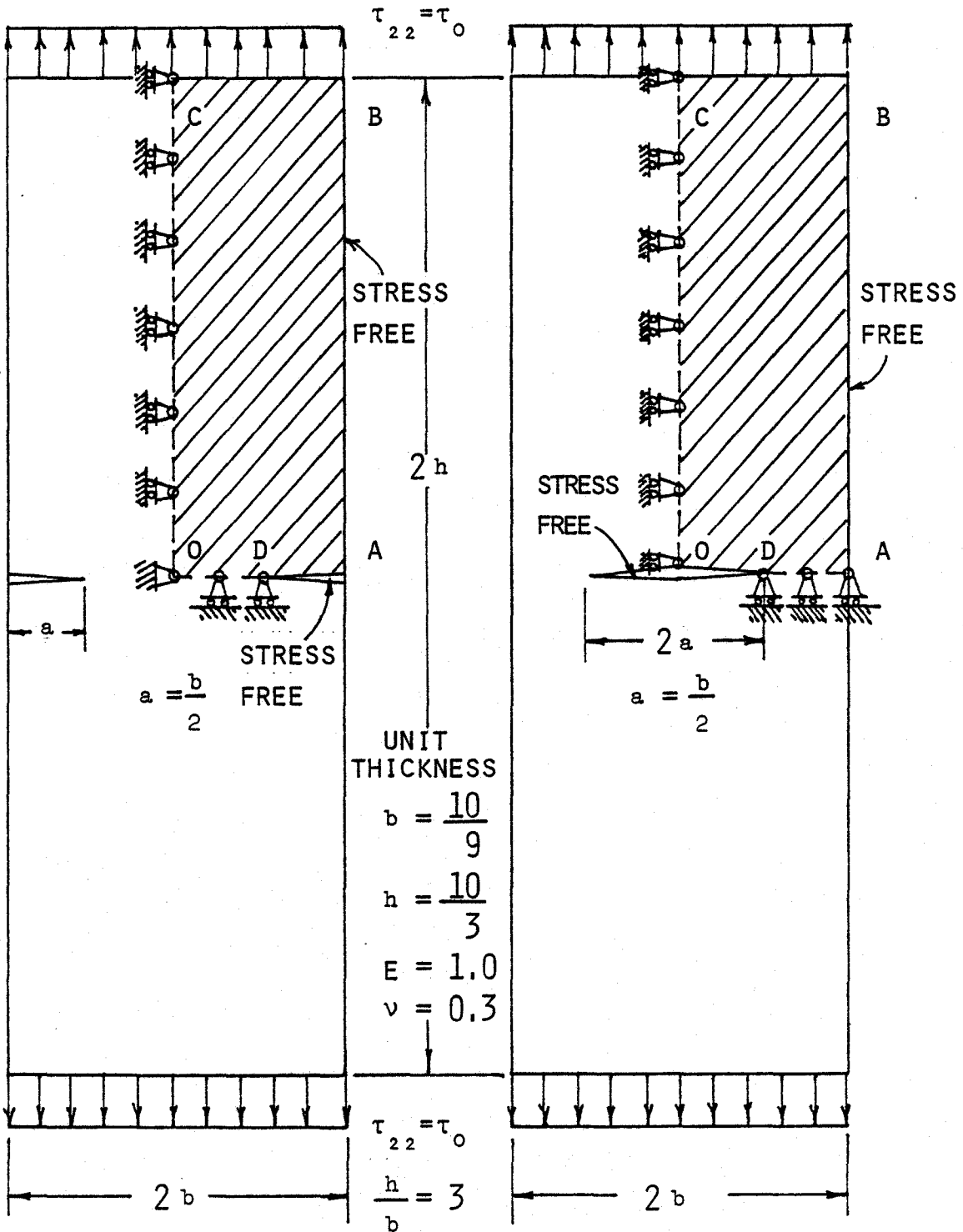


FIG. 4.5 b : ACCOMODATION OF CRACK EXTENSION  $\Delta a$  BY ADVANCING NODES ON PATH  $\Gamma_0$  IN FIGURE 4.5 a,



a) SYMMETRIC EDGE CRACKS

b) CENTRAL CRACK

FIG. 4.6: RECTANGULAR PLATES WITH CRACKS USED FOR DETERMINING THE CRACK INTENSITY FACTOR  $K_I$ . THE QUARTER PLATE CONSIDERED FOR THE FINITE ELEMENT ANALYSIS ALONG WITH BOUNDARY CONDITIONS SHOWN AS SHADED AREA.

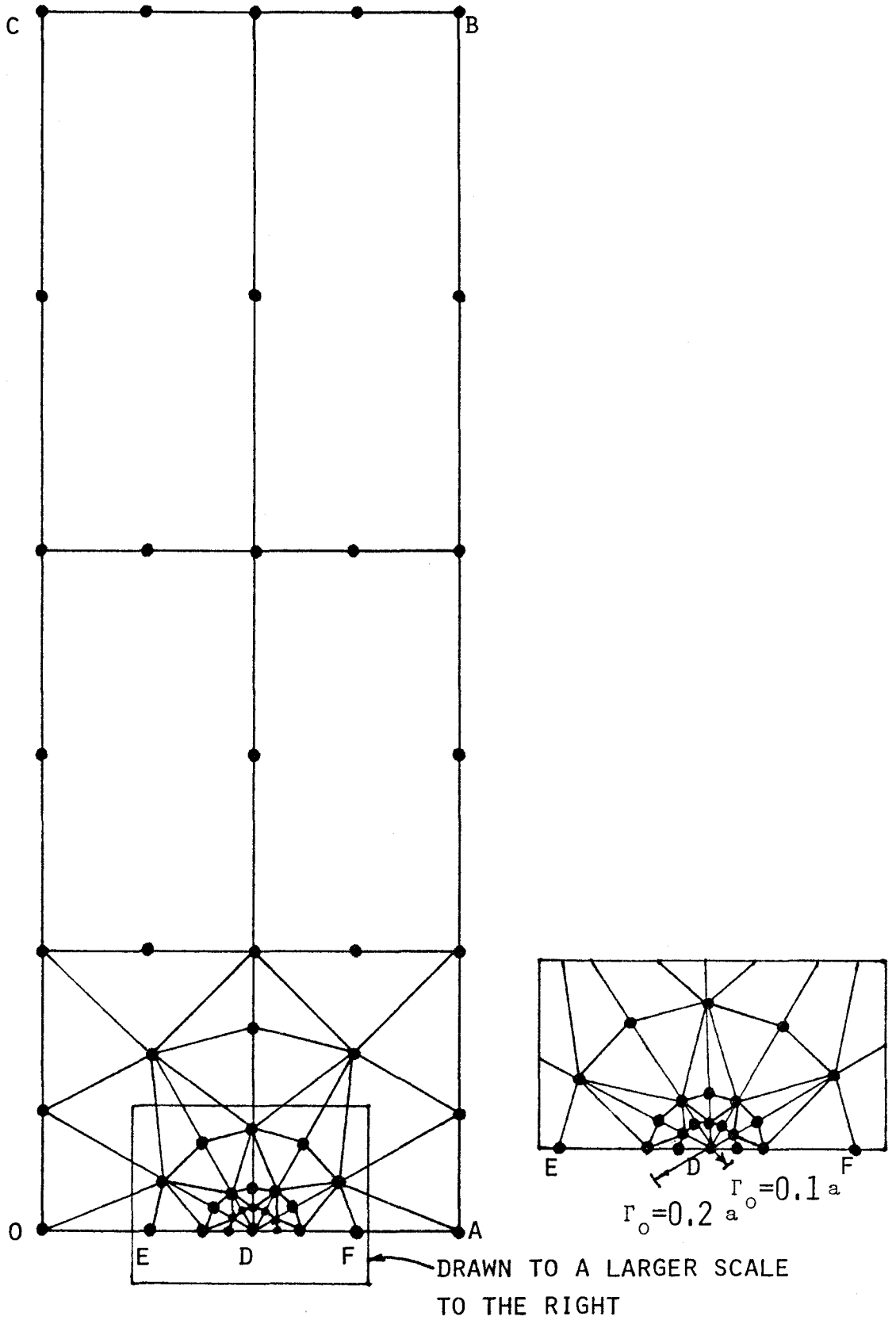


FIG. 4.7: FINITE ELEMENT MESH USED FOR DETERMINING THE CRACK INTENSITY FACTOR  $K_I$ , USED FOR BOTH SYMMETRIC EDGE CRACKS AND CENTRAL CRACKS.

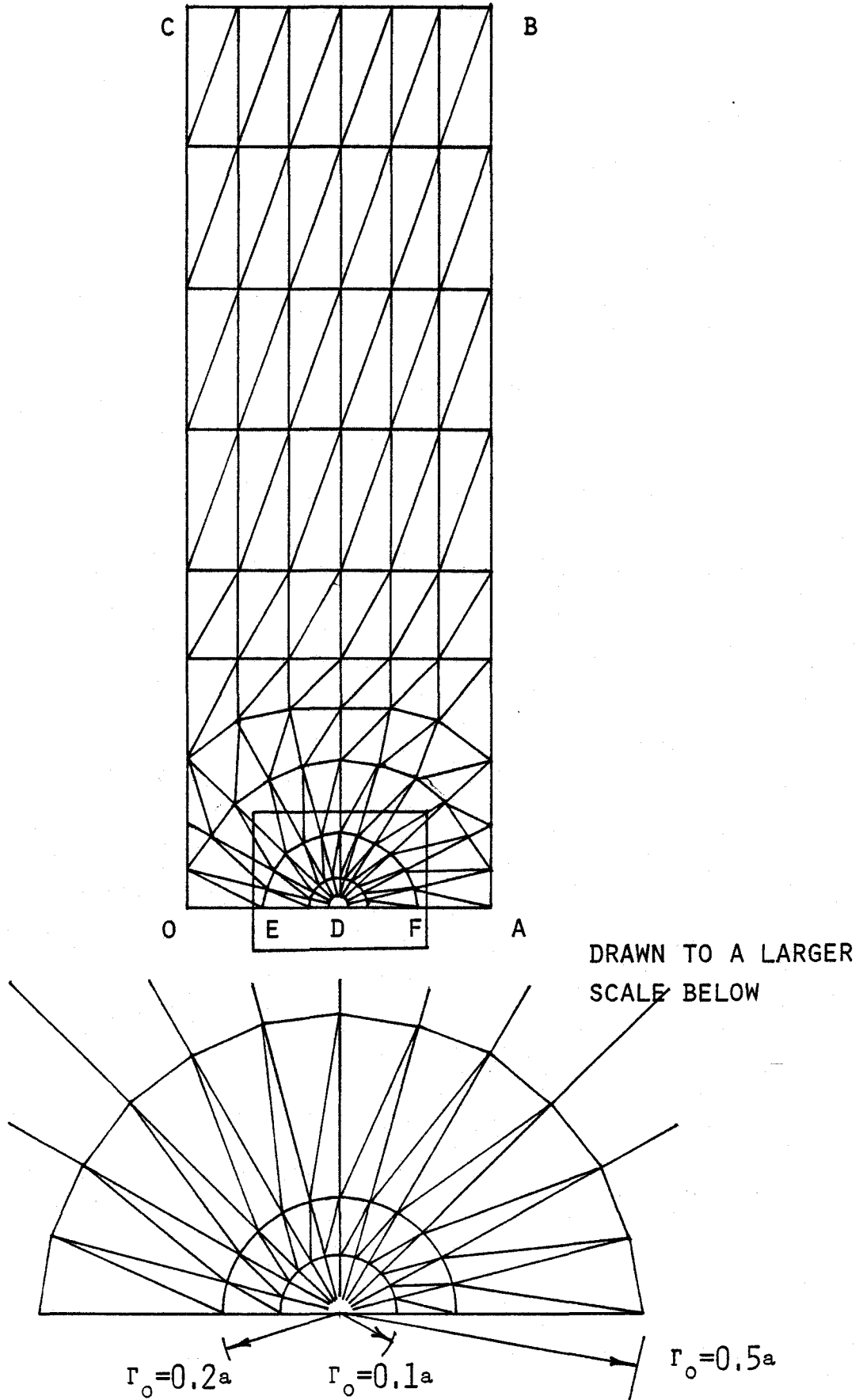
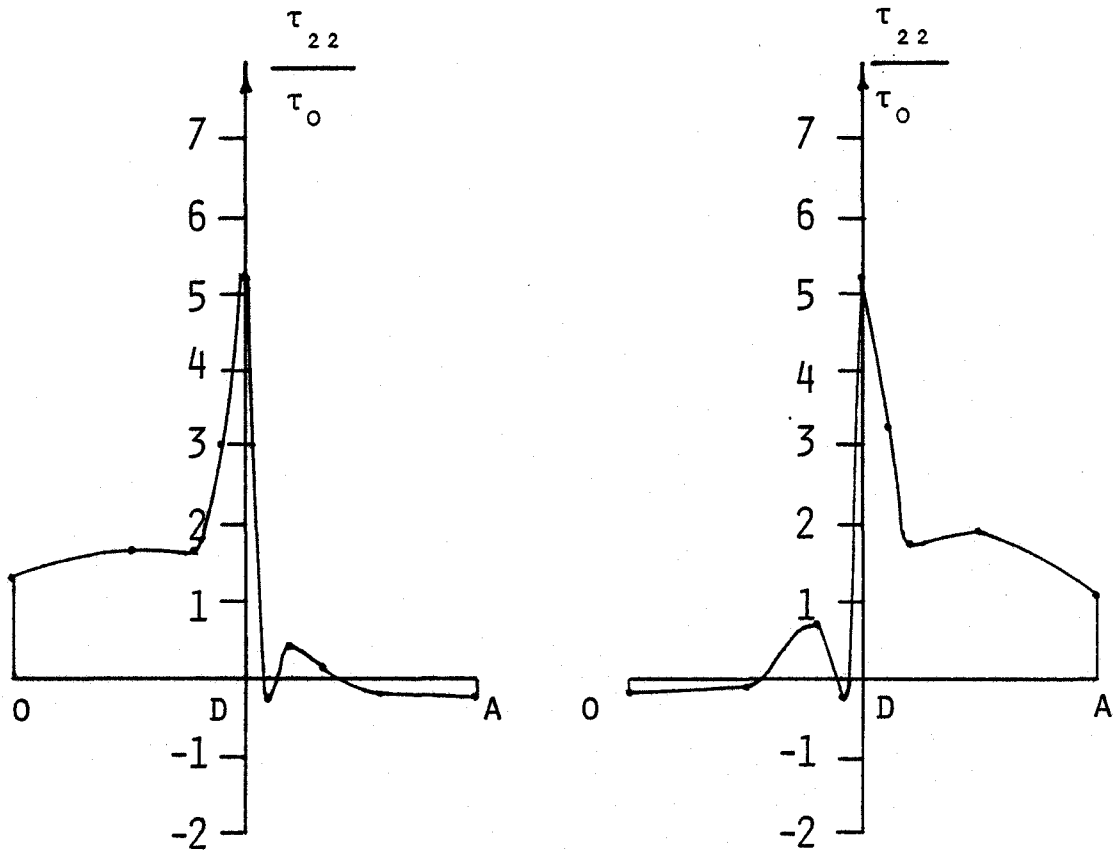


FIG. 4.8: FINITE ELEMENT MESH USED FOR DETERMINING THE CRACK INTENSITY FACTOR  $K_{I,}$  USED FOR BOTH SYMMETRIC EDGE AND CENTRAL CRACKS, REFERENCE [ 33 ].



a) SYMMETRIC EDGE CRACKS

b) CENTRAL CRACK

FIG, 4.9: NORMAL STRESS DISTRIBUTION ALONG THE EDGE OA OF THE RECTANGULAR PLATE WITH CRACKS-FIGURE 4.6.

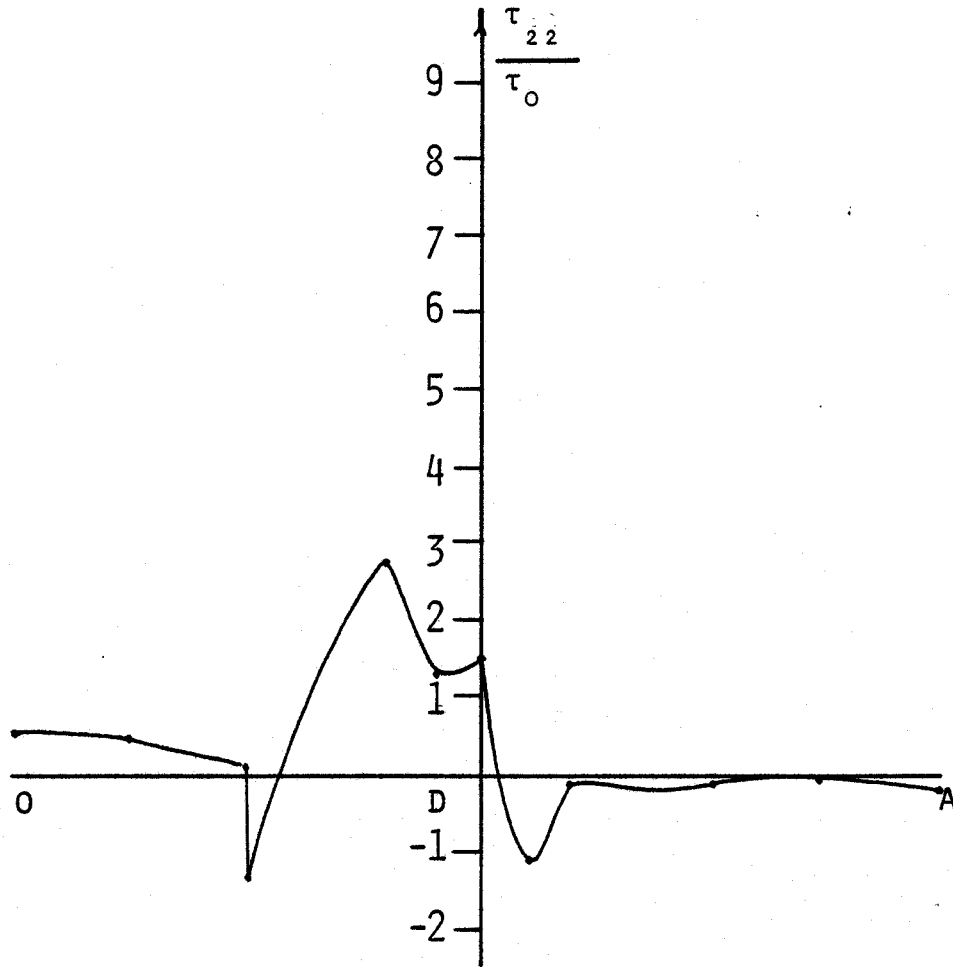


FIG. 4.10: FLUCTUATIONS OF NORMAL STRESS ALONG THE EDGE OA OF THE RECTANGULAR PLATE WITH SYMMETRIC EDGE CRACKS-FIGURE 4.6a,

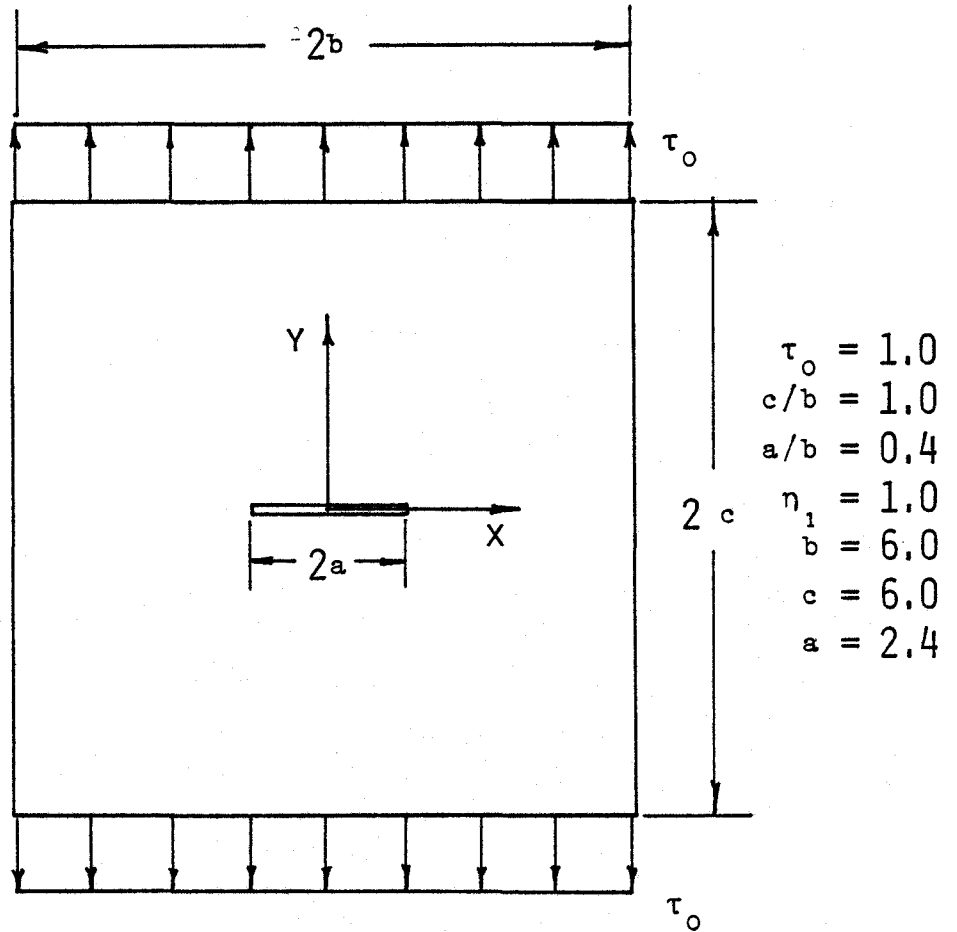


FIG. 4.11: ORTHOTROPIC SQUARE PLATE WITH A CENTRAL CRACK USED FOR DETERMINING THE STRESS INTENSITY FACTOR  $K_I$ .

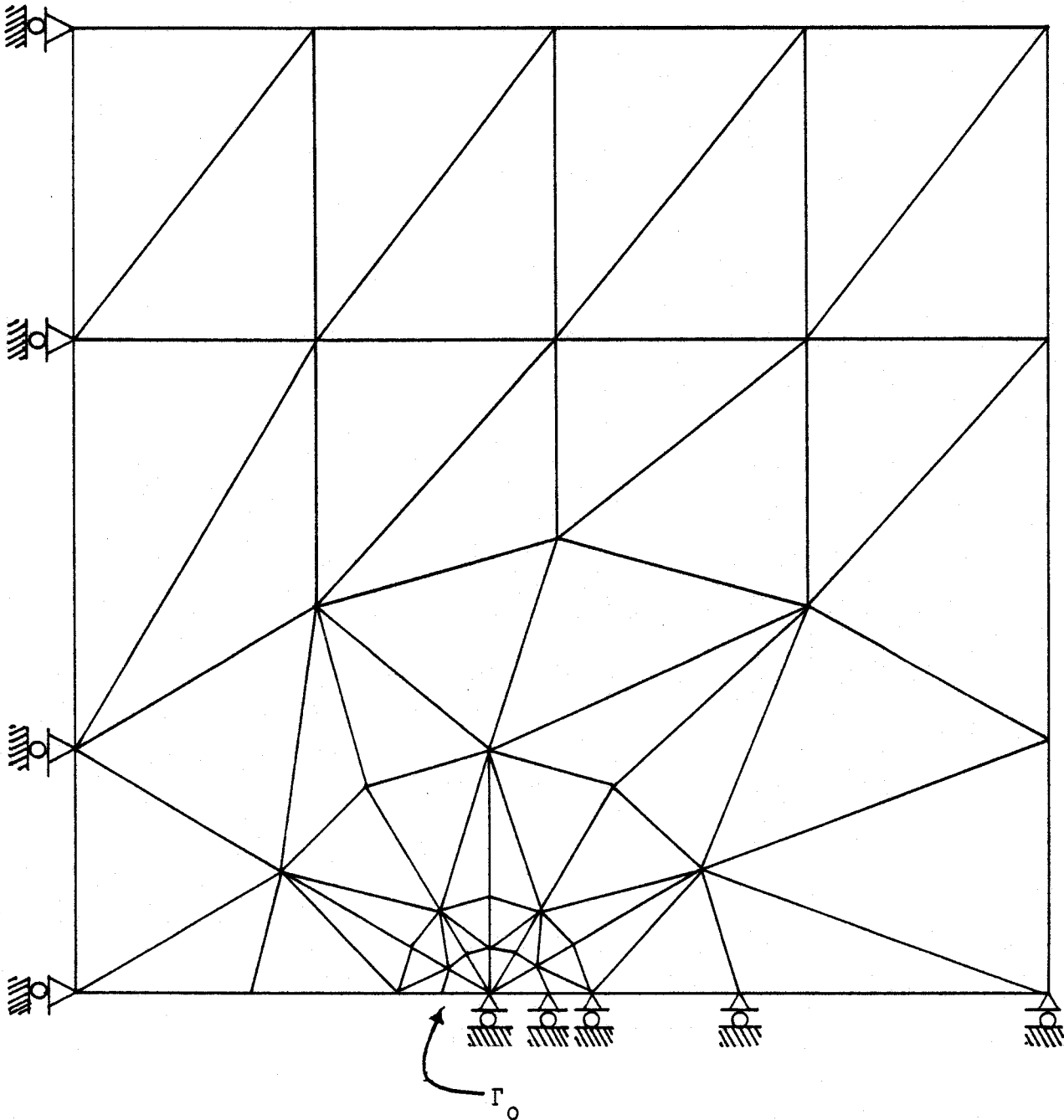


FIG. 4.12: FINITE ELEMENT MESH USED FOR DETERMINING THE CRACK INTENSITY FACTOR  $K_I$  FOR THE SQUARE PLATE WITH A CENTRAL CRACK-FIGURE 4.11.

CHAPTER 5

CRACK EXTENSION UNDER COMBINED MODES

A brief theory and applications of linear elastic fracture mechanics have been presented in the previous chapter. For a cracked body, loaded symmetrically about the crack plane (Mode I type), the crack will extend in a plane coincident with the original crack and it is sufficient to consider only the Mode I stress intensity factor  $K_I$  or the corresponding energy release rate  $G_I$ . For a cracked body under general loading (planar), both  $K_I$  and  $K_{II}$  in Equation (4.1.1) exist and combined mode (Mode I and Mode II) situation results. The initial direction of crack extension will be different from that of the original crack plane and is referred to as crack branching or non-coplanar crack growth. In general, both  $K_I$  and  $K_{II}$  have to be calculated and fracture criteria have to be found in order to predict the initial direction of crack extension and the onset of crack growth under such combined modes. The determination of the stress intensity factors  $K_I$  and  $K_{II}$  by the finite element method using the energy release rate will be presented. Also, currently available fracture criteria for fracture under combined modes will be discussed and used to predict the direction of crack extension.

5.1 Finite Element Analysis for Calculation of Stress Intensity Factors  $K_I$  and  $K_{II}$  Under Combined Modes

The determination of  $K_I$  for a cracked body under symmetrical,

Mode I, loading has been discussed in Chapter 4. To analyze combined mode fracture problems, the stress intensity factors  $K_I$  and  $K_{II}$  have to be determined. The extrapolation techniques and special finite elements with proper stress singularity embedded and reported in the previous chapters, could be used for such calculations. However, such procedures require special and much more difficult treatment of the region surrounding the crack tip and will not be used in this work. The energy approach for calculating stress intensity factors does not require special grid refinement in the crack tip region and has been shown to result in large reductions in the computer storage required. It is the purpose here to investigate such an energy approach. In particular, the direct derivative technique presented previously for the calculation of  $K_I$  for Mode I crack problems will be extended for the calculation of  $K_I$  and  $K_{II}$  for combined mode crack problems in linear elastic fracture mechanics.

#### 5.1.1 Calculation of $K_I$ and $K_{II}$ using Energy Approach

The path independent J-integral introduced in Chapter 4 is equivalent to the potential energy release rate  $G$  calculated by assuming that the crack extends in a plane coincident with the original crack. For a cracked body under symmetric (Mode I) loading, this is indeed the actual direction of crack propagation and there is no contribution to the energy release rate due to Mode II ( $K_{II} = 0$ ). Therefore

$$J = G = G_I = \frac{(\kappa + 1)}{8\mu} K_I^2 \quad (5.1.1.1)$$

The direct derivative technique can be used to calculate  $G_I$  as indicated in the previous chapter and  $K_I$  can be determined using Equation (5.1.1.1).

In combined mode crack problems (planar), crack extension will not be coplanar with the original crack plane. However, the potential energy release rate for an imaginary or a virtual crack extension assuming coplanar crack growth, i.e.  $J$ , can always be calculated using the direct derivative technique. In such cases, both  $K_I$  and  $K_{II}$  exist and therefore the energy release rate will have contributions from both Modes I and II. Equation (5.1.1.1) then takes the following form [27]:

$$J = G = G_I + G_{II} = \frac{(\kappa + 1)}{8\mu} K_I^2 + \frac{(\kappa + 1)}{8\mu} K_{II}^2 \quad (5.1.1.2)$$

where  $G_I$  and  $G_{II}$  are the energy release rates due to Modes I and II, respectively. Computation of  $G$  can be performed using the direct derivative technique in the same manner as presented in the previous chapter, i.e.  $G = -\frac{1}{2} \langle \underline{\tilde{u}}^T \underline{\tilde{\tau}} \rangle^T \frac{\Delta S}{\Delta a} \left\{ \begin{array}{c} \underline{\tilde{u}} \\ \underline{\tilde{\tau}} \end{array} \right\}$ . However, one cannot distinguish between contributions due to Modes I and II. Thus the energy release rate  $G$  has to be separated into the two components  $G_I$  and  $G_{II}$  in order to determine the stress intensity factors  $K_I$  and  $K_{II}$ .

The method of separating  $G$  into  $G_I$  and  $G_{II}$  is due to Ishikawa et al. [39, 40]. The cracked body is first analyzed using the finite element method. The displacement and stress solutions  $\underline{\tilde{u}}$ ,  $\underline{\tilde{\tau}}$  near the crack

tip are then separated into components  $\tilde{u}^I, \tilde{\tau}^I$  and  $\tilde{u}^{II}, \tilde{\tau}^{II}$  for modes I and II, respectively. Displacements and stresses of mode I and mode II are symmetric and skewsymmetric (See Equation (4.1.1)), respectively, with respect to the  $X_1$  axis shown in Figure (5.1). The displacements  $\tilde{u}$  at point  $P(X_1, X_2)$  can be separated in such a form that  $\tilde{u}$  is the sum of displacements  $\tilde{u}^I$  due to mode I and  $\tilde{u}^{II}$  due to mode II which have been expressed in terms of the displacements  $\tilde{u}$  at point  $P(X_1, X_2)$  and the displacements  $\tilde{u}'$  at point  $P'$ , with coordinates  $(X_1, -X_2)$ , in the following equations:

$$\tilde{u} = \tilde{u}^I + \tilde{u}^{II} \quad (5.1.3)$$

$$\begin{Bmatrix} \tilde{u}_1^I \\ \tilde{u}_2^I \end{Bmatrix} = \frac{1}{2} \begin{Bmatrix} \tilde{u}_1 + \tilde{u}'_1 \\ \tilde{u}_2 + \tilde{u}'_2 \end{Bmatrix} \quad \text{and} \quad \begin{Bmatrix} \tilde{u}_1^{II} \\ \tilde{u}_2^{II} \end{Bmatrix} = \frac{1}{2} \begin{Bmatrix} \tilde{u}_1 - \tilde{u}'_1 \\ \tilde{u}_2 - \tilde{u}'_2 \end{Bmatrix} \quad (5.1.4)$$

where  $\tilde{u}'_1$  are the displacements of point  $P'$ , and  $P$  and  $P'$  always form a pair of symmetric points about the  $X_1$  axis. Similarly, for stresses  $\tilde{\tau}$ , we have the following:

$$\tilde{\tau} = \tilde{\tau}^I + \tilde{\tau}^{II} \quad (5.1.1.5)$$

$$\begin{Bmatrix} \tilde{\tau}_{11}^I \\ \tilde{\tau}_{22}^I \\ \tilde{\tau}_{12}^I \end{Bmatrix} = \frac{1}{2} \begin{Bmatrix} \tilde{\tau}_{11} + \tilde{\tau}'_{11} \\ \tilde{\tau}_{22} + \tilde{\tau}'_{22} \\ \tilde{\tau}_{12} + \tilde{\tau}'_{12} \end{Bmatrix} \quad \text{and} \quad \begin{Bmatrix} \tilde{\tau}_{11}^{II} \\ \tilde{\tau}_{22}^{II} \\ \tilde{\tau}_{12}^{II} \end{Bmatrix} = \frac{1}{2} \begin{Bmatrix} \tilde{\tau}_{11} - \tilde{\tau}'_{11} \\ \tilde{\tau}_{22} - \tilde{\tau}'_{22} \\ \tilde{\tau}_{12} - \tilde{\tau}'_{12} \end{Bmatrix} \quad (5.1.1.6)$$

Therefore by using the displacement and stress components,  $\underline{\tilde{u}}^I$ ,  $\underline{\tilde{\tau}}^I$  and  $\underline{\tilde{u}}^{II}$ ,  $\underline{\tilde{\tau}}^{II}$ , and the direct derivative technique discussed earlier, the energy release rates  $G_I$  and  $G_{II}$  for a combined mode, planar crack problem are given by [39]

$$G_I = -\frac{1}{2} \langle \underline{\tilde{u}}^I \quad \underline{\tilde{\tau}}^I \rangle \frac{\Delta S}{\Delta a} \begin{pmatrix} \underline{\tilde{u}}^I \\ \underline{\tilde{\tau}}^I \end{pmatrix} \quad (5.1.1.7)$$

$$G_{II} = -\frac{1}{2} \langle \underline{\tilde{u}}^{II} \quad \underline{\tilde{\tau}}^{II} \rangle \frac{\Delta S}{\Delta a} \begin{pmatrix} \underline{\tilde{u}}^{II} \\ \underline{\tilde{\tau}}^{II} \end{pmatrix}. \quad (5.1.1.8)$$

It should be emphasized again that the energy release rates  $G_I$  and  $G_{II}$  are calculated by assuming that the crack extends in a plane coincident with the original crack, which is not necessarily the actual direction of the crack growth for a mixed mode type crack. With  $G_I$  and  $G_{II}$  given by Equations (5.1.1.7) and (5.1.1.8), the stress intensity factors  $K_I$  and  $K_{II}$  can be calculated using the following equations.

$$G_I = \frac{(\kappa + 1)}{8\mu} K_I^2, \quad G_{II} = \frac{(\kappa + 1)}{8\mu} K_{II}^2 \quad (5.1.1.9)$$

Thus using Equations (5.1.1.3) to (5.1.1.9) together with a solution for displacements and stresses from a finite element analysis,  $K_I$  and  $K_{II}$  of a combined mode crack can be determined through a virtual crack extension in the direction of the original crack. This has been implemented in the finite element program. Since only a virtual crack extension is

needed,  $\Delta S/\Delta a$  is calculated only once. Also, in calculating  $G_I$  and  $G_{II}$ , only the element matrices for the mixed elements within the contours  $\Gamma_0$  and  $\Gamma_1$  are altered (Figure (4.4)). Hence the separations of  $\tilde{u}$  and  $\tilde{r}$  for points P and P' need only be performed for those nodes located on contours  $\Gamma_0$  and  $\Gamma_1$ , respectively. This numerical scheme has been implemented in the subroutine 'DENERG' and will be illustrated through examples subsequently. The above scheme will hereafter be referred to as Ishikawa's scheme.

Another energy approach that requires calculation of the potential energy release rates for two virtual crack extensions in two mutually orthogonal directions has been investigated by Hellen et al., [41, 42] and Vanderglas and Pick [43]. The path independent J-integral was generalized to be a vector  $J_K$  by Knowles and Sternberg [44] and for two-dimensional problems the components are given by:

$$J_1 = \int \left\{ W n_1 - \bar{T} \frac{\partial \bar{u}}{\partial X_1} \right\} dS \quad (5.1.1.10)$$

$$J_2 = \int \left\{ W n_2 - \bar{T} \frac{\partial \bar{u}}{\partial X_2} \right\} dS \quad (5.1.1.11)$$

where  $n_1$  and  $n_2$  are the direction cosines of the unit outward normal  $\bar{n}$ , and  $W$ ,  $\bar{n}$ ,  $\bar{T}$  and  $\bar{u}$  have been defined previously. It has also been mentioned in reference [42] that  $J_K$  gives the energy release rates if the crack were to extend in the  $X_K$  directions. Thus  $J_1$  is the energy release rate calculated by assuming that the crack extends along axes  $x_1$

and  $J_2$  is the energy release rate calculated assuming that the crack extends along axes  $X_2$ , i.e. perpendicular to the direction of the crack, Figure (5.1). It is important to note that a continuous variation of stress field, as crack extension approaches zero, is assumed even when the crack does not extend in its own plane. Apparently this is not strictly correct; Hussain et al. [45] have calculated the stress field around the crack with a branched tip and found that by letting the length of the branch go to zero, the stress field near the crack tip in the limit does not coincide with the one for the unbranched crack. Thus there exist a discontinuity in the stress field when the crack does not extend in a coplanar manner. This will be commented upon later.

Using the assumption of continuity, Hellen and Blackburn [42] have shown that in two-dimensional elasticity problems with combined mode loadings, the stress intensity factors are related to  $J_1$  and  $J_2$  by:

$$J_1 = \frac{(1 + \nu)(1 + \kappa)}{4E} (K_I^2 + K_{II}^2) \quad (5.1.1.12)$$

$$J_2 = \frac{-(1 + \nu)(1 + \kappa)}{2E} K_I + K_{II} \quad (5.1.1.13)$$

where  $\nu$  is the Poisson's Ratio,  $E$  is the modulus of elasticity and  $\kappa$  has been defined previously. Also, the energy release rate of crack extension at any angle  $\theta$  is given as

$$G(\theta) = J_1 \cos\theta + J_2 \sin\theta \quad (5.1.1.14)$$

From Equation (5.1.1.14), the maximum energy release rate occurs at

$$\theta = \arctan \left( \frac{J_2}{J_1} \right) = \arctan \left( \frac{-2K_I K_{II}}{K_I^2 + K_{II}^2} \right) \quad (5.1.1.15)$$

and has the value

$$G_{\max} = (J_1^2 + J_2^2)^{1/2} = \frac{(1 + \nu)(1 + \kappa)}{4E} (K_I^4 + 6K_I K_{II} + K_{II}^4)^{1/2} \quad (5.1.1.16)$$

The direct derivative technique can again be used to calculate:

$$J_1 = - \frac{\partial \Pi}{\partial a} \Big|_{\theta=0} \cong - \frac{1}{2} \langle \underline{\tilde{u}}^T \quad \underline{\tilde{\tau}}^T \rangle \frac{\Delta S}{\Delta a} \Big|_{\theta=0} \left\{ \begin{array}{c} \underline{\tilde{u}} \\ \underline{\tilde{\tau}} \end{array} \right\} \quad (5.1.1.17)$$

$$J_2 = - \frac{\partial \Pi}{\partial a} \Big|_{\theta=\pi/2} \cong - \frac{1}{2} \langle \underline{\tilde{u}}^T \quad \underline{\tilde{\tau}}^T \rangle \frac{\Delta S}{\Delta a} \Big|_{\theta=\pi/2} \left\{ \begin{array}{c} \underline{\tilde{u}} \\ \underline{\tilde{\tau}} \end{array} \right\} \quad (5.1.1.18)$$

In Equations (5.1.1.17) and (5.1.1.18),  $\underline{\Delta S}/\Delta a \Big|_{\theta=0}$  and  $\underline{\Delta S}/\Delta a \Big|_{\theta=\pi/2}$  are the changes in the global matrix when the crack has extended by a small amount in the direction of the crack and perpendicular to the crack, respectively. Thus,  $\underline{\Delta S}/\Delta a$  has to be calculated twice.

As mentioned above this approach assumes continuity of the stress field and all derivations (e.g. Equations (5.1.1.2) and (5.1.1.3)) are based on the stress and displacement fields of the cracked body before crack branching occurs. Since in the direct deriva-

tive technique of calculating  $J_1$  and  $J_2$  (Equations (5.1.1.17) and (5.1.1.18)), the finite element solution  $\tilde{u}$  and  $\tilde{r}$  of the cracked body without branching is used, the stress continuity assumption is maintained. Therefore,  $J_1$  and  $J_2$  can be evaluated using the direct derivative method as indicated in Equations (5.1.1.17) and (5.1.1.18) and the stress intensity factors  $K_I$  and  $K_{II}$  can then be calculated using Equations (5.1.1.12) and (5.1.1.13). Moreover, if the direct derivative method is used to calculate the energy release rate for different angles  $\theta$  of crack extension, the variation of  $G(\theta)$  versus  $\theta$  will be expected to follow a sinusoidal variation as indicated in Equation (5.1.1.14). However, because of the assumed continuity of stress field, the calculated values of  $J_K$  and  $G(\theta)$  may not be the correct values of energy release rates for the corresponding angle of crack extension  $\theta$ .

In the finite element analysis, the virtual crack extension in the direction of the crack, i.e.  $\theta = 0.0$ , can be accommodated as discussed previously in Chapter 4. The modelling of the virtual crack extension in any other direction, i.e.  $\theta \neq 0.0$ , presents some difficulties. The finite element grid around the crack tip is shown in Figure (5.2.a). If the crack tip is used as  $\Gamma_0$ , i.e.  $r_{\Gamma_0} = 0.0$ , and the virtual crack extension for non-zero  $\theta$  is accommodated in the same manner as presented previously for  $\theta = 0.0$ , the finite element grid after the virtual crack extension will be that indicated in Figure (5.2.b). Thus it can be observed that the deflected crack is not modelled exactly by just moving the crack tip by a small amount  $\Delta a$  in the direction under investigation. If the deflected crack tip is to be modelled exactly,

two new elements will have to be introduced as shown in Figure (5.2.c) and the stiffness of such elements should be added to  $\Delta S/\Delta a$  when calculating  $G(\theta)$ . However, this would introduce uncertainty in the finite element grid error regarding the differences between that of Figure (5.2.a) and (5.2.c), thus affecting the strain energy change associated with the change in crack length  $\Delta a$ . It is found that although the geometry of the original crack plus the virtual extension will not be modelled exactly, accommodation of the virtual crack extension as shown in Figure (5.2.b) usually gives better results for  $K_I$  and  $K_{II}$  than those obtained by using Figure (5.2.c) when using Hellen et al.'s [41] approach. The same problem with modelling has been pointed out by Hellen [42] and it is anticipated that the modelling shown in Figure (5.2.b) has been used in his works.

The modelling of a virtual crack extension in any arbitrary direction using the crack tip as contour  $\Gamma_0$  can be performed using the Subroutine DENERG written previously for Mode I crack problems. Hence  $J_1$  and  $J_2$  can be calculated easily and  $K_I$  and  $K_{II}$  determined. However, it was observed in previous calculations of  $K_I$  in Chapter 4 that the most accurate results are usually obtained by using the first ring of nodes around the crack tip as  $\Gamma_0$  to be moved and using the crack tip as  $\Gamma_0$  will give results of lesser accuracy. A closer examination of Figure (5.2.b) shows that it is difficult to extend this method of modelling to the case when the crack tip is not used as  $\Gamma_0$ . Thus, in order to obtain accuracy comparable to that when the first ring of nodes is used as  $\Gamma_0$ , the finite element grid around the crack tip has to be more refined or

special elements as in reference [43] have to be used. On the other hand, when Ishikawa's scheme is used, only a virtual crack extension in the direction of the crack, i.e.  $\theta = 0.0$ , is needed and the first ring of nodes can readily be used as  $\Gamma_0$  with no difficulties. In view of this advantage, Ishikawa's scheme will be used to calculate  $K_I$  and  $K_{II}$  and, together with the fracture criteria to be presented later, to predict the direction of a crack extension.

Finally, it should be mentioned that a contour integral computation of combined mode stress intensity factors has been introduced by Stern, Becker and Dunham [46] and Wang, Yan and Corten [47]. The approach is based on Betti's reciprocal work theorem for plane elastic states and requires no special treatment of the finite element grid around the crack tip. However a path independent integral involving the use of an auxiliary elastic state of stresses and displacements has to be computed and it is found that the use of the energy release rate method utilizing Ishikawa's scheme is much simpler to implement in the present work.

### 5.1.2 Numerical Examples

To illustrate calculations of  $K_I$  and  $K_{II}$  for combined mode crack problems using the energy release rate concept via Ishikawa's scheme, two combined mode, plane stress problems are analyzed.

The first problem is a deep cantilevered beam subjected to end shear shown in Figure (5.3). The original crack length is half the

width of the plate and the modulus of elasticity and the Poisson's ratio are 1.0 and 0.25, respectively. The finite element grid is shown in Figure (5.4). Solutions for  $K_I$  and  $K_{II}$  from the finite element analyses are given in Table (5.1) and are compared with those obtained by Stern, Becker and Dunham [46] using contour integral computations for different contours and boundary collocation procedures. The results from a fairly coarse grid used are quite satisfactory and the values of  $K_I$  and  $K_{II}$  calculated using the first ring of nodes about the crack tip as  $\Gamma_0$ , i.e.  $r_{\Gamma_0} = 0.1a$ , show deviations of only 0.62% and 3.74% from the collocation method results. Thus very accurate results can be expected using the present energy release rate scheme and the mixed finite elements.

	$K_I$	$K_{II}$
Contour Integral Computations [46]	34.25	4.79
	33.20	4.50
	33.42	4.68
	33.52	4.76
Collocation [46]	34.0	4.55
Present Analysis $r_{\Gamma_0} = 0.0$  $r_{\Gamma_0} = 0.1a$	30.38	4.06
	33.79	4.72

TABLE 5.1: Results for  $K_I$  and  $K_{II}$  for a deep cantilevered beam subjected to end shear, Figure 5.3.

The second problem analyzed is shown in Figure (5.5). The geometry is essentially the same as that of the first problem analyzed

except that the plate is subjected to both end shear and tension. The same finite element grid shown in Figure (5.4) is used and results using Ishikawa's approach are given in Table (5.2) for  $r_{\Gamma_0} = 0.0$  and  $r_{\Gamma_0} = 0.1a$ . The stress intensity factors  $K_I$  and  $K_{II}$  calculated using the Hellen and Blackburn approach, i.e. Equations (5.1.1.12) and (5.1.1.13), are also given for comparison. As mentioned previously the stress intensity factors can only be calculated using the crack tip as  $\Gamma_0$ , i.e.  $r_{\Gamma_0} = 0.0$ . The stress intensity factors  $K_I$  and  $K_{II}$  are in good agreement with those calculated using Ishikawa's approach for  $r_{\Gamma_0} = 0.0$  and the deviations are 4.58% and 4.56%, respectively. Also the energy release rates for different assumed angles of virtual crack extension are calculated using the model of Figure (5.2.b) and tabulated in Table (5.3). Using the values of energy release rates for  $\theta = 0^\circ$  and  $90^\circ$  as  $J_1$  and  $J_2$  respectively, values of energy release rates for different angles of propagation are also calculated using Equation (5.1.1.14), and plotted in Figure (5.6). It can be observed that the finite element solutions are in excellent agreement with those calculated using Equation (5.1.1.14) as expected. It should be noted that these values of energy release rates are not strictly correct due to the continuity assumption mentioned earlier. However, for small angles of crack extensions, the error involved is very small.

	$G_I$	$G_{II}$	$K_I$	$K_{II}$
Ishikawa's Approach $r_{\Gamma_0} = 0.0$	1050.097	14.243	34.405	3.774
$r_{\Gamma_0} = 0.1a$	1290.345	19.825	35.921	4.452
Hellen and Blackburn's Approach (Equation 5.1.1.12 and 5.1.1.13) $r_{\Gamma_0} = 0.0$	$J_I$ 1063.341	$J_2$ -236.478	$K_1$ 32.824	$K_2$ 3.602

TABLE 5.2: Results for  $K_I$  and  $K_{II}$  for a deep cantilever beam subject to both end shear and tension, Figure 5.5.

$\theta^\circ$	Energy Release Rate, $G(\theta)$	
	Finite Element Solution	$J_1 \cos\theta + J_2 \sin\theta$
0	( $J_1$ ) 1064.341	1064.341
15	966.8689	966.8692
30	803.5066	803.5069
45	585.3867	585.3870
60	327.3737	327.3739
75	47.0506	47.0507
90	( $J_2$ ) -236.4788	-236.4788
105	-503.8926	-503.8927
120	-736.9670	-736.9671
135	-919.8183	-919.8185
150	-1039.985	-1039.9857
165	-1089.279	-1089.279
180	-1064.4341	-1064.4347

TABLE 5.3: Energy release rates for different angles of crack extension for the deep cantilever beam subjected to end shear and tension, Figure 5.5.

## 5.2 Fracture Criteria for Prediction of Direction of Crack Extension

A method for determining the stress intensity factors  $K_I$  and  $K_{II}$  by using the finite element method and Ishikawa's scheme has been presented. For combined mode crack problems, the crack extension will not be coplanar. Thus, in addition to calculation of the stress intensity factors, a fracture criterion must be established in order to analyze the linear elastic fracture problems with crack branching. The remainder of this work will deal with the prediction of the direction of crack extension for a cracked body under combined modes I and II.

There are currently three fracture criteria available for analyzing combined mode crack problems, namely the maximum stress criterion [48 - 51], the minimum strain energy density criterion [52, 53] and the maximum energy release rate criterion which is a generalization of Griffith's original energy release rate concept. These fracture criteria are presented in the following subsections.

### 5.2.1 Maximum Stress Criterion

For a general loading in a two-dimensional problem, the near crack tip stress field will be determined by the stress intensity factors  $K_I$  and  $K_{II}$  of the original crack. The maximum stress criterion [48] postulates that the crack will start to extend from the crack tip in the direction along which the tangential stress  $\tau_\theta$  is a maximum and the shear stress  $\tau_{r\theta}$  is zero (Figure (5.7)). Thus, once  $K_I$  and  $K_{II}$  have

been determined, the angle  $\theta_0$  for which the tangential stress is a maximum will be given by the following relationship

$$K_I \sin \theta_0 + K_{II} (3 \cos \theta_0 - 1) = 0 \quad (5.2.1.1)$$

### 5.2.2 Minimum Strain Energy Density Criterion

Sih [52, 53] proposed that the governing quantity for fracture process is the local strain energy density at a certain critical distance from the crack tip. The minimum strain energy density criterion postulates that for a crack under a two-dimensional combined stress field, the initial crack extension takes place in the direction  $\theta_0$  along which the strain energy density attains a stationary (minimum) value and reaches a certain critical value, i.e.

$$\frac{\partial W(\theta)}{\partial \theta} = 0 \text{ at which } \theta = \theta_0 \quad (5.2.2.1)$$

where  $W(\theta)$  is the strain energy density and takes the following form:

$$W(\theta) = a_{11} K_I^2 + 2a_{12} K_I K_{II} + a_{22} K_{II}^2 \quad (5.2.2.2)$$

and

$$a_{11} = \frac{1}{16\pi\mu} (1 + \cos \theta)(\kappa - \cos \theta)$$

$$a_{12} = \frac{\sin \theta}{16\pi\mu} [2 \cos \theta - (\kappa - 1)] \quad (5.2.2.3)$$

$$a_{22} = \frac{1}{16\pi\mu} [(\kappa + 1)(1 - \cos \theta) + (1 + \cos \theta)(3 \cos \theta - 1)]$$

where  $\mu$  and  $\kappa$  have been defined previously.

Using Equations (5.2.2.1) to (5.2.2.3), the angle  $\theta_0$  for which the strain energy density attains a stationary value is given by the relation:

$$\begin{aligned} \cos 2\theta_0 [(1 - 3\lambda^2) \tan 2\theta_0 + 4\lambda] - (\kappa - 1) \cos \theta_0 [(1 - \lambda^2) \tan \theta_0 + \\ 2\lambda] = 0 \end{aligned} \quad (5.2.2.4)$$

where  $\lambda$  is used to denote the ratio  $K_{II}/K_I$ . Also, in order to verify that the solution to (5.2.2.4) does correspond to a minimum, the additional condition of  $\partial^2 W(\theta)/\partial \theta^2 > 0$  has to be checked.

### 5.2.3 Maximum Energy Release Rate Criterion

The maximum energy release rate criterion for combined mode crack problems is a generalization of Griffith's energy release rate concept [15, 16]. This criterion implies that the crack will grow in a direction  $\theta_0$  for which the energy release rate  $G(\theta)$  is maximum. Since

direction of a crack extension will not be coplanar with the crack plane, it would be necessary to determine the energy release rate as a function of the direction of crack extension and then maximize it.

It was shown previously that by assuming continuity of the stress field, the energy release rate for a crack extension at any angle  $\theta$  is given by Equation (5.1.1.14), i.e.  $G(\theta) = J_1 \cos \theta + J_2 \sin \theta$ . However, it has also been mentioned that such continuity cannot be claimed to be true. Therefore, the elasticity solution of a branched crack with an infinitesimal branch must first be obtained. There have been many attempts to solve the problem of a branched crack [45, 54 - 62] and all of them indicate a discontinuity in the stress field as the crack branches. This comprises the work of : Hussain, Pu and Underwood [45], Wang [54], Palaniswamy and Knauss [55], Bilby et al. [56, 57], Lo [58], Wu [59 - 61] and Hayashi et al., [62]. A review in this area was presented by Palaniswamy and Knauss [63]. Most of these analyses were based on the Muskhelishvili potential formulation and conformal mapping of the branched crack geometry onto a unit circle. The solution is then reduced to either an infinite series expansion or integral equations. However, in spite of all these attempts, there are some disagreements reported in the literature. For example, Lo [58] showed that his results for the stress intensity factors for a branched crack with an infinitesimal branch agree with the results of Palaniswamy and Knauss [55] and Bilby et al., [56, 57] and are at variance with those of Hussain et al., [45]. It was also pointed out that the calculations for the maximum energy release rate, however, agree with those of the above authors and that of Wu [59 - 61]. Wang [54] pointed out that the analy-

sis by Hussain et al., was not satisfactory and solved the problem again. His results contain Hussain's results as a special case but are again at variance with those in References [55 - 57]. It is beyond the scope of present numerical work to draw a conclusive statement as to which result is correct. However, it has been observed that for small angles of crack branching, the energy release rate and the stress intensity factors given by all of the references quoted above are in a reasonably good agreement. For predicting the direction of crack growth using the energy release rate criterion, the expressions derived by Wang [54] will be used in this work.

The problem of a singly branched crack shown in Figure (5.8) was solved by Wang [54]. It was shown in reference [54] that as the length of the branch  $r_2$  approaches zero, the stress intensity factors at the branch tip approach the following limiting values.

$$K_I - i K_{II} = \frac{(\alpha - \bar{\alpha}\beta)}{1 - \beta\bar{\beta}} \quad (5.2.3.1)$$

Where

$$\alpha = (\overset{\circ}{K}_I - i \overset{\circ}{K}_{II}) e^{\gamma i \left( \frac{1 - \gamma/\pi}{1 + \gamma/\pi} \right)^{\gamma/2\pi}} \quad (5.2.3.2)$$

$$\beta = \frac{1}{4} (e^{2\gamma i} - 1) (C_1^* + iC_2^*) \quad (5.2.3.3)$$

and  $\overset{\circ}{K}_I$  and  $\overset{\circ}{K}_{II}$  are the stress intensity factors of a crack which does

not have a branch, i.e. before crack extension,  $i = \sqrt{-1}$ ,  $\bar{\alpha}$  and  $\bar{\beta}$  are the complex conjugates of  $\alpha$  and  $\beta$ , respectively, and  $C_1^*$  and  $C_2^*$  are constants evaluated from an integral equation [54]. The values of  $C_1^*$  and  $C_2^*$  are given in Table (5.4) for  $\gamma$  ranging from 0 to 90 degrees.

$\gamma$	0°	5°	10°	15°	20°
$C_1^*$	1.00	1.0003	1.0010	1.0023	1.0042
$-C_2^*$	0	$4.137 \times 10^{-3}$	$8.297 \times 10^{-3}$	$1.250 \times 10^{-2}$	$1.678 \times 10^{-2}$
$\gamma$	25°	30°	35°	40°	45°
$C_1^*$	1.0066	1.0095	1.0131	1.0173	1.0222
$-C_2^*$	$2.116 \times 10^{-3}$	$2.566 \times 10^{-2}$	$3.031 \times 10^{-2}$	$3.515 \times 10^{-2}$	$4.022 \times 10^{-2}$
$\gamma$	50°	55°	60°	65°	70°
$C_1^*$	1.0279	1.0343	1.0417	1.0500	1.0591
$-C_2^*$	$4.555 \times 10^{-2}$	$5.118 \times 10^{-2}$	$5.178 \times 10^{-2}$	$6.361 \times 10^{-2}$	$7.054 \times 10^{-2}$
$\gamma$	75°	80°	85°	90°	
$C_1^*$	1.0700	1.0821	1.0957	1.1110	
$-C_2^*$	$7.804 \times 10^{-2}$	$8.624 \times 10^{-2}$	$9.524 \times 10^{-2}$	0.1052	

TABLE 5.4: Values of  $C_1^*$  and  $C_2^*$  (Wang [54]).

Using Equations (5.2.3.1) to (5.2.3.3), the stress intensity

factors at the branch tip can also be expressed as:

$$K_I = \overset{\circ}{K}_I F_{11}(\gamma) + \overset{\circ}{K}_{II} F_{12}(\gamma) \quad (5.2.3.4)$$

$$K_{II} = \overset{\circ}{K}_I F_{21}(\gamma) + \overset{\circ}{K}_{II} F_{22}(\gamma)$$

where  $F_{ij}(\gamma)$  have been evaluated numerically and are tabulated in Table (5.5). With the values of  $K_I$  and  $K_{II}$  calculated, the energy release rate for the branched crack is calculated by:

$$G(\theta) = \frac{\kappa + 1}{16\mu} \{ \overset{\circ}{K}_I f_1 + \overset{\circ}{K}_{II} f_2 \} \quad (5.2.3.5)$$

$$f_1 = \{ \overset{\circ}{K}_I (1 + \cos \theta) - \overset{\circ}{K}_{II} \cdot 3 \sin \theta \} \cos \frac{\theta}{2} \quad (5.2.3.6)$$

$$f_2 = \{ \overset{\circ}{K}_I \sin \theta + \overset{\circ}{K}_{II} (3 \cos \theta) \} \cos \frac{\theta}{2}$$

where the superscript  $\circ$  denotes the functions and the quantities associated with the crack before branching. The crack branch configuration in Figure (5.8) is equivalent to the case  $\theta = -\gamma$ . Thus the energy release rate as a function of the direction of crack extension can be calculated and the critical direction found by maximizing the energy release rate.

$\gamma$	$F_{11}(\gamma)$	$F_{12}(\gamma)$	$F_{21}(\gamma)$	$F_{22}(\gamma)$
0°	1.0	0.0	0.0	1.0
5	0.996376669	0.110221389	-0.045633761	0.996376669
10	0.985501784	0.256654362	-0.090886746	0.985501784
15	0.967367377	0.383060001	-0.135350614	0.967367378
20	0.941967671	0.507089163	-0.178607225	0.941967671
25	0.909303233	0.627801413	-0.220228709	0.909303233
30	0.869402901	0.744154821	-0.259745176	0.869402901
35	0.822369570	0.855052729	-0.296606014	0.822369569
40	0.768350721	0.959157299	-0.330288315	0.768350721
45	0.707627245	1.055065146	-0.360189344	0.707627245
50	0.640632778	1.141274706	-0.385678123	0.640632778
55	0.567936288	1.216022443	-0.406171714	0.567936289
60	0.491122705	1.280995092	-0.420303864	0.491122706
65	0.409066648	1.324790179	-0.429702338	0.409066648
70	0.325268794	1.355572731	-0.431764605	0.325268794
75	0.240590462	1.368882254	-0.426909399	0.240590412
80	0.156851952	1.364080076	-0.415023175	0.156851952
85	0.075980844	1.340635356	-0.396294661	0.075980843
90	0.0	1.298875746	-0.371167000	0.0

TABLE 5.5: Values of  $F_{11}(\gamma)$ ,  $F_{12}(\gamma)$ ,  $F_{21}(\gamma)$  and  $F_{22}(\gamma)$ .

### 5.3 Numerical Examples

The fracture criteria for crack branching presented in the previous section are used to analyze the following examples. The stress intensity factors  $K_I$  and  $K_{II}$  of the unbranched crack are calculated using the energy release rate and Ishikawa's scheme. These are then used along with the fracture criteria to predict the direction of a crack extension.

The first problem considered is the deep cantilevered beam sub-

jected to end shear and tension as shown in Figure (5.3). The stress intensity factors  $K_I$  and  $K_{II}$  have been calculated in Section (5.1.2) and that corresponding to  $r_{T_0} = 0.1a$  are equal to 35.921 and 4.452, respectively. The predicted values of the direction of crack extension calculated using the fracture criteria presented previously are given in Table (5.6). The predicted values are in reasonably good agreement. The predicted angle calculated using Equation (5.1.1.15) i.e. Hellen et al.'s approach, is also given in Table (5.6) and is in reasonably good agreement with the other values. This may be because the error introduced by the continuity assumption in Hellen et al.'s approach is not very significant for small angles of crack branching as mentioned before.

	Calculated Angle of Crack Extension
Maximum Stress Criterion	-13.7°
Minimum Strain Energy Criterion	-12.5°
Maximum Energy Release Rate Criterion	
Wang: Equation (5.2.3.5)	-11.6°
Hellen: Equation (5.1.1.15)	-13.72°

TABLE 5.6: Predicted angles of crack extension for the deep cantilevered beam with end shear and tension, Figure 5.5.

The second problem analyzed is that of a plate with an oblique crack subjected to uniaxial tension  $\tau_0$  (Figure (5.9)). The crack makes an angle  $\beta$  with the direction of loading and the direction of crack extension is shown as  $\theta$  in the figure. The plane stress plate is analy-

zed for different angles of crack orientation,  $\beta$ . The finite element grid used, for  $\beta = 45^\circ$ , is shown in Figure (5.10). Again, it is noted that the configurations of the four-node mixed transitional finite elements conform with the requirements stated in Chapter 3. Also, the grid in the crack tip region is considered to be relatively coarse and, except for  $\beta = 45^\circ$ , only the crack tip can be used as  $\Gamma_0$  to be moved when using Ishikawa's scheme to calculate the stress intensity factors  $\overset{\circ}{K}_I$  and  $\overset{\circ}{K}_{II}$  for the unbranched crack. The calculated stress intensity factors are given in Table (5.7) together with the following stress intensity factors for an infinite plate, i.e.

$$\overset{\circ}{K}_I = \tau_0 a^{1/2} \sin^2 \beta, \quad \overset{\circ}{K}_{II} = \tau_0 a^{1/2} \sin \beta \cos \beta \quad (5.3.1)$$

$\beta$	$\overset{\circ}{K}_I$			$\overset{\circ}{K}_{II}$		
	Infinite Plate	Finite Element	Error %	Infinite Plate	Finite Element	Error %
15°	0.0669	0.0732	9.42	0.250	0.2937	17.5
30°	0.250	0.2925	17.0	0.4330	0.5072	17.1
45°	0.500	0.5372	7.4	0.50	0.6009	20.0
60°	0.7499	0.8013	6.9	0.4330	0.4960	14.5
75°	0.9330	1.0281	10.2	0.250	0.3153	26.1

TABLE 5.7: Stress intensity factors for the square plate with an oblique crack subjected to uniaxial tension, Figure 5.9.

It is observed that the calculated stress intensity factors  $\overset{\circ}{K}_I$  and  $\overset{\circ}{K}_{II}$  are not very accurate and the deviations from the infinite plate solution range from about 6.9% to 26.1%. This is because of the lack of

a finer grid around the crack tip. The predicted values of the angle of crack extension,  $\theta$ , calculated using Wang's equation (Equation (5.2.3.5)), Hellen et al.'s approach (Equation (5.1.1.15)) and the finite element method using different virtual crack extensions and crack branch model of Figure (5.2.b) are tabulated in Table (5.8) and plotted in Figure (5.11). Erdogan and Sih's [48] theoretical results using the maximum stress criterion and the stress intensity factors for an infinite plate are also shown in the same figure. It can be observed that the predicted values of  $\theta$  using Wang's equation and the stress intensity factors calculated using Ishikawa's scheme are in very good agreement with that of Erdogan and Sih. Although a coarse finite element grid has been used which resulted in relatively large errors in the stress intensity factors as mentioned above, the direction of crack extension can still be predicted fairly accurately. Results calculated using Hellen et al.'s approach agree well with those calculated using Wang's equation and the maximum stress criterion for  $\beta$  angles of  $60^\circ$  and above. For  $\beta$  below  $60^\circ$ , considerable divergence occurs. This is not surprising because the continuity assumption involved in Hellen et al.'s work (i.e. the derivation of Equation (5.1.1.15)) is not valid. Again, good agreement for  $\beta$  larger than  $60^\circ$  is observed because the error due to continuity assumption is not very significant when the angle of crack branching is relatively small. Finally, the predicted values using the virtual crack extension method are not satisfactory and, perhaps, can be improved by grid refinements near the crack tip. However, this is not feasible because of the storage limitation on the McMaster University CDC CYBER computer. Hence, the foregoing analyses indicate that the direction of crack extension can be satisfactorily predicted using the

energy release rate expression given by Wang (Equation 5.2.3.5) with the stress intensity factors calculated by the direct derivative method using Ishikawa's scheme and mixed finite elements.

	Angle of Crack Extension ( $\theta$ )		
$\beta$	Wang's Formula Equation (5.2.3.5)	Hellen's Formula Equation (5.1.1.15)	Finite Element Using Virtual Crack Extension
15°	62.7	29.3	75.4
30°	58.2	40.9	59.8
45°	51.3	44.8	45.3
60°	41.4	41.8	24.9
75°	25.6	25.2	-17.2

TABLE 5.8: Predicted angles of crack extension for the square plate with an oblique crack subjected to uniform tension, Figure 5.9.

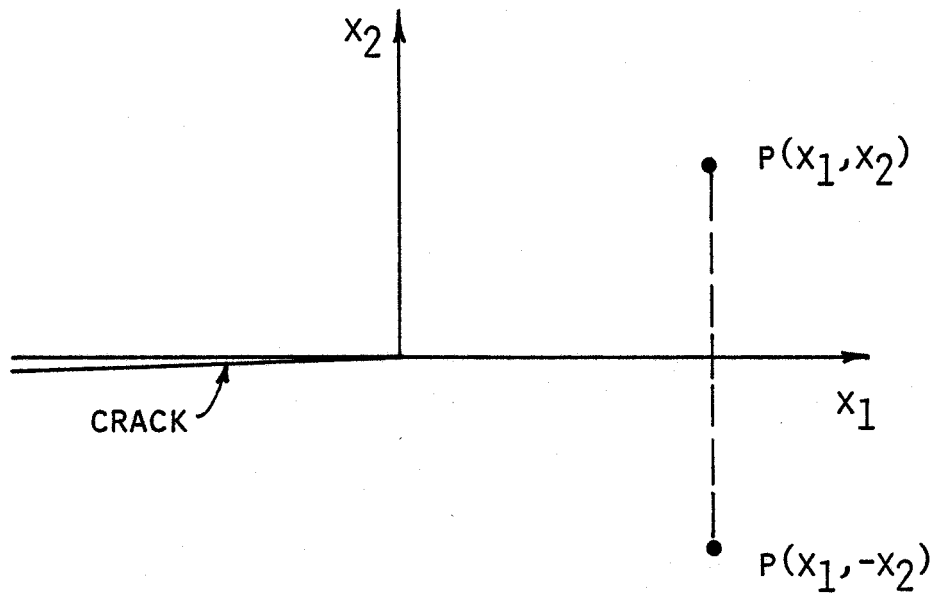


FIG. 5.1: CRACK TIP COORDINATE SYSTEM.

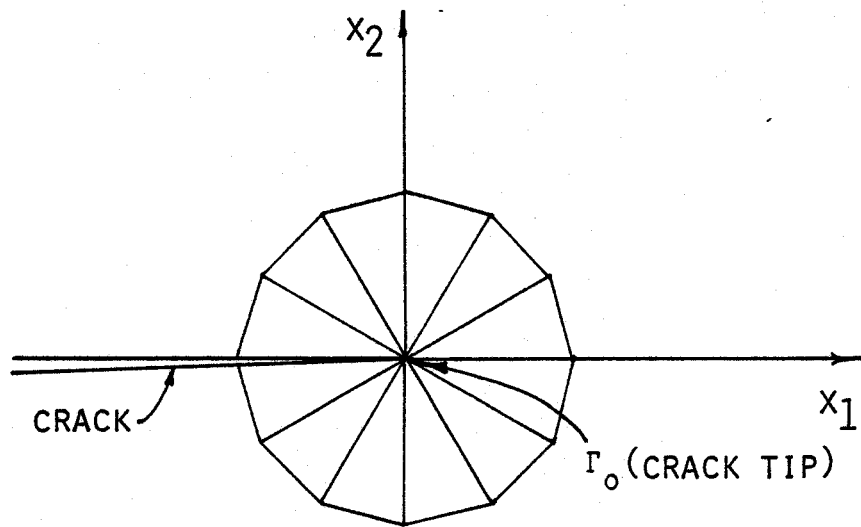


FIG. 5.2 a: FINITE ELEMENT GRID AROUND THE CRACK TIP.

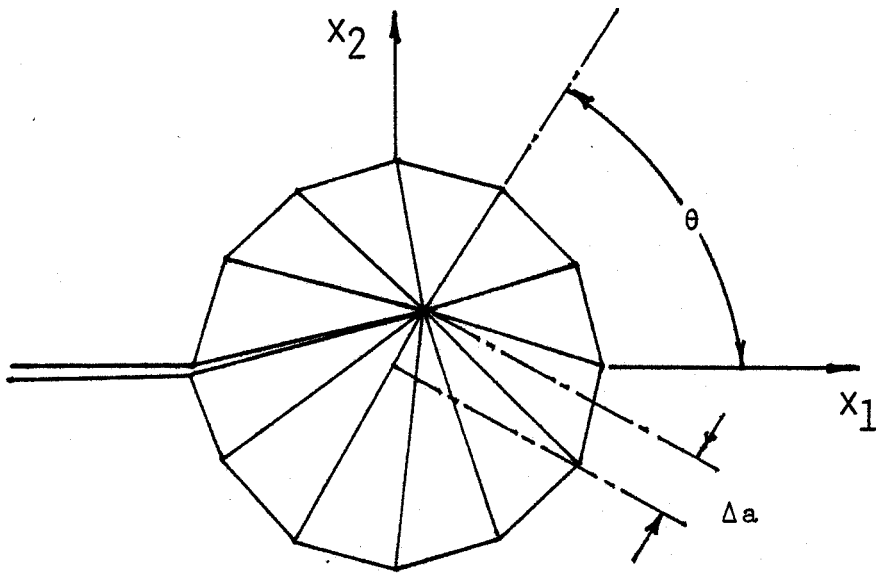


FIG. 5.2 b: MODELLING OF CRACK BRANCHING BY MOVING THE NODE AT THE CRACK TIP ONLY.

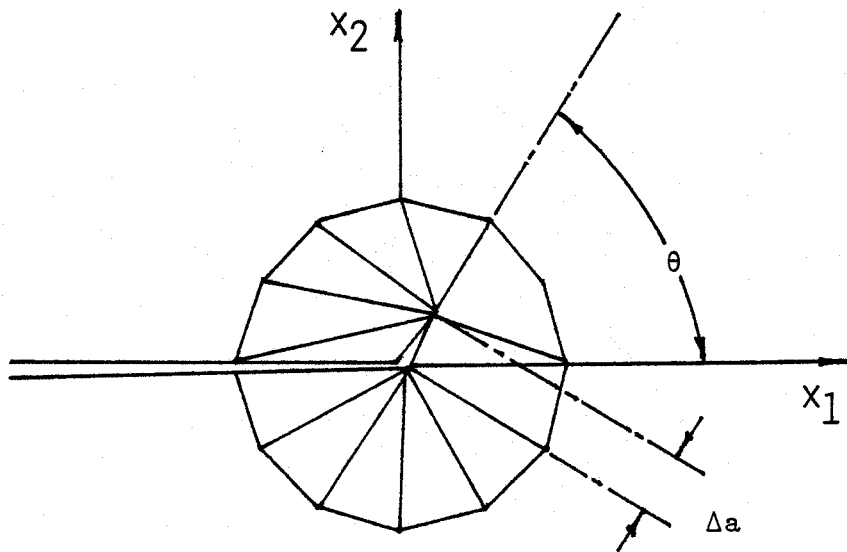


FIG. 5.2 c: MODELLING OF CRACK BRANCHING BY INTRODUCING TWO EXTRA ELEMENTS.

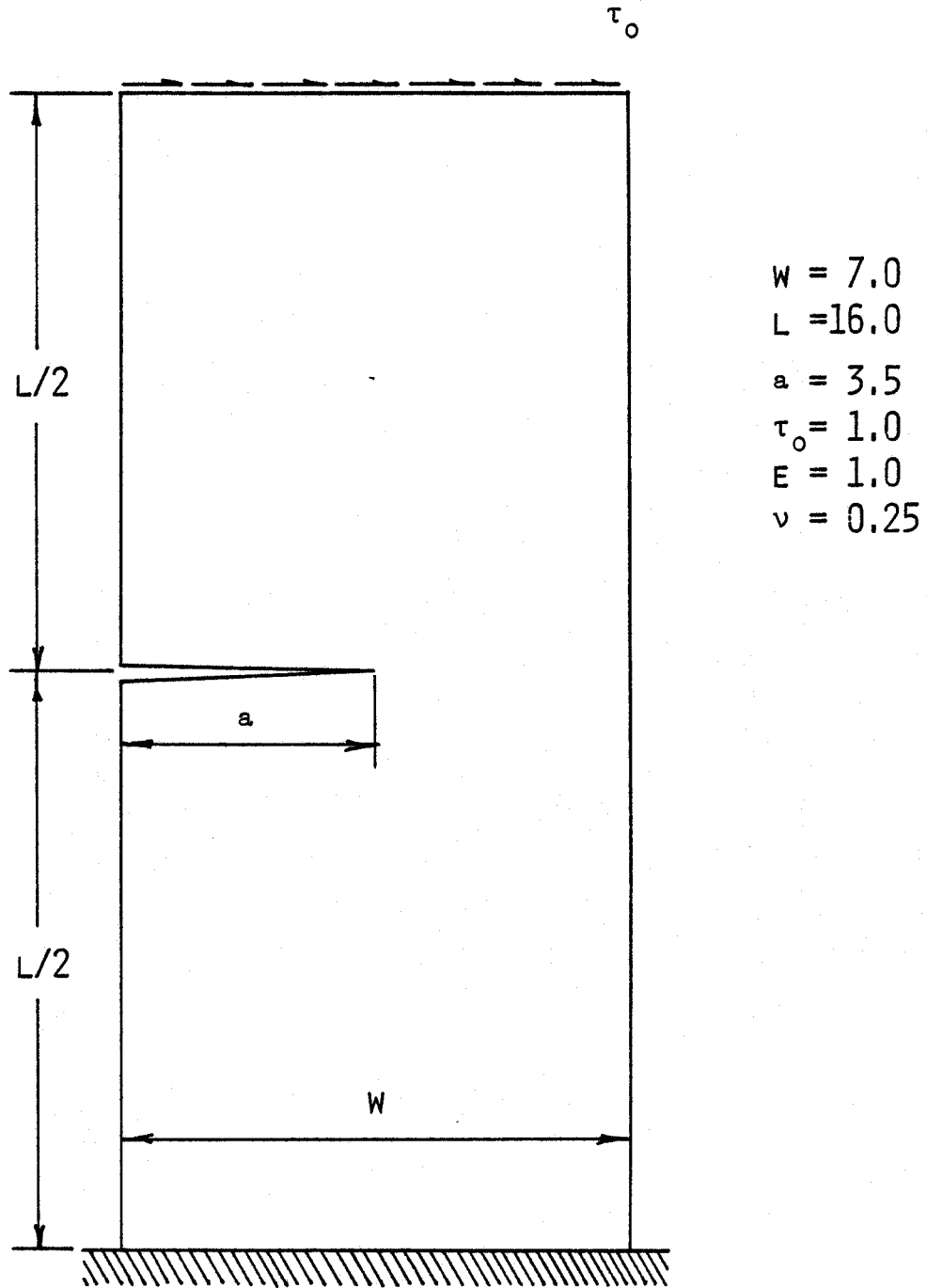


FIG. 5.3: DEEP CANTILEVERED BEAM SUBJECTED TO END SHEAR USED FOR DETERMINING THE CRACK INTENSITY FACTOR  $K_I$  AND  $K_{II}$ .

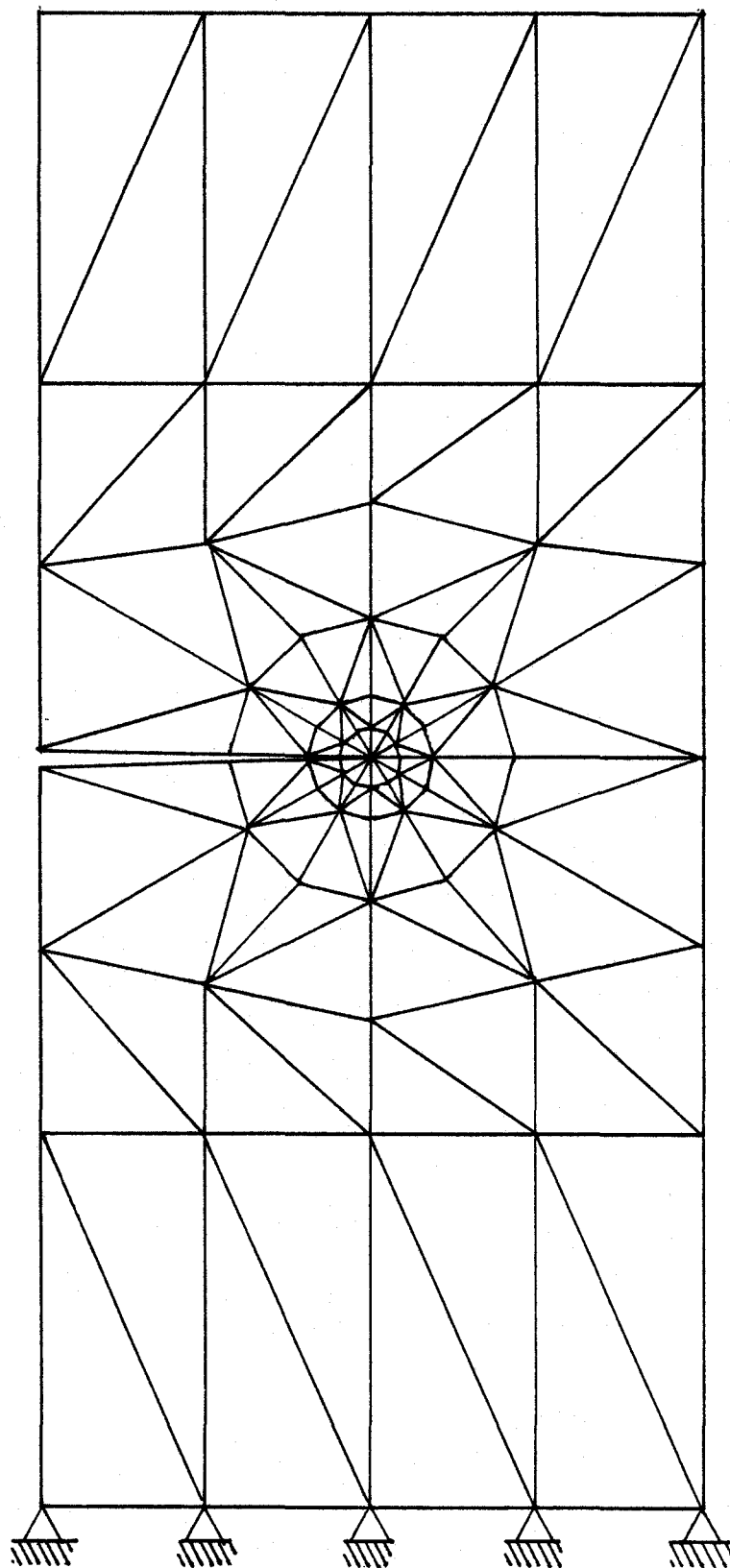


FIG. 5.4: FINITE ELEMENT MESH USED FOR DETERMINING THE CRACK INTENSITY FACTORS  $K_I$  AND  $K_{II}$  FOR THE DEEP CANTILEVERED BEAM SUBJECTED TO END SHEAR.

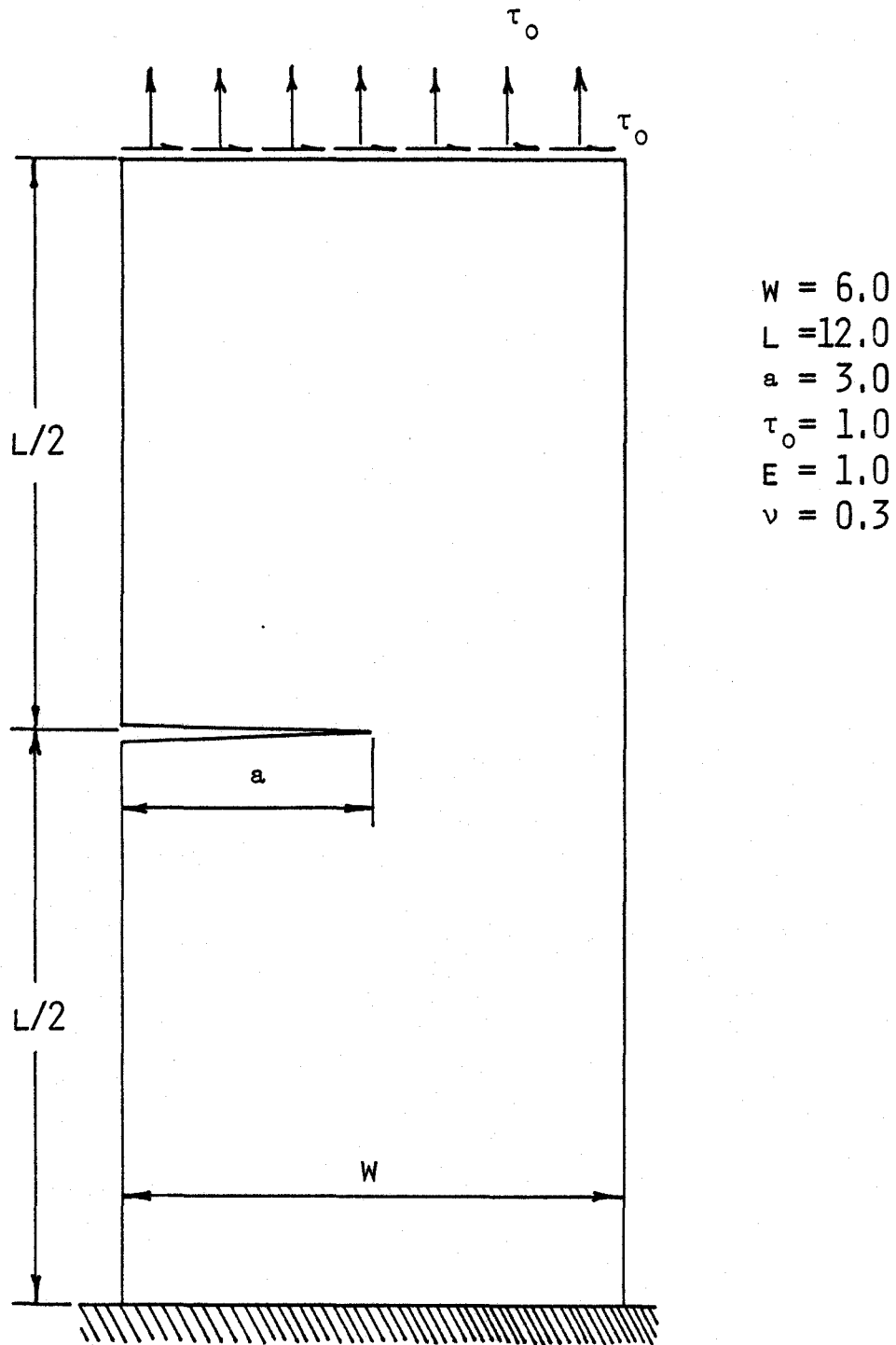


FIG. 5.5: DEEP CANTILEVERED BEAM SUBJECTED TO BOTH TENSION AND END SHEAR USED FOR DETERMINING THE CRACK INTENSITY FACTORS  $K_I$  AND  $K_{II}$ .

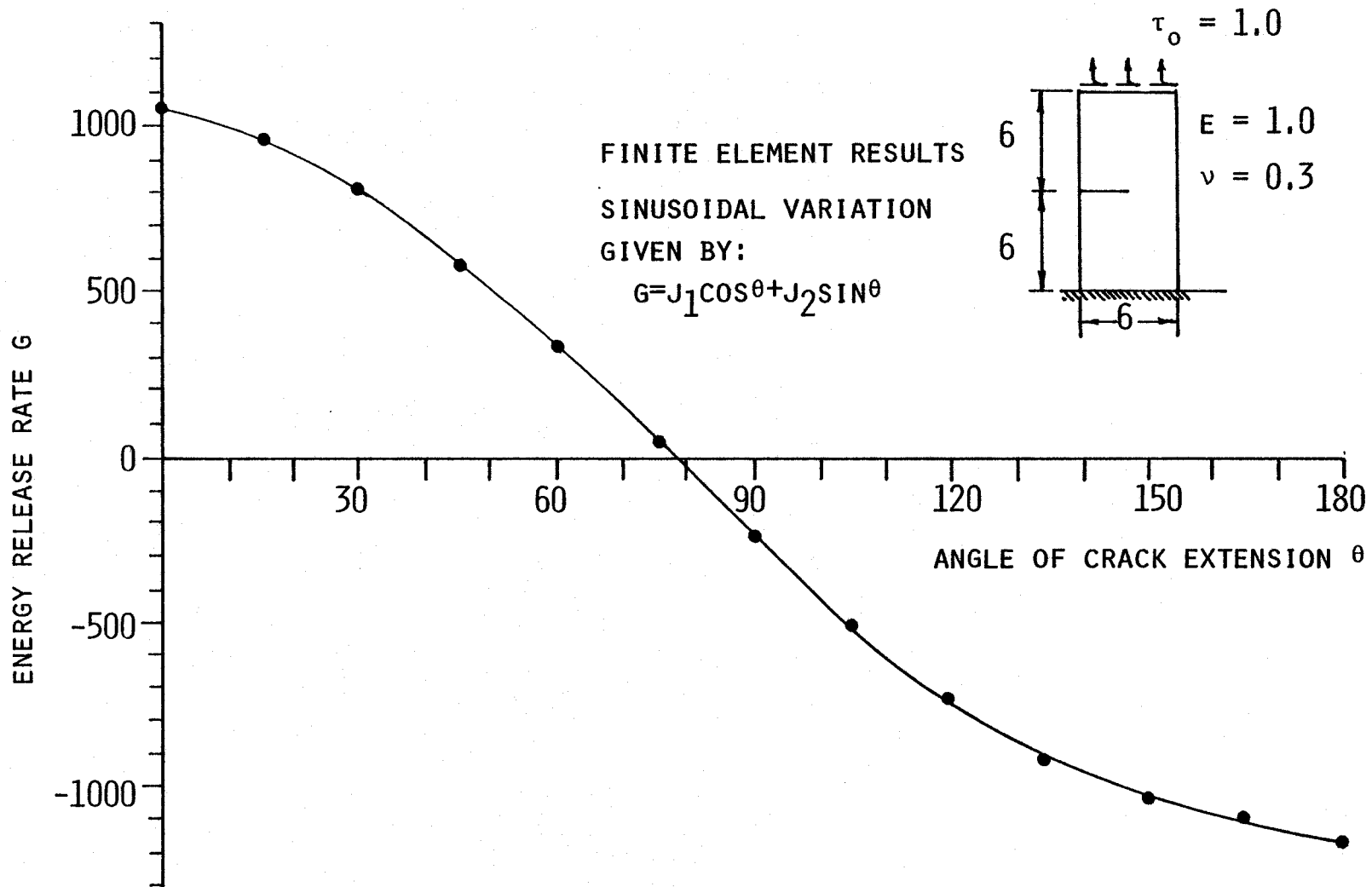


FIG. 5.6: PLOT OF ENERGY RELEASE RATE G AGAINST ANGLE OF CRACK EXTENSION  $\theta$  FOR THE DEEP CANTILEVERED BEAM SUBJECTED TO BOTH TENSION AND END SHEAR - FIGURE 5.5.

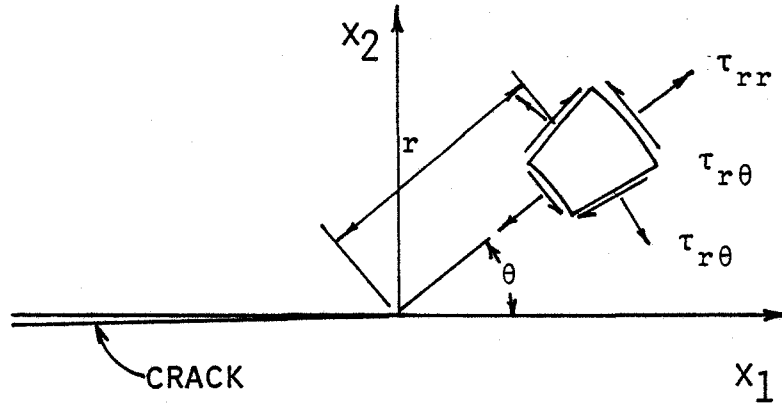


FIG. 5.7: STRESS COMPONENTS NEAR THE CRACK TIP IN POLAR COORDINATES.

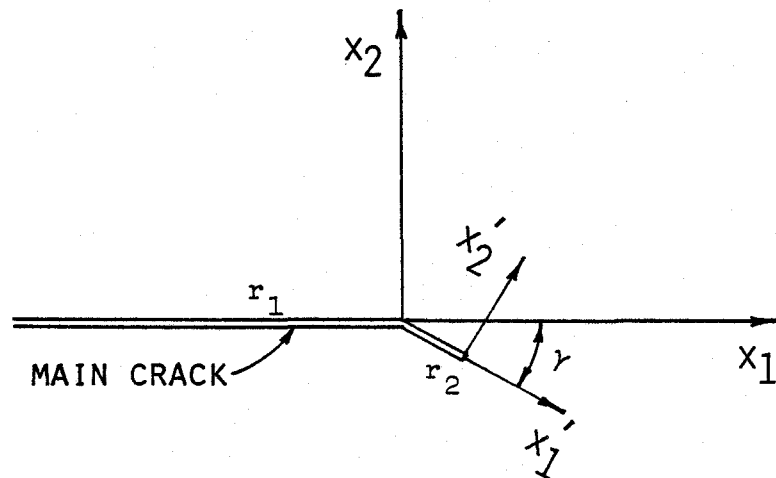


FIG. 5.8: PROBLEM OF A BRANCHED CRACK.

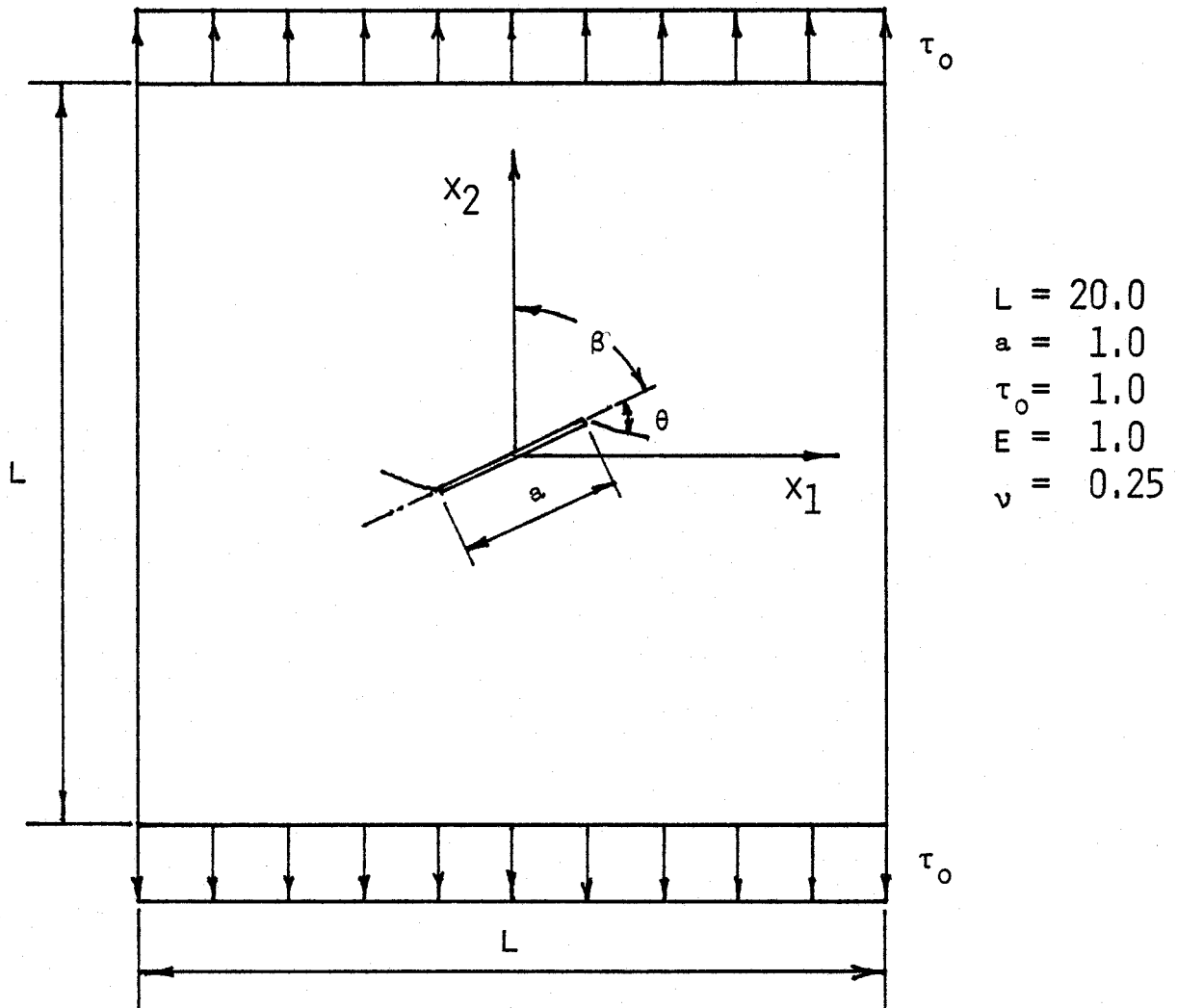


FIG. 5.9: SQUARE PLATE WITH OBLIQUE CRACK SUBJECTED TO TENSILE LOADING USED FOR DETERMINING THE CRACK INTENSITY FACTORS  $K_I$  AND  $K_{II}$  AND THE ANGLE OF CRACK BRANCHING  $\theta$ .

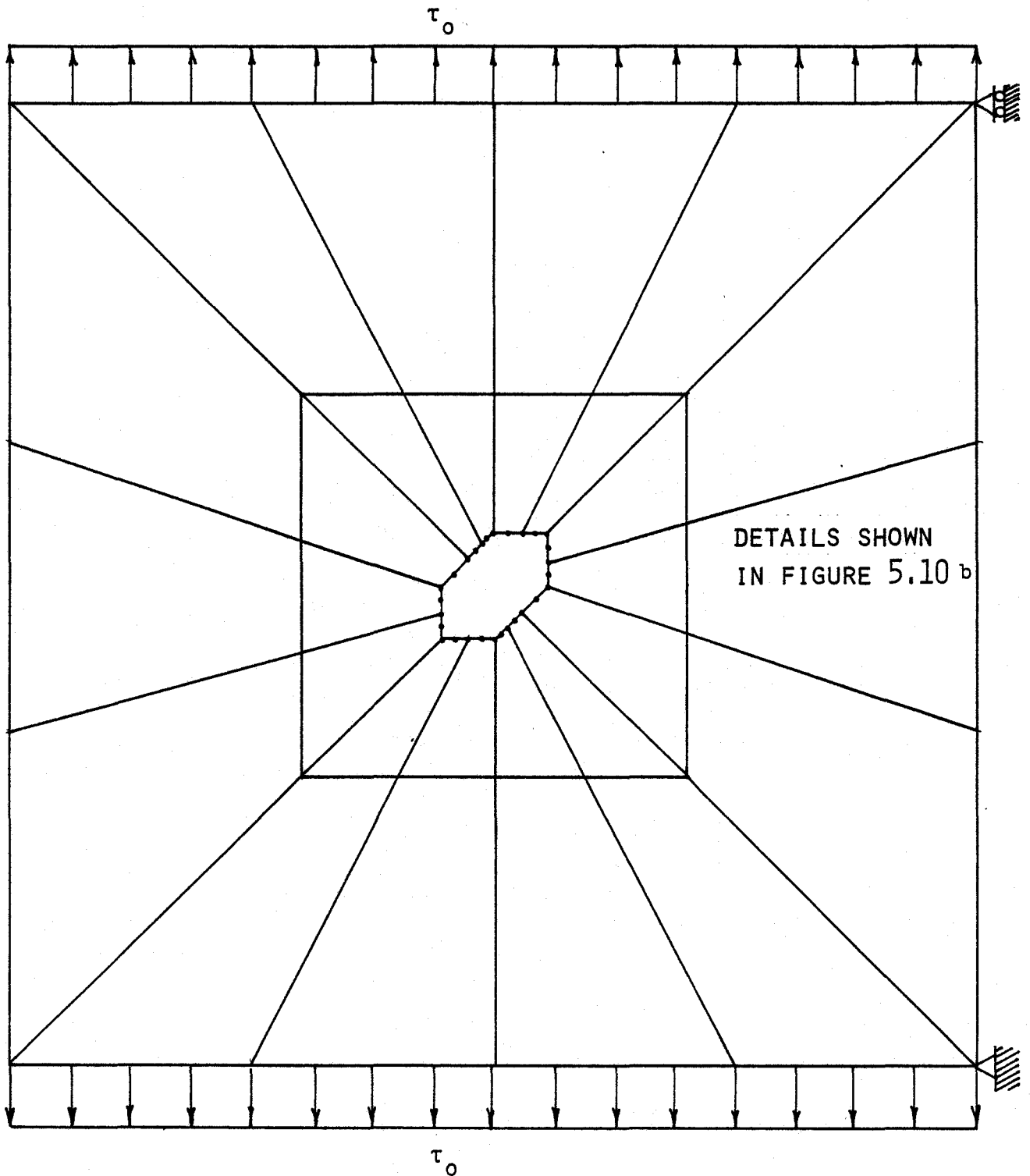


FIG. 5.10 <sub>a</sub> : FINITE ELEMENT MESH USED FOR DETERMINING THE CRACK INTENSITY FACTOR  $K_I$  AND  $K_{II}$  AND THE ANGLE OF CRACK BRANCHING FOR THE SQUARE PLATE WITH AN OBLIQUE CRACK SUBJECTED TO UNIAXIAL TENSION  $\tau_0$ .

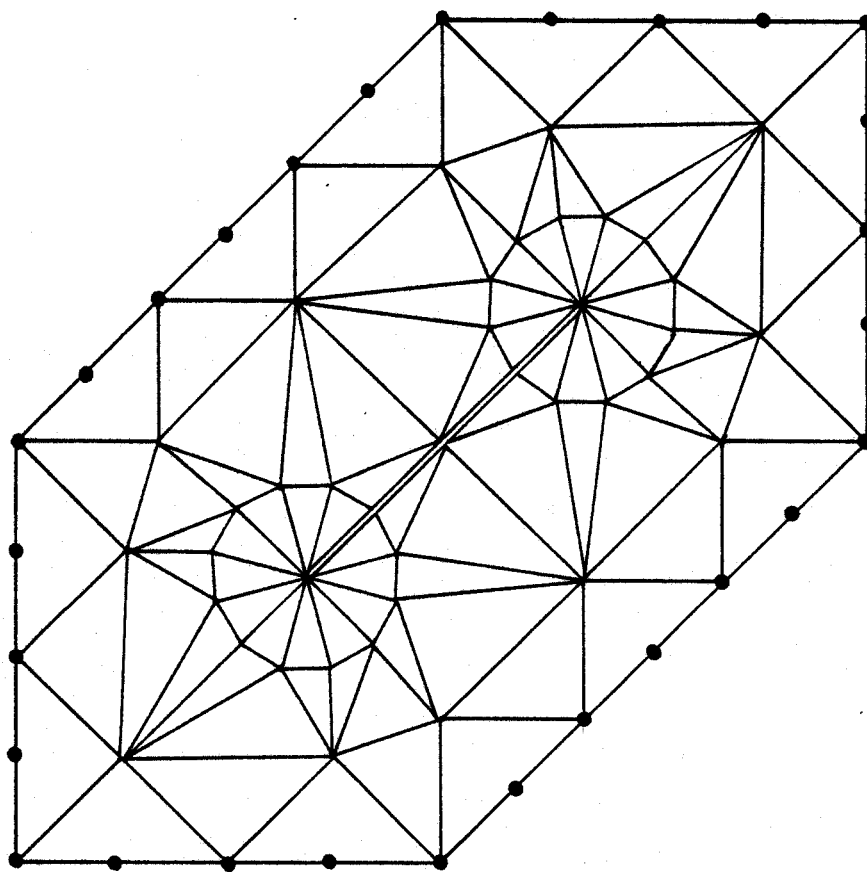


FIG. 5.10 b :      DETAILS OF THE FINITE ELEMENT MESH AROUND THE  
THE CRACK TIP FOR THE SQUARE PLATE WITH AN  
OBLIQUE CRACK SUBJECTED TO UNAXIAL TENSION.

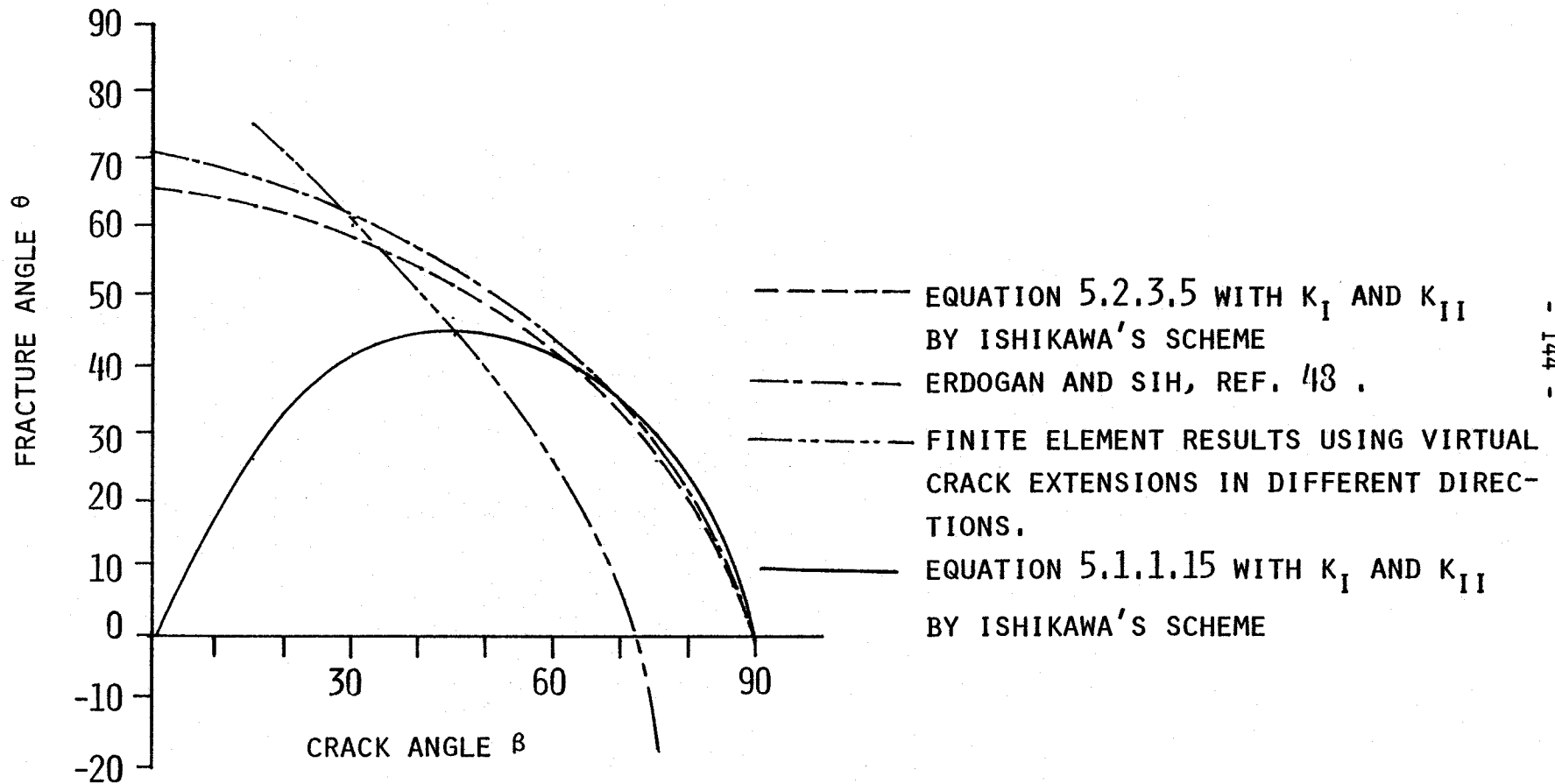


FIG. 5.11: FRACTURE ANGLE  $\theta$  AGAINST CRACK ANGLE  $\beta$  FOR A SQUARE PLATE WITH AN OBLIQUE CRACK SUBJECTED TO TENSION.

CHAPTER 6

CONCLUSIONS

Mixed transitional finite elements, which enable the use of the three-node triangular mixed and eight-node isoparametric displacement finite elements simultaneously, have been developed and tested numerically. Applications of the combination of the above three types of finite elements to both Mode I and mixed mode problems in linear elastic fracture mechanics have also been carried out.

The mixed finite element method [7] via the Hellinger-Reissner's Principle was shown to give much better results than the corresponding displacement finite element method via the Principle of Minimum Potential Energy. However, the mixed method requires more degrees of freedom than the displacement method for the same number of elements, which leads to a tremendous increase in the computer storage required. Mixed transitional finite elements have been developed in this work to enable the use of the mixed and displacement type finite elements in the same finite element grid, with the mixed finite elements used in the region where high stress gradients are expected due to a stress concentration or singularity. In particular, a four-node triangular and a three-node triangular mixed transitional elements have been developed to connect the three-node triangular mixed finite elements by Mirza and Olson [7] and the conventional eight-node isoparametric displacement elements. In general, the computer storage requirement, when using the above mixed,

mixed transitional and displacement finite elements in a single application, has been found to be much less than that required when only the mixed finite elements are used. This is especially so if the region of high stress gradients influenced by a stress singularity is much smaller than some typical dimension of a problem to be analyzed.

The matrix equations in plane elasticity, when the mixed finite elements are used, are always symmetric and indefinite. The master finite element matrix, when premultiplied by its own transpose, becomes positive definite. The matrix equations were solved using a computer subroutine that utilizes the skyline technique, Bathe and Wilson [12], and Gaussian elimination making full use of properties of a symmetric positive definite matrix.

Numerical tests revealed that very large values (around  $10^6$ ) of the modulus of elasticity  $E$  caused ill-conditioning of the matrix equation in mixed finite element applications. For linear elastic problems considered in this work, this problem has been avoided by using a small value of  $E$  ( $=1.0$ ) and the solution was scaled accordingly. Orientation problems with the four-node transitional finite element have also been observed and it is found that the uncondensed, four-node transitional element works well provided that:

1. the element sides form a triangle with  $m_{12} = -m_{13}$ , Figure (3.5); and
2. the element sides 1-2 and 1-3 form a right angle and are parallel to the global coordinate axes, Figure (3.6).

The strain energy convergence rate of the uncondensed transitional finite element was found to be  $O(N^{-4})$ . For the plane stress cantilever subjected to a parabolic end shear stress, it was found that the energy convergence rate of  $O(N^{-4})$  of both the three-node triangular mixed and eight-node isoparametric displacement finite elements is maintained when all three types of finite elements are used in the analysis. The strain energy convergence rate of the condensed transitional element was found to be  $O(N^{-2})$  and with use of these elements, the strain energy convergence rate for the above-mentioned cantilever became  $O(N^{-3})$ .

The analysis of a plane, linear elastic, square plate with a circular hole in the middle, using the mixed, mixed transitional and displacement finite elements indicated that the computer storage required is about a quarter of that required when only the mixed finite elements are used. A reasonably good accuracy was also obtained for the stress concentration factors. A faster convergence rate (nearly  $O(N^{-2})$ ) has been obtained by Mirza [8] for the stress singular problem of a plane stress square plate with symmetric edge cracks for which the strain energy converges only linearly with  $N$ , even with higher order displacement or hybrid type finite elements, Tong and Pian [34]. The use of the combination of mixed, mixed transitional and displacement finite elements in the analysis of such singular problems, using mixed elements in the vicinity of the singularity, is still expected to result in an improved convergence and accuracy.

The direct derivative energy release rate technique was used to analyze two isotropic rectangular plates with symmetric edge cracks and

a central crack, respectively. The computer storage required was about one-tenth of that when only the mixed finite elements are used, with errors in  $K_I$  of about 3 to 6% only. An orthotropic square plate with a central crack has also been analyzed for different values of the ratio  $E_x/E_y$ . In most cases, the errors in computation of the stress intensity factor  $K_I$  were less than one percent.

The direct derivative technique has been extended by incorporating Ishikawa's scheme to calculate stress intensity factors  $K_I$  and  $K_{II}$  for combined mode fracture problems. For the plane stress cantilever with an edge crack and subjected to end shear, stress intensity factors  $K_I$  and  $K_{II}$  have been obtained with errors of 0.62% and 3.74%, respectively. Combined mode stress intensity factors can also be calculated using the direct derivative technique via Hellen et al.'s approach [41, 42]. However, in such calculations, only the crack tip can be used as  $\Gamma_0$  in applying the direct derivative technique and relatively more refined finite element mesh is required to obtain moderately accurate values of  $K_I$  and  $K_{II}$ .

The maximum energy release rate criterion was used, together with the stress intensity factors calculated using Ishikawa's scheme, to predict direction of a crack extension for combined mode, plane elasticity fracture problems. The energy release rate, as a function of the branch angle derived by Wang [54], was used. A square plate with an oblique crack has also been analyzed and the calculated directions of crack extensions are found to be very close to those given by Erdogan

and Sih [48] using the maximum stress criterion. The virtual crack extension method can also be used to search for the direction of maximum energy release rate by introducing virtual extensions in different directions and calculating the corresponding energy release rates. However, this approach requires a more refined finite element grid in the crack tip region than the one used in the present work. Further investigation is not feasible because of the storage limitation on the CDC CYBER computer at McMaster University.

In summary, the use of mixed transitional finite elements, which enable the use of the three-node triangular and eight-node isoparametric displacement finite elements in a single finite element mesh, results in much saving on computer storage required compared to that when only the mixed finite elements are used while still maintaining reasonably good accuracy. The stress intensity factors  $K_I$  and  $K_{II}$  calculated using Ishikawa's scheme can be used along with an energy release rate expression to fairly accurately predict the direction of a crack extension; especially when the lack of large central memory on a computer does not allow the use of a very refined finite element mesh. However, some disagreements among the researchers exist regarding the expression for the energy release rate when the crack branches and are reported in the literature. Further investigation into this discrepancy is recommended. There is also a need for development of a numerical algorithm to extend the present investigation so that it can be applied to crack propagation problems.

APPENDIX A

FINITE ELEMENT MATRIX FOR THE THREE-NODE TRIANGULAR MIXED ELEMENT  
WITH LINEAR DISPLACEMENT AND STRESS APPROXIMATIONS

The element matrix equation for plane linear elasticity is given here for linear displacement and linear stress approximations within the triangular element shown in Figure (2.1). The material properties are incorporated through the compliance matrix:

$$\underline{C} = \begin{bmatrix} \alpha & -\beta & 0 \\ -\beta & \gamma & 0 \\ 0 & 0 & \delta \end{bmatrix} \quad (A.1)$$

where  $\alpha$ ,  $\beta$ ,  $\gamma$  and  $\delta$  depend upon elasticity properties.

The element matrix equation is of the following form:

$$\begin{bmatrix} \underline{0} & \underline{0} & \underline{a}^T & \underline{0} & \underline{b}^T \\ \underline{0} & \underline{0} & \underline{0} & \underline{b}^T & \underline{a}^T \\ \underline{a} & \underline{0} & \underline{\alpha C} & \underline{-\beta C} & \underline{0} \\ \underline{0} & \underline{b} & \underline{-\beta C} & \underline{\gamma C} & \underline{0} \\ \underline{b} & \underline{a} & \underline{0} & \underline{0} & \underline{\delta c} \end{bmatrix} \begin{Bmatrix} \underline{u} \\ \underline{\tau} \end{Bmatrix} = \begin{Bmatrix} \underline{d} \\ \underline{e} \\ 0 \end{Bmatrix} \quad (A.2)$$

$$\text{or } \underline{S} \tilde{\underline{\Lambda}} = \underline{p}. \quad (\text{A.3})$$

where the submatrices a, b, c, d, e, u and r in Equation (A.2) are given by:

$$a_{ij} = \int_{\Omega} L_i L_j d\Omega; \quad i = j = 1, 2, 3 \quad (\text{A.4})$$

$$b_{ij} = \int_{\Omega} L_i L_j x_2 d\Omega; \quad i = j = 1, 2, 3 \quad (\text{A.5})$$

$$c_{ij} = \int_{\Omega} L_i L_j d\Omega; \quad i = j = 1, 2, 3 \quad (\text{A.6})$$

*minus*

$$d_i = \int_{\Omega} f_1 L_i d\Omega; \quad i = j = 1, 2, 3 \quad (\text{A.7})$$

$$e_i = \int_{\Omega} f_2 L_i d\Omega; \quad i = j = 1, 2, 3 \quad (\text{A.8})$$

$$\tilde{\underline{u}} = \langle u_1^1 \ u_1^2 \ u_1^3 \ u_2^1 \ u_2^2 \ u_2^3 \rangle^T \quad (\text{A.9})$$

$$\tilde{\underline{r}} = \langle \tau_{11}^1 \ \tau_{11}^2 \ \tau_{11}^3 \ \tau_{22}^1 \ \tau_{22}^2 \ \tau_{22}^3 \ \tau_{12}^1 \ \tau_{12}^2 \ \tau_{12}^3 \rangle^T \quad (\text{A.10})$$

It is simple to evaluate the submatrices a, b, and c. If  $(x_{1_i}, x_{2_i})$  are the coordinates of the  $i^{\text{th}}$  node of the triangular element (Figure (2.1)), then the matrices a, b and c in terms of nodal coordinates are:

$$\frac{\underline{a}}{3 \times 3} = \frac{t}{6} \begin{bmatrix} 2 - x_2 & 3 - x_2 & 1 - x_2 \\ x_2 - x_2 & x_2 - x_2 & x_2 - x_2 \\ x_2 - x_2 & x_2 - x_2 & x_2 - x_2 \end{bmatrix} \quad (\text{A.11})$$

$$\frac{\underline{b}}{3 \times 3} = \frac{t}{6} \begin{bmatrix} 3 - x_1 & 1 - x_1 & 2 - x_1 \\ x_1 - x_1 & x_1 - x_1 & x_1 - x_1 \\ x_1 - x_1 & x_1 - x_1 & x_1 - x_1 \end{bmatrix} \quad (\text{A.12})$$

$$\underline{c} = -\frac{At}{12} \begin{bmatrix} 2 & 1 & 1 \\ 1 & 2 & 1 \\ 1 & 1 & 2 \end{bmatrix} \quad (\text{A.13})$$

where  $A$  and  $t$  are the area and thickness of the triangular element, respectively. Since  $\underline{c}$  is symmetric, the matrix of coefficients  $\underline{S}$  in Equation (A.3) is also symmetric as expected. The derivation of the load vector  $\langle \underline{d}^T \underline{e}^T \rangle$  is identical to its generation in the displacement method.

Next, the degrees of freedom  $\tilde{\Lambda}$  are rearranged by interchanging the corresponding rows and columns of  $\underline{S}$  such that:

$$\tilde{\Lambda} = \langle u_1^1 \ u_2^1 \ \tau_{11}^1 \ \tau_{22}^1 \ \tau_{12}^1 \ u_1^2 \ u_2^2 \ \tau_{11}^2 \ \tau_{22}^2 \ \tau_{12}^2 \ u_1^3 \ u_2^3 \ \tau_{11}^3 \ \tau_{22}^3 \ \tau_{12}^3 \rangle^T \quad (\text{A.14})$$

and the matrix  $\underline{S}$  becomes:

$$\frac{\bar{S}}{15 \times 15} =$$

0	0	a <sub>11</sub>	0	b <sub>11</sub>	0	0	a <sub>21</sub>	0	b <sub>21</sub>	0	0	a <sub>31</sub>	0	b <sub>31</sub>
0	0	b <sub>11</sub>	a <sub>11</sub>	0	0	0	0	b <sub>21</sub>	a <sub>21</sub>	0	0	0	b <sub>31</sub>	a <sub>31</sub>
	h <sub>11</sub>	f <sub>11</sub>	0	a <sub>12</sub>	0	h <sub>12</sub>	f <sub>12</sub>	0	a <sub>13</sub>	0	h <sub>13</sub>	f <sub>13</sub>	0	0
		i <sub>11</sub>	0	0	b <sub>12</sub>	f <sub>12</sub>	i <sub>12</sub>	0	0	b <sub>13</sub>	f <sub>13</sub>	i <sub>13</sub>	0	0
			g <sub>11</sub>	b <sub>12</sub>	a <sub>12</sub>	0	0	g <sub>12</sub>	b <sub>13</sub>	a <sub>13</sub>	0	0	g <sub>13</sub>	0
				0	0	a <sub>22</sub>	0	b <sub>22</sub>	0	0	a <sub>32</sub>	0	b <sub>32</sub>	0
					0	0	b <sub>22</sub>	a <sub>22</sub>	0	0	0	b <sub>32</sub>	a <sub>32</sub>	0
						h <sub>22</sub>	f <sub>22</sub>	0	a <sub>23</sub>	0	h <sub>23</sub>	f <sub>23</sub>	0	0
							i <sub>22</sub>	0	0	b <sub>23</sub>	f <sub>23</sub>	i <sub>23</sub>	0	0
								g <sub>22</sub>	b <sub>23</sub>	a <sub>23</sub>	0	0	g <sub>23</sub>	0
									0	0	a <sub>33</sub>	0	b <sub>33</sub>	0
										0	0	b <sub>33</sub>	a <sub>33</sub>	0
											h <sub>33</sub>	f <sub>33</sub>	0	0
												i <sub>33</sub>	0	0
														g <sub>33</sub>

s y m m e t r i c

where  $\underline{f} = -\beta \underline{c}$

$\underline{g} = \delta \underline{c}$

$\underline{h} = \alpha \underline{c}$

$\underline{i} = \gamma \underline{c}$

and  $\alpha$ ,  $\beta$ ,  $\gamma$  and  $\delta$  are elements of the compliance matrix  $\underline{C}$  in Equation (A.1). The corresponding entries in the load vector  $\underline{p}$  are also interchanged and the modified load vector becomes:

$$\bar{\underline{p}} = \langle d_1 \ e_1 \ 0 \ 0 \ 0 \ d_2 \ e_2 \ 0 \ 0 \ 0 \ d_3 \ e_3 \ 0 \ 0 \ 0 \rangle^T.$$

Equation (A.3) alters to:

$$\bar{\underline{S}} \bar{\underline{\Lambda}} = \bar{\underline{P}}. \tag{A.16}$$

The compliance matrix in Equation (A.1) for plane stress isotropic case is given by:

$$\underline{C} = \frac{1}{E} \begin{bmatrix} 1 & -\nu & 0 \\ -\nu & 1 & 0 \\ 0 & 0 & 2(1+\nu) \end{bmatrix} \tag{A.17}$$

where  $E$  and  $\nu$  are the modulus of elasticity and the Poisson's ratio, respectively. For isotropic plane strain case, the compliance matrix  $\underline{C}$  takes on the following form:

$$\underline{C} = \frac{1 - \nu^2}{E} \begin{bmatrix} 1 & \frac{\nu}{1-\nu} & 0 \\ -\frac{\nu}{1-\nu} & 1 & 0 \\ 0 & 0 & \frac{2}{1-\nu} \end{bmatrix} \quad (\text{A.18})$$

The compliance matrix  $\underline{C}$  can also be switched to incorporate the orthotropic cases and the coefficients  $\alpha$ ,  $\beta$ ,  $\gamma$  and  $\delta$  can be found in Reference [14].

APPENDIX B

FINITE ELEMENT MATRIX FOR THE FOUR-NODE TRIANGULAR MIXED  
TRANSITIONAL ELEMENT (UNCONDENSED)

The element matrix equation for plane linear elasticity is presented for the four-node triangular mixed finite element shown in Figure (2.6). The material properties are again given by the compliance matrix  $\underline{C}$  in Equation (A.1) which for isotropic plane stress and plane strain cases are given by Equations (A.17) and (A.18).

The element matrix equation has been given in Equation (2.3.19)

as:

$$\begin{bmatrix} \underline{0} & \underline{0} & \underline{a}^T & \underline{0} & \underline{b}^T \\ \underline{0} & \underline{0} & \underline{0} & \underline{b}^T & \underline{a}^T \\ \underline{a} & \underline{0} & \underline{\alpha c} & -\underline{\beta c} & \underline{0} \\ \underline{0} & \underline{b} & -\underline{\beta c} & \underline{\gamma c} & \underline{0} \\ \underline{b} & \underline{a} & \underline{0} & \underline{0} & \underline{\delta c} \end{bmatrix} \begin{Bmatrix} \underline{\tilde{u}} \\ \underline{\tilde{\tau}} \end{Bmatrix} = \begin{Bmatrix} \underline{d} \\ \underline{e} \\ \underline{0} \end{Bmatrix} \quad (\text{B.1})$$

$$\text{or } \underline{\tilde{S}} \underline{\tilde{\Lambda}} = \underline{p} \quad (\text{B.2})$$

and the submatrices  $\underline{\tilde{u}}$ ,  $\underline{\tilde{\tau}}$ ,  $\underline{a}$ ,  $\underline{b}$ ,  $\underline{c}$ ,  $\underline{d}$  and  $\underline{e}$  are as defined in Equations (2.3.11), (2.3.12) and Equations (2.3.20) to (2.3.24). If  $(x_{1_i}, y_{1_i})$  are the coordinates of the  $i^{\text{th}}$  node of the triangular element (Figure

(2.6)), the matrices a, b and c in terms of nodal coordinates are given by:

$$\underline{a} = t \begin{bmatrix} \frac{b_1}{6} & \frac{b_2}{12} - \frac{b_3}{12} & \frac{-b_2}{12} + \frac{b_3}{12} & \frac{b_2}{6} + \frac{b_3}{6} \\ \frac{b_1}{12} & \frac{b_2}{15} - \frac{b_3}{10} & \frac{-b_2}{60} - \frac{b_3}{60} & \frac{b_2}{30} + \frac{b_3}{5} \\ \frac{b_1}{12} & \frac{-b_2}{60} - \frac{b_3}{60} & \frac{-b_2}{10} + \frac{b_3}{15} & \frac{b_2}{5} + \frac{b_3}{30} \\ \frac{b_1}{6} & \frac{b_2}{30} - \frac{4b_3}{30} & \frac{-4b_2}{30} + \frac{b_3}{12} & \frac{8b_2}{30} + \frac{8b_3}{30} \end{bmatrix} \quad (\text{B.3})$$

$$\underline{b} = t \begin{bmatrix} \frac{a_1}{6} & \frac{a_2}{12} - \frac{a_3}{12} & \frac{-a_2}{12} + \frac{a_3}{12} & \frac{a_2}{6} + \frac{a_3}{6} \\ \frac{a_1}{12} & \frac{a_2}{15} - \frac{a_3}{10} & \frac{-a_2}{60} - \frac{a_3}{60} & \frac{a_2}{30} + \frac{a_3}{5} \\ \frac{a_1}{12} & \frac{-a_2}{60} - \frac{a_3}{60} & \frac{-a_2}{10} + \frac{a_3}{15} & \frac{a_2}{5} + \frac{a_3}{30} \\ \frac{a_1}{6} & \frac{a_2}{30} - \frac{4a_3}{30} & \frac{-4a_2}{30} + \frac{a_3}{12} & \frac{8a_2}{30} + \frac{8a_3}{30} \end{bmatrix} \quad (\text{B.4})$$

$$\underline{c} = -t \times A \begin{bmatrix} \frac{1}{6} & & & \\ & \frac{1}{20} & & \\ & & \frac{1}{20} & \\ & & & \frac{1}{15} \\ & & & & \frac{7}{90} & -\frac{1}{180} & \frac{2}{45} \\ & & & & & & \frac{7}{90} & \frac{2}{45} \\ & & & & & & & & \frac{8}{45} \end{bmatrix} \quad (\text{B.5})$$

where t and A are the thickness and area of the triangle, respectively;

$a_i$  and  $b_i$  are defined in terms of the nodal coordinates by:

$$a_1 = x_1^3 - x_1^2$$

$$a_2 = x_1^1 - x_1^3 \tag{B.6}$$

$$a_3 = x_1^2 - x_1^1$$

$$b_1 = x_2^2 - x_2^3$$

$$b_2 = x_2^3 - x_2^1 \tag{B.7}$$

$$b_3 = x_2^1 - x_2^2$$

The derivation of the load vector  $\langle \underline{d}^T \underline{e}^T \rangle$  is identical to its generation in the displacement method.

The degrees of freedom  $\underline{\tilde{\Lambda}}$  are then rearranged by interchanging the corresponding rows and columns of  $\underline{S}$  such that:

$$\underline{\tilde{\Lambda}} = \langle u_1^1 \ u_2^1 \ \tau_{11}^1 \ \tau_{22}^1 \ \tau_{12}^1 \ u_1^2 \ u_2^2 \ \tau_{11}^2 \ \tau_{22}^2 \ \tau_{12}^2 \ u_1^3 \ u_2^3 \ \tau_{11}^3 \ \tau_{22}^3 \ \tau_{12}^3 \ u_1^4 \ u_2^4 \ \tau_{11}^4 \ \tau_{22}^4 \ \tau_{12}^4 \rangle^T \tag{B.8}$$

and the matrix  $\underline{S}$  is shown in Equation (B.9).

(S) - S -  
20 x 20

0	0	a <sub>11</sub>	0	b <sub>11</sub>	0	0	0	a <sub>21</sub>	0	b <sub>21</sub>	0	0	0	a <sub>31</sub>	0	b <sub>31</sub>	0	0	0	a <sub>41</sub>	0	b <sub>41</sub>	a <sub>41</sub>
0	0	0	b <sub>11</sub>	a <sub>11</sub>	0	0	0	0	b <sub>21</sub>	a <sub>21</sub>	0	0	0	0	b <sub>31</sub>	a <sub>31</sub>	0	0	0	0	0	b <sub>41</sub>	a <sub>41</sub>
αC <sub>11</sub>	-βC <sub>11</sub>	0	a <sub>12</sub>	0	αC <sub>12</sub>	-βC <sub>12</sub>	0	a <sub>13</sub>	0	αC <sub>13</sub>	-βC <sub>13</sub>	0	a <sub>14</sub>	0	αC <sub>14</sub>	-βC <sub>14</sub>	0	0	0	0	0	0	0
γC <sub>11</sub>	0	0	b <sub>12</sub>	-βC <sub>12</sub>	γC <sub>12</sub>	0	0	b <sub>13</sub>	-βC <sub>13</sub>	γC <sub>13</sub>	0	0	b <sub>14</sub>	-βC <sub>14</sub>	γC <sub>14</sub>	0	0	0	0	0	0	0	0
δC <sub>11</sub>	b <sub>12</sub>	a <sub>12</sub>	0	0	δC <sub>12</sub>	b <sub>13</sub>	a <sub>13</sub>	0	0	δC <sub>13</sub>	b <sub>14</sub>	a <sub>14</sub>	0	0	δC <sub>14</sub>	0	0	0	0	0	0	0	δC <sub>14</sub>
0	0	0	a <sub>22</sub>	0	b <sub>22</sub>	0	0	0	a <sub>32</sub>	0	b <sub>32</sub>	0	0	0	a <sub>42</sub>	0	0	0	0	0	0	b <sub>42</sub>	a <sub>42</sub>
0	0	0	b <sub>22</sub>	a <sub>22</sub>	0	0	0	0	b <sub>32</sub>	a <sub>32</sub>	0	0	0	0	b <sub>42</sub>	a <sub>42</sub>	0	0	0	0	0	b <sub>42</sub>	a <sub>42</sub>
0	0	0	0	0	αC <sub>22</sub>	-βC <sub>22</sub>	0	a <sub>23</sub>	0	αC <sub>23</sub>	-βC <sub>23</sub>	0	a <sub>24</sub>	0	αC <sub>24</sub>	-βC <sub>24</sub>	0	0	0	0	0	0	0
0	0	0	0	0	γC <sub>22</sub>	0	0	b <sub>23</sub>	-βC <sub>23</sub>	γC <sub>23</sub>	0	0	b <sub>24</sub>	βC <sub>24</sub>	γC <sub>24</sub>	0	0	0	0	0	0	0	0
0	0	0	0	0	δC <sub>22</sub>	b <sub>23</sub>	a <sub>23</sub>	0	0	δC <sub>23</sub>	b <sub>24</sub>	a <sub>24</sub>	0	0	δC <sub>24</sub>	0	0	0	0	0	0	0	δC <sub>24</sub>
0	0	0	0	0	0	0	0	a <sub>33</sub>	0	b <sub>33</sub>	0	0	0	a <sub>43</sub>	0	0	0	0	0	0	0	b <sub>43</sub>	a <sub>43</sub>
0	0	0	0	0	0	0	0	0	0	b <sub>33</sub>	a <sub>33</sub>	0	0	0	0	0	0	0	0	0	0	b <sub>43</sub>	a <sub>43</sub>
0	0	0	0	0	0	0	0	0	0	0	0	0	0	αC <sub>33</sub>	-βC <sub>33</sub>	0	a <sub>34</sub>	0	αC <sub>34</sub>	-βC <sub>34</sub>	0	0	0
0	0	0	0	0	0	0	0	0	0	0	0	0	0	γC <sub>33</sub>	0	0	b <sub>34</sub>	-βC <sub>34</sub>	γC <sub>34</sub>	0	0	0	0
0	0	0	0	0	0	0	0	0	0	0	0	0	0	δC <sub>33</sub>	b <sub>34</sub>	a <sub>34</sub>	0	0	0	δC <sub>34</sub>	0	0	0
0	0	0	0	0	0	0	0	0	0	0	0	0	0	0	0	0	a <sub>44</sub>	0	0	0	0	b <sub>44</sub>	a <sub>44</sub>
0	0	0	0	0	0	0	0	0	0	0	0	0	0	0	0	0	0	0	b <sub>44</sub>	a <sub>44</sub>	0	0	a <sub>44</sub>
0	0	0	0	0	0	0	0	0	0	0	0	0	0	0	0	0	0	0	αC <sub>44</sub>	-βC <sub>44</sub>	0	0	0
0	0	0	0	0	0	0	0	0	0	0	0	0	0	0	0	0	0	0	0	γC <sub>44</sub>	0	0	0
0	0	0	0	0	0	0	0	0	0	0	0	0	0	0	0	0	0	0	0	0	0	0	δC <sub>44</sub>

(B.9)

α, β, γ and δ are the elements of the compliance matrix in Equation (A.1). The corresponding entries in the load vector  $\underline{p}$  are also interchanged and the modified load vector takes the following form:

$$\bar{\underline{p}} = \langle d_1 e_1 000 \ d_2 e_2 000 \ d_3 e_3 000 \ d_4 e_4 000 \rangle^T \quad (B.10)$$

The equation (B.2) alters to:

$$\bar{\underline{S}} \bar{\underline{\Lambda}} = \bar{\underline{p}} \quad (B.11)$$



where

$$\underline{M} = \frac{1}{360A} \begin{bmatrix} 81.25b_1^2 & 21.25b_1b_2-60b_1b_3 & -60b_1b_2+21.25b_1b_3 & 120b_1b_2+120b_1b_3 \\ 21.25b_2^2-60b_2b_3+60b_3^2 & 21.25b_2b_3 & & -120b_3^2 \\ \text{symmetric} & 60b_2^2+2.125b_3^2-60b_2b_3 & & -120b_2^2 \\ & & & 240(b_2^2+b_3^2+b_2b_3) \end{bmatrix} \quad (C.2)$$

$$\underline{N} = \frac{1}{360A} \begin{bmatrix} 81.25a_1^2 & 21.25a_1a_2-60a_1a_3 & -60a_1a_2+21.25a_1a_3 & 120a_1a_2+120a_1a_3 \\ 21.25a_2^2-60a_2a_3+60a_3^2 & 21.25a_2a_3 & & -120a_3^2 \\ \text{symmetric} & 60a_2^2+2.125a_3^2-60a_2a_3 & & -120a_2^2 \\ & & & 240(a_2^2+a_3^2+a_2a_3) \end{bmatrix} \quad (C.3)$$

$$\underline{P} = \frac{1}{360A} \begin{bmatrix} 81.25a_1 b_1 & 21.25b_1 a_2 & -60b_1 a_2 & 120b_1 a_1 \\ & -60b_1 a_3 & +21.25b_1 a_3 & +120b_1 a_3 \\ 21.25b_2 a_1 & 21.25b_2 a_2 - 30b_3 a_2 & 30b_3 a_2 & -120b_3 a_3 - 60b_3 a_2 \\ -60b_3 a_1 & -30b_2 a_3 + 60b_3 a_3 & -8.75b_2 a_3 & +60b_2 a_3 \\ -60b_2 a_1 & 30b_2 a_3 & 21.25b_3 a_3 - 30b_3 a_2 & -120b_2 a_2 - 60b_2 a_3 \\ +21.25b_3 a_1 & -8.75b_3 a_2 & -30b_2 a_3 + 60b_2 a_2 & +60b_3 a_2 \\ 120b_2 a_1 & -120b_3 a_3 + 60a_3 b_2 & -120b_2 a_2 + 60b_2 a_3 & 240b_3 a_3 + 240b_2 a_2 \\ +120b_3 a_1 & -60b_2 a_3 & -60b_3 a_2 & +120b_2 a_3 + 120b_3 a_2 \end{bmatrix} \quad (C.4)$$

$$\underline{Q} = \frac{17.5}{360} \langle b_1 \ b_2 \ b_3 \ 0 \rangle^T \quad (C.5)$$

$$\underline{R} = \frac{17.5}{360} \langle a_1 \ a_2 \ a_3 \ 0 \rangle^T \quad (C.6)$$

The vectors  $\underline{d}$  and  $\underline{e}$  are the same as the consistent load vectors for the uncondensed elements;  $t$  and  $A$  are the thickness and area of the triangular element, respectively;  $a_i$  and  $b_i$  are defined by:

$$\begin{aligned} a_1 &= x_1^3 - x_1^2 \\ a_2 &= x_1^1 - x_1^3 \\ a_3 &= x_1^2 - x_1^1 \end{aligned} \quad (C.7)$$

$$\begin{aligned} b_1 &= x_2^2 - x_2^3 \\ b_2 &= x_2^3 - x_2^1 \\ b_3 &= x_2^1 - x_2^2 \end{aligned} \tag{C.8}$$

where  $x_{1_i}$  and  $x_{2_i}$  are the coordinates of the  $i^{\text{th}}$  corner node; and  $\alpha$ ,  $\beta$ ,  $\gamma$  and  $\delta$  are elements of the compliance matrix  $\underline{C}$  (Equation (A.1)) given

by:

$$\underline{C} = \begin{bmatrix} \alpha & -\beta & 0 \\ -\beta & \gamma & 0 \\ 0 & 0 & \delta \end{bmatrix} \tag{C.9}$$

For the three-node mixed element with the stress degrees of freedom at node 3 condensed out, the element matrix equation is given by:

$$\begin{array}{l}
 \left[ \begin{array}{l}
 \frac{\gamma}{6(\gamma\alpha-\beta^2)A} \underline{\tilde{b}}^T \underline{\tilde{b}} \quad \frac{\beta}{6(\gamma\alpha-\beta^2)A} \underline{\tilde{b}}^T \underline{\tilde{a}} \\
 + \frac{1}{6\delta A} \underline{\tilde{a}}^T \underline{\tilde{a}} \quad + \frac{1}{6\delta A} \underline{\tilde{a}}^T \underline{\tilde{b}} \\
 \\
 \frac{\alpha}{6(\gamma\alpha-\beta^2)A} \underline{\tilde{a}}^T \underline{\tilde{a}} \\
 + \frac{1}{6\delta A} \underline{\tilde{b}}^T \underline{\tilde{b}} \\
 \\
 \text{symmetric}
 \end{array} \right]
 \begin{array}{l}
 \frac{1}{12} \underline{\tilde{b}}^{-T} \quad 0 \quad \frac{1}{12} \underline{\tilde{a}}^{-T} \\
 \\
 0 \quad \frac{1}{12} \underline{\tilde{a}}^{-T} \quad \frac{1}{12} \underline{\tilde{b}}^{-T} \\
 \\
 \frac{-\alpha A}{24} \begin{bmatrix} 3 & 1 \\ 1 & 3 \end{bmatrix} \quad \frac{\beta A}{24} \begin{bmatrix} 3 & 1 \\ 1 & 3 \end{bmatrix} \quad 0 \\
 \\
 \frac{-\gamma A}{24} \begin{bmatrix} 3 & 1 \\ 1 & 3 \end{bmatrix} \quad 0 \\
 \\
 \frac{-\delta A}{24} \begin{bmatrix} 3 & 1 \\ 1 & 3 \end{bmatrix}
 \end{array}
 \begin{array}{l}
 \left. \begin{array}{l}
 u_1^1 \\
 u_1^2 \\
 u_1^3 \\
 u_2^1 \\
 u_2^2 \\
 u_2^3 \\
 \tau_{11}^1 \\
 \tau_{11}^2 \\
 \tau_{22}^1 \\
 \tau_{22}^2 \\
 \tau_{12}^1 \\
 \tau_{12}^2
 \end{array} \right\} = \left\{ \begin{array}{l}
 \underline{d} \\
 \underline{e} \\
 \\
 \\
 \\
 \\
 \\
 \\
 \\
 \\
 \\
 \underline{0}
 \end{array} \right.
 \end{array}
 \end{array}$$

(C.10)

where  $\underline{\tilde{a}} = \langle a_1 \ a_2 \ a_3 \rangle$

(C.11)

$\underline{\tilde{b}} = \langle b_1 \ b_2 \ b_3 \rangle$

(C.12)

$$\underline{\tilde{a}} = \begin{bmatrix} a_1 & a_2 & a_3 \\ a_1 & a_2 & a_3 \end{bmatrix}$$

(C.13)

$$\underline{b} = \begin{bmatrix} b_1 & b_2 & b_3 \\ b_1 & b_2 & b_3 \end{bmatrix}$$

(C.14)

The vectors d and e and the constants t, A,  $a_i$ ,  $b_i$ ,  $\alpha$ ,  $\beta$ ,  $\gamma$  and  $\delta$  have been defined previously.

APPENDIX D

DIRECT DERIVATIVE METHOD OF CALCULATING ENERGY RELEASE RATE

The potential energy release rate has been given in Equation (4.3.10) as:

$$\frac{\Delta \Pi_M}{\Delta a} = \frac{1}{2} \sum_{i=1}^{E^0} \frac{\langle \underline{u}_i^e \quad \underline{\tau}_i^e \rangle^T [ \underline{S}_{i,a+\Delta a}^0 - \underline{S}_{i,a}^0 ]}{\Delta a} \begin{Bmatrix} \underline{u}_i^e \\ \underline{\tau}_i^e \end{Bmatrix}$$

where  $\Pi_M$  is the potential energy;  $\Delta a$  is the change in crack length;  $E^0$  is the number of elements between contours  $\Gamma_0$  and  $\Gamma_1$  between which the element matrices are altered;  $\underline{S}_{i,a}^0$  is the element matrix calculated for the initial crack length  $a$ ;  $\underline{S}_{i,a+\Delta a}^0$  when the crack length has been incremented by an amount  $\Delta a$ ; and  $\underline{u}_i^e$  and  $\underline{\tau}_i^e$  are the nodal displacement and stress degrees of freedom for the nodes corresponding to the  $i^{\text{th}}$  element within the contours  $\Gamma_0$  and  $\Gamma_1$ . The calculation of  $[ \underline{S}_{i,a+\Delta a}^0 - \underline{S}_{i,a}^0 ]$  for the three-node triangular mixed element is given below.

The three-node mixed finite elements between  $\Gamma_0$  and  $\Gamma_1$  (Figure (D.1)) can be classified into two types depending on their orientations with respect to  $\Gamma_0$ . The first type (type I) has two nodes located on contour  $\Gamma_0$ , while the second type (type II) has only one node located on

contour  $\Gamma_0$ . The change in element matrices for both types of elements, i.e.  $[\underline{S}_i^0 - \underline{S}_i^0]_{a+\Delta a}$ , are considered separately.

The element matrix for the three-node triangular mixed finite element is given in Appendix A as:

$$\underline{S} = \begin{bmatrix} \underline{0} & \underline{0} & \underline{a}^T & \underline{0} & \underline{b}^T \\ \underline{0} & \underline{0} & \underline{0} & \underline{b}^T & \underline{a}^T \\ \underline{a} & \underline{0} & \underline{\alpha C} & \underline{-\beta C} & \underline{0} \\ \underline{0} & \underline{b} & \underline{-\beta C} & \underline{\gamma C} & \underline{0} \\ \underline{b} & \underline{a} & \underline{0} & \underline{0} & \underline{\delta c} \end{bmatrix} \quad (D.1)$$

$$\underline{a} = \frac{t}{6} \begin{bmatrix} x_2^2 - x_2^3 & x_2^3 - x_2^1 & x_2^1 - x_2^2 \\ x_2^2 - x_2^3 & x_2^3 - x_2^1 & x_2^1 - x_2^2 \\ x_2^2 - x_2^3 & x_2^3 - x_2^1 & x_2^1 - x_2^2 \end{bmatrix} \quad (D.2)$$

$$\underline{b} = \frac{t}{6} \begin{bmatrix} x_1^3 - x_1^2 & x_1^1 - x_1^3 & x_1^2 - x_1^1 \\ x_1^3 - x_1^2 & x_1^1 - x_1^3 & x_1^2 - x_1^1 \\ x_1^3 - x_1^2 & x_1^1 - x_1^3 & x_1^2 - x_1^1 \end{bmatrix} \quad (D.3)$$

$$\underline{c} = \frac{-t \times A}{12} \begin{bmatrix} 2 & 1 & 1 \\ 1 & 2 & 1 \\ 1 & 1 & 2 \end{bmatrix} \quad (D.4)$$

The constants  $\alpha$ ,  $\beta$ ,  $\gamma$ ,  $\delta$  in Equation (D.1) are elements of the compliance matrix  $\underline{C}$  in Equation (A.1);  $x_{1_i}$ ,  $x_{2_i}$  are the coordinates of the  $i^{\text{th}}$  node of the triangular element; and  $t$  and  $A$  are the thickness and area of the triangular element, respectively, and  $A$  is given by:

$$A = \frac{1}{2} (x_1^2 x_2 + x_1 x_2^2 + x_1^2 x_3 - x_1 x_2^2 - x_1 x_3^2 - x_1^2 x_3). \quad (\text{D.5})$$

In general, the increment in the crack length  $\Delta a$  can be oriented in a direction other than the directions of the coordinate axes. Therefore, both the  $x_1$  and  $x_2$  coordinates of nodes located on contour  $\Gamma_0$  will change and the increments in the  $x_1$  and  $x_2$  coordinates are denoted by  $\Delta x_1$  and  $\Delta x_2$ , respectively. For the first type of element (type I), only nodes 1 and 2 are located on  $\Gamma_0$ . Thus  $\Delta x_1^3 = \Delta x_2^3 = 0$  and from

Equations (D.2) to (D.3):

$$\underline{\Delta a}^I = \frac{1}{6} \begin{bmatrix} \Delta x_2^{2I} & - \Delta x_2^{1I} & \Delta x_2^{1I} & - \Delta x_2^{2I} \\ \Delta x_2^{2I} & - \Delta x_2^{1I} & \Delta x_2^{1I} & - \Delta x_2^{2I} \\ \Delta x_2^{2I} & - \Delta x_2^{1I} & \Delta x_2^{1I} & - \Delta x_2^{2I} \end{bmatrix} \quad (\text{D.6})$$

$$\underline{\Delta b}^I = \frac{1}{6} \begin{bmatrix} -\Delta x_1^2 & \Delta x_1^1 & \Delta x_1^2 & -\Delta x_1^1 \\ -\Delta x_1^2 & \Delta x_1^1 & \Delta x_1^2 & -\Delta x_1^1 \\ -\Delta x_1^2 & \Delta x_1^1 & \Delta x_1^2 & -\Delta x_1^1 \end{bmatrix} \quad (D.7)$$

$$\underline{\Delta c}^I = \frac{-\Delta A^I}{12} \begin{bmatrix} 2 & 1 & 1 \\ 1 & 2 & 1 \\ 1 & 1 & 2 \end{bmatrix} \quad (D.8)$$

where the superscript I denotes the quantities associated with element type I;  $\underline{\Delta a}^I$ ,  $\underline{\Delta b}^I$  and  $\underline{\Delta c}^I$  are the changes in the submatrices  $\underline{a}^I$ ,  $\underline{b}^I$  and  $\underline{c}^I$ , respectively, due to a crack increment  $\Delta a$ ; and  $\Delta A^I$  is given by:

$$\Delta A^I = \frac{1}{2} [ (x_2^2 - x_2^3) \Delta x_1^1 + (x_2^3 - x_2^1) \Delta x_1^2 + (x_1^3 - x_1^2) \Delta x_2^1 + (x_1^1 - x_1^3) \Delta x_2^2 ] \quad (D.9)$$

With  $\underline{\Delta a}^I$ ,  $\underline{\Delta b}^I$  and  $\underline{\Delta c}^I$  given by Equations (D.6) to (D.8), the change in the element matrix for element type I due to a crack increment  $\Delta a$  is given by:

$$[\underline{s}_i^0 - \underline{s}_i^0]_{\Delta a + a}^I = \begin{bmatrix} \underline{0} & \underline{0} & \underline{\Delta a}^{IT} & \underline{0} & \underline{\Delta b}^{IT} \\ \underline{0} & \underline{0} & \underline{0} & \underline{\Delta b}^{IT} & \underline{\Delta a}^{IT} \\ \underline{\Delta a}^I & \underline{0} & \alpha \underline{\Delta C}^I & -\beta \underline{\Delta C}^I & \underline{0} \\ \underline{0} & \underline{\Delta b}^I & -\beta \underline{\Delta C}^I & \gamma \underline{\Delta C}^I & \underline{0} \\ \underline{\Delta b}^I & \underline{\Delta a}^I & \underline{0} & \underline{0} & \delta \underline{\Delta C}^I \end{bmatrix} \quad (D.10)$$

For the second type of element (type II), only node 1 is located on  $\Gamma_0$ . Therefore  $\Delta x_2^{1II} = \Delta x_2^{2II} = \Delta x_1^{3II} = \Delta x_2^{3II} = 0$  and from Equations (D.2) to (D.3):

$$\underline{\Delta a}^{II} = \frac{1}{6} \begin{bmatrix} 0 & -\Delta x_2^{1II} & \Delta x_2^{1II} \\ 0 & -\Delta x_2^{1II} & \Delta x_2^{1II} \\ 0 & -\Delta x_2^{1II} & \Delta x_2^{1II} \end{bmatrix} \quad (D.11)$$

$$\underline{\Delta b}^{II} = \frac{1}{6} \begin{bmatrix} 0 & -\Delta x_1^{1II} & \Delta x_1^{1II} \\ 0 & -\Delta x_1^{1II} & \Delta x_1^{1II} \\ 0 & -\Delta x_1^{1II} & \Delta x_1^{1II} \end{bmatrix} \quad (D.12)$$

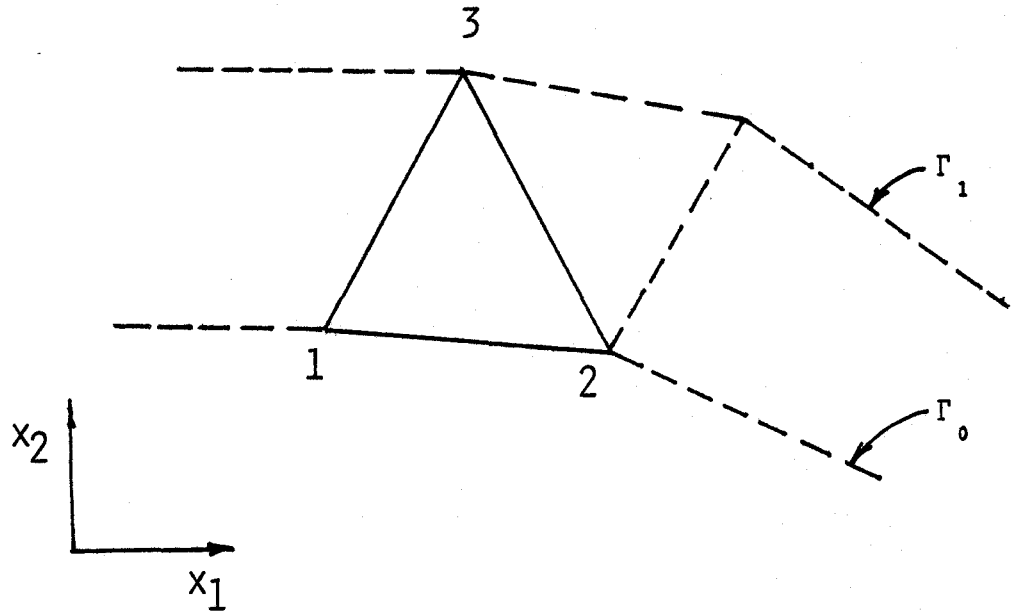
$$\underline{\Delta c}^{II} = \frac{-\Delta A^{II}}{12} \begin{bmatrix} 2 & 1 & 1 \\ 1 & 2 & 1 \\ 1 & 1 & 2 \end{bmatrix} \quad (D.13)$$

where the superscript II denotes quantities associated with element type II. In this case  $\Delta A^{II}$  is given by:

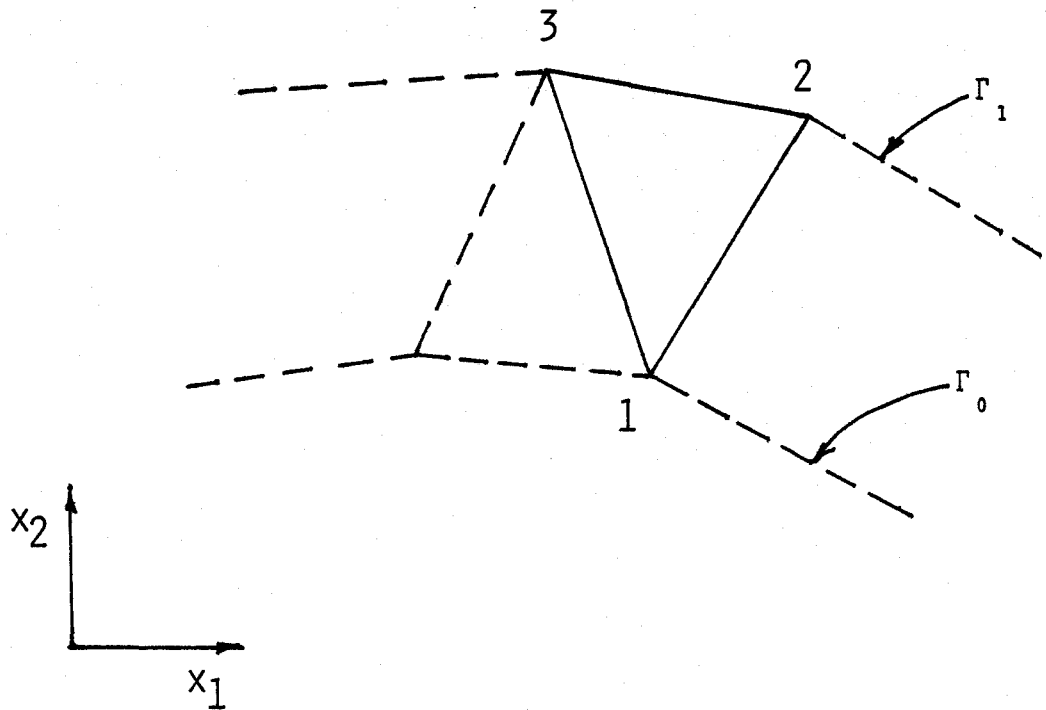
$$\Delta A^{II} = \frac{1}{2} [(x_2^{2II} - x_2^{3II}) \Delta x_1^{1II} + (x_1^{3II} - x_1^{1II}) \Delta x_2^{1II}] \quad (D.14)$$

The change in the element matrix for element type II due to a crack increment  $\Delta a$  is then given by:

$$[S_{i \Delta a + a}^0 - S_{i a}^0]^{II} = \begin{bmatrix} \underline{0} & \underline{0} & \underline{\Delta a}^{II T} & \underline{0} & \underline{\Delta b}^{II T} \\ \underline{0} & \underline{0} & \underline{0} & \underline{\Delta b}^{II T} & \underline{\Delta a}^{II T} \\ \underline{\Delta a}^{II} & \underline{0} & \underline{\alpha \Delta C}^{II} & \underline{-\beta \Delta C}^{II} & \underline{0} \\ \underline{0} & \underline{\Delta b}^{II} & \underline{-\beta \Delta C}^{II} & \underline{\gamma \Delta C}^{II} & \underline{0} \\ \underline{\Delta b}^{II} & \underline{\Delta a}^{II} & \underline{0} & \underline{0} & \underline{\delta \Delta C}^{II} \end{bmatrix} \quad (D.15)$$



a) TYPE I ELEMENT



b) TYPE II ELEMENT

FIG. D.1: TYPICAL TYPE I AND TYPE II ELEMENTS BETWEEN CONTOURS  $\Gamma_0$  AND  $\Gamma_1$ .

**APPENDIX E**  
**PROGRAM LISTINGS**

```
PROGRAM TST(INPUT=101B,OUTPUT=301B,TAPE5=INPUT,TAPE6=OUTPUT,
1TAPE1=520,TAPE2=520,TAPE3=520,TAPE4=520)
DIMENSION ICC(10),LJ(20),S(20,20),X(8),Y(8),FL(20),U(20),D(3,3),
1AA(4,4),BA(4,4),CA(4,4),AT(3),BT(3),AN(8),ANS(8),ANT(8),V(3,16),
2PX(3),PY(3)
DIMENSION A(10000),B(500),BB(500),IX(1050),MHT(501),MDIA(501),
1XX(300),YY(300),CPLN(3,3)
WRITE(6,1)
READ(5,2) NPROB,IPS,IGR,MT,NS,THICK,GR
IF(IPS.EQ.0) WRITE(6,2E)
IF(IPS.EQ.1) WRITE(6,2E)
WRITE(6,27) MT,NS,IGR,THICK,GR
CALL LAYOUT(XX,YY,X,Y,ICO,IX,LJ,NEM,NEMTR,NET,NEI,NNCD,NVAM,NVAI,
1NNCM,NNOT,NNOI,NVEM,NVET,NVEI,NMAT,NNET,MHT,NE NEW)
CALL DIAADD(MDIA,MHT,NNET,LBAND,NVA)
WRITE(6,5) NPROB,NNET,LBAND,NVA
NNNN=NNET+2
CALL PSET(A,NVA)
CALL PSET(B,NNET)
CALL PSET(BB,NNET)
CALL PRESET(D,3,3)
CALL PRESET(CPLN,3,3)
CALL PRESET(S,20,20)
READ(5,6) EX,EY,ANUYX,ANUZY,GXY
XN=EX/EY
ANUXY=ANUYX/XN
WRITE(6,7) EX,ANUXY,EY,ANUYX,GXY,ANUZY
IF(IPS.EQ.1) GO TO 55
D(1,1)=EX/(1-XN*ANUYX**2)
D(1,2)=D(1,1)*ANUXY
D(2,1)=D(1,2)
D(2,2)=D(1,1)/XN
D(3,3)=GXY
CPLN(1,1)=1.000/EX
CPLN(1,2)=-XN*ANUXY/EX
CPLN(2,1)=CPLN(1,2)
CPLN(2,2)=XN/EX
CPLN(3,3)=1.000/GXY
GO TO 56
55 CONTINUE
CPLN(1,1)=(1.0-(ANUYX**2)*EY/EX)/EX
CPLN(1,2)=-ANUYX*(1.0+ANUZY)/EX
CPLN(2,1)=CPLN(1,2)
CPLN(2,2)=(1.0-ANUZY**2)/EY
CPLN(3,3)=1.000/GXY
DDD=EX/((1.0+ANUZY)*(1.0-ANUZY-2.0*ANUYX*ANUYX/XN))
D(1,1)=(1.0-ANUZY**2)*DDD
D(1,2)=ANUYX*(1.0+ANUZY)*DDD/XN
D(2,1)=D(1,2)
D(2,2)=(1.0-ANUYX**2/XN)*DDD/XN
D(3,3)=GXY
56 CONTINUE
REWIND 1
READ(1) (IX(I),I=1,NMAT)
IF(NEM.EQ.0) GO TO 95
DO 9 IEL=1,NEM
CALL FREADI(X,Y,IS,IB,LJ,NNCM,NVEM)
```

```
CALL MIXEL(S,AA,BA,CA,X,Y,AT,BT,AR,CPLN,IS,THICK)
CALL MIXBON(X,Y,S,FL,AR,GR,THICK,IB,IGR,IS,NVEM,PX,PY)
CALL SETUP(A,B,MDIA,S,LJ,NVEM,FL)
9 CONTINUE
95 IF(NEMTR.EQ.0) GC TO 10
   DC 96 IEL=1,NEMTR
   CALL FREADI(X,Y,IS,IB,LJ,NNOM,NVEM)
   CALL MIXTRAN(S,AA,BA,CA,X,Y,AT,BT,AR,CPLN,IS,THICK)
   CALL MIXBON(X,Y,S,FL,AR,GR,THICK,IB,IGR,IS,NVEM,PX,PY)
96 CALL SETUP(A,B,MDIA,S,LJ,NVEM,FL)
   CCNTINUE
10 IF(NET.EQ.0) GO TO 12
   DO 11 IEL=1,NET
   CALL FREADI(X,Y,IS,IB,LJ,NNOT,NVET)
   CALL TRANEL(S,AA,EA,CA,X,Y,AT,BT,AR,CPLN,IS,THICK)
   CALL MIXBON(X,Y,S,FL,AR,GR,THICK,IB,IGR,IS,NVET,PX,PY)
   CALL SETUP(A,B,MDIA,S,LJ,NVET,FL)
11 CONTINUE
12 IF(NEI.EQ.0) GO TO 13
   DO 14 IEL=1,NEI
   CALL FREADI(X,Y,IS,IB,LJ,NNCI,NVEI)
   CALL ISOPAR(X,Y,S,FL,V,D,AN,ANS,ANT,THICK,GR,IS,IGR)
   CALL ISOBON(FL,X,Y,AN,ANS,ANT,THICK,IS,IB,IEL,PX,PY)
   CALL SETUP(A,B,MDIA,S,LJ,NVEI,FL)
14 CONTINUE
13 IF(NENEW.EQ.0) GO TO 777
   DO 888 IEL=1,NENEW
   CALL FREADI(X,Y,IS,IB,LJ,NNOM,NVEM)
888 CONTINUE
777 CONTINUE
   REWIND 3
   WRITE(3) (A(I),I=1,NVA),(B(I),I=1,NNET)
   CALL MULTIP(A,BB,B,MHT,MDIA,NNET,LBAND,IX,NVB)
   WRITE(6,5) NPROB,NNET,LBAND,NVB
   REWIND 4
   WRITE(4) (A(I),I=1,NVB)
   REWIND 3
   READ(3) (A(I),I=1,NVA),(B(I),I=1,NNET)
   CALL MULT(A,B,BB,NNET,IX,MHT,1,NNET)
   REWIND 4
   READ(4) (A(I),I=1,NVB)
   CALL COLSOL(A,BB,MDIA,NNET,NVB,1)
   REWIND 1
   READ(1) (IX(I),I=1,NMAT)
   CALL EXPAND(EB,NMAT,IX,FL,NNOD,NVAM)
   IF(NEI.EQ.0) GO TO 30
   WRITE(6,15)
   IF(NEI.EQ.0) GO TO 30
   WRITE(6,15)
   IF(NEM.EQ.0) GO TO 85
   DO 16 I=1,NEM
   CALL FREADI(X,Y,IS,IB,LJ,NNOM,NVEM)
16 CONTINUE
85 IF(NEMTR.EQ.0) GC TO 17
   DC 86 I=1,NEMTR
   CALL FREADI(X,Y,IS,IB,LJ,NNOM,NVEM)
86 CCNTINUE
```

```
17 IF(NET.EQ.0) GO TO 18
   DO 29 I=1,NET
   CALL FREADI(X,Y,IS,IB,LJ,NNOT,NVET)
20 CONTINUE
18 CONTINUE
   WRITE(6,24)
   DO 19 IEL=1,NEI
   CALL FREADI(X,Y,IS,IB,LJ,NNOI,NVEI)
   DO 20 J=1,NVEI
   IKK=LJ(J)
   IF(IKK) 21,22,21
22 U(J)=0.D0
   GO TO 20
21 U(J)=PB(IKK)
20 CONTINUE
   WRITE(6,23) IEL
   CALL SIGISC(X,Y,V,D,U,AN,ANS,ANT,MT,NS)
19 CONTINUE
30 REWIND 3
   READ(3) (A(I),I=1,NVA),(B(I),I=1,NNET)
   STENER=0.0
   DO 31 I=1,NNET
31 STENER=STENER+B(I)*BB(I)
   STENER=STENER/2.0
   WRITE(6,32) STENER
   NE=NEM+NEMTR+NET+NEI
   PIE=4.0*ATAN(1.0)
   CALL DENERG(PIE,X,Y,CPLN,THICK,BB,U,FL,S,NVEM,NMAT,LJ,
1 IX,AA,BA,CA,AT,BT,NE,MCIA)
   WRITE(6,996)
1 FORMAT("1",5X,"*** FINITE ELEMENT SOLUTION TO PLANE ELASTICITY PRO
1ELEM USING ",//,5X," MIXED,TRANSITIONAL AND ISOPARAMETRIC ELE
2MENTS***",//)
2 FORMAT(5I5,2F10.0)
4 FORMAT(4I5)
5 FORMAT(/,5X,"PROBLEM NO.",I5,10X,"TOTAL UNKNOWNNS",I5,//,5X,"BANDWI
10TH",I5,10X,"MATRIX SIZE",I8,/)
6 FORMAT(6F10.0)
7 FORMAT(/,5X,"MODULUS OF ELASTICITY IN X =",F15.1,10X,"ANUXY =",
1F8.4,/,5X,"MODULUS OF ELASTICITY IN Y =",F15.1,10X,"ANUYX =",
2F8.4,/,5X,"SHEAR MODULUS IN X-Y =",F15.2,10X,"ANUZY =",F8.4,//)
15 FORMAT(//,5X,"STRESSES IN ISOPARAMETRIC ELEMENTS",//)
23 FORMAT(/,5X,"***** STRESSES IN ELEMENT NUMBER",I5,"*****")
24 FORMAT(//,9X,"N",9X,"M",12X,"XX",12X,"YY",8X,"RADIUS",9X,"THETA",6
1X,"SIGMA-XX",6X,"SIGMA-YY",6X,"SIGMA-XY",//)
25 FORMAT(//,35X,"***** PLANE STRESS CASE *****",//)
26 FORMAT(//,35X,"***** PLANE STRAIN CASE *****",//)
27 FORMAT(//,5X,"NUMBER OF STRESS CALCULATIONS IN T-DIRECTION = MT ="
1,I5,//,5X,"NUMBER OF STRESS CALCULATIONS IN S-DIRECTION = NS ="
2,I5,//,5X,"IGR = ",I5,15X,"THICKNESS = ",F10.5,15X,"DENSITY = ",F10.5
3,//)
32 FORMAT(//,5X,"STRAIN ENERGY IN THE SYSTEM = ",E20.13,//)
996 FORMAT(//,5X,"***** END *****",//)
STOP
END
```

```
1) SUBROUTINE ARRANG(S,A,B,C,CPLN,M,N)
   DIMENSION S(20,1),A(4,1),B(4,1),C(4,1)
   DIMENSION CPLN(3,3)
   DO 3 I=1,M
     II=5*(I-1)
     I1=II+1
     I2=II+2
     I3=II+3
     I4=II+4
     I5=II+5
   DO 4 J=1,N
     JJ=5*(J-1)
     J1=JJ+1
     J2=JJ+2
     J3=JJ+3
     J4=JJ+4
     J5=JJ+5
     S(I1,J3)=A(J,I)
     S(I1,J5)=B(J,I)
     S(I2,J4)=B(J,I)
     S(I2,J5)=A(J,I)
     S(I3,J1)=A(I,J)
     S(I3,J3)=C(I,J)*CPLN(1,1)
     S(I3,J4)=C(I,J)*CPLN(1,2)
     S(I4,J2)=B(I,J)
     S(I4,J3)=C(I,J)*CPLN(2,1)
     S(I4,J4)=C(I,J)*CPLN(2,2)
     S(I5,J1)=B(I,J)
     S(I5,J2)=A(I,J)
     S(I5,J5)=C(I,J)*CPLN(3,3)
   CCONTINUE
   CCONTINUE
   RETURN
   END
```

4  
3

```
2) SUBROUTINE BMATRIX(ANS,ANT,X,Y,B,AJ,AI,DET)
   DIMENSION ANS(1),ANT(1),X(1),Y(1),B(3,1),AJ(2,2),AI(2,2)
   CALL PRESET(AJ,2,2)
   DO 1 K=1,8
     AJ(1,1)=AJ(1,1)+ANS(K)*X(K)
     AJ(1,2)=AJ(1,2)+ANS(K)*Y(K)
     AJ(2,1)=AJ(2,1)+ANT(K)*X(K)
     AJ(2,2)=AJ(2,2)+ANT(K)*Y(K)
   1 DET=AJ(1,1)*AJ(2,2)-AJ(1,2)*AJ(2,1)
     AI(1,1)=AJ(2,2)/DET
     AI(1,2)=-AJ(1,2)/DET
     AI(2,1)=-AJ(2,1)/DET
     AI(2,2)=AJ(1,1)/DET
   DO 2 K=1,8
     K1=2*K-1
     B(1,K1)=AI(1,1)*ANS(K)+AI(1,2)*ANT(K)
     B(2,K1)=AI(2,1)*ANS(K)+AI(2,2)*ANT(K)
     B(2,K1+1)=B(3,K1)
   2 B(3,K1+1)=B(1,K1)
   RETURN
   END
```

```

3) SUBROUTINE COLSOL(A,V,MAXA,NN,NWK,KKK)
C PFCGRAM
C TC SOLVE FINITE ELEMENT STATIC EQUILIBRIUM EQUATIONS IN CCRE, USING
C PFCGRAM
C TC SOLVE FINITE ELEMENT STATIC EQUILIBRIUM EQUATIONS IN CCRE, USING
C COMPACTED STORAGE AND COLUMN REDUCTION SCHEME
C INPUT VARIABLES
C A(NWK) = STIFFNESS MATRIX STORED IN COMPACTED FORM
C V(NN) = RIGHT-HAND-SIDE LOAD VECTOR
C A(NWK) = STIFFNESS MATRIX STORED IN COMPACTED FORM
C V(NN) = RIGHT-HAND-SIDE LOAD VECTOR
C MAXA(NNM) = VECTOR CONTAINING ADDRESSES OF DIAGONAL ELEMENTS OF
C STIFFNESS MATRIX IN A
C NN = NUMBER OF EQUATIONS
C NWK = NUMBER OF ELEMENTS BELOW SKYLINE OF MATRIX
C NNM = NN + 1
C KKK = INPUT FLAG
C EG. 1 TRIANGULARIZATION OF STIFFNESS MATRIX
C EG. 2 REDUCTION AND BACK-SUBSTITUTION OF LOAD VECTOR
C OUTPUT
C A(NWK) = C AND L - FACTORS OF STIFFNESS MATRIX
C V(NN) = DISPLACEMENT VECTOR
C THIS PROGRAM IS USED IN SINGLE PRECISION ARITHMETIC ON CDC EQUIPMENT
C AND DOUBLE PRECISION ARITHMETIC ON IBM OR UNIVAC MACHINES. ACTIVATE,
C DEACTIVATE OR ADJUST ABOVE CARD FOR SINGLE OR DOUBLE PRECISION
C ARITHMETIC
C DIMENSION A(1),V(1),MAXA(1)
C NNM=NN+1
C PERFORM L*D*L(T) FACTORIZATION OF STIFFNESS MATRIX
40 IF(KKK-2)40,150,150
DC 140 N=1,NN
KN=MAXA(N)
KL=KN+1
KU=MAXA(N+1) - 1
KT=KU - KL
50 IF(KH)110,90,50
K=N-KH
IC=0
KLT=KU
DC 80 J=1,KH
IC=IC + 1
KLT=KLT - 1
KI=MAXA(K)
ND=MAXA(K+1) - KI - 1
60 IF(ND)80,90,60
KK=MINO(IC,ND)
C=0.
DC 70 L=1,KK
70 C=C+A(KI+L)*A(KLT+L)
A(KLT)=A(KLT) - C
80 K=K+1
90 K=N
B=0.
DC 100 KK=KL,KU
K=K - 1
KI=MAXA(K)
C=A(KK)/A(KI)

```

```
B=B + C*A(KK)
100 A(KK)=C
A(KN)=A(KN) - B
110 IF (A(KN))120,120,140
120 WRITE(6,2000) N,A(KN)
STOP
140 CCONTINUE
C REDUCE RIGHT-HAND-SIDE LOAD VECTOR
150 DC 180 N=1,NN
KL=MAXA(N) + 1
KU=MAXA(N+1) - 1
IF(KU-KL)180,160,160
160 K=N
C=0.
DC 170 KK=KL,KU
K=K - 1
170 C=C+A(KK)*V(K)
V(N)=V(N) - C
180 CCONTINUE
C BACK-SUBSTITUTE
DC 200 N=1,NN
K=MAXA(N)
200 V(N)=V(N)/A(K)
IF (NN.EQ.1) RETURN
N=NN
DC 230 L=2,NN
KL=MAXA(N) + 1
KU=MAXA(N+1) - 1
IF(KU-KL)230,210,210
210 K=N
DC 220 KK=KL,KU
K=K - 1
220 V(K)=V(K)-A(KK)*V(N)
230 N=N-1
RETURN
2000 FCRMAT(//,5X,"STOP-STIFFNESS MATRIX IS NOT POSITIVE DEFINITE",//,
15X,"NONPOSITIVE PIVOT FOR EQUATION",I5,//,5X,"PIVCT =",E20.12)
END
```

```
4) SUBROUTINE COLHT(MHT,NVEL,LJ)
DIMENSION MHT(1),LJ(1)
LS=10000000
DC 100 I=1,NVEL
IF(LJ(I)) 110,100,110
110 IF(LJ(I)-LS) 120,100,100
120 LS=LJ(I)
100 CCONTINUE
DC 200 I=1,NVEL
II=LJ(I)
IF(II.EQ.0) GO TO 200
ME=II-LS
IF(ME.GT.MHT(II)) MHT(II)=ME
200 CCONTINUE
RETURN
END
```

```
5) SUBROUTINE ELDATA(ICC,LJ,MHT,XX,YY,X,Y,NE,NVAM,NVAI,NNODEL,NVEL,  
1 IX)  
  DIMENSION ICO(1),LJ(1),MHT(1),XX(1),YY(1),X(1),Y(1),IX(1)  
  WRITE(6,4)  
  NV=NVAM  
  IF(NNODEL.EQ.8) NV=NVAI  
  NNN=NNODEL+2  
  DO 1 I=1,NE  
  READ(5,2) (ICO(J),J=1,NNN)  
  IS=ICO(NNN-1)  
  IB=ICO(NNN)  
  DO 3 J=1,NNODEL  
  J1=(J-1)*NV  
  J2=NVAI*(ICO(J)-1)  
  XX(J)=X(ICO(J))  
  YY(J)=Y(ICO(J))  
  DO 3 K=1,NV  
  LJ(K+J1)=IX(J2+K)  
  CALL COLHT(MHT,NVEL,LJ)  
  WRITE(6,5) I,(ICO(J),J=1,NNN)  
  WRITE(1) (XX(J),J=1,NNODEL),(YY(J),J=1,NNODEL),IS,IB,(LJ(J),J=1,N  
1 VEL)  
  CCONTINUE  
  FCRMAT(10I3)  
  4 FCRMAT(//,5X,"ELEMENT",3X,"NODE NUMBERS",2X,"LAST TWO COLUMNS ARE  
1 IS AND IB",//)  
  5 FCRMAT(5X,I5,8X,10I4)  
  RETURN  
  END
```

```
6) SUBROUTINE EXPAND(B,NMAT,IX,FL,NNCD,NVAR)  
  DIMENSION B(1),IX(1),FL(1)  
  WRITE(6,40)  
  DO 1 I=1,NNCD  
  I2=NVAR+I  
  I1=I2-NVAR+1  
  II=1  
  DO 2 J=I1,I2  
  FL(II)=0.00  
  IF(IX(J).NE.0) FL(II)=B(IX(J))  
  II=II+1  
  2 CONTINUE  
  1 WRITE(6,41) I,(FL(K),K=1,5)  
  RETURN  
  40 FCRMAT(///," NODE",9X,"U",18X,"V ",17X,"TXX ",17X,"TYY",17X,  
  1 "TXY",/)  
  41 FCRMAT(1X,I5,5E20.8)  
  END
```

```
7) SUBROUTINE FREADI(X,Y,IS,IB,LJ,NNCD,NVEL)  
  DIMENSION X(1),Y(1),LJ(1)  
  READ(1) (X(J),J=1,NNCD),(Y(J),J=1,NNCD),IS,IB,(LJ(J),J=1,NVEL)  
  RETURN  
  END
```

```
8) SUBROUTINE ISOBON(FL,X,Y,AN,ANS,ANT,H,IS,IB,IEL,PX,PY)
   DIMENSION FL(1),X(1),Y(1),AN(1),ANS(1),ANT(1),W(3),XI(3),
1  FX(3),PY(3),JE(3)
   DATA W/0.5555555555555556,0.888888888888889,0.555555555555556/
   DATA XI/-0.77459666924148,0.0,0.77459666924148/
   IF(IS.EQ.0) GO TO 1000
   CALL PSET(FL,16)
   IF(IB.EQ.0) GO TO 1000
   DO 1 L=1,IB
   READ(5,2) IE,(JE(I),I=1,3),COR
2  FORMAT(4I5,F10.0)
   READ(5,3) PX(1),PY(1),FX(2),PY(2),PX(3),PY(3)
3  FORMAT(6F10.0)
   JL=JE(1)
   JM=JE(2)
   JN=JE(3)
   DO 4 I=1,3
   IF(IE.NE.1) GO TO 5
   T=COR
   S=XI(I)
   CALL SHAPE(AN,ANS,ANT,S,T,1)
   DXS=ANS(JL)*X(JL)+ANS(JM)*X(JM)+ANS(JN)*X(JN)
   DYS=ANS(JL)*Y(JL)+ANS(JM)*Y(JM)+ANS(JN)*Y(JN)
   CL=SQRT(DXS*DXS+DYS*DYS)
   GO TO 6
5  S=COR
   T=XI(I)
   CALL SHAPE(AN,ANS,ANT,S,T,1)
   DXT=ANT(JL)*X(JL)+ANT(JM)*X(JM)+ANT(JN)*X(JN)
   DYT=ANT(JL)*Y(JL)+ANT(JM)*Y(JM)+ANT(JN)*Y(JN)
   CL=SQRT(DXT*DXT+DYT*DYT)
6  DO 7 J=1,3
   J2=2*JE(J)
   J1=J2-1
   ZZ=0.00
   XX=0.00
   DO 8 K=1,3
   XX=XX+DL*AN(JE(J))*(AN(JE(K)))*H*PX(K)*W(I)
8  ZZ=ZZ+DL*AN(JE(J))*(AN(JE(K)))*H*PY(K)*W(I)
   FL(J1)=FL(J1)+XX
   FL(J2)=FL(J2)+ZZ
7  CONTINUE
4  CONTINUE
1  CONTINUE
   WRITE(6,499) IEL
   WRITE(6,500) (FL(I),I=1,16)
1000 RETURN
499 FORMAT(//,5X,"LOAD VECTOR FOR ELEMENT NUMBER = ",I5,2X,"IS",/)
500 FORMAT(8F15.7)
END
```

```
9) SUBROUTINE ISOPAR(X,Y,ST,FL,B,C,AN,ANS,ANT,H,GR,IS,IGR)
   DIMENSION X(1),Y(1),ST(20,1),FL(1),B(3,1),D(3,1),AN(1),ANS(1),
1  ANT(1),W(3),XI(3),AK(16,16),C(3,16),AJ(2,2),AI(2,2)
   DATA W/0.5555555555555556,0.888888888888889,0.555555555555556/
   DATA XI/-0.77459666924148,0.0,0.77459666924148/
   IF(IS.EQ.0) GO TO 1000
   CALL PRESET(ST,20,16)
   CALL PRESET(B,3,16)
   CALL PSET(FL,16)
   DO 26 I=1,3
   DO 27 J=1,3
   S=XI(I)
   T=XI(J)
   CALL SHAPE(AN,ANS,ANT,S,T,IGR)
   CALL BMATRIX(ANS,ANT,X,Y,B,AJ,AI,DET)
   CALL MULT1(D,B,AK,C,3,16,3)
```

```

DET=H*DET
DO 3 K=1,16
DO 4 L=1,16
4 ST(K,L)=ST(K,L)+(W(I)*W(J)*AK(K,L)*DET)
3 CONTINUE
IF(IGR.EQ.0) GO TO 27
DET=GR*DET
DO 5 K=1,8
L=2*K
5 FL(L)=FL(L)+(DET*W(I)*W(J)*AN(K))
27 CONTINUE
26 CONTINUE
1000 RETURN
END

```

```

SUBROUTINE LAYOUT(X,Y,XX,YY,ICO,IX,LJ,NEM,NEMTR,NET,NEI,NNOD,NVAM
1,NVAI,NNOM,NNOT,NNCI,NVEM,NVET,NVEI,NMAT,NNET,MHT,NENEW)
DIMENSION X(1),Y(1),XX(1),YY(1),ICO(10),IX(1),LJ(1),MHT(1)
REWIND 1
READ(5,1) NEM,NEMTR,NET,NEI,NNOD,NVAM,NVAI,NNOM,NNOT,NNOI
WRITE(6,2) NEM,NEMTR,NET,NEI,NNOD,NVAM,NVAI,NNOM,NNOT,NNOI
READ(5,777) NENEW
777 FORMAT(I5)
WRITE(6,888) NENEW
888 FORMAT(//,5X,"NO. OF NEW ELEMENTS = ",I5,/)
NVEM=NVAM*NNOM
NVET=NVAM*NNOT
NVEI=NVAI*NNCI
NEM=NUMBER OF MIXED FINITE ELEMENTS
NEMTR=NUMBER OF MIXED-TRANSITIONAL FINITE ELEMENTS
NET=NUMBER OF TRANSITIONAL ELEMENTS
NEI=NUMBER OF ISOPARAMETRIC ELEMENTS (8 NODE QUADS)
NNOD=TOTAL NODES
NVAM=DEGREES OF FREEDOM PER NODE FOR MIXED ELEMENTS
NVAI=DEGREES OF FREEDOM PER NODE FOR ISOPARAMETRIC ELEM.
NVAM=DEGREES OF FREEDOM PER NODE FOR MIXED ELEMENTS
NVAI=DEGREES OF FREEDOM PER NODE FOR ISOPARAMETRIC ELEM.
NCTE TRANSITIONAL ELEM. HAS THE SAME D.O.F. PER NODE AS M.F.E.S.
NNCM=NO OF NODES PER M.F.E.
NNCI=NO. OF NODES PER ISOPARAMETRIC ELEM.
NNOT=NO OF NODES PER TRANSITIONAL ELEM.
NVEM=NVAM*NNOM D.O.F./M.F.E.
NVET=NVAM*NNOT D.O.F./T.F.E.
NVEI=NVAI*NNCI D.O.F./I.F.E.
NNCD=TOTAL NO. OF NODES.
CALL NODATA(X,Y,IX,NNCD,NVAM)
NMAT=NNOD*NVAM
NNET=0
DC 12 I=1,NMAT
IF(IX(I) -1) 13,14,15
14 NNET=NNET+1
IX(I)=NNET
GO TO 12
13 IX(I)=0
GO TO 12
15 II=I-5
IX(I)=IX(II)
12 CCONTINUE
WRITE(1) (IX(I),I=1,NMAT)
DC 20 I=1,NNET
20 MHT(I)=0

```

```
IF(NEM.EQ.0) GO TO 25
CALL ELDDATA(ICO,LJ,MHT,XX,YY,X,Y,NEM,NVAM,NVAI,NNOM,NVEM,IX)
25 IF(NEMTR.EQ.0) GO TO 16
CALL ELDDATA(ICO,LJ,MHT,XX,YY,X,Y,NEMTR,NVAM,NVAI,NNOM,NVEM,IX)
16 IF(NET.EQ.0) GO TO 17
CALL ELDDATA(ICO,LJ,MHT,XX,YY,X,Y,NET,NVAM,NVAI,NNOT,NVET,IX)
17 IF(NEI.EQ.0) GO TO 18
CALL ELDDATA(ICO,LJ,MHT,XX,YY,X,Y,NEI,NVAM,NVAI,NNOI,NVEI,IX)
18 IF(NENEW.EQ.0) GO TO 19
CALL ELDDATA(ICO,LJ,MHT,XX,YY,X,Y,NENEW,NVAM,NVAI,NNOM,NVEM,IX)
19 CONTINUE
1  FORMAT(10I5)
2  FORMAT(/,5X,"NO. OF MIXED F.E.=",I5,5X,"NO. OF MIXED-TRANS. F.E.
1= ",I5,5X,"NO. OF TRANSITIONAL F.E.=",I5,/,5X,"NO. OF ISOPARAMETRIC
2 F.E.=",I5,5X,"TOTAL NO. OF NODES=",I5,/,5X,"NO. OF D.O.F. PER NOD
3E FOR M.F.E. AND M.T.F.E. AND T.F.E.=",I5,5X,"
4NO. OF D.O.F. PER NODE FOR ISOPAR.F.E.=",I5,/,5X,"NO. OF NODES PER
5 M.F.E.=",I5,5X,"NO. OF NODES PER T.F.E.=",I5,5X,"NO. OF NODES PER
6 ISOPARA.F.E.=",I5,/)
RETURN
END
```

```
11 SUBROUTINE MIXBON(X,Y,S,FL,AR,GR,H,IB,IGR,IS,NVEL,PX,PY)
DIMENSION X(1),Y(1),S(20,1),FL(1),PX(1),PY(1)
IF (IS.EQ.0) GO TO 1000
CALL PSET(FL,NVEL)
IF (IGR.EQ.0) GO TO 11
GRAV = -AR*H+GR/3.00
FL(2) =GRAV
FL(7) = GRAV
FL(12) =GRAV
IF(NVEL.EQ.15) GO TO 11
FL(7)=GRAV/2.0
FL(12)=FL(7)
FL(17)=GRAV
11 IF (IB.EQ.0) GO TO 1000
XL =SQRT(((X(2)-X(1))**2)+((Y(2)-Y(1))**2))
XL=XL*H
IF (IB.EQ.2) GO TO 12
READ(5,5) PX(1),PY(1),PX(2),PY(2),PX(3),PY(3)
WRITE(6,6)PX(1),PY(1),PX(2),PY(2),PX(3),PY(3)
E  FORMAT(/,5X,6F10.2)
FL(1)=FL(1)+XL*(2.00*PX(2)+PX(1))/6.00
FL(2)=FL(2)+XL*(2.00*PY(2)+PY(1))/6.00
FL(6)=FL(6)+XL*(2.00*PX(2)+PX(3))/6.00
FL(7)=FL(7)+XL*(2.00*PY(2)+PY(3))/6.00
WRITE(6,7) (FL(II),II=1,15)
7  FORMAT(/,5X,5F10.2,/,5X,5F10.2,/,5X,5F10.2)
GO TO 1000
12 READ(5,2) UK1,UK2,VK1,VK2
S(1,1)=S(1,1)+XL*((UK1/4.00)+(UK2/12.00))
S(1,6)=S(1,6)+XL*((UK1/12.00)+UK2/12.00)
S(6,1)=S(1,6)
S(6,6)=S(6,6)+XL*((UK1/12.00)+(UK2/4.00))
S(2,2)=S(2,2)+XL*((VK1/4.00)+(VK2/12.00))
S(2,7)=S(2,7)+XL*((VK1/12.00)+(VK2/12.00))
S(7,2)=S(2,7)
S(7,7)=S(7,7)+XL*((VK1/12.00)+(VK2/4.00))
2  FORMAT(4F15.0)
1000 FORMAT(6F10.0)
RETURN
END
```

```
1) SUBROUTINE MULT(A, BB, E, NN, MDIA, MHT, M1, M2)
   DIMENSION A(1), BB(1), E(1), MDIA(1), MHT(1)
   DC 20 I=1, NN
   B(I)=0.0
   DC 1 I=1, NN
   J1=I-(MDIA(I+1)-MDIA(I)-1)
   J2=I+MHT(I)
   IF(J1.LE.0) J1=1
   IF(J2.GT.NN) J2=NN
   AA=0.0
   IF(J2.LT.M1.OR.J1.GT.M2) GO TO 10
   DO 3 J=J1, J2
   MC=MDIA(J+1)-MDIA(J)-1
   MD=J-I
   IF(MD.GT.MC) GO TO 3
   IF(MD) 210, 215, 215
210 MJ=MDIA(I)
   MC=-MD
   GO TO 216
215 MJ=MDIA(J)
216 K=MJ+MD
   AA=AA+A(K)*BB(J)
3 CONTINUE
10 B(I)=AA
1 CONTINUE
RETURN
END
```

```
1) SUBROUTINE MULTIP(A, BB, B, MHT, MDIA, NN, MK, IX, NVB)
   DIMENSION A(1), BB(1), E(1), MHT(1), MDIA(1), IX(1)
   REWIND 2
   DC 1 J=1, NN
   MH=0
   JM=J+1
   MP=MK+J-1
   IF(MP.GT.NN) MP=NN
   DC 3 I=JM, MP
   MC=MDIA(I+1)-MDIA(I)-1
   MD=I-J
   IF(MD.GT.MC) GO TO 3
3 MH=I-J
   CCNTINUE
1 MHT(J)=MH
   DC 4 J=1, NN
   JM=J-(MDIA(J+1)-MDIA(J))
   MH=0
   DC 5 I=1, J
   MC=I+MHT(I)
   IF(MH.EQ.1) GO TO 5
   IF(MC.LE.JM) GO TO 5
5 MH=1
   IX(J)=J-I
4 CCNTINUE
   CCNTINUE
   DC 6 J=1, NN
   JM=MDIA(J+1)-MDIA(J)
   M1=J-JM+1
7 DC 7 I=1, NN
   BB(I)=0.0
   DC 8 I=1, JM
   MC=MDIA(J)+I-1
   MH=J+1-I
```

```

8      BB(MH)=A(MC)
      MP=J+MHT(J)
      JM1=J+1
      DC 9 I=JM1,MP
      MC=MDIA(I+1)-MDIA(I)-1
      MD=I-J
      IF(MD.GT.MC) GO TO 9
      MH=MDIA(I)+I-J
9      BB(I)=A(MH)
      CCONTINUE
      M2=MHT(J)+J
      IF(M1.LE.0)M1=1
      IF(M2.GT.NN)M2=NN
      CALL MULT(A,BB,B,NN,MCIA,MHT,M1,M2)
6      WRITE(2) (B(I),I=1,NN)
      CCONTINUE
      NNN=NN+1
      WRITE(2) (MDIA(I),I=1,NNN)
      REWIND 2
      CALL DIAADD(MDIA,IX,NN,MK,NVB)
40     WRITE(6,40)NVE
      FORMAT(/,5X,"NVB =",I20)
      CALL PSET(A,NVB)
      DC 10 J=1,NN
      READ(2) (B(I),I=1,NN)
      JM=MDIA(J+1)-MDIA(J)
      DC 11 I=1,JM
      MC=MDIA(J+1)-I
      MH=J-JM+I
11     A(MC)=B(MH)
10     CCONTINUE
      READ(2) (IX(I),I=1,NNN)
      RETURN
      END

```

C  
C  
C

```

14) SUBROUTINE MULT1(X,Y,S,Z,M1,M2,M3)
MULTIPLIES THE MATRICES Y (TRANSPOSE) * X * Y .
DIMENSION X(M1,1),Y(M1,1),Z(M3,1),S(M2,1)
DO 1 I=1,M1
DO 2 K=1,M2
XX=0.00
DO 3 J=1,M1
3 XX=XX+X(I,J)*Y(J,K)
2 Z(I,K)=XX
1 CONTINUE
DO 4 I=1,M2
DO 5 K=1,M2
XX=0.00
DO 6 J=1,M1
6 XX=XX+Y(J,I)*Z(J,K)
5 S(I,K)=XX
4 CONTINUE
RETURN
END

```

```
11 DC 10 J=1,NN
10 READ (2) (B(I),I=1,NN)
JM=MDIA(J+1)-MDIA(J)
DC 11 I=1,JM
MC=MDIA(J+1)-I
MH=J-JM+I
A(MC)=B(MH)
CONTINUE
READ(2) (IX(I),I=1,NNN)
RETURN
END
```

```
(5) SUBROUTINE DIAADD(MDIA,MHT,NNET,MK,NVA)
DIMENSION MDIA(1),MHT(1)
NN=NNET+1
DC 20 I=1,NN
20 MDIA(I)=0
MDIA(1)=1
MDIA(2)=2
MK=0
IF(NNET.EQ.1) GO TO 100
DC 10 I=2,NNET
10 IF(MHT(I).GT.MK) MK=MHT(I)
100 MDIA(I+1)=MDIA(I)+MHT(I)+1
MK=MK+1
NVA=MDIA(NN)-MDIA(1)
RETURN
END
```

```
(6) SUBROUTINE MIXEL(S,A,B,C,X,Y,AT,BT,AR,CPLN,IS,H)
DIMENSION S(20,1),A(4,1),B(4,1),C(4,1),X(1),Y(1),AT(1),BT(1)
DIMENSION CPLN(3,3)
IF(IS.EQ.0) RETURN
CALL PRESET(S,20,15)
CALL PRESET(A,4,3)
CALL PRESET(B,4,3)
CALL PRESET(C,4,3)
AT(1)=(X(3)-X(2))/6.00
AT(2)=(X(1)-X(3))/6.00
AT(3)=(X(2)-X(1))/6.00
BT(1)=(Y(2)-Y(3))/6.00
BT(2)=(Y(3)-Y(1))/6.00
BT(3)=(Y(1)-Y(2))/6.00
AR=(X(1)*Y(2)+X(2)*Y(3)+X(3)*Y(1)-Y(1)*X(2)-Y(2)*X(3)-Y(3)*X(1))/
1 2.00
DC 1 I=1,3
DC 2 J=1,3
A(I,J)=BT(J)*H
B(I,J)=AT(J)*H
C(I,J)=-AR*H/12.00
IF(I.EQ.J) C(I,J)=2.00*C(I,J)
2 CCNTINUE
1 CCNTINUE
CALL ARRANG(S,A,B,C,CPLN,3,3)
RETURN
END
```

```
2) SUBROUTINE NODATA (X,Y,IX,NN,NVAR)
   DIMENSION X(1),Y(1),IX(1)
   WRITE(6,1)
   DC 2 I=1,NN
   I2=NVAR*I
   I1=I2-NVAR+1
   READ(5,3) X(I),Y(I),(IX(J),J=I1,I2)
   WRITE(6,4)I,X(I),Y(I),(IX(J),J=I1,I2)
   CCNTINUE
1  FCRMAT(//,4X,"NOCE",7X,"X-CORD",6X,"Y-CORD",8X,"U",3X,"V",3X,"TXX
3  ",1X,"TYY",1X,"TXY",//)
4  FCRMAT(2F10.0,6I3)
   FCRMAT(1X,I5,5X,F20.9,2X,F20.9,5X,6I4)
   RETURN
   END
```

```
5) SUBROUTINE PRESET(A,M,N)
   DIMENSION A(M,1)
   CO 1 I=1,M
   DO 2 J=1,N
2  A(I,J)=0.00
1  CONTINUE
   RETURN
   END
```

```
4) SUBROUTINE PSET(A,M)
   DIMENSION A(1)
   DO 1 I=1,M
1  A(I)=0.00
   RETURN
   END
```

```
20) SUBROUTINE SETUP(A,B,MDIA,S,LJ,NVEL,FL)
   DIMENSION A(1),B(1),MCIA(1),S(20,1),LJ(1),FL(1)
   DC 200 I=1,NVEL
   LJR=LJ(I)
100  IF(LJR) 200,200,100
   B(LJR)=B(LJR)+FL(I)
   DC 220 J=I,NVEL
   LJC=LJ(J)
110  IF(LJC) 220,220,110
   IJ=LJR-LJC
210  IF(IJ) 210,215,215
   MJ=MDIA(LJC)
   IJ=-IJ
   GC TC 216
215  MJ=MDIA(LJR)
216  KK=MJ+IJ
   A(KK)=A(KK)+S(I,J)
220  CCNTINUE
200  CCNTINUE
   RETURN
   END
```

```

20) SUBROUTINE SHAPE(AN,ANS,ANT,S,T,N)
DIMENSION AN(1),ANS(1),ANT(1)
IF(N.EQ.0) GO TO 1
AN(1)=-((1.00-S)*(1.00-T)*((1.00+S+T)/4.00
AN(2)=-((1.00+S)*(1.00-T)*((1.00-S+T)/4.00
AN(1)=-((1.00-S)*(1.00-T)*((1.00+S+T)/4.00
AN(2)=-((1.00+S)*(1.00-T)*((1.00-S+T)/4.00
AN(3)=-((1.00+S)*(1.00+T)*((1.00-S-T)/4.00
AN(4)=-((1.00-S)*(1.00+T)*((1.00+S-T)/4.00
AN(5)=-((1.00-S*S)*(1.00-T)/2.00
AN(6)=-((1.00-T*T)*(1.00+S)/2.00
AN(7)=-((1.00-S*S)*(1.00+T)/2.00
AN(8)=-((1.00-T*T)*(1.00-S)/2.00
1 ANS(1)=-((1.00-T)*(2.00*S+T)/4.00
ANS(2)=-((1.00-T)*(2.00*S-T)/4.00
ANS(3)=-((1.00+T)*(2.00*S+T)/4.00
ANS(4)=-((1.00+T)*(2.00*S-T)/4.00
ANS(5)=-S*(1.00-T)
ANS(6)=-((1.00-T*T)/2.00
ANS(7)=-S*(1.00+T)
ANS(8)=-((1.00-T*T)/2.00
ANT(1)=-((1.00-S)*(S+2.00*T)/4.00
ANT(2)=-((1.00+S)*(2.00*T-S)/4.00
ANT(3)=-((1.00+S)*(2.00*T+S)/4.00
ANT(4)=-((1.00-S)*(2.00*T-S)/4.00
ANT(5)=-((1.00-S*S)/2.00
ANT(6)=-T*(1.00+S)
ANT(7)=-((1.00-S*S)/2.00
ANT(8)=-T*(1.00-S)
RETURN
END

```

```

20) SUBROUTINE SIGISO(X,Y,E,D,U,AN,ANS,ANT,M,N)
DIMENSION X(1),Y(1),B(3,1),D(3,1),U(1),AN(1),ANS(1),ANT(1),
1 STFAIN(3),STRESS(3),AJ(2,2),AI(2,2)
CALL PRESET(B,3,16)
AA=N-1
BB=M-1
DO 50 J=1,N
CC=J-1
S=-1.00+CC*2.00/AA
DO 51 I=1,M
DD=I-1
T=-1.00+DD*2.00/BB
CALL SHAPE(AN,ANS,ANT,S,T,1)
CALL BMATRX(ANS,ANT,X,Y,B,AJ,AI,DET)
XX=0.00
YY=0.00
DO 4 K=1,8
XX=XX+X(K)*AN(K)
4 YY=YY+Y(K)*AN(K)
XX=XX+1.E-8
RATIO=YY/XX
THETA=ATAN(RATIO)*180.00/3.1415926
RADIUS=SQRT(XX*XX+YY*YY)
DO 5 K=1,3
ZZ=0.00
DO 6 L=1,16
6 ZZ=ZZ+B(K,L)*U(L)
5 STRAIN(K)=ZZ
DO 7 K=1,3
ZZ=0.00
DO 8 L=1,3
8 ZZ=ZZ+D(K,L)*STRAIN(L)
7 STRESS(K)=ZZ
WRITE(6,52) J,I,XX,YY,RADIUS,THETA,(STRESS(K),K=1,3)
51 CONTINUE
50 CONTINUE
RETURN
52 FORMAT(2I10,7E14.5)
END

```

```
27) SUBROUTINE TRANEL(S,A,B,C,X,Y,AT,BT,AR,CPLN,IS,H)
  DIMENSION S(20,1),A(4,1),B(4,1),C(4,1),X(1),Y(1),AT(1),BT(1)
  DIMENSION CPLN(3,3)
  IF (IS.EQ.0) GO TO 1000
  CALL PRESET (S,20,20)
  CALL PRESET (A,4,4)
  CALL PRESET (B,4,4)
  CALL PRESET (C,4,4)
  AT(1)=X(3)-X(2)
  AT(2)=X(1)-X(3)
  AT(3)=X(2)-X(1)
  BT(1)=Y(2)-Y(3)
  BT(2)=Y(3)-Y(1)
  BT(3)=Y(1)-Y(2)
  AR=(X(1)*Y(2)+X(2)*Y(3)+X(3)*Y(1)-Y(1)*X(2)-Y(2)*X(3)-Y(3)*X(1))/
1 2.0
  EA=H/(360.0*AR)
  E1=CPLN(2,2)/(CPLN(1,1)*CPLN(2,2)-CPLN(1,2)**2)
  E2=1.0/CPLN(3,3)
  E3=-CPLN(1,2)/(CPLN(1,1)*CPLN(2,2)-CPLN(1,2)**2)
  E4=CPLN(1,1)*E1/CPLN(2,2)
  CALL TRANAB(A,BT,BT,EA)
  CALL TRANAB(B,AT,AT,EA)
  CALL TRANAB(C,BT,AT,EA)
  DO 1 I=1,4
  I1=(I-1)*5+1
  I2=I1+1
  DO 2 J=1,4
  J1=(J-1)*5+1
  J2=J1+1
  S(I1,J1)=E1*A(I,J)+E2*B(I,J)
  S(I1,J2)=E3*C(I,J)+E2*C(J,I)
  S(I2,J1)=E3*C(J,I)+E2*C(I,J)
2 S(I2,J2)=E4*B(I,J)+E2*A(I,J)
  CONTINUE
  EA=H/360.0
  CALL TRANCC(A,B,AT,BT,EA)
  DO 3 I=1,4
  I1=(I-1)*5+1
  S(I1,3)=A(I,1)
  S(3,I1)=A(I,1)
  S(I1,5)=B(I,1)
  S(5,I1)=B(I,1)
3 CALL TRANCC(A,B,BT,AT,EA)
  DO 4 I=1,4
  I1=(I-1)*5+2
  S(I1,4)=A(I,1)
  S(4,I1)=A(I,1)
  S(I1,5)=B(I,1)
  S(5,I1)=B(I,1)
4 TERM1=-AR*H*7.0/72.0
  S(3,3)=CPLN(1,1)*TERM1
  S(4,4)=CPLN(2,2)*TERM1
  S(3,4)=CPLN(1,2)*TERM1
  S(4,3)=S(3,4)
  S(5,5)=CPLN(3,3)*TERM1
1000 RETURN
```

```

24) SUBROUTINE TRANAB(C,B,A,E)
    DIMENSION C(4,4),B(4),A(4)
    C(1,1)=81.25*A(1)*B(1)
    C(1,2)=21.25*B(1)*A(2)-60.0*B(1)*A(3)
    C(1,3)=-60.0*B(1)*A(2)+21.25*B(1)*A(3)
    C(1,4)=120.0*B(1)*A(2)+120.0*B(1)*A(3)
    C(2,1)=21.25*A(1)*B(2)-60.0*A(1)*B(3)
    C(2,2)=21.25*A(2)*B(2)-30.0*A(2)*B(3)-30.0*A(3)*B(2)+60.0*A(3)*
18(3)
    C(2,3)=30.0*A(2)*B(3)-8.75*A(3)*B(2)
    C(2,4)=-120.0*A(3)*B(3)-60.0*A(2)*B(3)+60.0*A(3)*B(2)
    C(3,1)=21.25*A(1)*B(3)-60.0*A(1)*B(2)
    C(3,2)=-8.75*A(2)*B(3)+30.0*A(3)*B(2)
    C(3,3)=21.25*A(3)*B(3)-30.0*A(2)*B(3)-30.0*A(3)*B(2)+60.0*A(2)*
18(2)
    C(3,4)=-120.0*A(2)*B(2)+60.0*A(2)*B(3)-60.0*A(3)*B(2)
    C(4,1)=120.0*A(1)*B(2)+120.0*A(1)*B(3)
    C(4,2)=60.0*A(2)*B(3)-60.0*A(3)*B(2)-120.0*A(3)*B(3)
    C(4,4)=240.0*A(2)*B(2)+120.0*A(2)*B(3)+120.0*A(3)*B(2)+240.0*A(3)
1*B(3)
    C(4,3)=-120.0*A(2)*B(2)+60.0*A(3)*B(2)-60.0*A(2)*B(3)
    DC 1 I=1,4
    DC 2 J=1,4
    C(I,J)=E*C(I,J)
    CCNTINUE
    RETURN
    END

```

2  
1

```

47) SUBROUTINE TRANCC(A,B,AT,BT,EA)
    DIMENSION A(4,1),B(4,1),AT(1),BT(1)
    A(1,1)=17.5*BT(1)*EA
    A(2,1)=17.5*BT(2)*EA
    A(3,1)=17.5*BT(3)*EA
    A(4,1)=0.0*EA
    B(1,1)=17.5*AT(1)*EA
    B(2,1)=17.5*AT(2)*EA
    B(3,1)=17.5*AT(3)*EA
    B(4,1)=0.0*EA
    RETURN
    END

```

```

26) SUBROUTINE MIXTRAN(S,A,B,C,X,Y,AT,BT,AR,CPLN,IS,H)
    DIMENSION S(20,1),A(4,1),B(4,1),C(4,1),X(1),Y(1),AT(1),BT(1)
    DIMENSION CPLN(3,3)
345 WRITE(6,345)(X(I),I=1,3),(Y(I),I=1,3)
    FORMAT(/,2(/,5X,3F15.3,/) )
    IF(IS.EQ.0) RETURN
    CALL PRESET(S,20,15)
    CALL PRESET(A,4,3)
    CALL PRESET(B,4,3)
    CALL PRESET(C,4,3)
    AT(1)=(X(3)-X(2))
    AT(2)=(X(1)-X(3))
    AT(3)=(X(2)-X(1))
    BT(1)=(Y(2)-Y(3))
    BT(2)=(Y(3)-Y(1))
    BT(3)=(Y(1)-Y(2))
    AR=(X(1)*Y(2)+X(2)*Y(3)+X(3)*Y(1)-Y(1)*X(2)-Y(2)*X(3)-Y(3)*X(1))/
1 2.00
    DDC=((CPLN(1,1)*CPLN(2,2)-CPLN(1,2)**2)*AR*6.0)
    E1=H*CPLN(2,2)/DDC
    E2=H/(CPLN(3,3)*AR*6.0)
    E3=-H*CPLN(1,2)/DDC
    E4=E1*CPLN(1,1)/CPLN(2,2)
    CALL TRANAC(A,BT,BT)
    CALL TRANAC(B,AT,AT)
    CALL TRANAC(C,BT,AT)

```

```

DC 10 I=1,3
I1=(I-1)*5+1
I2=I1+1
DC 20 J=1,3
J1=(J-1)*5+1
J2=J1+1
S(I1,J1)=E1*A(I,J)+E2*B(I,J)
S(I1,J2)=E3*C(I,J)+E2*C(J,I)
S(I2,J1)=E3*C(J,I)+E2*C(I,J)
10 20 S(I2,J2)=E4*B(I,J)+E2*A(I,J)
CCONTINUE
DC 1 I=1,3
DC 2 J=1,3
A(I,J)=BT(J)*H/12.0
B(I,J)=AT(J)*H/12.0
C(I,J)=-AR*H/(12.000)*0.5000
2 IF(I.EQ.J) C(I,J)=C(I,J)*3.000
CCONTINUE
1 CCONTINUE
DC 3 I=1,3
I1=(I-1)*5+1
S(I1,3)=A(1,I)
S(3,I1)=S(I1,3)
S(I1,5)=B(1,I)
S(5,I1)=S(I1,5)
S(I1,8)=S(I1,3)
S(8,I1)=S(I1,8)
3 S(I1,10)=S(I1,5)
S(10,I1)=S(I1,10)
DC 4 I=1,3
I1=(I-1)*5+2
S(I1,4)=B(1,I)
S(4,I1)=S(I1,4)
S(5,I1)=A(1,I)
S(I1,5)=S(5,I1)
S(I1,9)=S(I1,4)
S(9,I1)=S(I1,9)
4 S(I1,10)=S(I1,5)
S(10,I1)=S(I1,10)
DC 5 I=1,2
I1=(I-1)*5+3
DC 6 J=1,2
J1=(J-1)*5+3
J2=(J-1)*5+4
S(I1,J1)=C(I,J)*CFLN(1,1)
S(I1,J2)=C(I,J)*CFLN(1,2)
6 S(J2,I1)=S(I1,J2)
5 CCONTINUE
DC 7 I=1,2
I1=(I-1)*5+4
I2=I1+1
DC 8 J=1,2
J1=(J-1)*5+4
J2=J1+1
S(I1,J1)=C(I,J)*CFLN(2,2)
7 8 S(I2,J2)=C(I,J)*CFLN(3,3)
1000 CCONTINUE
RETURN
END

```

```

77 SUBROUTINE TRANAC(C,B,A)
DIMENSION C(4,1),B(1),A(1)
DC 1 I=1,3
DC 2 J=1,3
2 C(I,J)=B(I)*A(J)
1 CCONTINUE
RETURN
END

```



C

```
DO 601 K=1,NODE
I2=5*NODET(K)
I1=I2-5+1
I3=I1+1
I4=I3+1
I5=I4+1
I6=I5+1
A1=0.00
A2=0.00
```

```
CO=COS(ANGLE)
SI=SIN(ANGLE)
IF (IX(I1).NE.0) A1=B (IX(I1))
IF (IX(I3).NE.0) A2=B (IX(I3))
IF (IX(I1).NE.0) BBT (IX(I1))=A1*CO+A2*SI
IF (IX(I3).NE.0) BBT (IX(I3))=A2*CO-A1*SI
TX=B (IX(I4))
TY=B (IX(I5))
TXY=B (IX(I6))
BBT (IX(I4))=TX*CO*CO+TY*SI*SI+2.00*TXY*SI*CO
BBT (IX(I5))=TX*SI*SI+TY*CO*CO-2.00*TXY*SI*CO
BBT (IX(I6))=(TY-TX)*SI*CO+TXY*(CO*CO-SI*SI)
601 CONTINUE
```

C  
C  
C

SEPARATE BBT INTO SYMMETRICAL AND ANTISYMMETRICAL PARTS

```
DO 602 IKK=1,NODEN
NS1=NODE1 (IKK)
NS2=NODE2 (IKK)
NT1=(NS1-1)*5+1
NT2=(NS2-1)*5+1
NU1=NT1+1
NU2=NT2+1
ND1=NU1+1
NE1=ND1+1
NF1=NE1+1
ND2=NU2+1
NE2=ND2+1
NF2=NE2+1
U1=0.0
V1=0.0
U2=0.0
V2=0.0
IF (IX (NT1).NE.0) U1=BBT (IX (NT1))
IF (IX (NU1).NE.0) V1=BBT (IX (NU1))
IF (IX (NT2).NE.0) U2=BBT (IX (NT2))
IF (IX (NU2).NE.0) V2=BBT (IX (NU2))
TX1=BBT (IX (ND1))
TY1=BBT (IX (NE1))
TXY1=BBT (IX (NF1))
TX2=BBT (IX (ND2))
TY2=BBT (IX (NE2))
TXY2=BBT (IX (NF2))
SYMU=(U1+U2)/2.00
SYMV1=(V1-V2)/2.00
SYMV2=(V2-V1)/2.00
```

```

ASYMV=(V1+V2)/2.00
ASYMU1=(U1-U2)/2.00
ASYMU2=(U2-U1)/2.00
SYMTX=(TX1+TX2)/2.00
ASMTX1=(TX1-TX2)/2.00
ASMTX2=0.0-ASMTX1
SYMTY=(TY1+TY2)/2.00
ASMTY1=(TY1-TY2)/2.00
ASMTY2=0.0-ASMTY1
SMTXY1=(TXY1-TXY2)/2.00
SMTXY2=0.0-SMTXY1
ASMTXY=(TXY1+TXY2)/2.00
I1=IX(NT1)
I2=IX(NU1)
I3=IX(NT2)
I4=IX(NU2)
IF(I1.NE.0)SYMBB(I1)=SYMU*CO-SYMV1*SI
IF(I2.NE.0)SYMBB(I2)=SYMU*SI+SYMV1*CO
IF(I3.NE.0)SYMBB(I3)=SYMU*CO-SYMV2*SI
IF(I4.NE.0)SYMBB(I4)=SYMU*SI+SYMV2*CO
IF(I1.NE.0)ASYMBB(I1)=ASYMU1*CO-ASYMV*SI
IF(I2.NE.0)ASYMBB(I2)=ASYMU1*SI+ASYMV*CO
IF(I3.NE.0)ASYMBB(I3)=ASYMU2*CO-ASYMV*SI
IF(I4.NE.0)ASYMBB(I4)=ASYMU2*SI+ASYMV*CO
SYMBB(IX(ND1))=SYMTX*CO*CO+SYMTY*SI*SI-2.00*SMTXY1*SI*CO
SYMBB(IX(NE1))=SYMTX*SI*SI+SYMTY*CO*CO+2.00*SMTXY1*SI*CO
SYMBB(IX(NF1))=(SYMTX-SYMTY)*SI*CO+SMTXY1*(CO*CO-SI*SI)
SYMBB(IX(ND2))=SYMTX*CO*CO+SYMTY*SI*SI-2.00*SMTXY2*SI*CO
SYMBB(IX(NE2))=SYMTX*SI*SI+SYMTY*CO*CO+2.00*SMTXY2*SI*CO
SYMBB(IX(NF2))=(SYMTX-SYMTY)*SI*CO+SMTXY2*(CO*CO-SI*SI)
ASYMBB(IX(ND1))=ASMTX1*CO*CO+ASMTY1*SI*SI-2.00*ASMTXY*SI*CO
ASYMBB(IX(NE1))=ASMTX1*SI*SI+ASMTY1*CO*CO+2.00*ASMTXY*SI*CO
ASYMBB(IX(NF1))=(ASMTX1-ASMTX2)*SI*CO+ASMTXY*(CO*CO-SI*SI)
ASYMBB(IX(ND2))=ASMTX2*CO*CO+ASMTY2*SI*SI-2.00*ASMTXY*SI*CO
ASYMBB(IX(NE2))=ASMTX2*SI*SI+ASMTY2*CO*CO+2.00*ASMTXY*SI*CO
ASYMBB(IX(NF2))=(ASMTX2-ASMTY2)*SI*CO+ASMTXY*(CO*CO-SI*SI)

```

```

602 CONTINUE
401 CONTINUE
WRITE(6,95)(R(IK),IK=1,400)
WRITE(6,95)(SYMBB(IK),IK=1,400)
WRITE(6,95)(ASYMBB(IK),IK=1,400)
95 FORMAT(5X,/,20(/,5X,5E16.5))

```

C  
C  
C  
C  
C

NJJ=NO. OF ELEMENTS WHOSE STIFFNESS ARE ALTERED WITHIN THE SPECIFIC  
 CCNTOUR MOVED  
 IF=ELEMENT NO. OF ELEMENTS WITHIN THE SPECIFIC CONTOUR MOVED  
 MDIA=ELEMENT TYPE IDENTIFIER

```

DO 121 IJ=1,NCONTR
  READ(5,28)NJJ
28  FORMAT(2I5)
  READ(5,29)(IE(I),I=1,NJJ)
  READ(5,29)(MDIA(I),I=1,NJJ)
29  FORMAT(26I3)
  WRITE(6,30)IJ,(IE(I),I=1,NJJ)
  WRITE(6,31)IJ,(MDIA(I),I=1,NJJ)
30  FORMAT(/,5X,"CONTOUR NO.",I3,2X,"ELEMENT NO .",26I3,/)

```

```
31  FORMAT(//,5X,"CCNTOUR NO.",I3,2X,"ELEM TYPES",26I3,/)
    ALPHA=0.0
    DO 603 I=1,NN1
    YI=I-1
    ALPHA=PI*FLCAT(II)
    DXB=CELA*COS(ALPHA)
    CYB=0.0-DELA*SIN(ALPHA)
    DX=DXB*COS(ANGLE)-DYE*SIN(ANGLE)
    DY=DXB*SIN(ANGLE)+DYE*COS(ANGLE)
    WRITE(6,32)DX,DY,ALPHA
32  FORMAT(//,5X,"DISPL. IN X DIRECTION =",F15.8,/,5X,
1   "DISPL. IN Y DIRECTION =",F15.8,/,5X,"ALPHA =",F15.6,/)
    REWIND 1
    READ(1)(IX(MM),MM=1,NMAT)
    IM=0.0
    DENG=0.0
    DENG1=0.0
    DENG2=0.0
    CO 102 IL=1,NJJ
    IEL=IE(IL)
130  IM=IM+1
    READ(1)(X(J),J=1,3),(Y(J),J=1,3),IS,IB,(LJ(J),J=1,NVEL)
    IF(IM.EQ.IEL) GO TO 103
    GO TO 130
103  IS=1
    IB=MDIA(IL)
    IF(IB.EQ.2) GO TO 104
    AR=(Y(2)-Y(1))*DX+(X(1)-X(2))*DY
    AR=AR/2.00
    IF(IEI.GT.NE) GO TO 140
    X(1)=DX
    X(2)=DX
    X(3)=0.00
    Y(1)=DY
    Y(2)=DY
    Y(3)=0.00
    GO TO 105
140  X(1)=X(1)+DX
    Y(1)=Y(1)+DY
    X(2)=X(2)+DX
    Y(2)=Y(2)+DY
    GO TO 105
104  AR=(Y(2)-Y(3))*DX+(X(3)-X(2))*DY
    AR=AR/2.00
    IF(IEI.GT.NE) GO TO 141
    X(1)=DX
    X(2)=0.00
    X(3)=0.00
    Y(1)=DY
    Y(2)=0.00
    Y(3)=0.00
    GO TO 105
141  X(1)=X(1)+DX
    Y(1)=Y(1)+DY
105  IF(I.EG.1.AND.IEL.GT.NE) GO TO 102
    IF(I.EG.NN1.AND.IEL.GT.NE) GO TO 102
    CALL MIXEL2(S,AA,BA,CA,X,Y,AT,BT,AR,CPLN,IS,THICK)
```

```
IF(ALPHA.NE.0.0) GO TO 801
IF(K1K2.NE.1) GO TO 801
DO 604 J=1,NVEL
IKK=LJ(J)
IF(IKK) 308,309,308
309 UN1(J)=0.00
UN2(J)=0.00
GO TO 604
308 UN1(J)=SYMBB(IKK)
UN2(J)=ASYMBB(IKK)
604 CONTINUE
DO 605 K=1,NVEL
XEN1=0.0
XEN2=0.0
DO 606 J=1,NVEL
XEN1=XEN1+S(K,J)*UN1(J)
606 XEN2=XEN2+S(K,J)*UN2(J)
VN1(K)=XEN1
VN2(K)=XEN2
605 CONTINUE
XEN1=0.00
XEN2=0.00
DO 607 K=1,NVEL
XEN1=XEN1+(VN1(K)*UN1(K))/2.00
XEN2=XEN2+(VN2(K)*UN2(K))/2.00
607 CONTINUE
DENG1=DENG1+XEN1
DENG2=DENG2+XEN2
DENG=DENG1+DENG2
GO TO 102
801 CONTINUE
DO 107 J=1,NVEL
IKK=LJ(J)
IF(IKK) 108,109,108
109 U(J)=0.00
GO TO 107
108 U(J)=B(IKK)
107 CONTINUE
DO 110 K=1,NVEL
XEN=0.00
DO 111 J=1,NVEL
111 XEN=XEN+S(K,J)*U(J)
110 V(K)=XEN
XEN=0.00
DO 112 K=1,NVEL
112 XEN=XEN+(V(K)*U(K))/2.00
DENG=DENG+XEN
102 CONTINUE
DENG=DENG/DELA
IF(ALPHA.NE.0.0) GO TO 802
IF(K1K2.NE.1) GO TO 802
DENG1=DENG1/DELA
DENG2=DENG2/DELA
WRITE(6,33)IJ,DENG1,DENG2
33 FORMAT(/,5X,"CONTOUR NO.",I3,/,5X,"MODE 1 ENERGY RELEASE RATE=",
1E20.10,/,5X,"MODE 2 ENERGY RELEASE RATE=",E20.10,/)
802 CONTINUE
WRITE(6,34)IJ,DENG
34 FORMAT(/,5X,"CONTOUR NO.",I3,5X,"STRAIN ENERGY RELEASE RATE =",
1E20.10,/)
603 CONTINUE
121 CONTINUE
RETURN
END
```

```
SUBROUTINE TRANEL (S,A,B,C,X,Y,AT,BT,AR,E,ANU,XN,G,IS,H)
DIMENSION S(20,1),A(4,1),B(4,1),C(4,1),X(1),Y(1),AT(1),BT(1)
IF (IS.EQ.0) GO TO 1000
CALL PRESET (S,20,20)
CALL PRESET (A,4,4)
CALL PRESET (B,4,4)
CALL PRESET (C,4,4)
AT(1)=X(3)-X(2)
AT(2)=X(1)-X(3)
AT(3)=X(2)-X(1)
BT(1)=Y(2)-Y(3)
BT(2)=Y(3)-Y(1)
BT(3)=Y(1)-Y(2)
DO 12 I=1,3
BT(I)=H*BT(I)
12 AT(I)=H*AT(I)
AR=(X(1)*Y(2)+X(2)*Y(3)+X(3)*Y(1)-Y(1)*X(2)-Y(2)*X(3)-Y(3)*X(1))/
1 2.00
EE=-AR*H/E
C(1,1)=EE/6.00
C(1,2)=EE/20.00
C(1,3)=C(1,2)
C(1,4)=EE/15.00
C(2,2)=7.00*EE/90.00
C(2,3)=-EE/180.00
C(2,4)=2.00*EE/45.00
C(3,3)=C(2,2)
C(3,4)=C(2,4)
C(4,4)=8.00*EE/45.00
DO 1 I=1,4
DO 2 J=1,4
2 C(J,I)=C(I,J)
1 CONTINUE
CALL TRANAB(A,BT)
CALL TRANAB(B,AT)
CALL ARRANG(S,A,B,C,ANU,XN,G,4,4)
1000 RETURN
END
```

```
SUBROUTINE TRANAB(A,BT)
DIMENSION A(4,1),BT(1)
A(1,1)=BT(1)/6.00
A(1,2)=(BT(2)-BT(3))/12.00
A(1,3)=-A(1,2)
A(1,4)=(BT(2)+BT(3))/6.00
A(2,1)=BT(1)/12.00
A(2,2)=(BT(2)-1.5*BT(3))/15.00
A(2,3)=- (BT(2)+BT(3))/60.00
A(2,4)=(BT(2)+6.00*BT(3))/30.00
A(3,1)=A(2,1)
A(3,2)=A(2,3)
A(3,3)=(-1.5*BT(2)+BT(3))/15.00
A(3,4)=(6.00*BT(2)+BT(3))/30.00
A(4,1)=A(1,1)
A(4,2)=(BT(2)-4.00*BT(3))/30.00
A(4,3)=(-4.00*BT(2)+BT(3))/30.00
A(4,4)=8.00*(BT(2)+BT(3))/30.00
RETURN
END
```

BIBLIOGRAPHY

- [1] Pian, T.H.H., and Tong, P., "Basis of Finite Element Methods for Solid Continua", International Journal for Numerical Methods in Engineering, Vol. 1, 1969, pp. 3-28.
- [2] Reissner, E., "On a Variational Theorem in Elasticity", Journal of Mathematics and Physics, Vol. 29, 1950, pp. 90-95.
- [3] Sokolinkoff, I.S., Mathematical Theory of Elasticity, McGraw Hill, 1956.
- [4] Oden, J.T., "Some Contribution to the Mathematical Theory of Mixed Finite Element Approximations", Theory and Practice in Finite Element Analysis (Eds. Y. Yamada and R.H. Gallagher), University of Tokyo Press, 1973.
- [5] Oden, J.T., and Reddy, J.N., "On Mixed Finite Element Approximations", SIAM Journal of Numerical Analysis, Vol. 13, 1976, p. 392.
- [6] Oden, J.T., and Lee, J.K., "Theory of Mixed and Hybrid Finite Element Approximations in Linear Elasticity", Proceedings, IUTAM/IUM Symp. Applications of Methods of Functional Analysis to Problems of Mechanics, Marseilles, France, Sept. 1975.
- [7] Mirza, F.A., and Olson, M.D., "The Mixed Finite Element Method in Plane Elasticity", International Journal for Numerical Methods in Engineering, Vol. 15, 1980, pp. 273-289.
- [8] Mirza, F.A., "Convergence of Mixed Methods in Continuum Mechanics and Finite Element Analysis", Ph.D. Thesis, University of British Columbia, 1977.

- [9] Zienkiewicz, O.C., *The Finite Element Method in Engineering Science*, McGraw Hill, London, 1971.
- [10] Bradley, G.L., *A Primer of Linear Algebra*, Prentice-Hall, New Jersey, 1975.
- [11] Kanarachos, A., "Ritz-Galerkin and least squares finite element methods for incompressible viscous flow", Department of Mechanical Engineering, Ruhr University, Bochum, Germany, 1979.
- [12] Bathe, J.K., and Wilson, E.L., *Numerical Methods in Finite Element Analysis*, Prentice-Hall, 1976.
- [13] Timoshenko, S.P., and Goodier, J.N., *Theory of Elasticity*, 3rd Edition, McGraw Hill, New York, 1970.
- [14] Savin, G.N., *Stress Concentration Around Holes*, Pergamon Press, 1961.
- [15] Griffith, A.A., *Phil. Trans. Royal Society*, A221, 1921, pp. 163.
- [16] Griffith, A.A., *Proc. 1st Int. Congr. Applied Mech.*, Delft, 1924, p. 65.
- [17] Irwin, G.R., "Fracture", *Encyclopedia of Physics*, Vol. 6, Springer, pp. 551-590.
- [18] Irwin, G.R., "Relation of Crack-Toughness Measurements to Practical Applications", AWS-ASME Meeting, Cleveland, Ohio, 1962.
- [19] Irwin, G.R., "Fracture Mechanics", *Structural Mechanics*, Pergamon Press, New York, New York, 1960, pp. 557-592.
- [20] Sih, G.C., and Liebowitz, H., "Mathematical Fundamental of Fracture", *Academic Press*, New York, 1968, p. 67.

- [21] Williams, M-L., "On the Stress Distribution at the Base of a Stationary Crack", Journal of Applied Mechanics, Vol. 24, 1957, pp. 109-114.
- [22] Paris, D.C., and Sih, G.C., "Fracture Toughness Testing and Its Application", ASTM Special Technical Publication, No. 381, Philadelphia, Pa., 1965, pp. 30-81.
- [23] Chan, S.K., Tuba, I.S., and Wilson, W.K., "On the Finite Element Method In Linear Fracture Mechanics", Engineering Fracture Mechanics, Vol. 2, 1970, pp. 1-17.
- [24] Mowbray, D.F., "A Note on the Finite Element Method in Linear Fracture Mechanics", Engineering Fracture Mechanics, Vol. 2, 1970, pp. 173-176.
- [25] Hayes, D.J., "A Practical Formulation for Determining Stress Intensity Factors for Cracked Bodies", International Journal of Fracture Mechanics, Vol. 8, 1972, pp. 157-165.
- [26] Rice, J.R., "A Path Independent Integral and the Approximate Analysis of Strain Concentration by Notches and Cracks", Journal of Applied Mechanics, Vol. 35, 1968, pp. 379-386.
- [27] Rice, J.R., "Mathematical Analysis in the Mechanics of Fracture", An Advanced Treatise, Vol. 2 (ed. Liebowitz, H.), Academic Press, 1968, pp. 191-311.
- [28] Park, D.M., "A Stiffness Derivative Finite Element Technique for Determination of Crack Tip Stress Intensity Factors", International Journal of Fracture, Vol. 10, 1974, pp. 487-501.
- [29] Tracey, D.M., "Finite Element for Determination of Crack Tip Stress Intensity Factors", Engineering Fracture Mechanics, Vol. 3, 1972, pp. 255-267.

- [30] Byskov, E., "The Calculation of Stress Intensity Factors using the Finite Element Method with Cracked Elements", International Journal of Fracture Mechanics, Vol. 6, 1970, pp. 159-167.
- [31] Pian, T.H.H., Tong, P. and Luk, C.H., "Elastic Crack Analysis by a Finite Hybrid Method", 3rd Air Force Conf. Matrix Meth. Struct. Mech., Dayton, Ohio, 1971.
- [32] Alturi, S.N., Kobayashi, A.S., and Nakagaki, M., "Fracture Mechanics Application of an Assumed Displacement Hybrid Finite Element Procedure", AIAA Journal, Vol. 13, No. 6, 1975, pp. 734-739.
- [33] Mirza, F.A., and Olson, M.D., "Energy convergence and Evaluation of Stress Intensity Factor  $K_I$  for Stress Singular Problems by Mixed Finite Element Method", International Journal of Fracture, Vol. 14, 1978, pp. 555.
- [34] Tong, P., and Pian, T.H.H., "On the Convergence of the Finite Element Method for Problems with Singularity", International Journal of Solids and Structures, Vol. 9, 1973, pp. 313-321.
- [35] Bowie, O.L., "Rectangular Tensile sheet with Symmetric Edge Crack", Journal of Applied Mechanics, Vol. 31, 1964, pp. 208-212.
- [36] Bowie, O.L., and Neal, D.M., "A Note on the Central Crack in a Uniformly Stressed Strip", Engineering Fracture Mechanics, Vol. 2, 1970, pp. 181-182.
- [37] Bowie, O.L., and Freese, C.E., "Central Crack in Plane Orthotropic Rectangular Sheet", International Journal of Fracture Mechanics, Vol. 8, No. 1, March, 1972, pp. 49-58.

- [38] Sih, G.C., and Liebowitz, H., "Mathematical Theories of Brittle Fracture", An Advanced Teatise, Vol. 2, (ed. Liebowitz, H.), Academic Press, 1968, pp. 68-188.
- [39] Ishikawa, H., "A Finite Element Analysis of Stress Intensity Factor for Combined Tensile and Shear Loading by only a Virtual Crack Extension", International Journal of Fracture, Vol. 16, 1980, pp. 243-245.
- [40] Ishikawa, H., Kitagawa, H., and Okamura, H., "J Integral of a Mixed Mode Crack and Its Application", Proceedings of Third International Conference on Mechanical Behaviour of Materials, University of Cambridge, Vol. 3, 1979, pp. 447-455.
- [41] Hellen, T.K., and Blackburn, W.S., "The Calculation of Stress Intensity Factors for Combined Tensile and Shear Loading", International Journal of Fracture, Vol. 11, No. 4, 1975, pp. 605-617.
- [42] Hellen, T.K., "On the Method of Virtual Extensions", International Journal for Numerical Methods in Engineering, Vol. 9, 1975, pp. 187-207.
- [43] Vanderglas, M.L. and Pick, R.J., "On Virtual Crack Extension Methods for Combined Tensile and Shear Loadings", Fracture 1977, ICF4, Waterloo, Canada, Vol. 3, 1977, pp. 501-506.
- [44] Knowles, J.K., and Sternberg, E., "On a Class of Conservation Laws in Linearised and Finite Elastostatics", Arch. Rat. Mech. Anal., Vol. 44, 1972, pp. 187-211.

- [45] Hussain, M.A., Pu, S.L., and Underwood, J., "Strain Energy Release Rate for a Crack Under Combined Mode I and Mode II", Fracture Analysis, ASTM STP 560, American Society for Testing and Material, 1974, pp. 2-28.
- [46] Stern, M., Becker, E.B., and Dunham, R.S., "A Contour Integral Computation of Mixed-Mode Stress Intensity Factors", International Journal of Fracture, Vol. 12, No. 3, 1976, pp. 359-368.
- [47] Wang, S.S., Yan, J.F., and Corten, H.T., "A Mixed-Mode Crack Analysis of Rectilinear Anisotropic Solids using Conservation Laws of Elasticity", International Journal of Fracture, Vol. 16, No. 3, 1980, pp. 247-259.
- [48] Erdogan, F., and Sih, G.C., "On the Crack Extension in Plates Under Plane Loading and Transverse Shear", Journal of Basic Engineering, Vol. 85, D, 1963, pp. 519-527.
- [49] Williams, J.G., and Ewing, P.D., "Fracture under Complex Stress - The Angle Crack Problem", International Journal of Fracture Mechanics, Vol. 8, No. 4, 1972, pp. 441-446.
- [50] Sih, G.C., and Kipp, M.E., Discussion on "Fracture under Complex Stress - The Angle Crack Problem", International Journal of Fracture, Vol. 10, No. 2, 1974, pp. 261-265.
- [51] Finnie, I., and Saith, A., "A Note on the Angle Crack Problem and the Directional Stability of Cracks", International Journal of Fracture, Vol. 9, 1973, pp. 484-486.
- [52] Sih, G.C., "Strain-Energy-Density Factor applied to Mixed Mode Crack Problems", International Journal of Fracture, Vol. 10, No. 3, 1974, pp. 305-321.

- [53] Sih, G.C., "Applications of the Strain-Energy-Density Theory to Fundamental Problems in Fracture Mechanics", presented at the 10th Annual Meeting of the Society of Engineering Science, Raleigh, North Carolina, November, 1973.
- [54] Wang, T.C., "Fracture Criteria for Combined Mode Crack", Fracture, 1977, ICF4, Waterloo, Canada, Vol. 4, 1977, pp. 135-154.
- [55] Palaniswamy, K., and Knauss, W.G., "Propagation of a Crack under General In-Plane Loading", International Journal of Fracture Mechanics, Vol. 8, 1972, pp. 114-117.
- [56] Bilby, B.A., Cardew, G.E., and Howard, I.C., "Stress Intensity Factors at the Tips of Kinked and Forked Cracks", Fracture 1977, ICF4, Waterloo, Canada, Vol. 3, 1977, pp. 197-200.
- [57] Bilby, B.A. and Cardew, G.E., "The Crack with a Kinked Tip", International Journal of Fracture, Vol. 11, 1975, pp. 708-712.
- [58] Lo, K.K., "Analysis of Branched Crack", Journal of Applied Mechanics, Vol. 45, 1978, pp. 797-802.
- [59] Wu, C.H., "Elasticity Problem of a Slender Z-Crack", Journal of Elasticity, Vol. 8, No. 2, 1978, pp. 183-205.
- [60] Wu, C.H., "Maximum-Energy-Release-Rate Criterion Applied to a Tension-Compression Specimen with Cracks", Journal of Elasticity, Vol. 8, No. 3, 1978, pp. 235-257.
- [61] Wu, C.H., "Fracture Under Combined Loads by Maximum-Energy-Release-Rate Criterion", Journal of Applied Mechanics, Vol. 45, 1978, pp. 553-558.

- [62] Hayashi, K., and Nemat-Nasser, S., "Energy Release Rate and Crack Kinking", International Journal of Solids and Structures, Vol. 17, 1981, pp. 107-114.
- [63] Palaniswamy, K., and Knauss, W.G., in "Mechanics Today", Vol. 4, edited by S. Nemat-Nasser, Pergamon Press, 1978, pp. 87-130.